Cobalt catalyzed open-shell transformations: Synthetic applications & Mechanistic studies

Monography dissertation

in partial fulfillment of the requirements for the degree of

doctor rerum naturalium (Dr. rer. nat.)

at the University of Rostock

Faculty for Mathematics and Natural Sciences

submitted by

Le Quoc Phong Dam

Born October 06th 1996

in Hanoi, Vietnam

Leibniz Institute for Catalysis

at the University of Rostock

2024

https://doi.org/10.18453/rosdok_id00005135

The present work was accomplished at the Leibniz-Institute for Catalysis e.V. at the University of Rostock, at the “Modern Organic Chemistry” research group of Dr. Osama El-Sepelgy and the “In situ Catalytic Studies” department of Prof. Angelika Brückner during the period from August 2021 to October 2024.

Reviewers:

Dr. Osama El-Sepelgy, Leibniz-Institut für Katalyse e.V., Rostock

Prof. Dr. Johannes M. Wahl, Johannes-Gutenberg-Universität Mainz, Mainz

Year of the submission to the faculty: 2024

Year of oral defense: 2025

Selbstständigkeitserklärung

I hereby affirm that I have written the present work by myself without outside assistance. No other resources were utilised than stated. All references as well as verbatim extracts were quoted, and all sources of information were specifically acknowledged.

Ich versichere hiermit an Eides statt, dass ich die vorliegende Arbeit selbstständig angefertigt und ohne fremde Hilfe verfasst habe. Dazu habe ich keine außer den von mir angegebenen Hilfsmitteln und Quellen verwendet und die den benutzten Werken inhaltlich und wörtlich entnommenen Stellen habe ich als solche kenntlich gemacht.

Rostock, den 12.11.2024

_____

Le Quoc Phong Dam

Acknowledgements

First and foremost, I would like to express my sincere gratitude to my supervisor, Dr. Osama El-Sepelgy, for warmly welcoming me into the group and offering the opportunity to work on such fascinating topics, which ultimately led to the work presented in this thesis. I am especially thankful for your willingness to engage in discussions and for sharing your perspective and approach as an organic chemist, which inspires me to appreciate the beauty of chemistry.

I also want to express my gratefulness to my second supervisor, Prof. Angelika Brückner, whose support enabled me to work at LIKAT since my master's degree. I am grateful for the invaluable discussions enriched by your expertise and critical insights. These exchanges have been a source of motivation, which shapes my approach to scientific inquiry.

Special thanks go to the leader of "Magnetic Resonance & X-ray Methods" group, Dr. Jabor Rabeah, for his continuous support and guidance throughout my PhD journey. Thank you for always listening, generously offering support with your expertise and sense of humor, engaging in thoughtful discussions, which led to the majority of work presented here.

I would like to thank my daily lab mates, Dr. Chenyang Wang and Kaiming Zuo, for creating such a welcoming and collaborative working environment. In particular, I want to thank Chenyang for guiding me when I started my journey in the organic synthesis lab.

Furthermore, I want to acknowledge all the members of the former "In situ catalytic studies" department – of which I had the privilege to be part of – for all the supports and insightful discussions on spectroscopy and lab techniques, which have been helpful to the studies I conducted here.

My journey in Rostock would not have been the same without Dr. José "Cobra" Balena, Dr. Elizaveta Fedorova, Dr. Aleksandr Fedorov, Dr. Sebastian Cisneros, Dr. Hilario "Muchacho" Huerta, Evaristo Salaya, Pierre Fablet, Hendrik Kempf, Gustavo Alberto Alvarez, Mirjam Schröder, Dr. Tatiana Otroshchenko, Dr. Jan Günther Tönjes and Simon Haida. Thank you for onboarding me, accompanying me and making many unforgettable memories together with uncountable Bierabends, sunsets in the harbor or swims in Warnemünde.

Additionally, I am greatful to the Vietnamese community in Rostock, who welcomes and makes me feel less homesick when I am abroad. Specially, I want to thank the "Rostock gang" – anh Viên, em Hưng and em Tuấn – for being my best gym and nhậu buddies.

Thank you, Huyen, for always being by my side, supporting and encouraging me to be a better version of myself. Your “push” in those recent days is immensely meaningful to me.

Last but not least, I want to thank my family – my sister, my father and my mother – for their unconditional love and belief in me. Không có bố mẹ và chị Tít thì đã không có bài luận án ngày hôm nay. Cảm ơn bố mẹ đã nuôi nấng, luôn ủng hộ để con được tự do theo đuổi hành trình của riêng mình.

Zusammenfassung

Diese Dissertation untersucht das breite Potenzial der Kobaltkatalyse bei Open-Shell-Transformationen und positioniert Kobalt als eine nachhaltige, vielseitige Alternative zu Edelmetallen für die Durchführung komplexer organischer Reaktionen unter milden Bedingungen. Die Arbeit ist in vier Projekte gegliedert, von denen jedes einen einzigartigen Einblick in die Rolle von Kobalt bei der radikalischen Entsättigung und selektiven Funktionalisierung verschiedener organischer Moleküle bietet.

Die ersten drei Projekte befassen sich mit der Cobaloxim-Katalyse für radikalische Entsättigungsreaktionen (Kapitel 2-4). Im ersten Projekt werden innovative photoangeregte, basisch-metallkatalysierte Methoden zur selektiven Modifizierung von aliphatischen Amiden, Imiden und primären Aminen vorgestellt. Durch den Einsatz eines Katalysators auf Kobaltbasis unter Bestrahlung mit sichtbarem Licht wird eine selektive Entsättigung von aliphatischen Amiden und Imiden bei Raumtemperatur erreicht, was zu wertvollen zyklischen und azyklischen Enamiden und Enimiden führt. Darüber hinaus zeigt eine endoselektive intramolekulare Heck-Reaktion von Iodmethylsilylethern, die von Phenolen und Alkenolen abgeleitet sind, die Effizienz eines einfachen Cobaloxim-Katalysators zur Herstellung von Siloxycyclen, die anschließend in Allylalkohole umgewandelt werden können. Darauf aufbauend wird in Kapitel 4 eine biomimetische Strategie für die katalytische Deammonisierung von primären Aminen vorgestellt. Mit einer Kombination aus Acridiniumsalz und Cobaloxim als photoaktiven Katalysatoren werden bei diesem vielseitigen Ansatz Olefine aus erneuerbaren Rohstoffen erzeugt.

In Kapitel 5 wird ein bahnbrechender Ansatz für die γ-C-H-Funktionalisierung aliphatischer Alkohole durch Kobalt-Salen-Katalyse beschrieben. Diese Methodik ermöglicht eine selektive Modifizierung an der typischerweise nicht reaktiven γ-Position, wodurch verschiedene Umwandlungen wie Halogenierung, Aminierung, Cyanierung, Azidierung und Entsättigung mit hoher Selektivität möglich werden.

Um die zugrundeliegenden Mechanismen zu entschlüsseln, wurden fortschrittliche experimentelle Techniken wie UV-vis- und EPR-Spektroskopie zusammen mit der Analyse der Dichtefunktionaltheorie (DFT) eingesetzt. Die Spektroskopie bot Einblicke in die katalytische Aktivierung und die Bildung von Zwischenstufen, während die DFT einen detaillierten Überblick über die schnellen, mehrstufigen Reaktionswege lieferte. Dieser kombinierte Ansatz ermöglichte ein umfassendes Verständnis der Reaktivität und Selektivität

von Kobalt und unterstreicht sein Potenzial als nachhaltiger Katalysator für die organische Synthese.

Abstract

This dissertation investigates the broad potential of cobalt catalysis in open-shell transformations, positioning cobalt as a sustainable, versatile alternative to noble metals for conducting complex organic reactions under mild conditions. The thesis is organized into four projects, each contributing unique insights into cobalt's role in radical desaturation and selective functionalization of various organic molecules.

The first three projects center on cobaloxime catalysis for radical desaturation transformations (Chapter 2-4). The first project introduces innovative photoexcited, base-metal-catalyzed methods for the selective modification of aliphatic amides, imides, and primary amines. By employing a cobalt-based catalyst under visible-light irradiation, selective desaturation of aliphatic amides and imides is achieved at ambient temperature, resulting in valuable cyclic and acyclic enamides and enimides. Additionally, an *endo*-selective intramolecular Heck reaction of iodomethylsilyl ethers derived from phenols and alkenols demonstrates the efficiency of a straightforward cobaloxime catalyst for producing siloxycycles, which can subsequently be converted into allylic alcohols. Building on this, Chapter 4 presents a biomimetic strategy for the catalytic deammoniation of primary amines. Using a combination of acridinium salt and cobaloxime as photoactive catalysts, this versatile approach generates olefins from renewable feedstocks.

In Chapter 5, a pioneering approach for remote γ-C–H functionalization of aliphatic alcohols *via* cobalt salen catalysis is detailed. This methodology enables selective modification at the typically unreactive γ-position, allowing for diverse transformations including halogenation, amination, cyanation, azidation, and desaturation with high selectivity.

To unravel the underlying mechanisms, advanced experimental techniques, such as UV-vis and EPR spectroscopy, were employed alongside density functional theory (DFT) analysis. Spectroscopy offered insights into catalytic activation and intermediate formation, while DFT provided a detailed view of rapid, multi-step reaction pathways. This combined approach delivered a comprehensive understanding of cobalt’s reactivity and selectivity, underscoring its potential as a sustainable catalyst for organic synthesis.

Contents

List of publications:

1. **P. Dam**, K. Zuo, L. M. Azofra and O. El-Sepelgy. Biomimetic Photoexcited Cobaloxime Catalysis in Organic Synthesis, *Angewandte Chemie International Edition*, 2024, DOI: 10.1002/anie.202405775.
2. C. Wang, **P. Dam**, M. Elghobashy, A. Brückner, J. Rabeah, L. M. Azofra and O. El-Sepelgy, Biomimetic Dehydroamination of Primary Amines. *ACS Catalysis*, 2023, DOI: 10.1021/acscatal.3c04305.
3. C. Wang, L. M. Azofra, **P. Dam**, E. J. Espinoza-Suarez, H. T. Do, J. Rabeah, A. Brückner, and O. El-Sepelgy. Photoexcited cobalt catalysed endo-selective alkyl Heck reaction, *Chemical Communications*, 2023, DOI: 10.1039/D2CC06967A.
4. C. Wang, L. M. Azofra, **P. Dam**, M. Sebek, N. Steinfeldt, J. Rabeah, O. El-Sepelgy. Catalytic Desaturation of Aliphatic Amides and Imides Enabled by Excited-State Base-Metal Catalysis, *ACS Catalysis,* 2022, DOI: 10.1021/acscatal.2c01723.

The publications presented in this thesis are reprinted with permission from the corresponding publishers.

Chapter 1: Introduction

1.1. Open-shell transformation

Most stable chemical compounds have closed-shell electronic configurations. In this arrangement, all electrons are paired, and orbitals with the same energy are either fully occupied or completely empty.[1] In contrast, open-shell systems in chemistry refer to atomic or molecular structures where not all orbitals are filled with paired electrons.[1] In such configurations, some electrons remain unpaired in their orbitals, either due to an imbalance between the number of α (spin-up +1/2) and β (spin-down -1/2) electrons, or because some degenerate orbitals are only partially filled.[2] Open-shell systems are commonly found in *free radicals*, *transition metals* with partially filled d-orbitals, or *atoms and molecules in transition states* that have absorbed energy, causing an electron to move to a higher orbital.

Because unpaired electrons generate magnetic moment, open-shell species exhibit paramagnetic character, meaning that they are attracted to magnetic fields. This property makes open-shell systems prominent in spectroscopy.[3] Additionally, these species tend to be more reactive since unpaired electrons are unstable and seek to pair with electrons from other atoms or molecules. As a result, open-shell species are highly prone to chemical reactions.[4]

Open-shell transformations involve reactions or processes that include species with unpaired electrons, such as radicals or certain transition metal complexes. These transformations play a crucial role in various chemical processes, especially in organic chemistry, catalysis, and photochemistry, where bond formation and bond breaking involve radicals or unpaired electron species.[5]

1.1.1. General considerations on free radicals

Free radicals are generally defined as short-lived, unstable chemical species (atoms, molecules, or ions) which possess an unpaired electron.[6] Depending upon the core atom that owns this electron, the radicals can be categorized as carbon-, oxygen-, nitrogen-, metal-centered radicals.

The first organic free radical, triphenylmethyl, was identified by Gomberg in 1900.[7] Based on this foundation work, many studies have explored various aspects of free

radicals, including their electronic structures, spectroscopy, chemical kinetics, and reaction dynamics, as well as their roles in different reactive systems.[8] In 1929, Paneth and Hofeditz made another significant discovery by proving the existence of the methyl radical ($CH_3^{\bullet}$).[9] Their findings showed that organic reactions can probably occur *via* transient radical species that are unstable to be isolated. With this evidence, radical mechanism was assigned to several known synthetic transformations.[10] However, radical chemistry was not applied widely in organic synthesis as it was seen as unstable, unpredictable, and lacking selectivity.[11] In the 1980s, radical chemistry experienced significant growth, especially with the introduction of tin reagents as promoters of radical chain reactions to apply for polymer synthesis.[12] However, the requirement for high temperatures and toxic reagents posed challenges for their use on a synthetic scale. Until the last decade, the radical chemistry has changed dramatically with the rise of photoredox catalysis, which allows radicals to be accessed under much milder conditions.[13] These advancements have established radical as a valuable alternative approach to classical ionic method.

The selectivity of radical process comes from kinetic studies, where the formation of desired product should occur faster than all other possible reactions under the experimental conditions.[14] This behavior is largely influenced by the energy levels of the radical intermediates involved. The energy of these intermediates shapes the reaction pathway and has a significant impact on the final product distribution. Key factors that contributed to the energy of transition species are polar, stereoelectronic, and steric effects. Firstly, polar effects describe how the electronegativity of the constituent atoms affect the activation energy. This effect are significant in homolytic substitution reactions (e.g., hydrogen atom transfer (HAT), halogen atom transfer (XAT)), where the step of abstracting atoms to form polar transition state is required, or in intermolecular addition to π systems (e.g., Giese addition to olefins).[15] In these reactions, the polarity (i.e., electrophilic or nucleophilic character) of radical should be matched with that of the reactant to establish strong interaction and thus, control the chemoselectivity. Secondly, stereoelectronic effects are the influence of the orbital orientation to the energy of the transition state. This effect dominates in ring opening reactions, where the overlap of frontier orbital promotes the formation of a new π orbital to lower the activation energy of the ring opening step.[16] Finally, steric effects reflect the contribution of non-bonded interaction to the activation energy. This effect is important in radical transfer reactions, where bulky groups can hinder radicals from reaching specific sites or stabilizing them through electron delocalization, as well as affecting the formation of new radical.[17]

1.1.2. Generation of free radicals

Traditionally, free radical generation involved harsh conditions like UV irradiation, high temperatures, and the use of toxic tin reagents or peroxides. However, modern methods can enable the formation of free radicals under much milder conditions. The next subsections will focus on two of the most common strategies now available, namely *photoredox* and *transition metal* catalysis.

Outer-sphere electron transfer (Photoredox catalysis)

Over the past five decades, photoredox chemistry has been widely applied in inorganic fields, including water splitting, carbon dioxide reduction, and solar cell development.[18] However, pioneering work by researchers such as MacMillan, Stephenson, and Yoon revealed the potential of organic dyes and metal polypyridyl complexes in organic synthesis, leading to rapid growth in this area.[19] Today, the significant role of light as a clean, selective, and powerful energy source for driving chemical reactions is well-recognized and embraced in organic synthesis.[20] The main advantage of this method is the generation of highly reactive radical species under mild conditions simply by exposing the reaction to light. This approach enables the access to reactivity modes that are not available in the ground state. Importantly, advances in safe, tunable, and widely available light sources have further accelerated the adoption of photochemical methods, highlighting the critical role of these technical developments in advancing the field. Some of the valuable photocatalysts are listed in Figure 1.1.

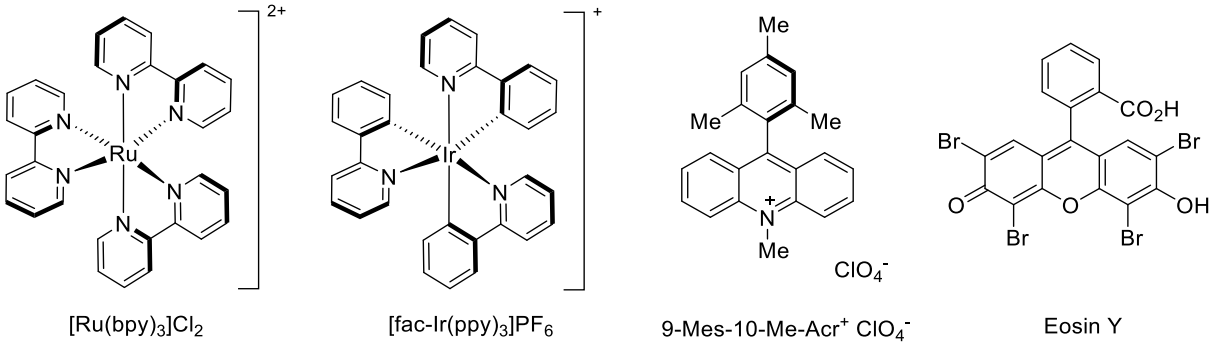

Figure 1.1. Examples of transition metal and organic photoredox catalysts.

In a typical photoredox cycle, the photocatalyst is excited by light, following by a single-electron transfer (SET) between the catalyst and an organic molecule to generate a reactive radical species. Since the photocatalyst is often activated at room temperature using low catalyst loading, radical formations are taken place under extremely mild conditions,

making it highly compatible with various functional groups. Additionally, because many organic molecules tend to absorb light at shorter wavelengths, using visible light helps avoid unwanted decomposition pathways.[21]

A photocatalyst can act as both an oxidizing and reducing agent at different stages of the catalytic cycle. When it absorbs light, the catalyst transitions from its ground state to an excited state. Depending on the redox potential match between the excited photocatalyst and the substrate in its ground state, either a reductive or oxidative quenching cycle can occur (Scheme 1.1).

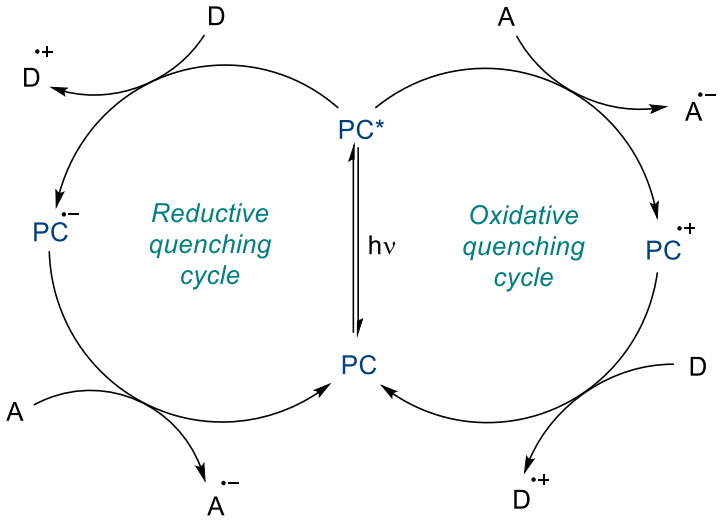

Scheme 1.1. Reductive and oxidative quenching cycles of photoredox catalysts.

If the oxidation potential of the excited photocatalyst exceed the ground state oxidation potential of the substrate, a reductive quenching cycle would take place (Scheme 1.1, left). Specifically, a SET from a donor D occurs to generate $PC^{\bullet-}$ as well as $D^{\bullet+}$, which may engage in subsequent radical reactions. The catalytic cycle is closed by the oxidation of the reduced photocatalyst by a suitable acceptor A. On the contrary, the oxidative quenching can be achieved if the reduction potential of the excited state photocatalyst is more negative than the ground state reduction potential of the elected substrate (Scheme 1.1, right). The excited photocatalyst PC* transfers an electron to an acceptor A, resulting in oxidized photocatalyst $PC^{\bullet+}$ that can would then be reduced by a donor D to close the catalytic cycle. This flexibility becomes one of the main advantages in photoredox catalysis as it allows to carry transformations that are overall redox neutral.

Inner-sphere electron transfer (organometallics)

Radical chemistry and transition metal catalysis are closely linked, though they evolved separately. Radical chemistry began to see widespread synthetic applications in polymer synthesis only in the early 1980s, while transition metal catalysis had already made significant development during the 1960s and 1970s, with landmark reactions such as the Mizoroki-Heck,[22] Suzuki-Miyaura,[23] and Negishi cross-couplings[24]. The connection between radicals and transition metal chemistry was brought together by Kochi and others, who highlighted the role of electron transfer in reactions containing organometallic intermediates and its importance in generating free radical species.[25] By using transition metal catalyzed process involving radical intermediates, the concentration of generated radical is controlled to not exceed than that of the metal catalyst. The low concentration of radical promotes the desired process and avoids competing homocoupling or disproportionation.[26] While late transition metals mostly take part in processes that involve two-electron changes, first-row transition metals frequently show one-electron reactivity. This means that often radicals are involved as intermediates in reactions using base-metal catalysts.[27] In the coordination sphere of a transition metal, radical-type reactions can proceed selectively.

Radical generation in transition metal complexes can be classified into two types based on electron flow: *reductive* or *oxidative* electron transfer.[28] Reductive electron transfer occurs when the metal donates an electron to an organic molecule. The reductive generation of radical is usually seen by using Ni, Cr.[25a] On the other hand, oxidative electron transfer involves the metal accepting an electron from a radical precursor. This is more common for 3d metals such as Mn, Fe, Co, Cu that can reach higher oxidation states more easily, and act as oxidants.[29]

Besides generating of radical in ground state, radical formation can be also achieved in excited state *via* direct excitation strategy.[30] By combining visible light with transition metal complexes, open-shell species are mostly generated through ligand-to-metal charge transfer (LMCT) excited states pathway.[31] LMCT states occur when light promotes an electron from a filled ligand-based orbital to an empty metal-centered orbital (Scheme 1.2).[32]

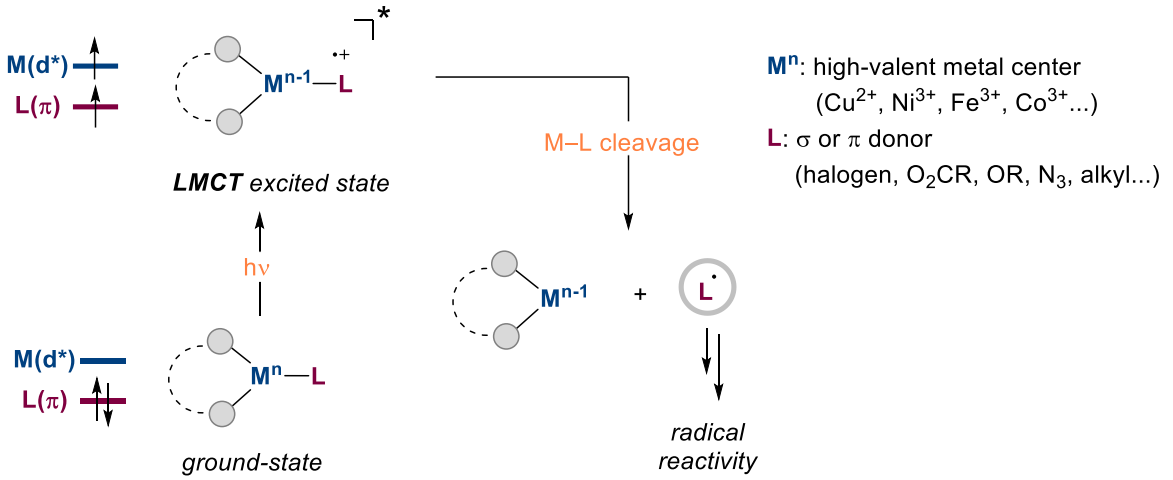

Scheme 1.2. Photophysics and photochemistry of LMCT states. The scheme is adapted with permission from ref [31].

To facilitate the access to this process, the energy of empty metal orbital (d*) must be relatively low, which is typical of complexes with electrophilic, high-valent metal centers (Ti^{IV}, Fe^{III}, Co^{II}).[33] Additionally, because the ligand serves as the electron donor reservoir in this transition, the presence of strong π and σ donating ligands (such as halides, carboxylates, or azides) supports the appearance of LMCT transitions at lower energy levels.[33] Regarding the electronic structure, LMCT transitions filled electron of a metal antibonding orbital (d*/dσ*) from ligand (π/σ). This process weakens the strength of metal–ligand bonds and thus, the bond cleavage is facilitated. This behavior often relates to a non-emissive deactivation of the excited state, which resulted in short lifetimes and low emission quantum yield.[34] Thus, these excited states are difficult to observe by classical fluorescence/phosphorescence spectroscopy.

In conclusion, open-shell organometallic chemistry enables the control of radical-type reactions within the coordination sphere of transition metals. Due to the high abundance and relatively low cost of the first-row transition metals, exploring novel reactivities using base metals is particularly desirable. Therefore, understanding these radical-type processes and applying them to develop sustainable methodologies paves the way for innovative chemical transformations that are challenging or even unattainable through conventional approaches.

1.2. Reactivity of cobaloxime catalysis

Vitamin B_{12}, a naturally occurring organocobalt compound, is regarded as the earliest and most studied molecule that can generate alkyl radical *via* excited states (Figure 1.2,

left).[35] This C-centered radical is generated through the reversible homolytic cleavage of Co–C bonds in the molecules under visible light. This feature plays a crucial role in their enzymatic functions.[36] For instance, the formation of weak Co–C bonds stabilizes the methyl radicals for sequential methylation on *p*-aminobenzoate peptidyl carrier protein.[37] These Co–C bonds can be broken easily by either thermolysis or photolysis due to the low bond dissociation energy.[38]

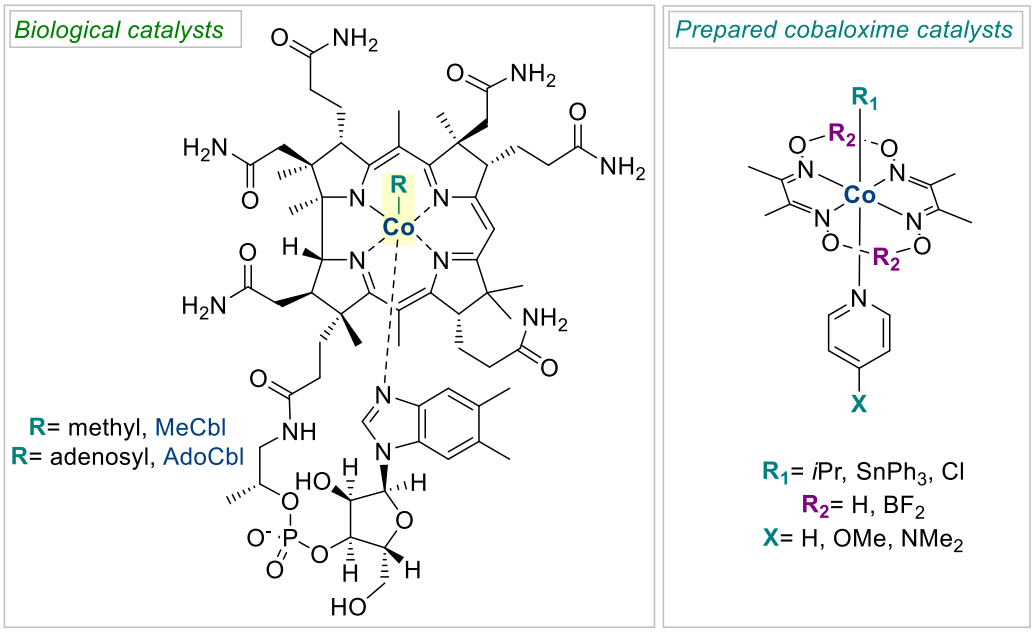

Figure 1.2. Structures of biological and bio-inspired cobaloxime.

To mimic the structure of natural alkylcobalamins and investigate their enzymatic mechanisms, simple cobaloxime complexes were synthesized.[39] These cobalt(III) complexes possess octahedral geometry and contain dioximate connected by hydrogen bonds or BF_2 bridges as equatorial ligands. The axial ligands are typically nitrogen-containing species like pyridine and halogens (Figure 1.2, right). In catalysis field, cobaloximes are well known for the role as proton reduction catalysts in water-splitting processes.[40] However, their use in organic synthesis has been extensively applied only recently. The first application of cobaloximes in organic synthesis is dated back to the 1980s from the seminal works of Tada, Pattenden, Branchaud, and Giese.[41] However, a significant limitation of cobaloxime chemistry was the catalytic turnover step, which required harsh reductive conditions. Several catalytic regeneration methods during this period were reported including electrochemical methods or the need of stoichiometric number of reductants like Zn, sodium borohydride, or Grignard reagents.[42] Until 2011, the first catalytic turnover of cobaloximes utilizing simple organic bases was reported by Carreira and coworkers, which marks as a significant milestone in cobaloxime catalysis.[43]

In 2015, the combination of cobaloxime and photoredox catalysis was established, which led to more innovative chemical transformations.[44]

1.2.1. General considerations to cobaloxime

The catalytic activity of cobaloxime complexes can be classified into *inner-sphere* and *outer-sphere* reactivity, which can occur in either ground or excited state (Scheme 1.3).

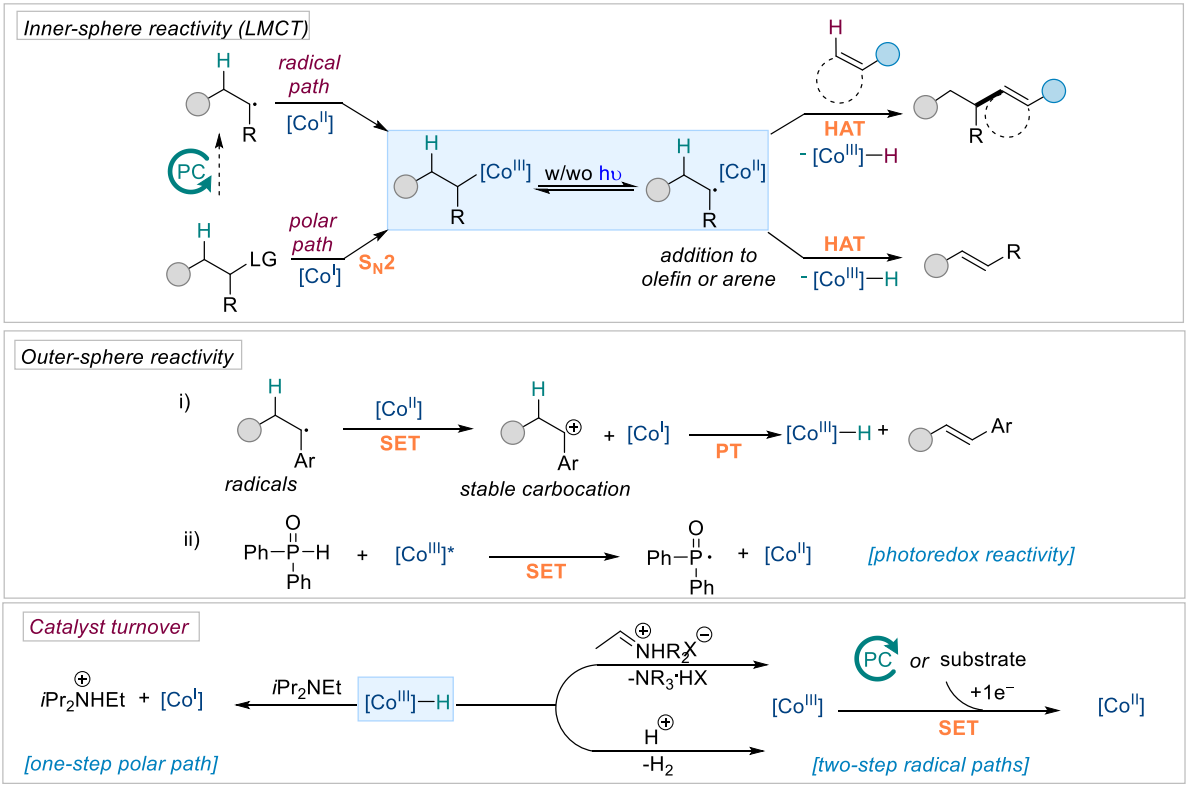

Scheme 1.3. General concept of catalytic activity and turnover of cobaloxime.

The inner-sphere reactivity, also referred to as the ligand-to-metal charge transfer (LMCT) pathway, closely mimics natural enzymatic processes via the formation of reversible Co–alkyl bonds between the catalyst and the substrate.[31] This [Co^{III}]–alkyl complexes can be generated through either radical or polar pathway. The former involves the capture of alkyl radicals by persistent [Co^{II}] radicals, while the latter encompasses the interaction between electrophilic alkyl species and highly nucleophilic [Co^{I}] via S_N2-type reactions. The reversible homolysis of Co–C bond in [Co^{III}]–alkyl intermediate into C-centered radical can be achieved under thermal or light-induced conditions. The formed reactive radical can undergo β-hydrogen elimination and HAT with [Co^{II}] to yield an olefin or aromatic compound. Otherwise, the organic radical may add to olefins or arenes, resulting in a new

radical intermediate. This intermediate can then be trapped by a metalloradical [Co^{II}] species, forming [Co^{III}]–H and a new olefin or functionalized aromatic compound.

On the other hand, outer-sphere reactivity involves electron transfer steps that occur outside the coordination sphere of the cobalt complex (Scheme 1.3). The electron transfer process is influenced by the matching of redox potential between reactant and [Co^{II}] metalloradicals, which possess low reduction potential ($E_{p/2}(Co^{II}/Co^{I})$ = −1.13 V vs SCE).[45] Thus, to promote a SET from [Co^{II}] species to organic radicals, the organic radicals also need low oxidative potential, such as benzylic and dibenzylic radicals (E_{ox} < 0 V vs SCE), to facilitate the oxidation.[46] This SET oxidation results in the generation of [Co^{I}] species and stable carbocations, which can subsequently undergo proton transfer (PT) to form [Co^{III}]–H and unsaturated compounds. Another type of SET from cobaloxime to the reactant includes the participant of the excited-state of [Co^{III}] complex. In this pathway, the excited state [Co^{III}]* species undergoes a SET to oxidize H-phosphines, leading to the formation P-radicals and [Co^{II}] species.

Depending on the active species of the system (i.e., [Co^{I}] or [Co^{II}]), the turnover from [Co^{III}]–H can occur *via* either polar or radical pathway. The nucleophlic [Co^{I}] can be regenerated *via* one-step polar route, where [Co^{III}]–H is deprotonated by a simple organic base (e.g., *i*Pr_2NEt) (Scheme 1.3). In contrast, in a radical pathway, [Co^{III}]–H is supposed to be convert to [Co^{III}] species by reacting with an imine salt intermediate or another proton to release H_2. This electron-deficient Co^{III} species is easily reduced to Co^{II} *via* SET with a substrate like H-phosphine or a photoredox catalyst ($E_{p/2}(Co^{III}/Co^{II})$ = −0.68 V vs SCE).[45]

The following sections cover the reactivity of cobaloxime in some specific chemical reactions.

1.2.2. Alkyl-Heck type reaction

Since its discovery in the early 1970s, the Mizoroki-Heck reaction, which couples unsaturated carbon electrophiles with nucleophiles, is one of the most versatile synthetic methods to form C–C bonds. Compared to aryl halides as common electrophiles for the reaction, the use of C(sp^3) halides faces more challenges, owing to the slow rate of oxidative addition.[47]

Polar Alkyl Heck-type reaction

In 2011, Carreira and coworkers reported the use of the simple **Co(dmgH)$_2$(pyr)(*i*Pr)** complex together with under visible light conditions for the intramolecular *exo*-selective Heck reaction of primary alkyl iodides (Scheme 1.4).[43] The key to success is the formal reduction of [Co^{III}]–H to an anionic [Co^{I}] species *via* deprotonation using an organic base (*i*Pr$_2$NEt). In 2016, the Morandi group demonstrated the use of epoxides and aziridines as electrophiles and intramolecular coupling with alkenes catalyzed by **Co(dmgH)$_2$(pyr)(*i*Pr)**.[48]

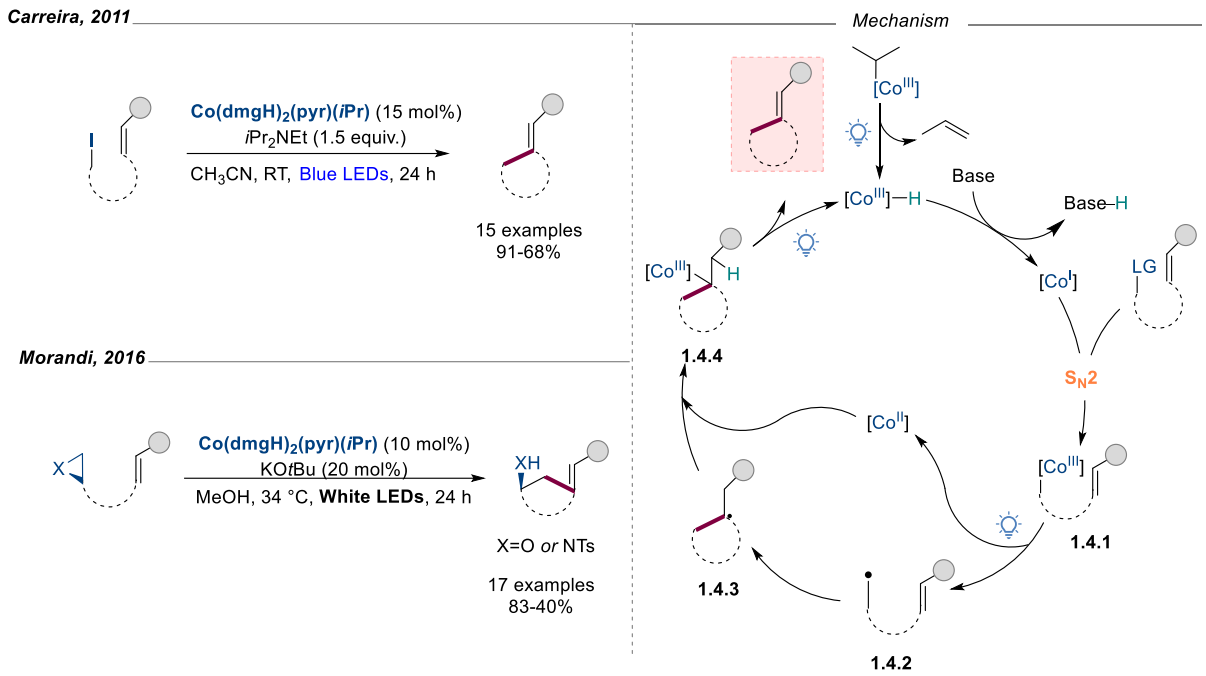

Scheme 1.4. Cobaloxime catalyzed polar alkyl-Heck reaction.

Herein, the initial activation of **Co(dmgH)$_2$(pyr)(*i*Pr)** under visible light irradiation leads to the formation of [Co^{III}]–H. This species is deprotonated by a suitable base to generate the nucleophilic [Co^{I}] species, which undergoes S$_N$2 process with an electrophile substrate to give the corresponding alkyl–[Co^{III}] intermediate (**1.4.1**). This Co–C bond is cleaved under the irradiation to produce [Co^{II}] and alkyl radical intermediate (**1.4.2**), following by intramolecular radical addition to furnish intermediate (**1.4.3**). The radical species (**1.4.3**) can recombine with [Co^{II}] to form another alkyl–[Co^{III}] intermediate (**1.4.4**). Upon β-hydrogen elimination under irradiation, this intermediate affords the desired product as well as regenerates [Co^{III}]–H to complete the catalytic cycle.

Radical Alkyl-Heck reaction

The previously discussed polar-based Heck reactions are primarily restricted to intramolecular transformations involving primary alkyl iodides. To address these

limitations, efforts have been made to generate alkyl radicals under visible light using a co-catalyst. These radicals are then added to olefins, while a suitable cobaloxime regenerates the double bond, forming alkene products (Scheme 1.5). In this context, Wu and colleagues were the first to report a decarboxylative alkyl Heck reaction employing dual photoredox and cobaloxime catalysis.[49] They used carboxylic acids as precursors for a wide variety of primary, secondary, and tertiary alkyl radicals under oxidative photoredox conditions. Two years later, Leonori and his team introduced an alkyl Heck reaction involving alkyl iodides and bromides, utilizing a halogen atom transfer (XAT) strategy to generate radicals.[50] This XAT pathway was achieved using an aminoalkyl radical reagent generated *in situ* by Et_3N and a photocatalyst (4CzIPN). More recently, Melchiorre and his group demonstrated the combination of alkyl radical generation *via* electron-donating acceptor (EDA) photoactivation with cobalt-catalyzed dehydrogenation.[51] They used electron-rich radical precursors, such as 1,4-dihydropyridines, silicates, and trifluoroborates, along with tetrachlorophthalimides as EDA acceptor catalysts.

In all cases, the alkyl radicals add to the olefin, followed by β-hydrogen elimination via cobaloxime catalysis, producing the desired Heck product and a $[Co^{III}]$–H intermediate. For catalytic turnover, $[Co^{III}]$–H is initially converted to $[Co^{III}]$ through reaction with a proton or iminium salt intermediate. The electron-deficient $[Co^{III}]$ then undergoes single electron transfer (SET) reduction, regenerating $[Co^{II}]$ and the photocatalyst or EDA catalyst.

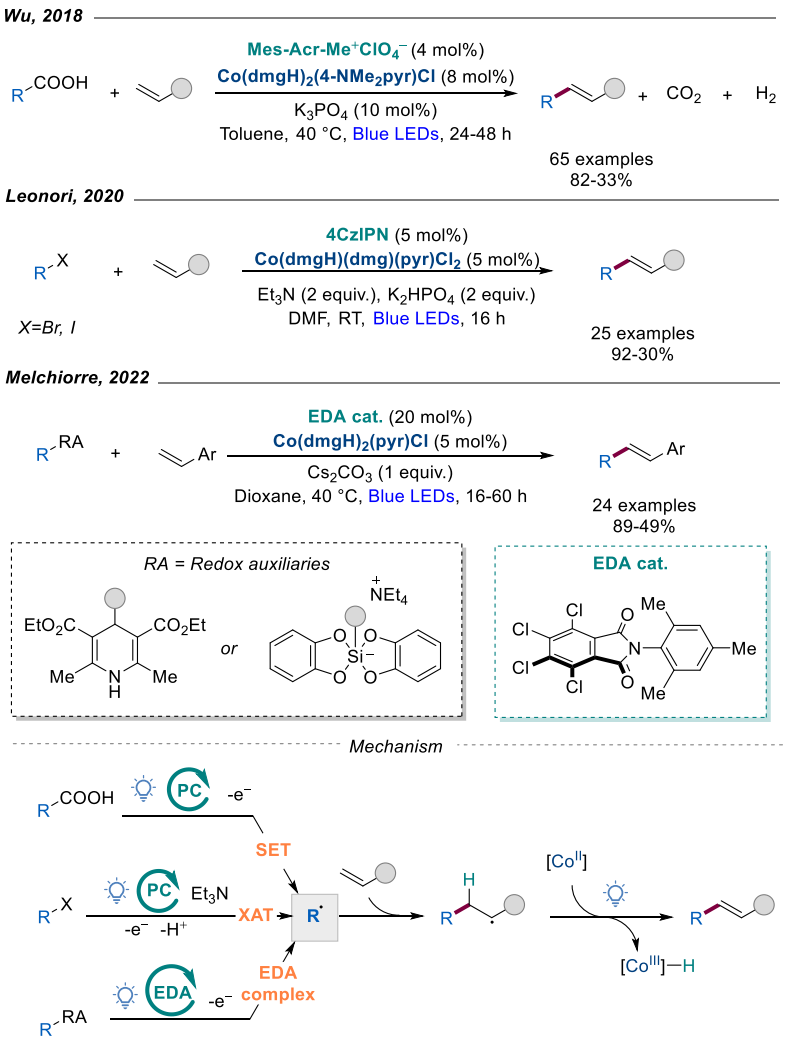

Scheme 1.5. Cobaloxime catalyzed radical-type alkyl Heck reaction.

1.2.3. Desaturation of aliphatic compounds

Olefination by desaturation process to transform saturated alkyl motifs from a diverse and easy access feedstock (e.g., non-/functionalized aliphatics) is a fundamental method in industrial application.[52] To initiate the reaction, the activation of C–H bonds can ideally enable *via* the generation of alkyl radicals by different methodologies (e.g., thermal condition, photoredox catalyst).[53] The ability of capturing these radicals through weak Co–C bonds, which can be easily cleaved under visible light irradiation to give the desired olefins, makes cobaloxime as a suitable catalysis for this method.

Nondirected desaturation

In 2015, the group of Sorensen developed a landmark approach for acceptorless dehydrogenation of alkanes to alkenes by merging a photoredox catalyst - tetrabutylammonium decatungstate and **Co(dmgH)$_2$(pyr)Cl** in one catalytic system for the first time (Scheme 1.6).[44b] Due to a challenging activation of C–H bonds though HAT

process by the tungsten photocatalyst as well as using near-UV irradiation, which are absorbed by many functional groups, the reaction scope was limited and resulted in modest yield. Nevertheless, this work still presents the big potential of conducting desaturation process under mild conditions with earth-abundant element in organic synthesis.

Indeed, the group of Huang further improved the nondirected desaturation of unactivated alkanes by using organophotoredox (2-chloroanthraquinone)/ *in-situ* generated cobaloxime dual catalysis (Scheme 1.6).[54] By changing to this electrophilic organophotoredox catalyst, the system not only activated C(sp^3)–H bonds more effectively but also can work under visible range, resulting in high functional group tolerance in the reaction scope.

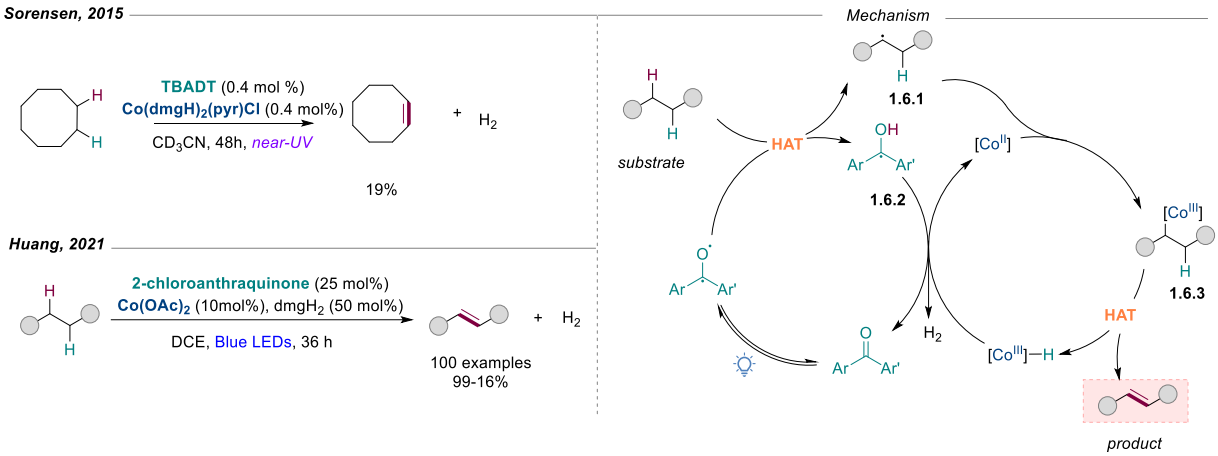

Scheme 1.6. Cobaloxime catalyzed the synthesis of olefins via nondirected desaturation of alkanes.

The reaction selectivity is governed by the strength and electronic properties of C(sp^3)–H bonds. For example, the catalytic system shows a very good reactivity and selectivity for the conversion of alkyl (hetero)arenes such as ethylbenzene to the corresponding styrenes. The detailed reaction mechanism is described in Scheme 1.6. The activation of C(sp^3)–H bonds in alkane was initiated though a HAT process with excited anthraquinone, resulting in ketyl radical (**1.6.2**) and alkyl radical (**1.6.1**). This alkyl radical intermediate (**1.6.1**) was captured by [Co^{II}] to generate [Co^{III}]–alkyl species (**1.6.3**), which under irradiation to facilitate another HAT process to yield desired olefin and [Co^{III}]–H species.

Dehydrofunctionalisation

Defunctionalization chemistry facilitates the transition from fossil-based to bio-based chemicals, promoting sustainability. By selectively removing functional groups and substituting them with alkenes, it streamlines the synthesis of bio-derived compounds from renewable feedstocks. This reduces reliance on finite fossil resources and minimizes

environmental impact. Through tailored catalysts and reaction conditions, defunctionalization enables the conversion of biomass into value-added chemicals while adhering to green chemistry principles.[55]

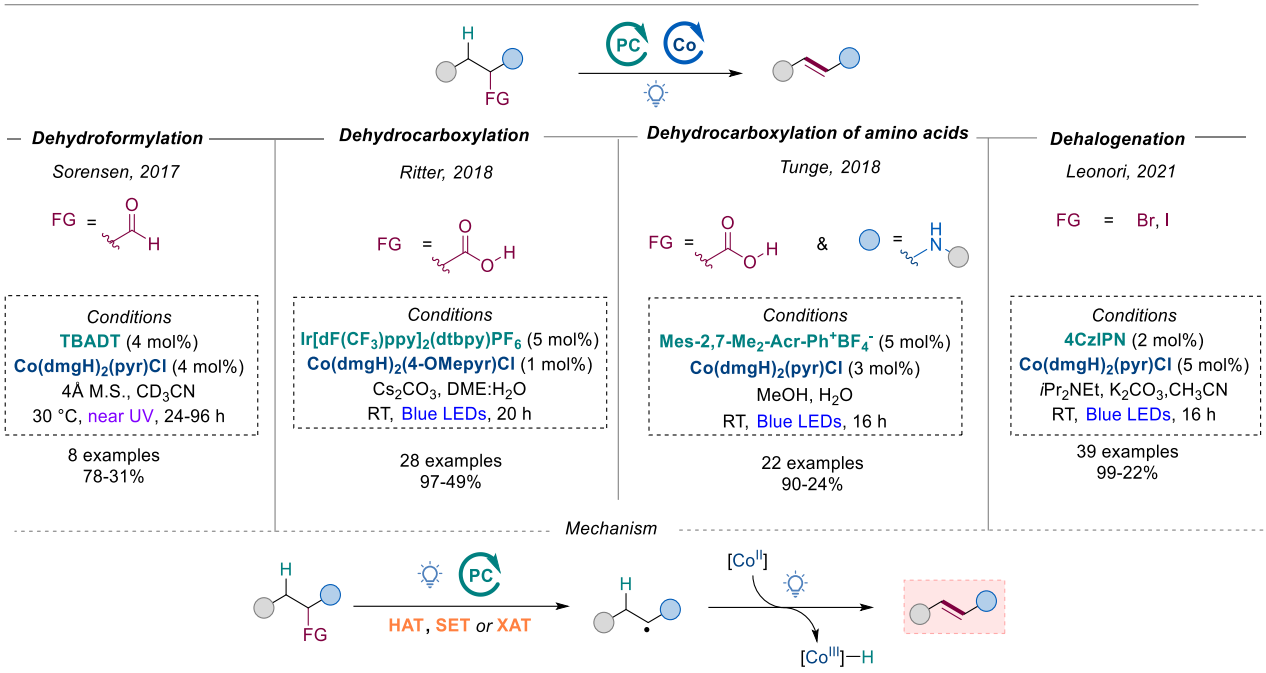

Scheme 1.7. Cobaloxime catalyzed dehydrofunctionalization enabled by the combination of photoredox catalysis.

By means of this photoredox/cobaloxime dual system, Sorensen and co-workers pioneered with a dehydroformylation method to form olefins from aldehydes.[56] Inspired by their previous work, the authors used the similar catalytic system to extend the reaction scope to α-quaternary aldehydes. The defunctionalization cycle begins with the deprotonation of aldehyde C–H bonds *via* a HAT mode to the excited state of tungsten catalyst. This process resulted in the formation of acyl radicals, which undergo decarbonylation to extrude CO and generate alkyl radicals. The key point of this transformation relies on the decarbonylative ability of acyl radicals, which belongs to the nature of α-position in the aldehydes. This explained the less tolerance of reaction scope when the non α-quaternary aldehydes were examined. Despite this limitation, the work still established a unique concept of a powerful transformation. In a related approach, the groups of Ritter and Tunge independently developed the decarboxylative olefination method of nature abundant carboxylic acids, using slightly different cobaloxime/photoredox system.[45, 57] Regardless of the redox potential of photosensitizer in each case, the photoredox catalysis still facilitated the oxidation of alkyl carboxylates though SET process to form carboxyl radicals, which followed by decarboxylation to produce CO_2 and alkyl radicals. This

strategy targets to generate more site-specific alkene regioisomer. In 2021, Leonori et al. reported a photochemical dehalogenative olefination of alkyl halides by using photoredox/cobaloxime system.[58] The radical generation from the alkyl halides is enable by XAT using α-amino radical that could be *in situ* generated using photocatalyst and simple organic base such as *i*Pr$_2$NEt. Notably, the authors have shown that the regioselectivity of products can be controlled by modulating suitable steric and electric properties of the cobalt catalysts.

Wu and Rueping utilized a photoredox/cobaloxime dual catalysis system for a defunctionalization reaction, synthesizing distally unsaturated ketones from alcohols (Scheme 1.8).[59] This process, applicable to both linear and cyclic alcohols, required electron-rich substituents (e.g., arenes) in α-position. The mechanism initiates with a SET from aryl substituents of alcohols to the excited state of the photoredox catalyst, generating cation radical species (**1.8.1**). These intermediates undergo intramolecular proton-coupled electron transfer (PCET) in the presence of base to yield alkoxyl radical species (**1.8.2**), which can cleave into alkyl radicals and carbonyl moieties (**1.8.3**) via β-scission of the neighboring C–C bond. The formed alkyl radicals subsequently take place the desaturation process via cobaloxime catalysis, resulting in the final product. This transformation, introducing keto and alkenyl groups simultaneously, holds significant potential for applications in organic and medicinal synthesis.

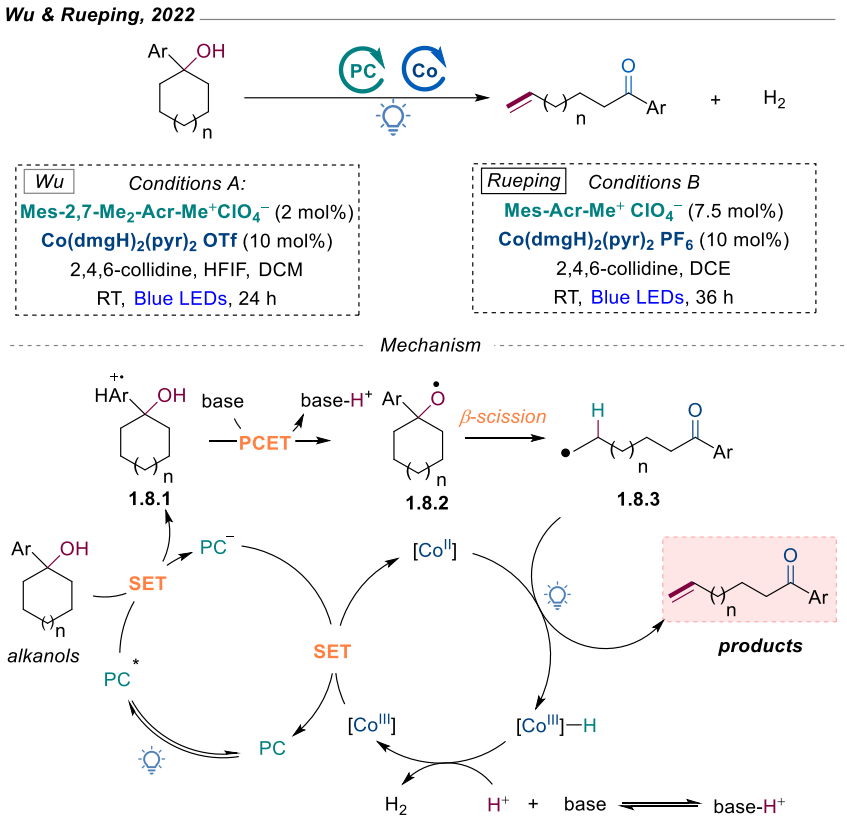

Scheme 1.8. Cobaloxime catalyzed the synthesis of distally unsaturated ketones via dehydrogenated alcohols.

1.2.4. Desaturation of aromatics

Recently, the Leonori group has developed several methodologies to convert aliphatic substrates into high-value aromatic compounds, utilizing dual catalytic systems that include cobaloxime catalysis for acceptorless dehydrogenation steps.[60]

In 2020, the group introduced a versatile and site-selective method for synthesizing anilines from cyclohexanes and ammonia, or primary and secondary amines (Scheme 1.9).[60a] This process begins with the condensation of the amine or ammonia with a cyclohexane derivative to form an enamine (**1.9.1**). The enamine is then oxidized by an iridium photocatalyst, generating an enaminium radical (**1.9.2**), which deprotonates to produce a β-enamine radical (**1.9.3**). This radical reacts with a [Co^{II}] metalloradical *via* hydrogen atom transfer (HAT), forming a di-enamine (**1.9.4**) and a [Co^{III}]–H species. A second round of oxidation and dehydrogenation, facilitated by the cobaloxime/photocatalyst system, leads to full aromatization, yielding the desired aniline derivatives. This reaction shows excellent tolerance to functional groups in various positions on the cyclohexanone ring and has been applied to the streamlined synthesis of numerous pharmaceuticals.

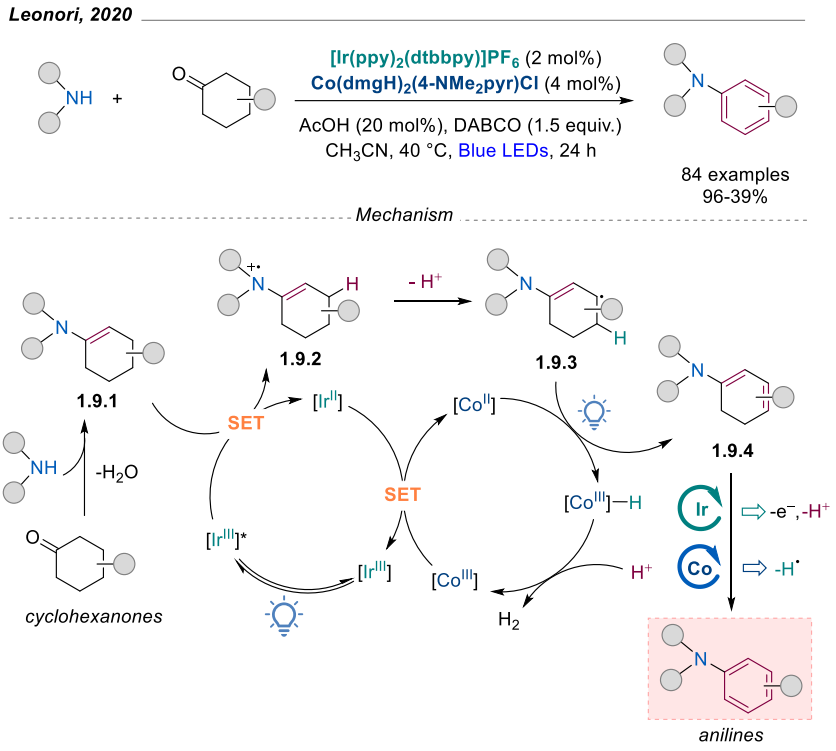

Scheme 1.9. Cobaloxime catalyzed the synthesis of anilines from amines and cyclohexanones

In 2021, Leonori and his colleagues introduced a method for producing a wide range of substituted aromatic aldehydes from cyclohexanecarbaldehydes (Scheme 1.10).[60b] This approach employs a triple catalytic system—an amine catalyst, a photocatalyst, and cobaloxime—to convert the starting materials into aromatic aldehydes with hydrogen gas as the only byproduct. In this process, morpholine reacts with the aldehyde to form an enamine, which undergoes two cycles of oxidation and deprotonation with an iridium photocatalyst, followed by desaturation with cobaloxime. Hydrolysis then yields the desired aldehydes.

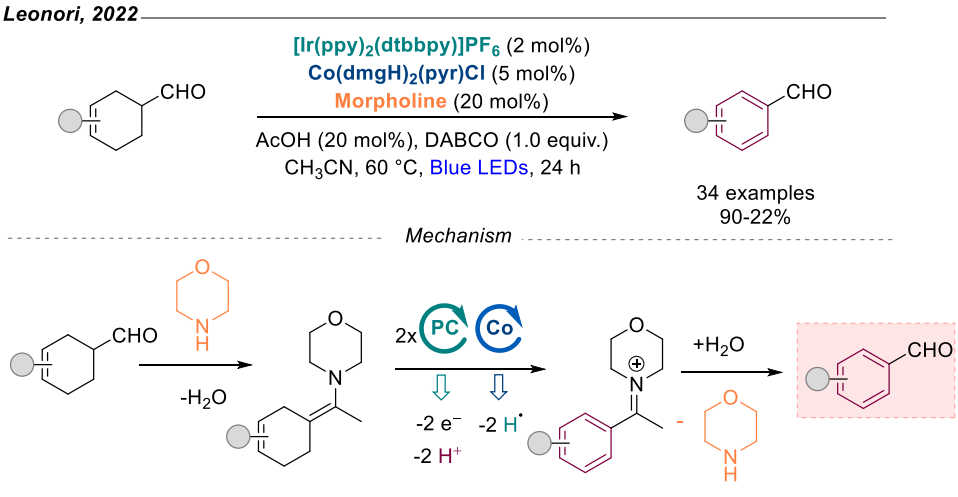

Scheme 1.10. Cobaloxime catalyzed dehydrogenative of aldehydes.

Most recently, the group have developed a method for fully aromatizing cyclohexanones into phenols (Scheme 1.11).[60c] This innovative approach leverages the synergistic action of photocatalytic HAT and cobalt catalysis, sequentially removing four hydrogen atoms from the saturated precursors. To optimize the HAT process, they first convert cyclohexenes into enol ethers or introduce electron-withdrawing groups (e.g., acetyl, ester) at the α-position to favor the enol tautomer over the ketone form. The catalysis begins with HAT, transferring hydrogen from the substrate to the excited triplet state of the HAT catalyst, forming an allylic radical (**1.11.1**) and a ketyl radical (**1.11.2**). The allylic radical undergoes desaturation with [Co^{II}] species, forming a diene (**1.11.3**), which then experiences further HAT and desaturation to produce phenol derivatives.

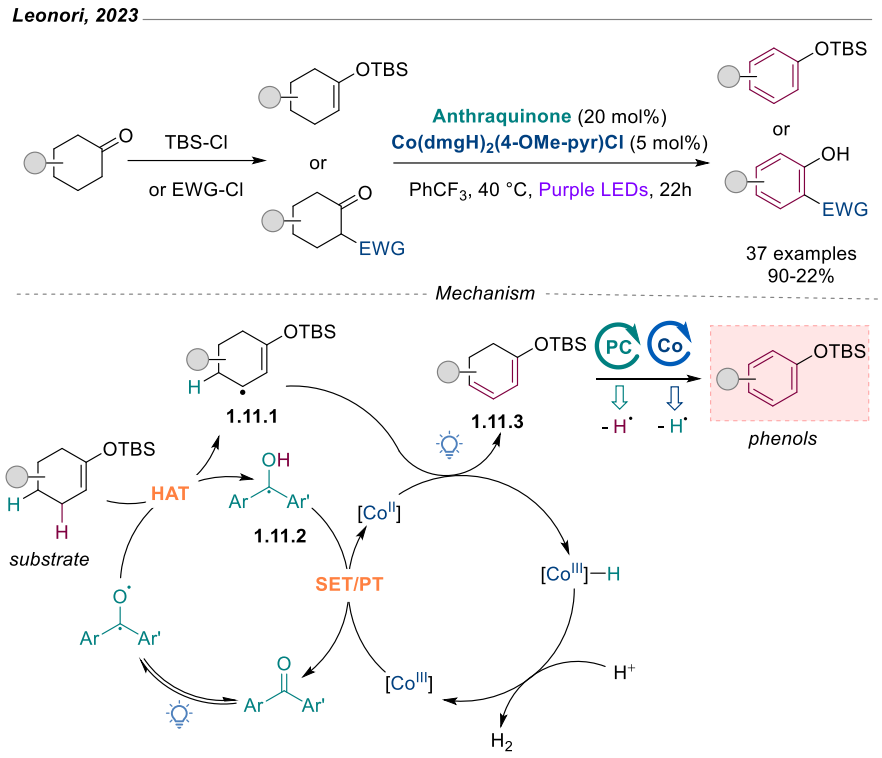

Scheme 1.11. Cobaloxime catalyzed the synthesis of phenols via desaturation of cyclohexanones

1.2.5. Asymmetric catalysis

The first application of cobaloxime in asymmetric synthesis was demonstrated by Luo and Wu in 2017.[61] A triple enamine/photoredox/cobaloxime catalysis was used for the asymmetric CDC of tetrahydroisoquinolines with carbonyl compounds. In 2022, the same group introduced another novel 3-in-1 catalysis system when performing asymmetric C–H dehydrogenative allylic alkylation (Scheme 1.12).[62] The reaction couples β-ketocarbonyls to olefins in a good yield and high enantioselectivities. The reaction also shows a high tolerance to β-ketocarbonyls, ranging from cyclic to aliphatic ketoesters, diketone or

ketoamides. However, the olefin component would be tricky as it tolerates only 2-aryl-1-propenes bearing various para- and meta-substituents. Finally, the group showed excellent application of the method in late-stage allylation as examining with complexed substrates bearing multichiral centers resulted in high yield and good diastereoselectivity. The reaction starts with chiral enamine (**1.12.1**) formation upon the condensation between chiral organocatalyst and the β-ketocarbonyl substrate. The photoredox catalyst oxidizes the chiral enamine (**1.12.1**) to α-imino radical intermediate which can be trapped by the [Co^{II}] metalloradical to form the radical-radical complex (**1.12.2**). Subsequent radical addition to alkene gave the complex (**1.12.3**), followed by β-hydrogen elimination under visible light irradiation afford the imine intermediate (**1.12.4**). Finally, the hydrolysis led to the allylation product and regeneration of the organocatalyst.

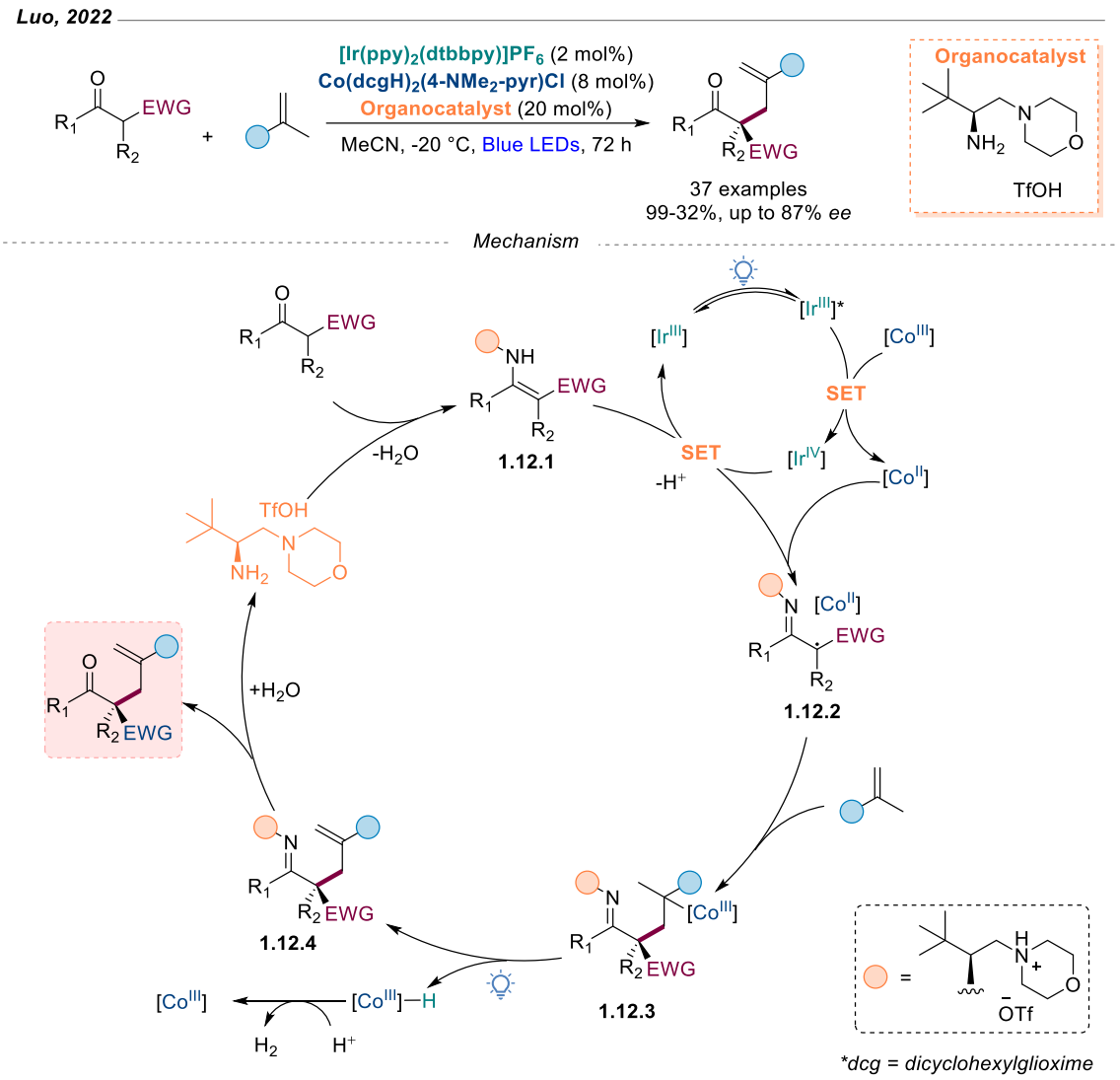

Scheme 1.12. Cobaloxime in asymmetric catalysis.

1.3. Spectroscopy – a mechanistic tool for open-shell transformations

Since unpaired electrons generate a magnetic moment, open-shell species exhibit paramagnetism, meaning they can be attracted to a magnetic field. This property makes open-shell electronic structures prevalent in spectroscopy. Among various spectroscopic techniques, *electron paramagnetic resonance* (EPR) and *UV-vis* spectroscopy are particularly effective for studying these species.

EPR spectroscopy

EPR spectroscopy is a powerful tool to elucidate the nature and role of open-shell species for catalytic processes.[63] The reason EPR is so useful is that it probes the magnetic properties of paramagnetic species, which are closely related to their geometric and electronic structures.[3] These properties influence their reactivity and offer valuable information for understanding reaction mechanisms. By identifying paramagnetic species, EPR can confirm radical-based reaction mechanisms or provide insights into transition metal ion oxidation states, coordination geometry, and ligand fields. Furthermore, these findings can be correlated with reaction conditions and catalytic performance.

The paramagnetism of a transition metal ion depends on the number of unpaired electrons, which varies based on its oxidation state, coordination geometry, and ligand field.[3] EPR can be used to analyze samples in both liquid and solid states, across a broad range of temperature and pressure conditions. However, some transition metal ions, like Co^{II}, exhibit short relaxation times after a spin-flip at room temperature, making their EPR signals detectable only at cryogenic temperatures. In such cases, freeze quenching is often employed as a *quasi-in situ* method. This technique rapidly freezes the sample at cryogenic temperatures, stabilizing otherwise short-lived species for analysis.

Short-lived radicals can also be captured for EPR analysis using spin traps, which react with radicals to form more stable radical adducts.[64] This allows the concentration of radicals, such as •OH or •OOH, to build up to detectable levels, providing insights into their formation as reaction intermediates or byproducts.[65]

Useful information that can be obtained by EPR in catalytic systems includes identifying and quantifying paramagnetic species, as well as determining electronic and geometric structure.

Identifying paramagnetic species:

The nature of free radicals, whether organic or metal-based, can be determined by their g-value in EPR.[66] Additionally, hyperfine splitting (or coupling) constants offer critical information about the identity of the trapped radical in spin trapping experiments. The line width and shape of the spectrum provide further details about the trapped radical's molecular size, intermolecular interactions (such as hydrogen bonding), revealing information on local molecular dynamics and rotation.

Free radicals can be directly detected via EPR spectroscopy. However, for highly transient radicals in aqueous solutions, indirect detection is possible using diamagnetic or paramagnetic probes to stabilize or probe the radicals. Nitrone and hydroxylamine are commonly used as spin trapping reagents, as their EPR spectra change in the presence of radicals, allowing researchers to study radical formation kinetics and the nature of the radicals themselves.

Quantifying paramagnetic species:

The area under an EPR absorption peak correlates with the number of paramagnetic species in a sample.[67] Signal intensity is influenced by both the physical properties of the species (e.g., spin state, relaxation times) and experimental factors (e.g., microwave power, temperature). Accurate quantification requires calibration with a standard sample of known concentration and electron spin count under similar conditions.

Electronic and geometric structure:

The magnetic parameters (g and hyperfine values) measured in EPR are highly sensitive to the electronic structure and the surrounding environment of paramagnetic species. These values can be compared with known systems from the literature, or analyzed using theoretical models like crystal field theory, which predicts how g-values change in response to variations in the electronic structure, such as geometric distortions in the coordination environment of transition metal ions.[68]

UV-vis spectroscopy

UV-vis spectroscopy measures the absorbance or transmittance of light in the ultraviolet (UV) and visible (vis) regions of the electromagnetic spectrum.[69] The principle of the technique is the interaction of light with matter, specifically how molecules absorb energy at different wavelengths, and a spectrum showing absorbance as a function of wavelength is shown.

By measuring the characteristic absorption wavelengths, UV-vis spectroscopy can provide the information about electronic transitions, the concentration of the compound or kinetics of reactions.[70] Specifically, when UV or visible light passes through a sample, certain wavelengths are absorbed, corresponding to the energy needed to excite electrons from lower energy orbitals to higher energy orbitals. The absorbance at a specific wavelength is directly proportional to the concentration of the absorbing species in the sample.[71] Therefore, one of the major applications of UV-vis spectroscopy is in quantitative analysis. This technique is also valuable in studying the kinetics of chemical reactions, as changes in absorbance over time can be monitored to track the progress of reactions in real-time.

UV-vis spectroscopy is a useful tool to monitor the transformation of transition metal complexes. In these species, the technique provides valuable insights into the electronic structure of the metal ion and its surrounding ligands, primarily through two types of transitions: *d-d transitions* and *charge transfer transitions*.[72] The nature and geometry of the complex significantly affect these transitions, leading to characteristic absorption bands in the UV-vis spectrum.

In d-d transitions, where an electron is excited from a lower-energy d-orbital to a higher-energy one, the energy difference between these orbitals corresponds to the energy of light in the UV-vis region that can be absorbed. According to crystal field theory, when a metal ion is surrounded by ligands, the degeneracy of the d-orbitals is broken due to the electrostatic interactions between the ligands and the metal ion. The gap between these energy levels is called crystal field splitting energy. The extent and pattern of this crystal field splitting depend on several factors, including the geometry of the complex (such as octahedral, tetrahedral, or square planar), the oxidation state of the metal ion, and the nature of the ligands involved. These transitions are usually weak in the UV-vis spectrum.

Beyond d-d transitions, the second type of absorption in the UV-vis spectrum of transition metal complexes is charge transfer transitions. These transitions occur when there is a movement of electronic charge between the metal ion and the ligands. Based on ligand field theory, charge transfer transitions can be categorized into two types: metal-to-ligand charge transfer (MLCT) or ligand-to-metal charge transfer (LMCT). Both MLCT and LMCT transitions tend to be intense compared to d-d transitions because they are not symmetry forbidden. These transitions often result in strong absorption bands in the UV-vis spectrum and can sometimes overshadow weaker d-d transitions. The energy and

intensity of charge transfer transitions are highly dependent on the oxidation state of the metal, the electronic structure of the ligands, and the overall coordination environment.

1.4. Motivation and outline of research

The motivation behind this dissertation arises from the growing demand for sustainable and efficient chemical processes in modern organic synthesis. Traditional methods often rely on expensive, rare, or toxic metals, alongside harsh reaction conditions, limiting their applicability in green chemistry. Cobalt, an earth-abundant and cost-effective metal, has shown promise in catalysis, particularly in facilitating radical-type reactions with open-shell species. However, the understanding of cobalt's mechanistic role in these reactions remains limited, and there is significant potential to explore and expand its applications in organic transformations.

This research aims to bridge that gap by exploring cobalt-catalyzed open-shell transformations. By employing advanced spectroscopic techniques along with computational analysis, the dissertation delves into the mechanistic pathways of several reactions, uncovering the role of cobalt in facilitating key steps. The outline of the research is as follows:

In **chapter 2**, an investigation into the remote desaturation of aliphatic amides and imides catalyzed by cobaloxime will be described. Cobaloxime was used as a single catalyst to enable the synthesis of valuable cyclic and acyclic enamides and enimides from abundant chemicals. DFT analysis, EPR and UV-vis studies rationalized the discovered reactivity of the cobalt catalyst for the photochemical $C(sp^3)$–H activation reaction.

In **chapter 3**, the role of cobaloxime in intramolecular *endo*-selective Heck reactions will be examined by using different experimental and theoretical tools. Rapid scan EPR experiments and DFT calculations suggests a concerted β-hydrogen elimination event to take place in the triplet state. The reaction leads to the formation of seven- and eight-membered siloxycycles in excellent yields.

In **chapter 4**, a detailed study of the cobalt-catalyzed dehydroamination of primary amines will be investigated. The synergistic effect of dual cobaloxime/ photoredox catalysis promoted conversion of various primary amines into their respective alkenes with selectivity for the *trans*-configured isomers. By combining different spectroscopic measurements (fluorescence, EPR) and computational studies, the mechanistic pathway was revealed.

Chapter 5 will deal with remote functionalization and γ, δ- desaturation of aliphatic alcohols using metal-hydride catalysis. This strategy enables the selective modification of alcohols at the γ position, a site typically challenging to functionalize. The method demonstrates broad versatility, facilitating a range of transformations including halogenation, amination, cyanation, azidation, and desaturation, all with excellent selectivity. Mechanistic insights were gained through spectroscopic experiments, which confirmed the formation of carbon-centered radicals as key intermediates in the reaction pathway.

Chapter 2: Cobaloxime-catalyzed remote desaturation of aliphatic amides and imides

2.1. Backgrounds

Enamines, enamides, and enimides are among the most common functional groups found in pharmaceutical and agrochemical industries.[73] Specifically, enamines are highly reactive nucleophiles that facilitate carbon–carbon bond formation, making them valuable in synthetic strategies for pharmaceuticals and agrochemicals.[74] On the other hand, enamides are key building blocks in drug discovery, enabling the development of bioactive compounds with enhanced stability and selectivity.[75] Meanwhile, enimides play an important role in polymer and material science due to their unique reactivity and structural properties. The ability to synthesize these compounds opens pathways to the efficient creation of complex molecules in both medicinal chemistry and industrial applications. Some examples of pharmaceutically attractive natural products such as antibiotics or the antitumor macrolides or important building blocks in synthesis of complex structure are presented in Figure 2.1 below.[76]

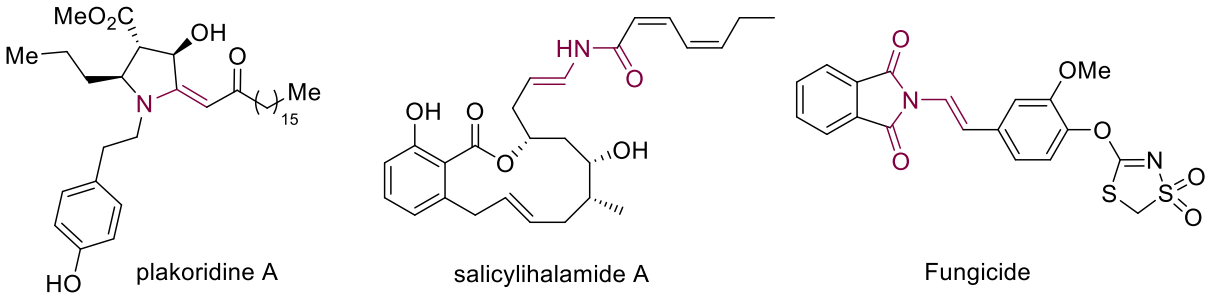

Figure 2.1. Selected examples of naturally occurring enamine, enamide and enimide.

To synthesize these important motifs, various methods have been established.[77] Conventional approaches for enamide synthesis include isomerizing allylamides,[78] condensing amides with carbonyl compounds,[79] olefination or dehydration of imides,[80] N-alkenylation of amides,[81] and using ynamides[82] or alkynes[83], as well as through Curtius rearrangements[84] or rearrangement-hydrolysis[85]. However, these strategies often require pre-functionalized substrates and generate equivalent amounts of waste byproducts. Additionally, while many of these methods are complementary, they frequently struggle with poor control over the *E/Z* stereoisomer ratio.

To alternate these methods, an ideal approach to prepare enamides and enimides would be direct and selective dehydrogenation or desaturation of aliphatic amides and imides at room temperature. In general, the design and development strategy to activate C(sp^3)–H bonds to C(sp^2)–H bonds remain a central challenge for synthetic chemists. To acquire this achievement, several groups have independently developed a few innovative approaches (Figure 2.2).

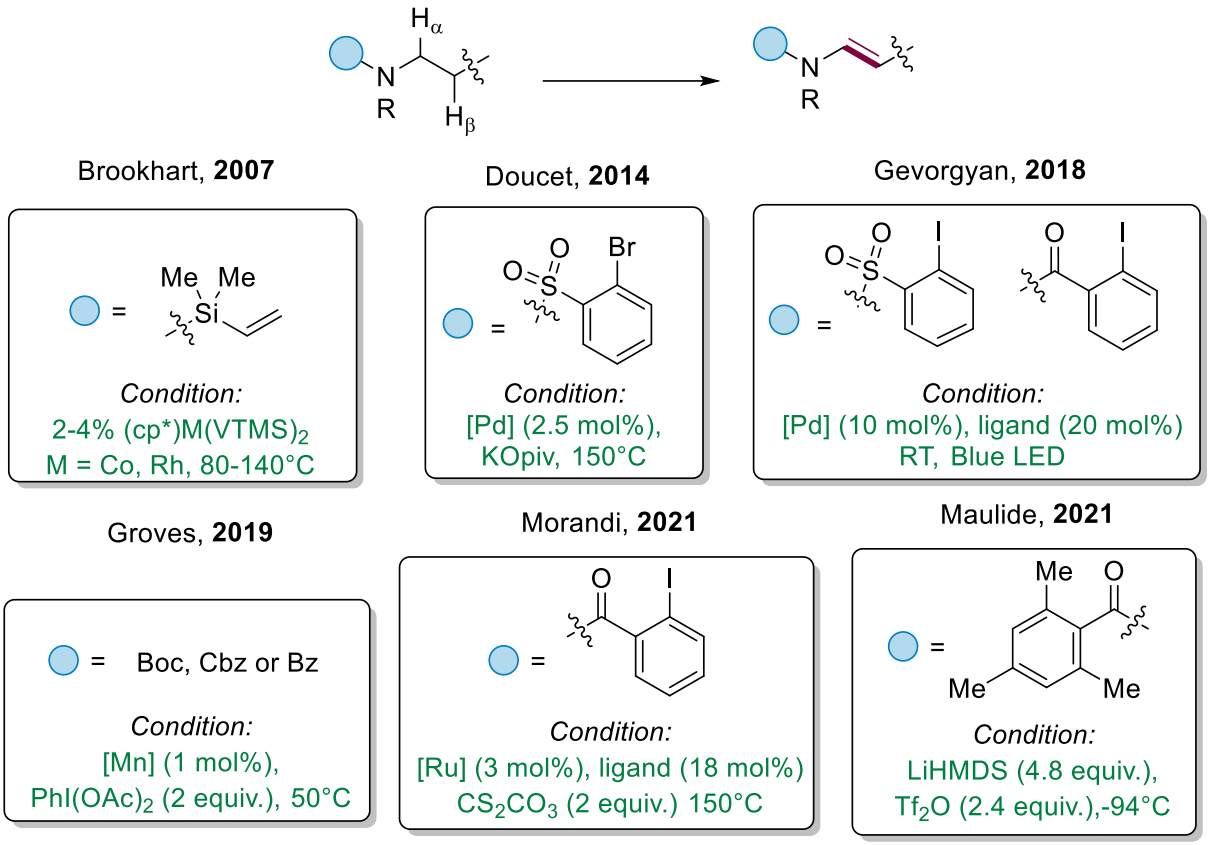

Figure 2.2. State-of-the-art of desaturation amines, amides to form enamines, enamides

Most methods for desaturation share a common approach of using directing groups to specifically target the Hα and Hβ positions of amines. These directing groups help guide the reaction, making it easier to desaturate the molecule by bypassing the challenging activation of C(sp^3)–H bonds. This strategy simplifies the process and improves efficiency in transforming amines. In details, Brookhart et al. introduced silyl tethers to nitrogen atom of cyclic amines, which acted both as directing groups and hydrogen acceptors, enabling desaturation through transfer hydrogenation.[86] Later, Doucet and Gevorgyan utilized halogenated aryl auxiliary in combination with noble Pd catalysis to promote amine desaturation via β-hydrogen elimination process.[87] However, their strategies differed: Doucet's approach relied on C–H activation through metallation–deprotonation event,

while Gevorgyan developed a radical-based system via internal hydrogen atom transfer (i-HAT) process. When using first-row metals like Mn along with a stochiometric amount of oxidant, the group of Groves presented a simple desaturation protocol with tolerance of air and moisture.[88] Recently, Maulide et al. introduced a novel direct dehydrogenation of amides using an unusual combination of lithiated organosilicon compound (LiHMDS) and triflic anhydride at cryogenic temperatures.[89] However, these methods suffer from several drawbacks including the use of highly sensitive substrates, large amount of noble metal and expensive ligands, the regioselectivity issues as well as the need of harsh temperature conditions.

Alternatively, the desaturation of fatty acid in nature can be transformed selectively under mild condition through the utilization of enzymes called desaturases.[90] The structure of these enzymes contain high valent di-iron as active sites.[91] These 3d-transition metals prefer to engage in single electron transfer (SET) processes than two-electron transfer events that popular in noble metal.[92] Inspired by these lessons, a goal of using non-enzymatic base-metal catalysis system for the desaturation of aliphatic chains under room temperature become feasible. Indeed, there was a report of using cyanocobalamin (vitamin B_{12}) to convert alkyl electrophiles to olefins under mild condition (Figure 2.3).[93]

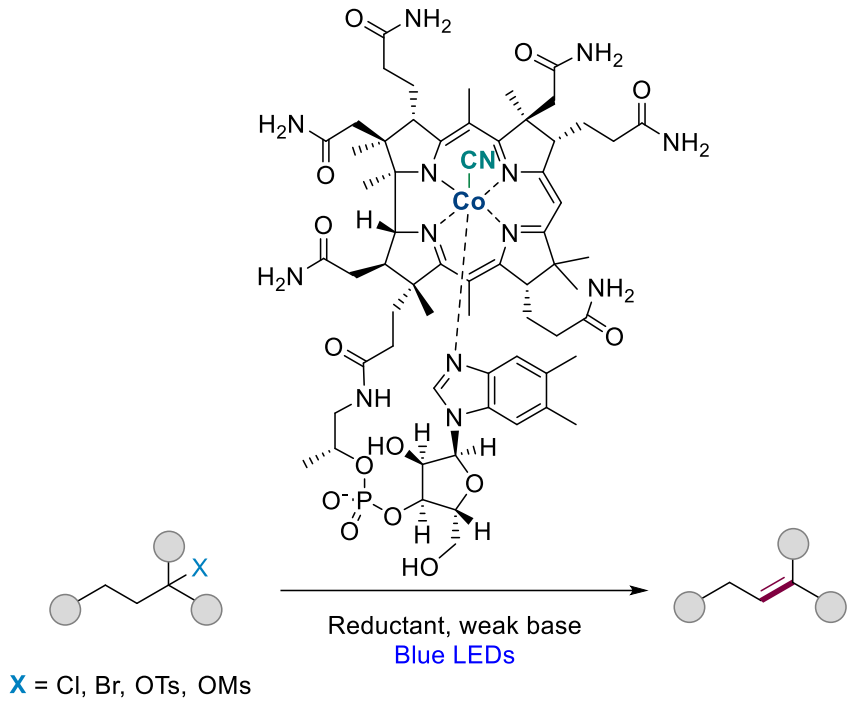

Figure 2.3. Desaturation of aliphatic chains by vitamin B_{12}.

The driving force of this transformation relies on the ability to cleave Co–C bonds by light to generate alkyl radical and Co^{II} metalloradical, which can abstract a hydrogen atom from

the position adjacent the carbon-centered radical to afford a terminal olefin. Based on this property, cobaloxime could be a suitable candidate to catalyze the selective desaturation step of aliphatic amines.

As the common approach to prepare enamides and enimides through direct desaturation process, an auxiliary at the nitrogen atom should be utilized to control the selectivity towards α, β- desaturation. Inspired by that, our strategy involves the installation of a commercially available benzoyl tether at the nitrogen atom of the aliphatic amine or the amide to form amide or imide, respectively (Scheme 2.1).

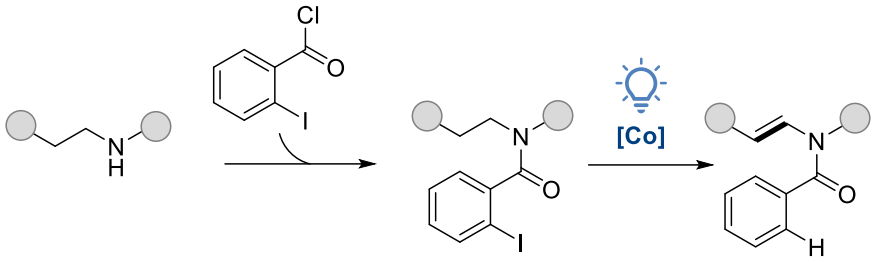

Scheme 2.1. Reaction design of desaturation of amides/imides by cobaloxime.

2.2. Screening of the reaction conditions

In this section, Dr. Chenyang Wang conducted a screening of reaction conditions for the desaturation of amides using **Co-1** (5 mol%) as the catalyst and i-Pr_2NEt as the base in CH_3CN. Morpholine, protected with commercially available o-iodobenzoyl chloride tether **1.1a**, was selected as the model substrate for developing the reaction. The results are shown in Table 2.1.

Table 2.1. Screening of the reaction conditions for the remote desaturation of amide 1.1a

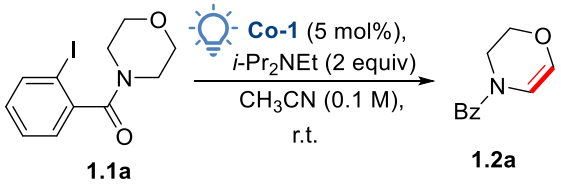

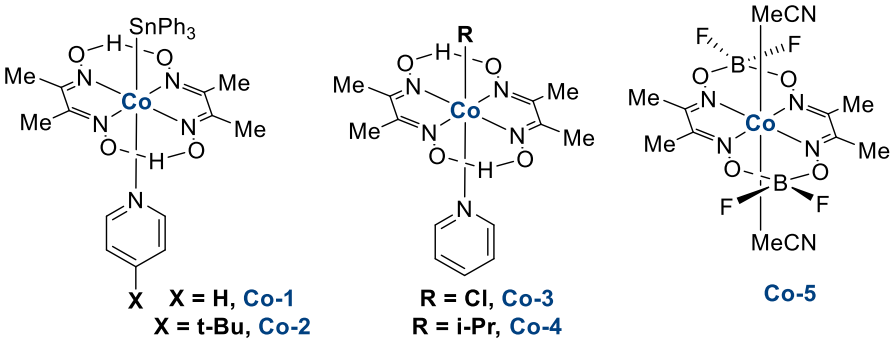

Entry	Deviations from the standard conditions	Yield (%)
1	None	99
2	No **Co-1** or no light	n.d.
3	70 ºC instead of light	Trace
4	**Co-2** instead of **Co-1**	99
5	**Co-3** and 4CzIPN (2 mol%)	n.d.
6	**Co-5** and 4CzIPN (2 mol%)	n.d.
7	**Co-4** instead of **Co-1**	n.d.
8	1 equiv. K_2CO_3 as base	59
9	1 equiv. K_2CO_3, 0.2 equiv. *i*-Pr_2NEt as base	99
10	DMAP as base	13
11	DABCO as base	29
12	DBU as base	Trace
13	No base, **Co-1** (50 mol%)	37
14	TEMPO was added	n.d.
15	o-bromobenzoyl as tether	95
16	o-chlorobenzoyl as tether	n.d.

Under these mild conditions, **1.1a** was successfully converted to **1.2a** with a 99% yield (entry 1), demonstrating the potential of combining 3d-metal catalysis with photochemistry in Co-catalyzed transformations. Control experiments showed no reactivity without the cobalt catalyst or in the absence of light (entries 2, 3). Notably, only trace amounts of **1.2a** were formed under thermal conditions, highlighting the importance of visible light irradiation. Using a pyridine-substituted **Co-2** catalyst with an electron-donating group produced similar results to the **Co-1** complex (entry 4).

Next, the catalytic activity of the **Co-3**/photoredox system, previously reported by Leonori for E2 eliminations of aliphatic alkyl halides, was tested.[58] Surprisingly, no desired product was formed (entry 5). Additionally, combining the photoredox catalyst 4CzIPN

with the Co^{II} catalyst **Co-5** showed no catalytic activity (entry 6), and **Co-4**, which contains an *i*-Pr ligand, also displayed no activity (entry 7). Various bases were then explored (entries 8-12). Using 1 equivalent of K_2CO_3 as a base resulted in a lower yield of 56%, but full reactivity was restored with the addition of catalytic amounts of *i*-Pr_2NEt. Bases such as DMAP, DABCO, and DBU significantly reduced the yield. When 50 mol% of **Co-1** was used without a base, the yield of **1.2a** dropped to 37% (entry 13). Moreover, adding the radical scavenger TEMPO completely suppressed product formation (entry 14).

Finally, different halogen-substituted benzoyl tethers were examined (entries 15, 16). The bromide-substituted tether gave results similar to the iodide analogue, while the chloride derivative was inactive under the tested conditions.

2.3. Scope for desaturation of aliphatic amides and imides

In this section, the work of Dr. Chenyang Wang showed a versatile approach of the method for different amides (Scheme 2.2). Cyclic amide derivatives with five, six, and seven-membered rings reacted efficiently, yielding the corresponding enamides in high to excellent yields (**1.2a-1.2l**). Specifically, unsubstituted piperidine **1.1b**, piperidines with an unprotected hydroxyl group **1.1c**, a 4-methyl substituent **1.1d**, and a sensitive spiro acetal group **1.1e** were well-tolerated, producing cyclic enamides with yields up to 96%. Similarly, substrate **1.1f** with double piperidine groups gave a double dehydrogenated product in 93% yield. Various unsymmetrical piperidine derivatives also reacted effectively, though they formed regioisomers (**1.2g**-**1.2i**). Notably, piperazine **1.1j**, with two amide groups, underwent double desaturation, yielding **1.2j** in 75%. Desaturation of proline ester **1.1k** produced **1.2k** with high regioselectivity (>20:1), while palladium-catalyzed reactions with amide **1.1k** yielded a 4:1 mixture of isomers. Unlike previous methods, increasing the ring size did not reduce substrate reactivity. Protected azepane and azocane underwent selective desaturation to form cyclic enamides **1.2l** and **1.2m**. These findings offer an efficient route to synthesize endocyclic enamides that are challenging to produce by traditional methods.

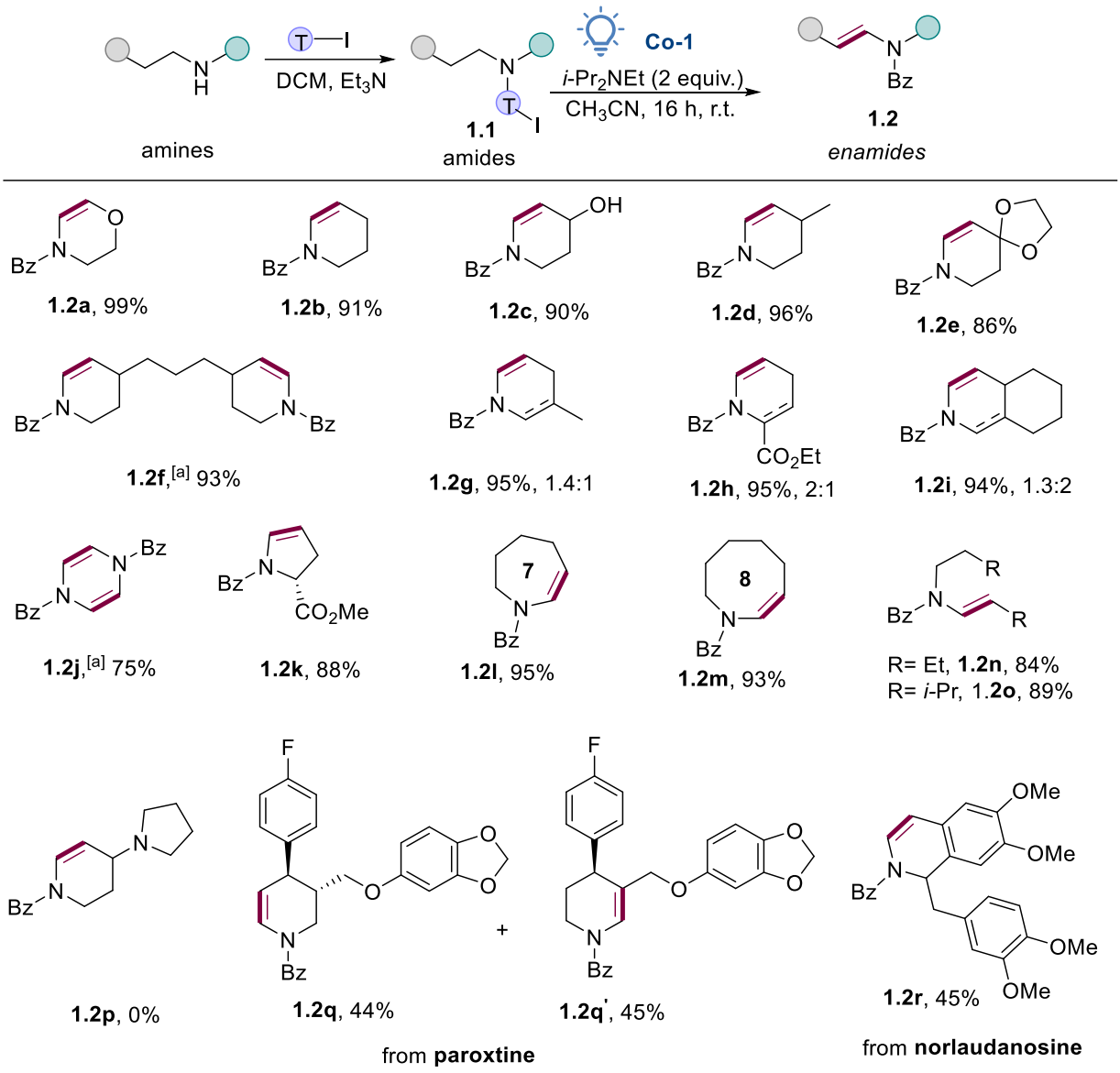

*Scheme 2.2. Desaturation of amides. Reaction conditions: substrate **1.1** (0.2 mmol), **Co-1** (0.01 mmol, 7.2 mg), i-Pr$_2$NEt (0.4 mmol, 70 µL), CH$_3$CN (2 mL), RT, Blue LED (10W, Ledxon), 16 h, isolated yields. [a] **Co-1** (0.02 mmol, 14.4 mg), i-Pr$_2$NEt (0.8 mmol, 140 µL).*

This photoexcited cobalt catalysis worked effectively for linear amides **1.1n** and **1.1o**, resulting in exclusively E-selectivity with very good yields. It is worth mentioning that substrates capable of forming α-aminoalkyl radicals, such as **1.1p**, were incompatible with this method. Next, we focused on applying our approach to the late-stage functionalization of commercially available drugs and natural products. The antidepressant drug paroxetine was desaturated, yielding two isolable enamides **1.2q** and **1.2q'** in 44% and 45% yields, respectively. Additionally, the benzoyl derivative of norlaudanosine **1.1r**, a dopamine metabolite, was desaturated to produce the corresponding enamide **1.2r** in moderate yield.

Following the successful development of this process, we decided to examine the more challenging imides using a modified catalytic system with catalytic amounts of organic

base and K_2CO_3. Notably, different aliphatic acetimides **1.3a-1.3i** were found to be amendable to this method and led to the formation of the corresponding enimides **1.4** in good to excellent yields (Scheme 2.3). Gratifyingly, we found that this photoexcited base metal catalytic system is also applicable to cyclic imides such as *δ*-valerolactam **1.3j**, leading to selective desaturation at an unusual reaction site.

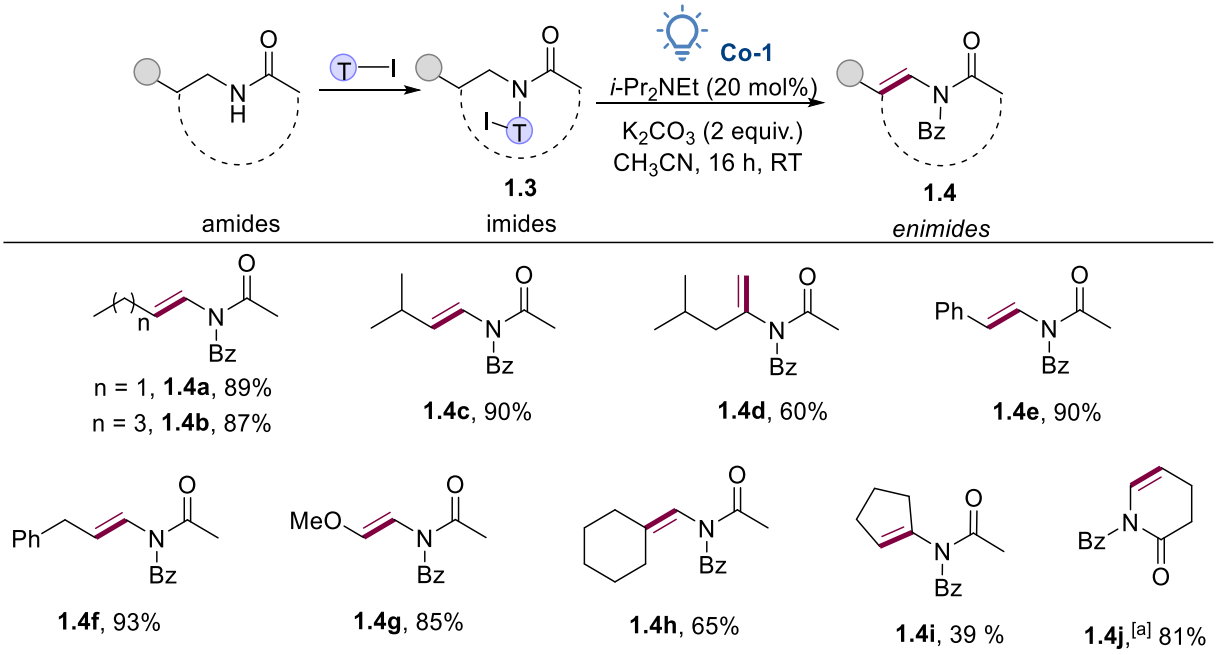

*Scheme 2.3. Desaturation of imides. Reaction conditions: substrate **1.3** (0.2 mmol), **Co-1** (0.02 mmol, 14.4 mg), i-Pr₂NEt (0.04 mmol, 7 µL), K_2CO_3 (55 mg, 0.4 mmol), CH_3CN (2 mL), RT, 16 h, Blue LED (Ledxon), isolated yields. [a] **Co-1** (0.01 mmol, 7.2 mg), i-Pr₂NEt (0.4 mmol, 70 µL).*

2.4. Mechanistic insights

2.4.1. Quantum yield and light on/off experiment

To determine the quantum yield, the initial rate of the product formation was required and thus, the reaction profile was examined. In this experiment, the reaction was conducted in standard conditions and the product formation of the desaturation of amide **1.1a** was monitored by calibrated GC using n-dodecane as internal standard. A 30-minute-interval was set to sample out for the first two hours. The results were shown in the Table 2.2 below.

*Table 2.2. Reaction profile of the desaturation amide **1.1a**.*

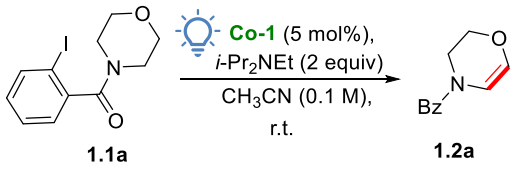

Time (second)	0	1800	3600	5400	7200	10800
Product (mmol)	0	0.016	0.033	0.040	0.049	0.062
Yield (%)	0	16.06	32.68	40.03	48.80	61.52

According to the table, the reaction profile was plotted in Figure 2.4.A. Based on this profile, the initial rate of the desaturation reaction of amide can be determined in the first hour. The reaction steadily proceeded for the following 2 hours and the amide **1.1a** was mostly converted after 6 hours.

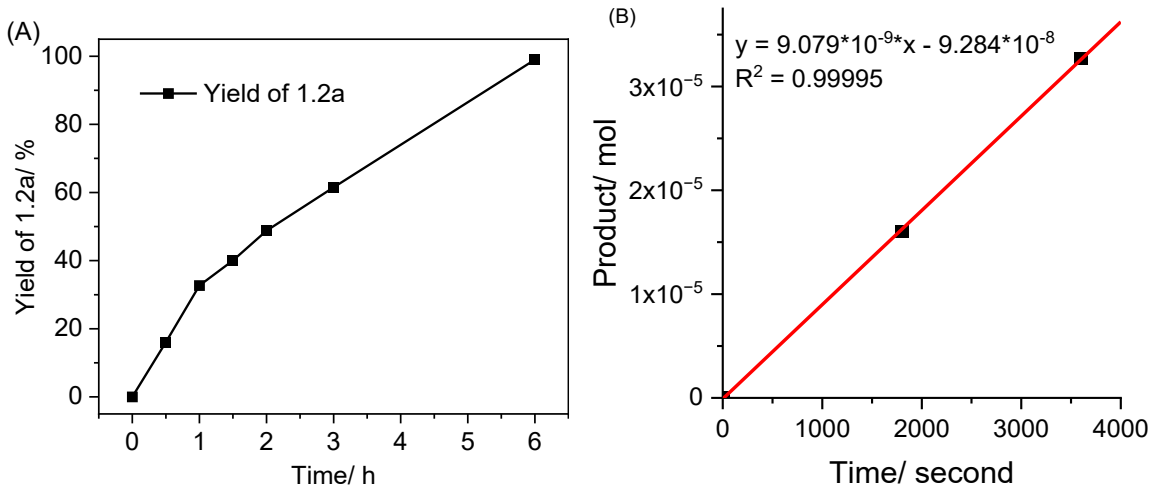

*Figure 2.4. **A**: Reaction monitoring by calibrated GC using n-dodecane as internal standard for desaturation amide 1.1a; **B**: Initial rate determination.*

By plotting the product formation against the time domain, the initial rate of the desaturation of the amide **1.1a** was determined by the slope of the linear fit (Figure 2.4.B). The fitting parameter was analyzed by Origin, which determining the initial rate of the reaction to be 9.079×10^{-9} mol/s.

By utilizing ferrioxalate solution as a standard actinometry, the photon flux of the blue LEDs setup was determined as 6.093×10^{-7} mol/s (see Appendix for more details). Thus, the quantum yield of the photoexcited cobalt for the desaturation reaction can be obtained by:

$$\phi = \frac{n_{product/s}}{photons/s} = \frac{9.079 \times 10^{-9}\ mol/s}{6.093 \times 10^{-7}\ mol/s} = 0.015$$

With the calculation of quantum yield of the reaction < 1, it can be demonstrated that the efficient radical chain propagations are not operating under these reaction conditions.

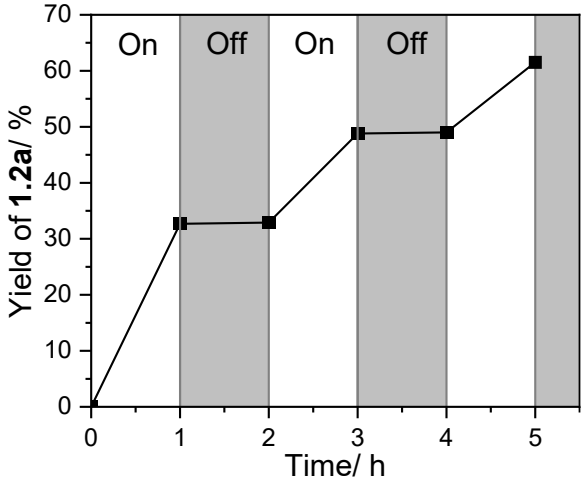

Figure 2.5. Light on-off experiment.

Additionally, the light on-off experiment was also carried out (Figure 2.5). The similar procedure was conducted as the reaction profile, with interruptions of 1-hour-interval to keep the mixture in the dark during 5 hours of irradiation. The result showed that the enamide **1.2a** was only formed in the presence of light. Meanwhile, during the light off-cycles, no reaction was observed. Therefore, together with the quantum yield, the possibility of a radical chain process can be excluded.

2.4.2. In situ UV-vis spectroscopy

In order to shed more light into the mechanism, we have performed preliminary experimental mechanistic studies. UV-Vis studies were performed to understand electronic properties of cobaloxime as well as the reaction system (Figure 2.6).

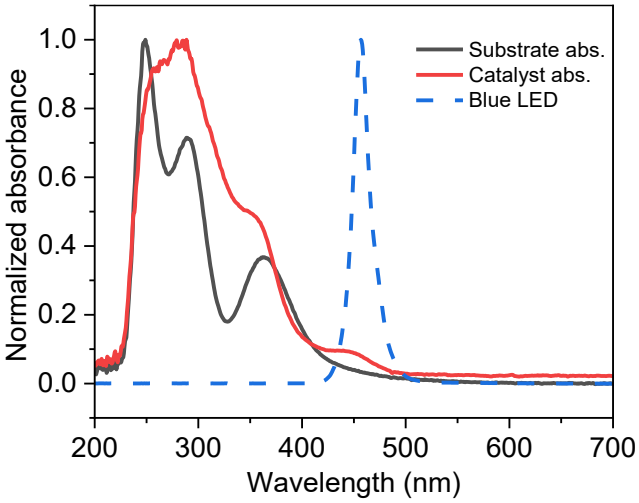

*Figure 2.6. UV-vis spectroscopy for amide **1.2a**, cobalt and emission of blue LEDs (dash, blue).*

In the case of cobaloxime, the charge transfer of oxime to Co (LMCT) showed the absorption maximum at 280-300 cm^{-1} region.[94] The Co–Sn charge transfer band, representing for [Co^{III}] species, is assigned at a shoulder of 358 nm.[95] The overlap between the absorption of the catalyst at 420 nm and the emission region of the blue LEDs showed the ability to activate the precatalyst under irradiation.

Next, the in-situ UV-vis spectroscopy was measured with the interval of 30 seconds to monitoring the transformation of cobalt species during the irradiation (Figure 2.7). Upon the irradiation of cobaloxime, the transformation of the precatalyst can be divided into two periods (Figure 2.7.A). The first phase represents the precatalyst activation period, which took place for the first 3 hours (Figure 2.7.A (top)). It can be seen by the gradual decrease in the absorption of Co–Sn CT and the simultaneous raise of the absorption band at 430 nm, which is assigned to the formation of [Co^{II}] species.[95] These observations support the hypothesis of precatalyst activation that blue lights cleaved off the Co–Sn bond to form [Co^{II}] species. After reaching maximum of [Co^{II}] species, the catalyst entered the second step, which occurred for another 3 hours (Figure 2.7.A (bottom)). This period demonstrates the deactivation step of the catalyst, as there was a continuing reduction of the amount of [Co^{II}] species. The further irradiation did not lead to any changes or resurrect the Co–Sn bond of the precatalyst.

In the presence of amide **1.1a** and diisopropylethylamine, the behavior of cobaloxime during the irradiation also exhibited in two phases as above (Figure 2.7.B). However, the time domain in each phase was much shorter, especially in the activation period only as it lasted for merely 1.5 hours (Figure 2.7.B (top)). The possible reason could lie on the rapid

interaction between catalytic active [Co^{II}] species with the substrate, which facilitate the reaction to take place. Meanwhile, the deactivation took place for nearly the same time in the absence of imide **1.1a** (Figure 2.7.B (bottom)).

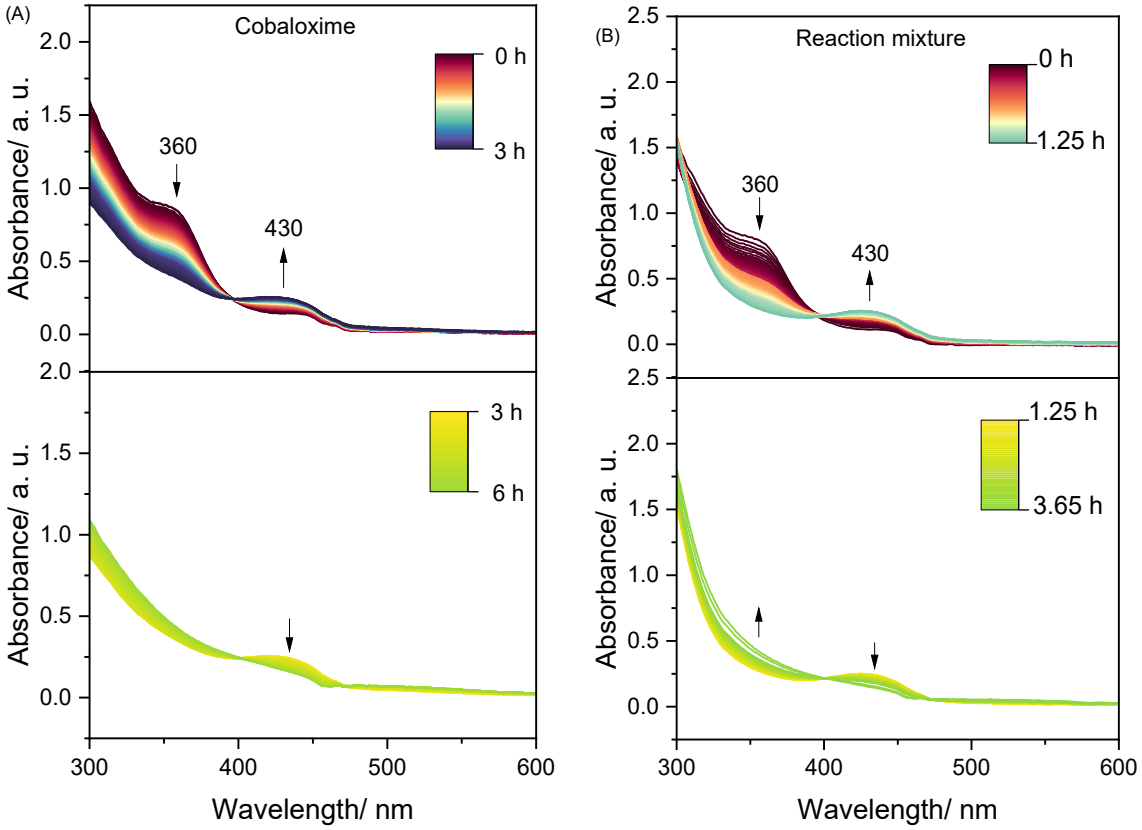

Figure 2.7. ***A****: In situ UV-vis spectra of cobaloxime during irradiation in the 1st phase (bottom) and the 2nd phase (top);* ***B****: In situ UV-vis spectra of reaction mixture during irradiation in the 1st phase (bottom) and the 2nd phase (top).*

2.4.3. EPR spectroscopy

To gain more details about the nature of cobalt during the reaction, EPR experiments at low temperature with different irradiation time were conducted (Figure 2.8).

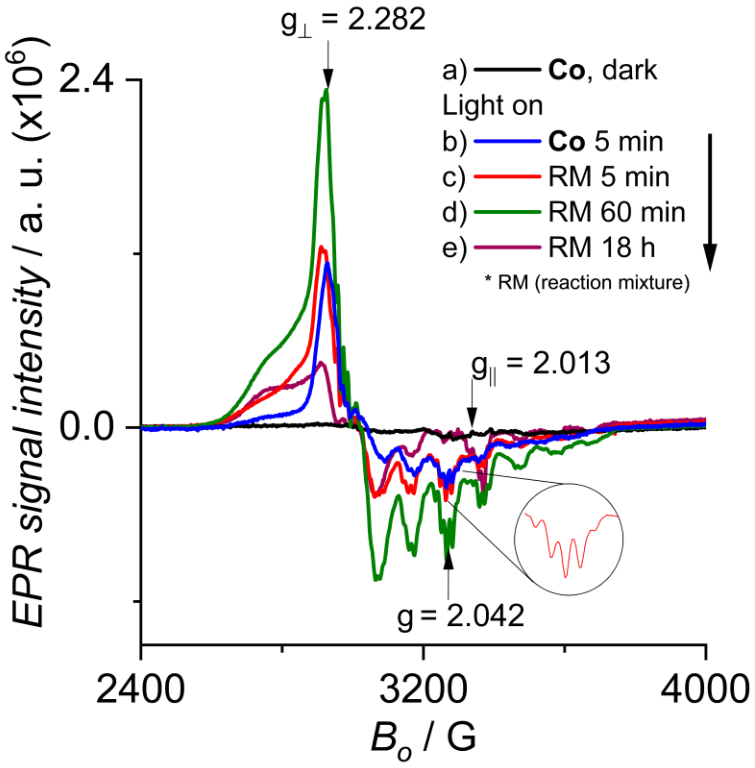

Figure 2.8. EPR spectra of Co-1 (5 mM) in CH_3CN at -173°C: a) Co-1 before irradiation; b) Co-1 after 5 min light on; c) reaction mixture of 1a (RM) after 5 min light on; d) RM after 60 min light on; e) RM after 18 h light on.

Initially, the pre-catalyst **Co-1** in dark showed no EPR signal, which is due to the EPR inactive by d^6 electronic configuration of [Co^{III}] complex (black line). Upon the irradiation with blue lights at room temperature, the frozen solution of X-band EPR spectrum showed the signal of typical low-spin d^7 (S = ½) electronic configuration of ^{59}Co (blue line). This is in agreement with UV-vis results as [Co^{II}] species are generated upon the irradiation to the precatalyst. The g-tensor of this species are axial signal at $g_\perp$ = 2.282 and $g_\parallel$ = 2.013 with resolvable hyperfine structure (I=7/2) of the parallel component A = 113 G. Notably, the hyperfine structure, especially the middle lines, exhibited a five-line signals as a super hyperfine splitting with approximately ratio of 1:2:3:2:1 (figure inset). This is probably due to the nearly equal interaction with two ^{14}N nucleus (I = 1) indicating the coordination of the doubly axial N ligands to the [Co^{II}] center.[96] These two nitrogen nucleus could be from two pyridine, two acetonitrile solvation or one pyridine and one solvated acetonitrile (Scheme 2.4). Additionally, there is a very weak signal superimposed with the hyperfine structure of [Co^{II}] at g = 2.042, most probably due to the formation of Ph_3Sn radical. It seems that the light induced homolytic cleavage of cobaloxime pre-catalyst **Co-1** leads to the formation of the EPR active [Co^{II}] species and Ph_3Sn radical.

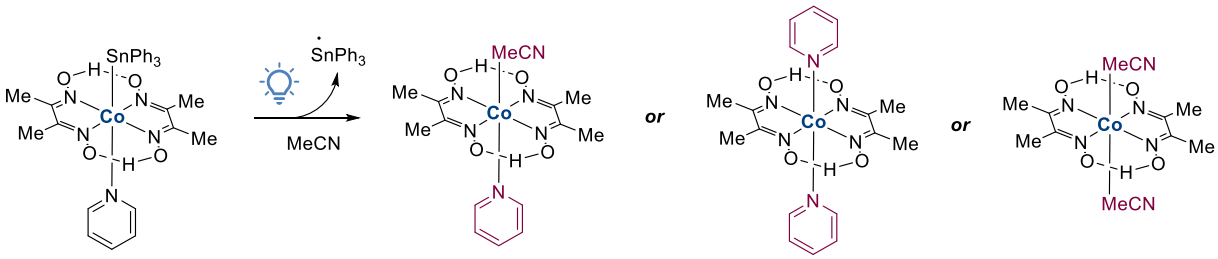

Scheme 2.4. Different possibility of ligation cobalt (II) complex upon the irradiation.

In the addition of substrate **1.1a** and the base, the EPR signal intensity of Co^{II} was continuously increased for the first hour of irradiation, as proved by UV-vis spectroscopy (Figure 2.8, red and green line). After 18 hours of irradiation and complete conversion, a dramatic decrease in the intensity of the EPR signals was observed (purple line). Additionally, the remaining signal exhibited broad feature, which is characteristic for cluster formation. This could be the deactivated form of the cobalt catalyst after the reaction.

2.4.4. Spin trapping experiments

To confirm the formation of radical species during the reaction, EPR experiments with the addition of 5,5-Dimethyl-1-pyrroline N-oxide (DMPO) as the spin trap were conducted. First, DMPO was added to the solution of cobaloxime in MeCN and the EPR signal were recorded while irradiating by blue LEDs at room temperature. In this case, only DMPO–H spin adducts were captured upon the irradiation (Figure 2.9). These hydrogen atoms trapped by DMPO could be from either the chelated hydrogen atom or α-carbon atom of the equatorial ligand.[97]

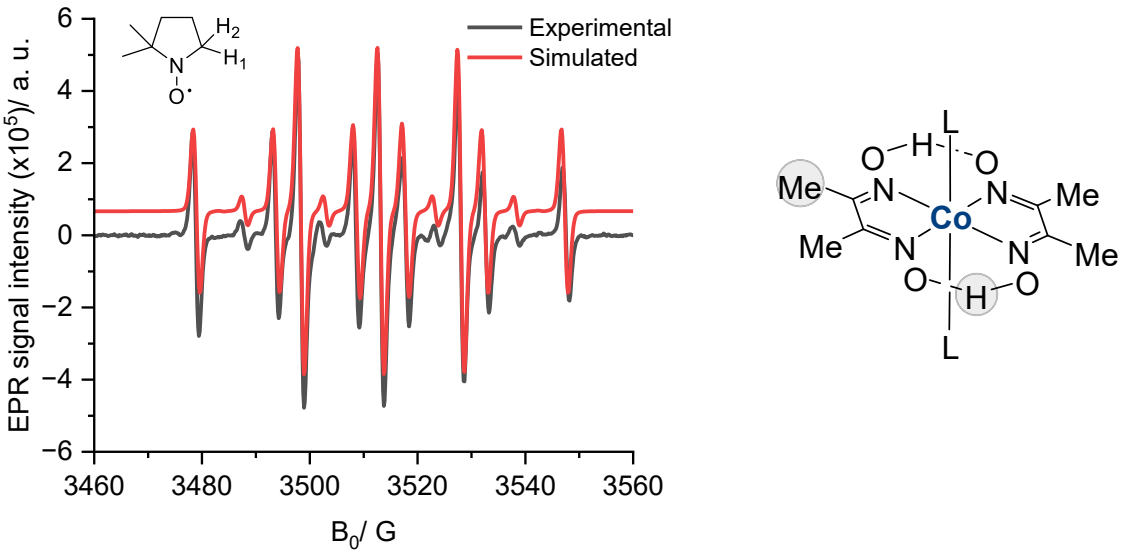

Figure 2.9. Experimental (black) and fitted EPR spectra (red) of DMPO–H spin adducts when irradiating Co-1. For fitting the following hfs parameters were used: a_N=14.8G, a_{H1}=19.3G, a_{H2}= 19.3 G for H•.

Furthermore, DMPO was subjected to the mixture between cobaloxime and different components in the reaction mixture to examine the interaction between them. In the presence of iPr$_2$NEt, a carbon-centered radical was also captured besides DMPO–H adducts (Figure 2.10). These adducts were unstable and quickly disappeared upon further irradiation. The generation of these organic radicals might be attributed to the α-amino radicals through the interaction of SnPh3• with the base.

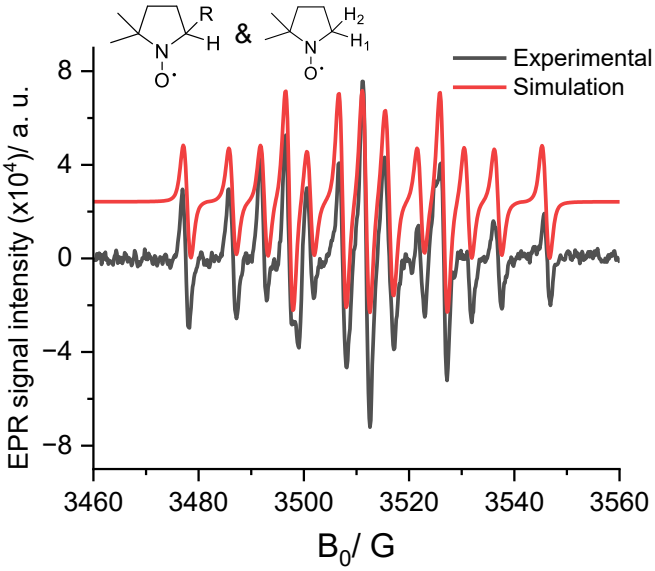

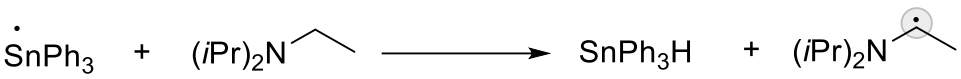

Figure 2.10. Experimental (black) and fitted EPR spectra (red) of DMPO spin adducts when irradiating the mixture of Co-1 and iPr$_2$NEt. For fitting the following hfs parameters were used: a_N=14.7G, a_{H1}=19.4G, a_{H2}= 19.3 G for H•; a_N=14.7 G, a_H= 21.0 G for C•.

2.4.5. Further control experiments

In order to determine the type of intramolecular HAT taking place in the reaction, Dr. Chenyang Wang prepared a series of substrates bearing different iodide position in the benzoyl tether (Scheme 2.5). The reactivity of these prepared substrates was tested under standard conditions afterwards. Interestingly, it was found that only 2-iodo benzoyl tether can facilitate the desaturation reaction, while 3- or 4-iodo benzoyl tethers are unsuitable tethers. This is attributed to the fact that selective 1,5-HAT is more favorable than 1,6 or 1,7-HAT process in this reaction.

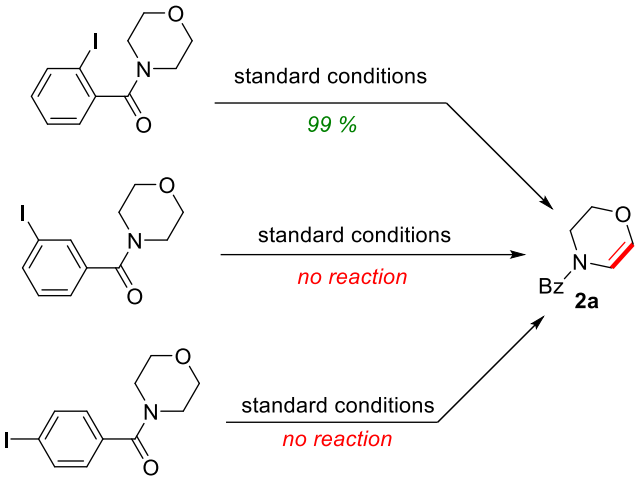

Scheme 2.5. Control experiments with different position of iodide in tether.

2.5. DFT calculation

In this section, the DFT calculation was conducted in a collaboration with Dr. Luis Miguel Azofra.

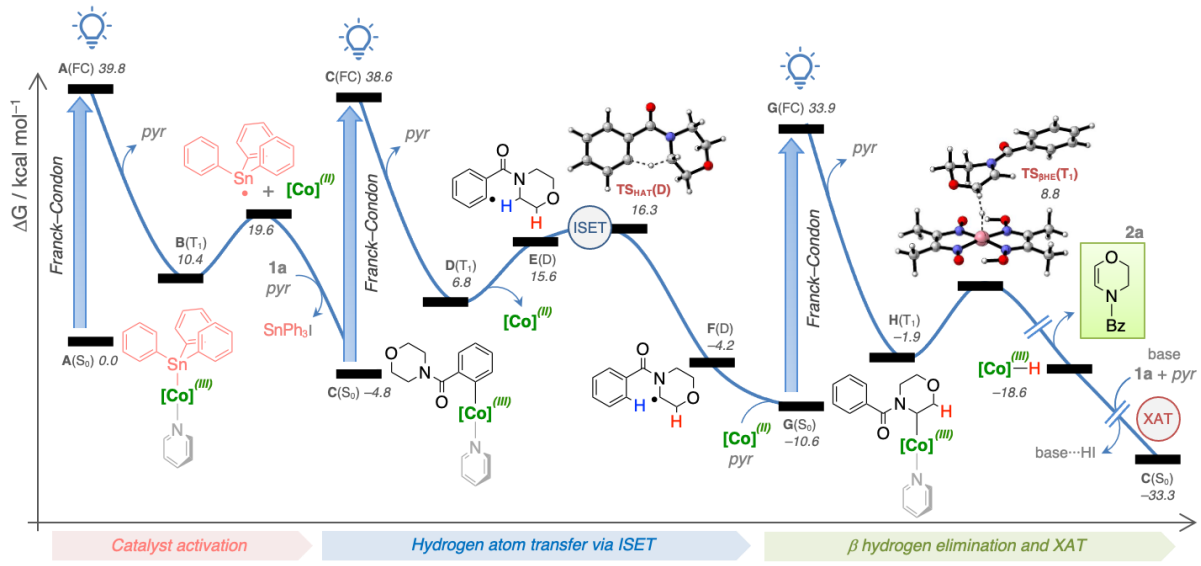

Figure 2.11. Detailed description of the potential energy surface (PES) for the pre-catalyst activation and metal-assisted desaturation cycle involving the hydrogen atom transfer (HAT) and the β hydrogen elimination (βHE) steps. Free energy results are shown in kcal mol^{-1} at the PBE96/TZVP//BP86/6-31G-SVP(Sn,I) level of theory in acetonitrile as solvent.

The reaction mechanism was investigated using DFT techniques (Figure 2.11). Initially, the triphenyl tin cobaloxime complex (**A**) is excited by light, causing it to split into [Co^{II}] and a Ph_3Sn radical. This Ph_3Sn radical then captures the iodide from substrate **1a**, and the resulting substrate radical combines with [Co^{II}] species to form complex **C**, at –4.8 kcal/mol. The key step, internal hydrogen atom transfer (HAT), which facilitates selective C(sp^3)–H activation at the α-position of the amide substrate, was also examined. Complex **C** is excited from its singlet ground state (S_0) to the triplet excited state (T_1) via vertical Franck–Condon (FC) excitation, reaching a high-energy state of 36.6 kcal/mol. This high-energy state is essential for enabling the transformation, which is not possible under thermal conditions. After relaxation, pyridine (pyr) is released, forming complex **D**(T_1), followed by cleavage of the [Co^{III}]–C bond, generating [Co^{II}] and radical species **E**, both in the doublet state (D), which corresponds to the EPR-active species. The transition state for hydrogen atom transfer (TS_{HAT}), driven by internal single electron transfer (ISET), lies just 0.6 kcal/mol above species **E** in relative free energy. This leads to the formation of complex **G**(S_0), stabilized at –10.6 kcal/mol, through the recombination of [Co^{II}], the alkyl radical species **F**, and pyridine.

The next step, product formation *via* β-hydrogen elimination, was also analyzed. Under visible light irradiation, complex **G**(S_0) undergoes a second vertical FC excitation, reaching an energy level of 33.9 kcal/mol. Pyridine is again released, forming complex **H**(T_1) at –1.9 kcal/mol. The β-hydrogen elimination occurs in the triplet state, resulting in

the formation of [Co^{III}]–H and the enamine product **1.2a**. Notably, the transition state for β-hydrogen elimination (TS $_{βHE}$) in the triplet state is only 11.1 kcal/mol higher in free energy relative to complex **H.**

2.6. Proposed mechanism

The results from EPR and UV-vis spectroscopy suggested the activation of the catalyst occurring via the generation of [Co^{II}] species and α-amino radicals from the base. To facilitate the remote desaturation of the amides, the initial radical generated in the benzoyl tether undergoes 1,5-HAT process to relocate to the desired position. The proposed reaction mechanism for the remote desaturation of amides and imides is depicted in Scheme 2.6 below. Upon visible light irradiation, the catalyst was activated through a homolytic cleavage of Co–$SnPh_3$ to generate a [Co^{II}] species alongside a triphenyltin radical. The latter is believed to promote the formation of an α-amino radical from iPr_2NEt, serving as a XAT reagent to abstract iodo groups from the substrate to generate aryl radical **1.5**. Subsequently, this radical undergoes 1,5-HAT process, leading to radical formation at an unactivated site of the alkyl chain **1.6**. The alkyl radical **1.6** then undergoes desaturation utilizing the [Co^{II}] species to furnish the unsaturated product along with [Co^{III}]–H. This hydride species facilitates the catalyst turnover by the reaction between $SnPh_3H$ and an iminium salt to regenerate the cobalt-tin catalyst.

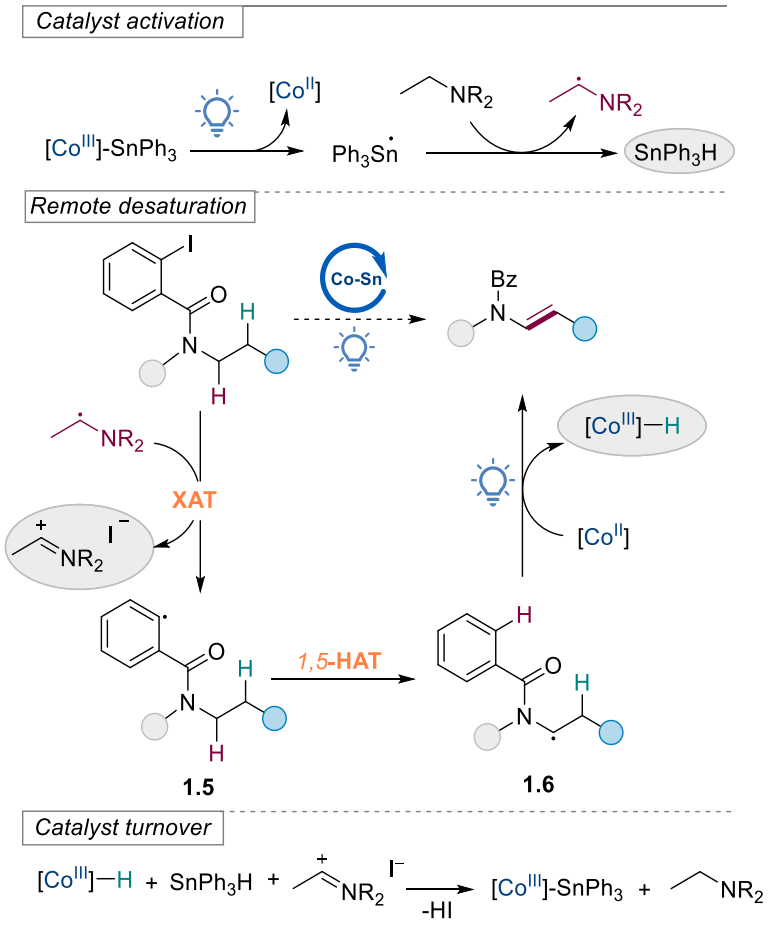

Scheme 2.6. Proposed mechanism for remote desaturation of amides utilizing cobaloxime.

2.7. Conclusion

In conclusion, comprehensive mechanistic experiments provided a detailed proposal on the reaction mechanism of desaturating amines. EPR and UV-vis spectroscopy results indicated that the catalyst is activated through the formation of [Co^{II}] species and α-amino radicals from the base. Moreover, a radical propagation mechanism can be ruled out based on the result of light on-off experiment and the determination of quantum yield. Further controlled experiments indicated the favor of 1,5-HAT process to facilitate the remote desaturation. Finally, a conceivable mechanism of a C(sp^3)–H activation reaction was postulated, which were further supported by DFT calculation.

Chapter 3: Cobaloxime-catalyzed intramolecular *endo*-selective Heck reaction

3.1. Backgrounds

Since its discovery in the early 1970s, the Mizoroki-Heck reaction, which couples unsaturated carbon electrophiles with nucleophiles, is one of the most versatile synthetic methods to form C–C bonds.[98] One of the most memorable milestones for this transformation was the recognition by the Nobel prize award in Chemistry in 2010.[22b, 99] The first intermolecular Heck reaction was reported by Heck in 1972, using aryl iodies as electrophiles to couple with styrenes (Scheme 3.1).[100] Development of the general intermolecular reaction suffered due to poor regiocontrol of the addition and elimination steps for electronically neutral olefins. Thus, only mono- and disubstituted olefins can participate in the reactions.

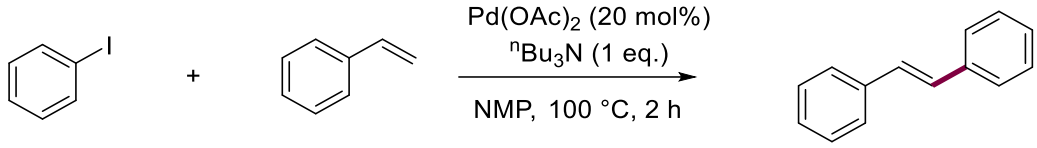

Scheme 3.1. The first intermolecular Heck reaction.

In contrast to the intermolecular Heck reaction, the intramolecular version can form highly sterically hindered C–C bonds. The first intramolecular Heck reaction, reported by Mori and Ban in 1977 for indole synthesis (Scheme 3.2), resulted in the indole product through Pd–H isomerization of the olefin.[101] Intramolecular Heck reactions are generally more efficient than their intermolecular counterparts because they eliminate entropic concerns.

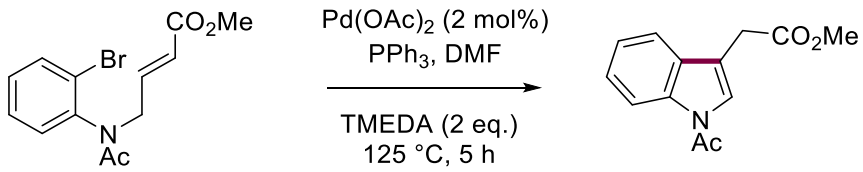

Scheme 3.2. The first intramolecular Heck reaction.

The regioselectivity of the intramolecular Heck reaction is determined by whether the migratory insertion of olefins occurs in an *endo* or *exo* fashion (Scheme 3.3). This selectivity depends on the formation of the ring, with a strong preference for *exo* mode in the case of 5-, 6-, and 7-membered rings. The transition state leading to *exo* products in small ring formations is energetically more favorable than the *endo* transition state due to

the shorter tether length. Longer and more flexible chains are required to achieve the appropriate conformation for *endo* insertion.

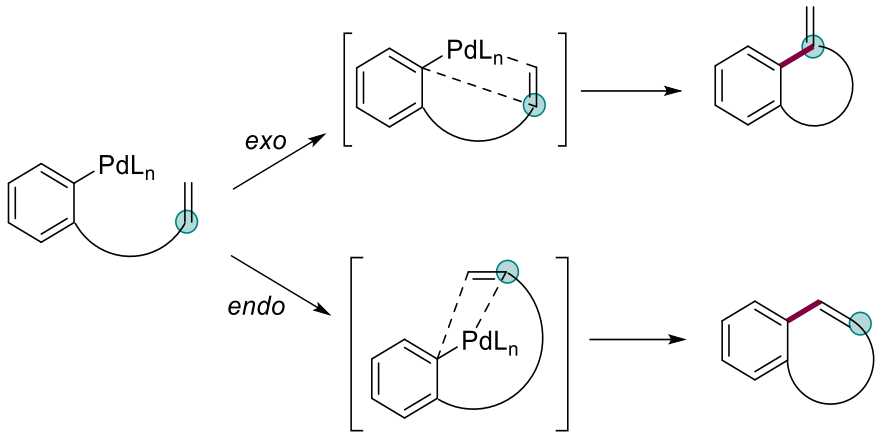

Scheme 3.3. The regioselectivity of intramolecular Heck reaction.

Historically, aryl halides have been the preferred electrophiles for all cross-coupling reactions, thus, including Heck reactions Heck reactions. Compared to these common electrophiles, using C(sp^3) halides faces more challenges due to their slower oxidative addition rates and the tendency for competing β-hydrogen elimination.[47] Despite these difficulties, the alkyl-Heck reaction can still be conducted in a mild condition using palladium or earth-abundant metal catalysis under improved conditions.[43, 102]

The first example of an intramolecular alkyl-Heck reaction catalyzed by palladium was reported by Fu in 2007, using an NHC ligand to achieve selective 5-*exo*-trig cyclization (Scheme 3.4).[103] This ligand helps to overcome the competitive β-hydride elimination pathway, promoting migratory insertion and supporting C–C bond formation *via* an alkylpalladium intermediate rather than a radical. Later, in 2011, Alexanian developed another *exo*-trig-cyclization for intramolecular alkyl-Heck reaction using palladium catalysis under thermal conditions.[104]

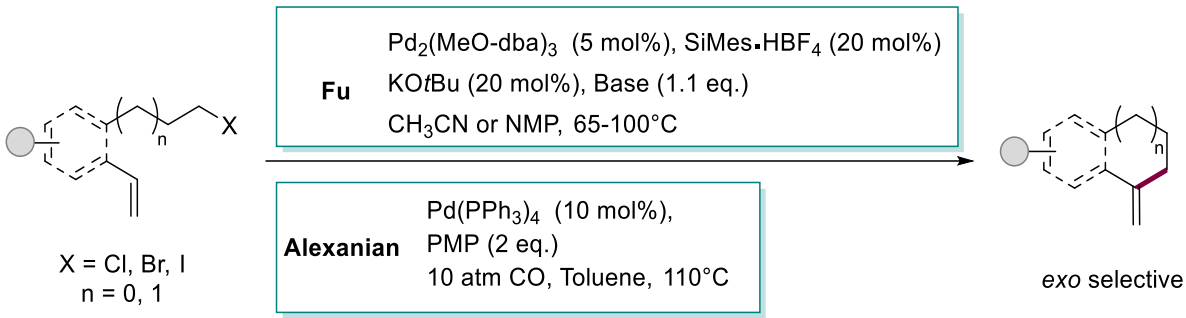

Scheme 3.4. Examples of intramolecular Alkyl Heck-type reaction catalyzed by Pd.

Instead of classical palladium catalysis, the use of other base-metal catalyst for alkyl-Heck reaction is feasible as the C–C bond forming step can generally occur *via* radical process.[105] In 1985, the intramolecular alkyl-Heck reaction with cobalt catalyst was reported for the first time using electrochemical method in 40% NaOH as medium and 50 mol% of chlorocobaloxime.[42b] Alternatively, the reaction can be conducted in a system consisting of catalytic amount of vitamin B_{12} with strong reductive reagents such as Zn, $NaBH_4$ under thermal conditions.[42d, 106]

Until 2011, the first practical catalytic use of cobaloxime complexes in organic synthesis was reported by the group of Carreira, demonstrating an intramolecular *exo*-selective Heck reaction of primary alkyl iodides under visible light.[43] The success of this approach relied on the reduction of the Co^{III}–H species to an anionic [Co^{I}] species via deprotonation using a simple organic base (iPr$_2$NEt). To date, all the strategies using cobalt catalysis have only resulted in *exo*-trig cyclization products.

On the other hand, the *endo*-trig alkyl-Heck reaction is extremely rare, with only three reported examples to date. The first was introduced by Koreeda's group in 1990 under reductive conditions (Scheme 3.5).[107] The approach involved the installation of (bromomethyl)silyl ethers onto hydroxyl group of the aliphatic alcohols, using in situ-generated of nBu$_3$SnH to form alkyl radicals. Two factors that promotes *endo* transition state during the radical cyclizations are the elongated of Si–C bond of this preinstalled tether and the slower rate of competitive *exo* cyclization. However, this method was limited to the substrates containing unsubstituted olefin, as this minimizes steric hindrance during radical attack on the sp^2 center. Inspired by this masking strategy, Gevorgean developed an intramolecular alkyl-Heck cyclization of iodomethysilyl ethers of phenols to the corresponding siloxycycles using palladium catalysis, and thus, eliminated the need for harsh reductive conditions.[108] The method enabled the formation of 7-, 8-, 9-membered-*endo*-trig cyclization products *via* a hybrid palladium radical mechanism under thermal conditions. However, the use of 20 mol% of expensive ferrocene-based phosphine (dtbdppf) and equivalent amounts of silver salts limits its scalability for larger applications.

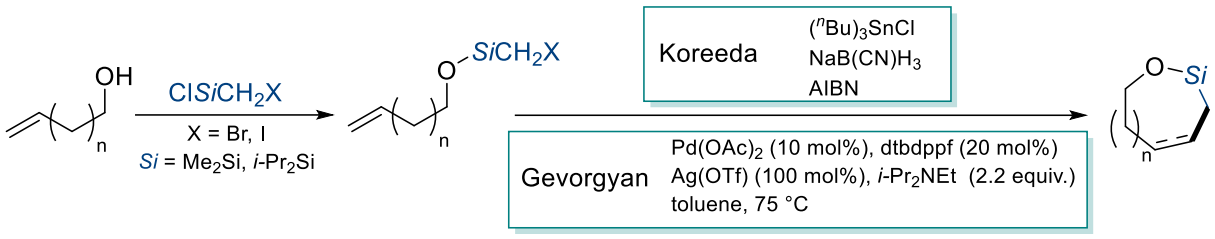

Scheme 3.5. Examples of endo-trig alkyl-Heck reaction.

Instead of relying on the elongated bond of a preinstalled tether, *endo*-trig-cyclization products can also be formed by generating a stable radical during the cyclization process to bypass the typical *exo* pathways. This strategy was employed by Liu and colleagues, reporting the synthesis of 5-phenyltetrahydropyridine derivatives from alkyl iodides containing a 1-aryl-substituted alkene moiety (Scheme 3.6).[109] This substituent serve as a reservoir for forming stable tertiary benzylic radicals, which drive the selective formation of 6-*endo*-trig products.

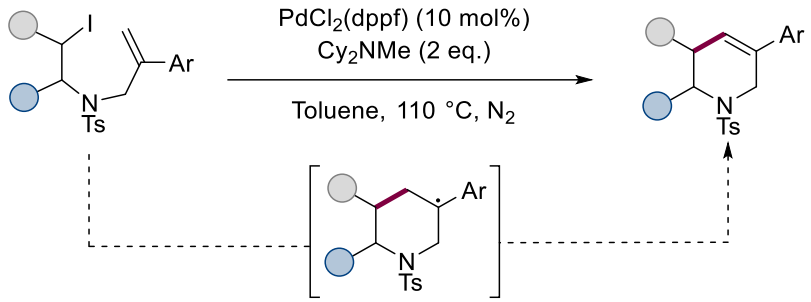

Scheme 3.6. Examples of 6-endo-trig alkyl-Heck reaction.

Based on the literature, there is a lack of base-metal catalysis for catalysed *endo*-selective alkyl Heck reactions to replace thermal palladium system. Inspired by the ability of cobaloxime to promote the alkyl-Heck reaction as well as the experience with this complex of the group, the idea of applying cobaloxime for the intramolecular Heck reaction is proposed. This cobalt complex, which possesses the reversible alkyl–cobalt bond under visible light, can facilitate the reaction *via* radical mechanism. The *endo*-selective cyclization should be achieved by the preinstallation of the iodomethylsilyl ethers into phenols and aliphatic alkenols.

3.2. Screening of reaction conditions

In this section, the screening of reaction conditions for intramolecular endo-selective Heck reaction was conducted by Dr. Chenyang Wang. The silyl-tethered *o*-hydroxystyrene **2.1a** was used as a model substrate for reaction development (Table 3.1).

*Table 3.1. Screening of the reaction conditions for intramolecular Heck-reaction of **2.1a**.*

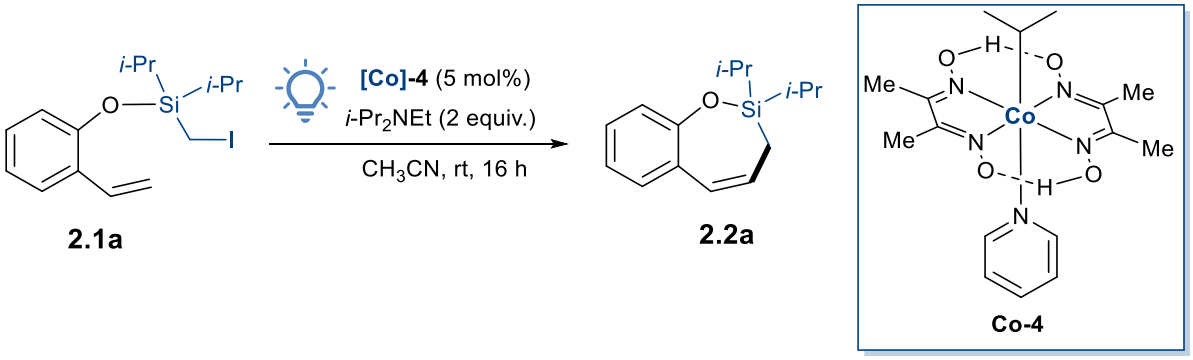

Entry	Deviation from standard conditions	Yield (%)
1	None	99
2	No **Co-4** or no light	n.d.
3	70 °C instead of light	trace
4	1 equiv. K_2CO_3 as base	72
5	1 equiv. K_2CO_3, 20 mol% *i*Pr_2NEt as base	81
6	DMAP as base	trace
7	DBU as base	trace
8	DCM as solvent	85
9	THF as solvent	71
10	TEMPO was added	n.d.

The optimal conditions for producing the 7-membered siloxycycle **2.2a** in quantitative yield involved using 5 mol% of **Co-4** and Hünig's base (DIPEA) in acetonitrile under blue LED irradiation at room temperature (entry 1). Notably, this catalytic system does not require an additional photoredox catalyst,[49] strong reductive conditions,[41b, 42a, 42b, 110] and Grignard reagents.[42e, 111] Control experiments confirmed that the reaction does not proceed without the cobalt catalyst or blue light (entries 2, 3). Examining various organic and inorganic bases showed that Hünig's base is optimal (entries 4-7). Switching solvent from CH_3CN to DCM or THF resulted in reduced yields (entries 8, 9). Finally, the addition of TEMPO completely suppressed product formation (entry 10).

3.3. Scope for intramolecular endo-selective Heck reaction

The reaction scope of the cobalt-catalyzed endo-selective Heck cyclization using various o-hydroxystyrenes and alkenols as substrates was examined by Dr. Chenyang Wang. The results are highlighted in Scheme 3.7.

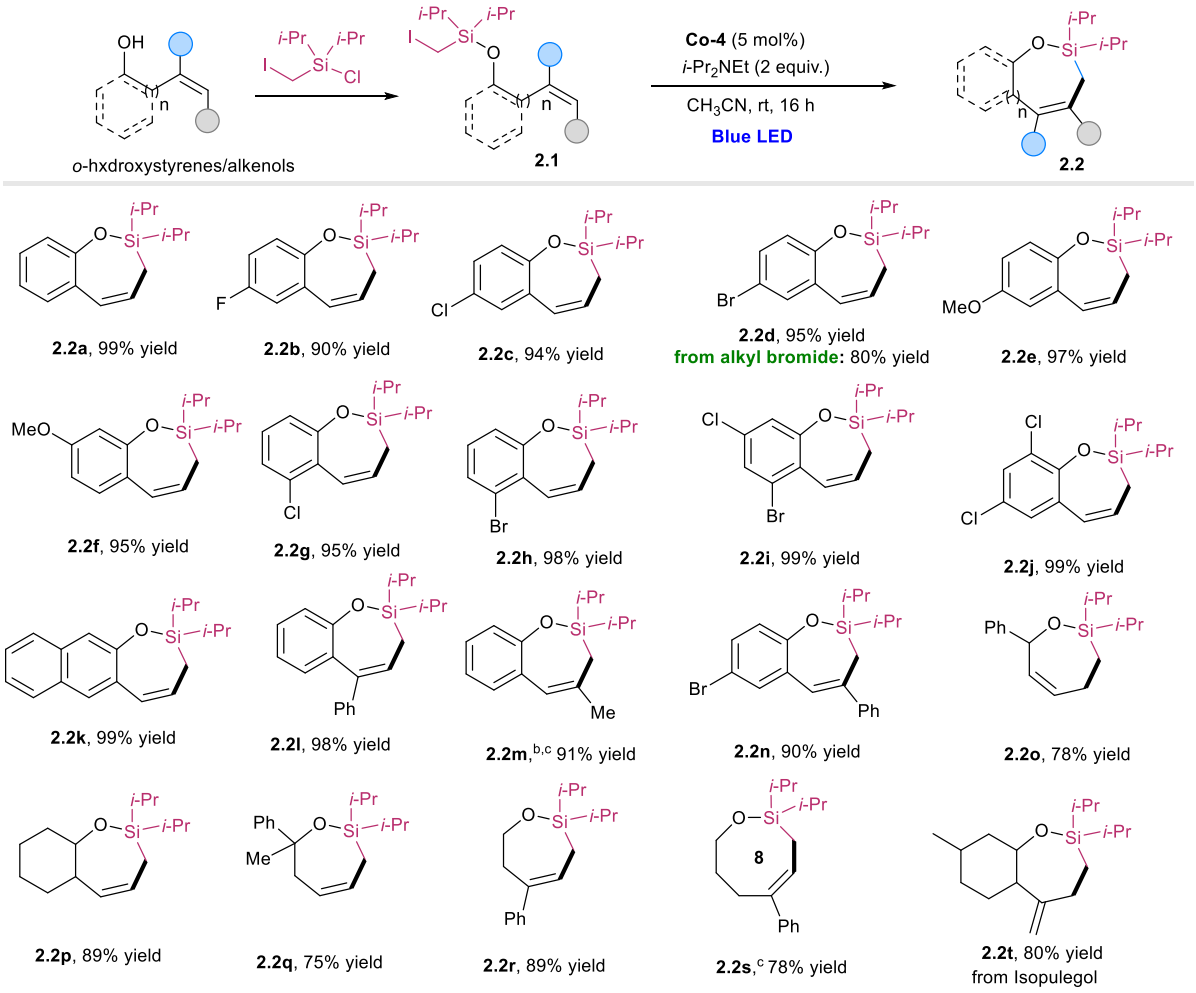

Scheme 3.7. Reaction scope of intramolecular endo-selective Heck reaction. a) Reaction conditions: 2.1 (0.2 mmol), Co-4 (0.01 mmol, 7.2 mg), i-Pr₂NEt (0.4 mmol, 70 μL), CH₃CN (2 mL), rt, Blue LED (19 W, Ledxon), 16h, isolated yields; b) mixture of isomers; c) NMR yield.

Substrates with different substituents (Cl, Br, F, Me and OMe) at the 4 different positions on the phenyl ring yielded the desired *endo*-products **2.2b**-**2.2j** in excellent yields, ranging from 90 to 99%. Notably, switching from alkyl iodide to alkyl bromide in the silyl tether also afforded the desired **2.2d** in 80% yield. Moreover, the naphthyl derivative also yielded the cyclic product **2.2k** in a quantitative amount, demonstrating the method's versatility with aromatic rings.

The reaction is also applicable to substrates bearing substituents at the olefin, producing the desired products with moderate to good selectivity. The α-substituted substrate gave

the *endo*-product **2.2l**. Meanwhile, substrate **2.1m**, which had β-position substituents, led to the formation of oxasilepine **2.2m** with moderate selectivity (60% of the major isomer). Building on these results, more challenging system such as aliphatic alkenol was examined. Specifically, the cyclization of the secondary homoallylic alcohol **2.1o** yielded the allylic siloxycycle **2.2o** in 78%. Besides, the substrate with two vicinal substitutions at the α- and β- positions of the tethered alcohol efficiently produced the siloxysilane **2.2p** in very good yield.

Importantly, the method showed tolerance to not only secondary alcohol substrates but also primary and tertiary ones. Indeed, the catalytic system tolerated the tethered tertiary alcohol **2.1q**, resulting in a 75% yield of the desired product. Furthermore, the tethered primary alcohols **2.1r** and **2.1s** underwent successful 7-*endo*-trig and 8-*endo*-trig cyclization, yielding 89% and 78%, respectively. The approach also works with naturally occurring isopulegol, yielding the *endo*-product **2.2t** with excellent selectivity and yield, showcasing the robustness and general applicability of the method across various structural frameworks.

3.4. Mechanistic studies

3.4.1. Quantum yield and light on-off experiment

To determine the quantum yield, the reaction profile was conducted to determine the initial rate of the product formation. In this experiment, the reaction was conducted in standard conditions and the product formation of the desaturation of amide **2.1d** was monitored by calibrated GC using n-dodecane as internal standard. A 30-minute-interval was set to sample out for the first two hours. The results were shown in the Table 3.2 below.

*Table 3.2. Reaction profile of the desaturation amide **2.1d.***

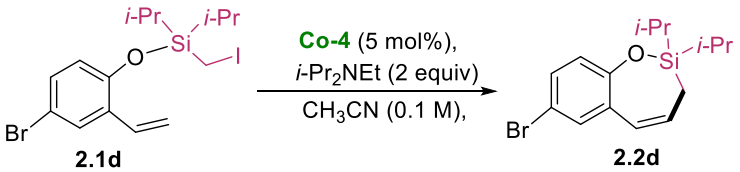

2.1d 2.2d

Time (s)	0	3600	7200	10800
Product (mol × 10^{-4})	0	4.856	6.629	7.026
Yield (%)	0	48.56	66.29	70.26

According to the table, the reaction profile was plotted in (Figure 3.1.A). Based on this profile, the initial rate of the desaturation reaction of amide can be determined in the first two hour. The reaction steadily proceeded for the following 2 hours and the amide **2.1a** was mostly converted overnight.

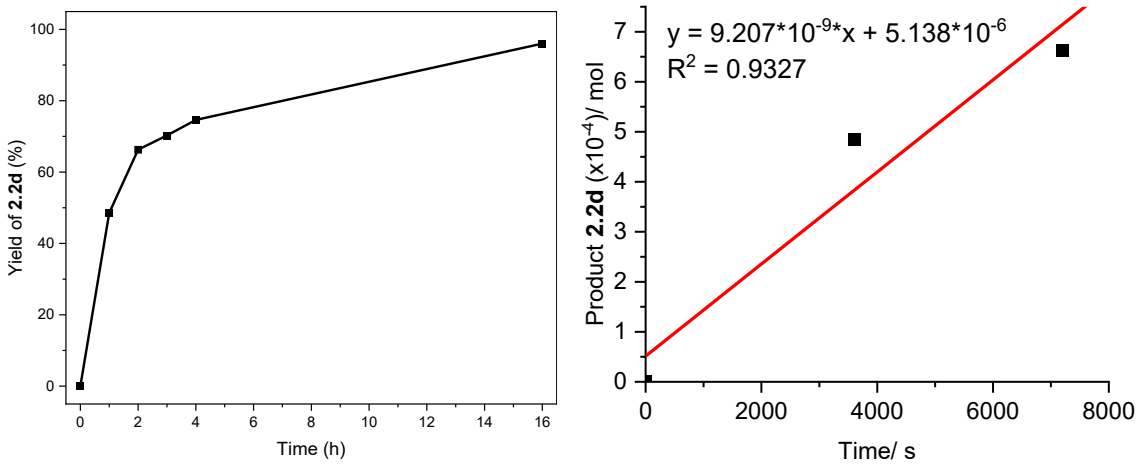

*Figure 3.1. **A**: Reaction monitoring by calibrated GC using n-dodecane as internal standard for desaturation amide **2.1d**; **B**: Initial rate determination.*

By plotting the product formation against the time domain, the initial rate of the desaturation of the amide **2.1d** was determined by the slope of the linear fit (Figure 3.1.B). The fitting parameter was analyzed by Origin, which determining the initial rate of the reaction to be 9.207×10^{-9} mol/s.

By utilizing ferrioxalate solution as a standard actinometry, the photon flux of the blue LEDs setup was determined as 6.093×10^{-7} mol/s (see Appendix for more details). Thus, the quantum yield of the photoexcited cobalt for the desaturation reaction can be obtained by:

$$\phi = \frac{n_{product/s}}{photons/s} = \frac{9.207 \times 10^{-9}\ mol/s}{6.093 \times 10^{-7}\ mol/s} = 0.015$$

With the calculation of quantum yield of the reaction < 1, it can be demonstrated that the efficient radical chain propagations are not operating under these reaction conditions.

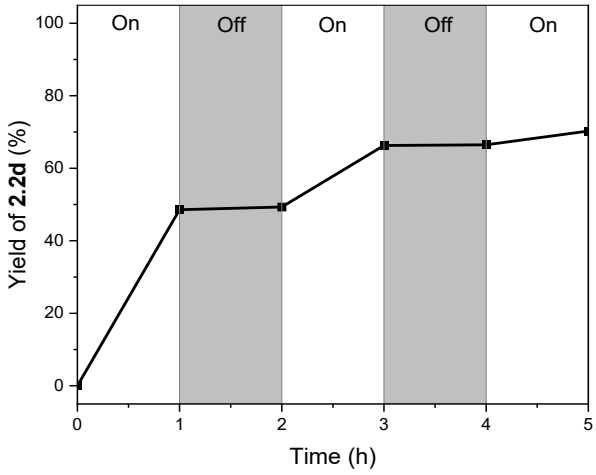

Figure 3.2. Light on-off experiments

Additionally, the light on-off experiment was also carried out (Figure 3.2). The similar procedure was conducted as the reaction profile, with interruptions of 1-hour-interval to keep the mixture in the dark during 5 hours of irradiation. The result showed that the enamide **2.2d** was only formed in the presence of light. Meanwhile, during the light off-cycles, no reaction was observed. Therefore, together with the quantum yield, the possibility of a radical chain process can be excluded.

3.4.2. NMR studies

To detect the formation of Co–H species by light, ^{1}H-NMR measurements of **Co-4** catalyst were conducted upon different irradiation time (Figure 3.3). **Co-4** was dissolved in deuterated DCM and measured in a J Young NMR tube. Initially, the ^{1}H spectrum in the absence of light exhibited sharp signals of the equatorial glyoxime ligands, indicating the diamagnetic property of [Co^{III}] species (top, blue line). Upon irradiating for 20 minutes, the signal became broaden, revealing for the formation of paramagnetic species in the system (middle, green line). Additionally, there were appearances of propene and hydride species in a low field region (marked as red and black, respectively). This indicates that the alkyl–cobalt bond of **Co-4** was cleaved upon the irradiation and released propene and Co–H species via β-hydride elimination process. The addition of diisopropylethylamine led to the vanishing of hydride signal, suggesting the deprotonation of Co–H with base to form nucleophilic [Co^{I}] species (bottom, red line). This [Co^{I}] species could react with alkyl halide *via* classical S_N2 pathway to yield the corresponding [Co^{III}]-alkyl intermediate.

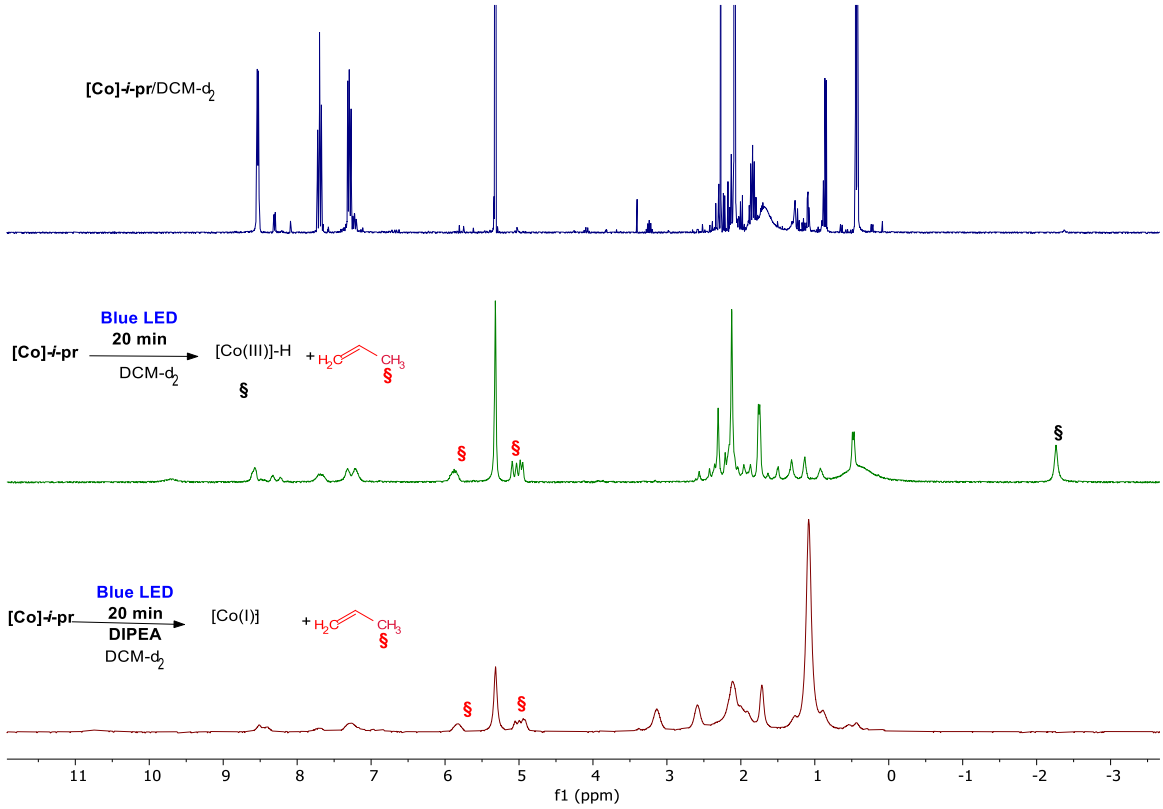

*Figure 3.3. ^{1}H-NMR spectra of **Co-4** upon irradiation of blue LEDs.*

3.4.3. Spin trapping experiments

To detect the formation of radical species during the reaction, spin trapping experiments were conducted using DMPO and measured by EPR spectroscopy. However, the initial attempt to capture radical species generated solely from **Co-4** at a normal 40-second interval was unsuccessful due to the rapid decomposition of DMPO-adducts, likely caused by the formation of unstable open-shell species. To address this, the spin trap experiments were repeated using a rapid scan technique, allowing for shorter measurement intervals to reveal these unstable radicals.

The results are shown in the Figure 3.4. During 18 seconds of irradiation, the DMPO–H adduct was predominantly detected, but with a short lifetime of just 6 seconds. According to the results from NMR spectroscopy above, the irradiation of **Co-4** led to the formation of Co–H and propene. However, the C radicals, which are presumably as propene precursors, appeared only as weak signals within the first 3 seconds. This suggests that hydrogen atoms react so quickly that DMPO struggles to trap alkyl radicals. Notably, the reaction of alkyl radicals with DMPO competes with their recombination with [Co^{II}], which reforms the Co–C bond. As a result, the spin density is very low, and DMPO may not capture enough alkyl radicals to produce significant signals. This behavior indicates

that the alkenes detected in NMR studies were likely generated *via* a concerted mechanism.

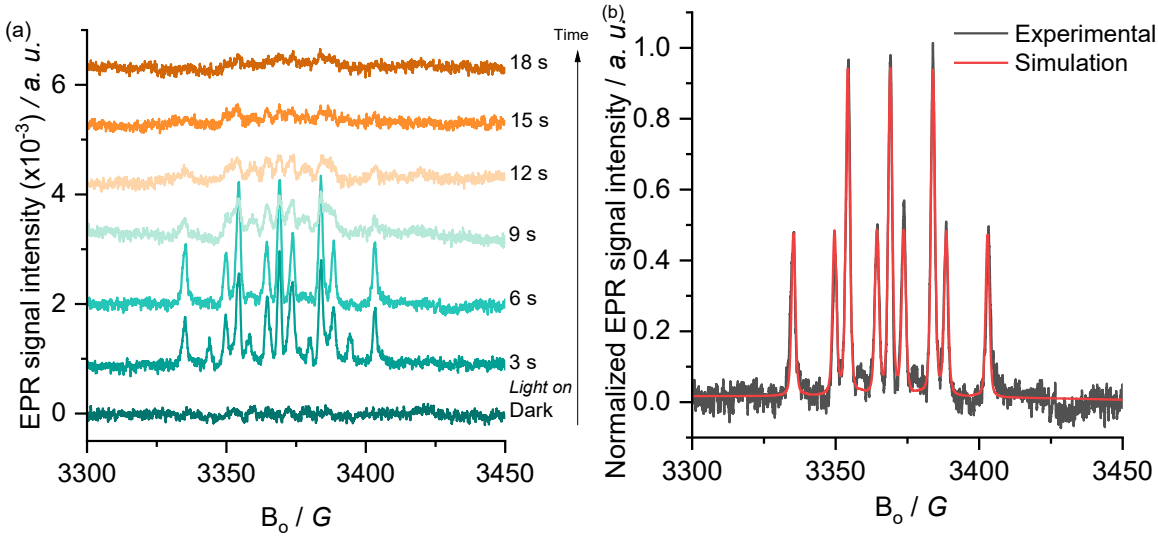

Figure 3.4. (a) EPR spectra for Co-4 with DMPO using rapid scan technique during the irradiation; (b) Experimental and simulated EPR spectra of DMPO–H adduct with the following hfs parameters were used: a_N=14.8G, a_{H1}=19.3G, a_{H2}= 19.3 G for fitting.

3.4.4. Low temperature EPR spectroscopy

To monitor the cobalt species during irradiation, low-temperature EPR spectroscopy was conducted, as shown in Figure 3.5. Initially, **Co-4** in the dark exhibited no EPR signal, which is expected due to the EPR-inactive d^6 electronic configuration of the [Co^{III}] complex (black line). Upon irradiation, the EPR spectrum displayed an axial signal with $g_\perp$ = 2.282 and $g_\parallel$ = 2.029, accompanied by a resolved ^{59}Co hyperfine structure (I = 7/2) in the parallel component. The appearance of [Co^{II}] observed in the spectrum likely results from the homolytic cleavage of the [Co^{III}]–H bond upon irradiation.[112]

In the presence of *i*-Pr_2NEt and substrate **2.1d**, the number of EPR-active [Co^{II}] species decreased by approximately 70% compared to that from the precatalyst upon 1 minute of irradiation. This amount of [Co^{II}] species remained nearly constant with prolonged exposure. This suggests that the catalyst rapidly achieves a steady state, where an efficient [Co^{I}]/[Co^{III}]/[Co^{II}] cycle is established, maintaining a constant level of [Co^{II}] over time.

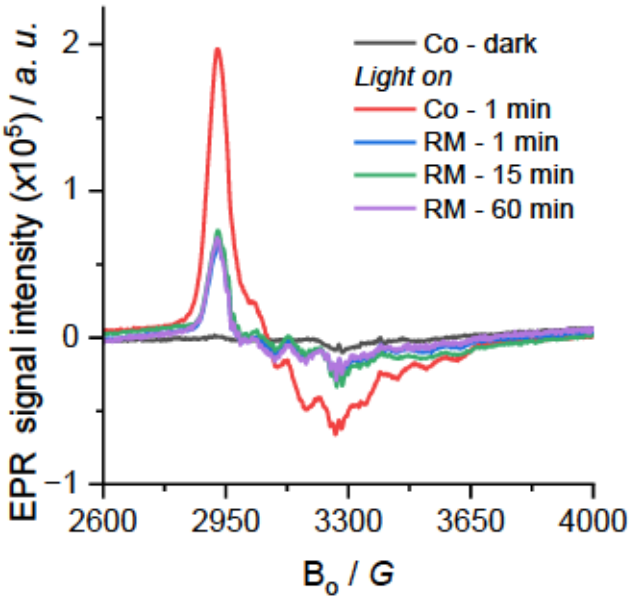

Figure 3.5. EPR spectra measured at -173 °C of (0.005 mmol Co-4, 1 ml MeCN) and reaction mixture (0.005 mmol Co-4, 0.1 mmol 1d, 0.2 mmol i-Pr$_2$NEt, 1 ml MeCN) before and after irradiation with time.

3.5. DFT calculations

To further rationalize the mechanism upon the catalytic activation, DFT calculations were carried out by Dr. Luis Miguel Azofra. The results of calculating potential energy surface using **2.1a** as model substrate are illustrated in Figure 3.6.

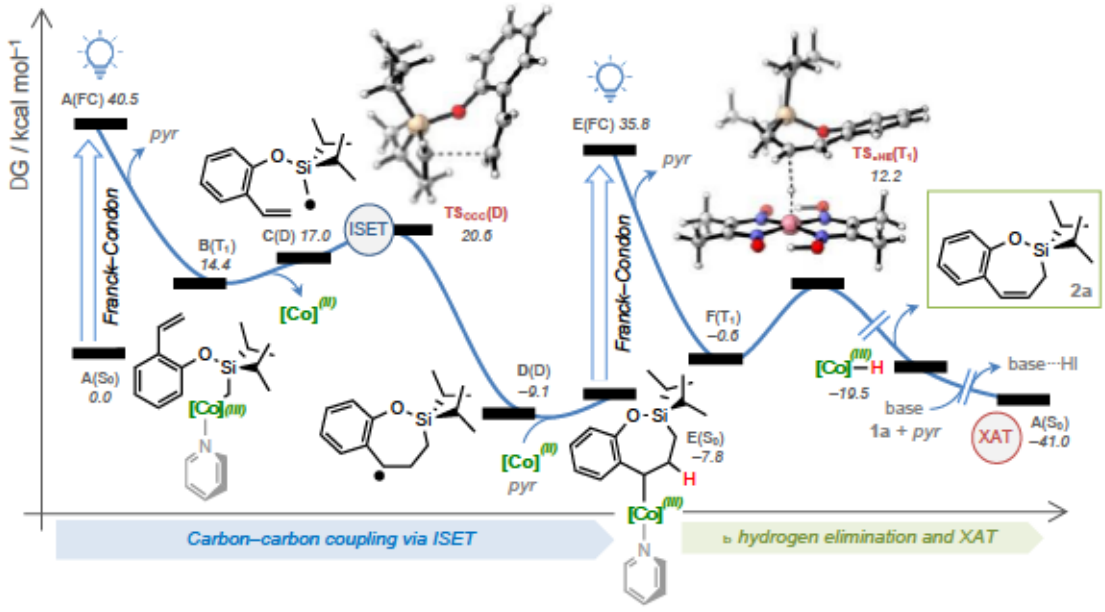

Figure 3.6. Detailed description of the potential energy surface (PES). Free energy results are shown in kcal mol^{-1} at the PBE96/TZVP//BP86/6-31G-SVP(Sn,I) level of theory in acetonitrile as solvent.

The mechanism proceeds through carbon-carbon bond formation via internal single electron transfer (ISET), followed by β-hydrogen elimination and an S_N2 pathway. The

process begins when complex **A** is excited from its singlet ground state (S_0) to a higher-energy triplet state (T_1) through vertical Franck–Condon (FC) excitation, raising the energy level to 40.5 kcal/mol. After relaxation, pyridine (pyr) is released, producing complex **B**(T_1). At this point, the [Co^{III}]–C bond breaks, forming [Co^{II}] and the radical species **C**, both in the doublet state (D). Notably, the formation of the high-energy radical species **C** by light, which is crucial for enabling this carbon-carbon coupling, could not be facilitated by thermal conditions. The radical species **C** has an unpaired electron on the terminal carbon connected to the tether, making it highly reactive. Through an ISET process, this radical carbon interacts with the C(sp^2) center of the vinyl group, leading to carbon-carbon bond formation. The transition state for this carbon-carbon coupling step (TS_{CCC}) is only 3.6 kcal/mol above **B** in free energy, resulting in the spontaneous formation of a seven-membered ring at **D**, with a highly exergonic energy of –9.1 kcal/mol relative to **A**. The radical **D** then recombines with [Co^{II}] and pyridine to form complex **E** (S_0).

Upon the excitation by visible light, this complex undergoes a second vertical (FC) excitation to a high-energy triplet state at 35.8 kcal/mol. In a similar sequence, pyridine is again released, forming **F** (T_1) at –0.6 kcal/mol. As shown in rapid scan EPR experiments, β-hydrogen elimination happens through a concerted process in the triplet state, with the transition state ($TS_{\beta HE}$) being 12.8 kcal/mol above **F**. This leads to the formation of the [Co^{III}]–H complex and product **2.2a**. Finally, complex **A** (S_0) is regenerated by the action of the organic base and substrate **2.1a** via an S_N2 reaction, allowing it to re-enter the photocatalytic cycle.

3.6. Proposed mechanism

By combining the results from experimental and theoretical methods, the proposed reaction mechanism for the intramolecular endo-selective Heck reaction is depicted in Scheme 3.8. NMR studies and spin trapping experiments suggested that the catalyst activation was initiated by light to release [Co^{III}]–H species *via* β hydrogen elimination. This hydride species could be deprotonated by the addition of base to generate a highly nucleophilic Co^{I} complex. This cobalt species could react with alkyl halide to yield the corresponding intermediate (**A**) *via* classical S_N2 pathway. The Co–C bond from this alkyl–[Co^{III}] intermediate can be easily cleaved under visible light irradiation to form an active [Co^{II}] species and an alkyl radical (**B**). Then the alkyl radical undergoes intramolecular radical addition followed by recombination with [Co^{II}] to generate species

(**D**). Upon irradiation, the β hydrogen elimination takes place to yield the Heck product together with [Co^{III}]–H to close the cycle.

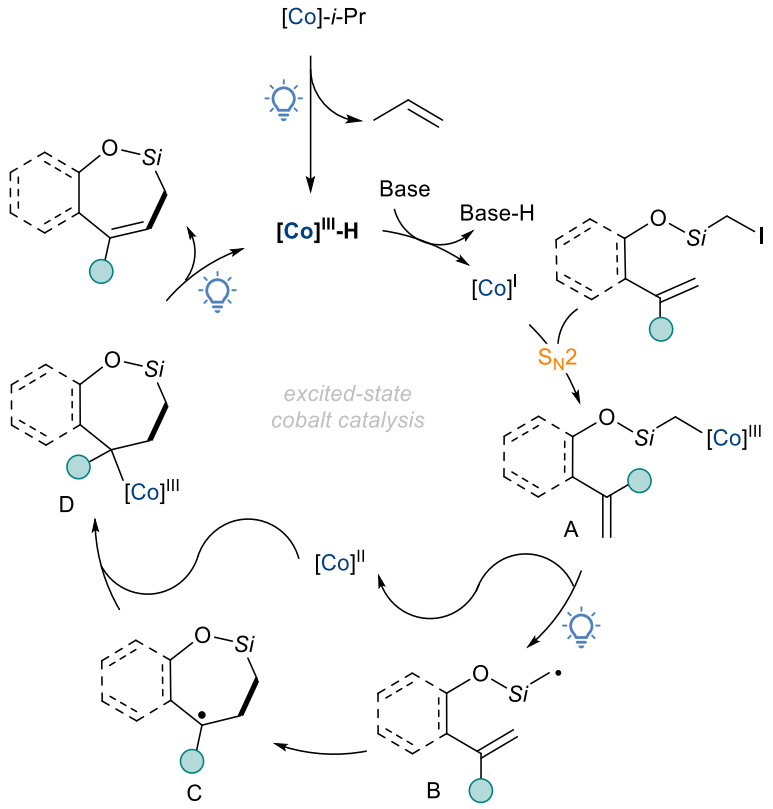

Scheme 3.8. Proposed mechanism for intramolecular endo-selective Heck reaction utilizing cobaloxime.

3.7. Conclusion

In conclusion, the *endo*-selective cyclization of iodomethylsilyl ethers derived from phenols and aliphatic compounds was catalyzed by cobaloxime under mild conditions. Through the integration of various experimental and theoretical approaches, a detailed mechanistic study was conducted. NMR spectroscopy revealed the catalytic activation steps upon irradiation, which were further validated by spin trapping experiments. Low-temperature EPR spectroscopy confirmed the formation of active [Co^{II}] species and the rapid establishment of a steady state during the reaction. Additionally, a radical propagation mechanism was ruled out based on light on-off experiments and the determination of quantum yield. Finally, a plausible mechanism for the intramolecular *endo*-selective Heck reaction was proposed, which were further supported by DFT calculations.

Chapter 4: Cobaloxime-catalyzed biomimetic dehydroamination of primary amines

4.1. Backgrounds

Amines are among the most common functional groups in organic molecules, playing a crucial role in the structure of many natural products, pharmaceuticals, and agrochemicals.[113] Given their significance, a variety of mild, site-selective, and straightforward methods for forming C–N bonds have been developed over the years.[114] Additionally, methods for constructing C–C and C–X bonds through deaminative processes are equally important.[115] These strategies can facilitate site- and stereoselective alkyl chain functionalization from such ubiquitous functionality, potentially offering new approaches to retrosynthetic planning and enabling late-stage functionalization of complex molecular structures. Additionally, due to the growing interest in replacing fossil-based chemicals with bio-based alternatives in the chemical industry, the demand for alkenes motifs is raising.[116]

In nature, deamination plays a crucial role in a range of biological processes, encompassing the biosynthesis of natural products and the metabolism of amino acids. For instance, phenylalanine ammonia lyase converts L-phenylalanine to cinnamic acid, a critical precursor for the biosynthesis of lignols, flavonoids, coumarins, aurones, and stilbenes (Scheme 4.1).[117] Based on the mechanism proposal, the activation of amines requires an electrophilic species.[118]

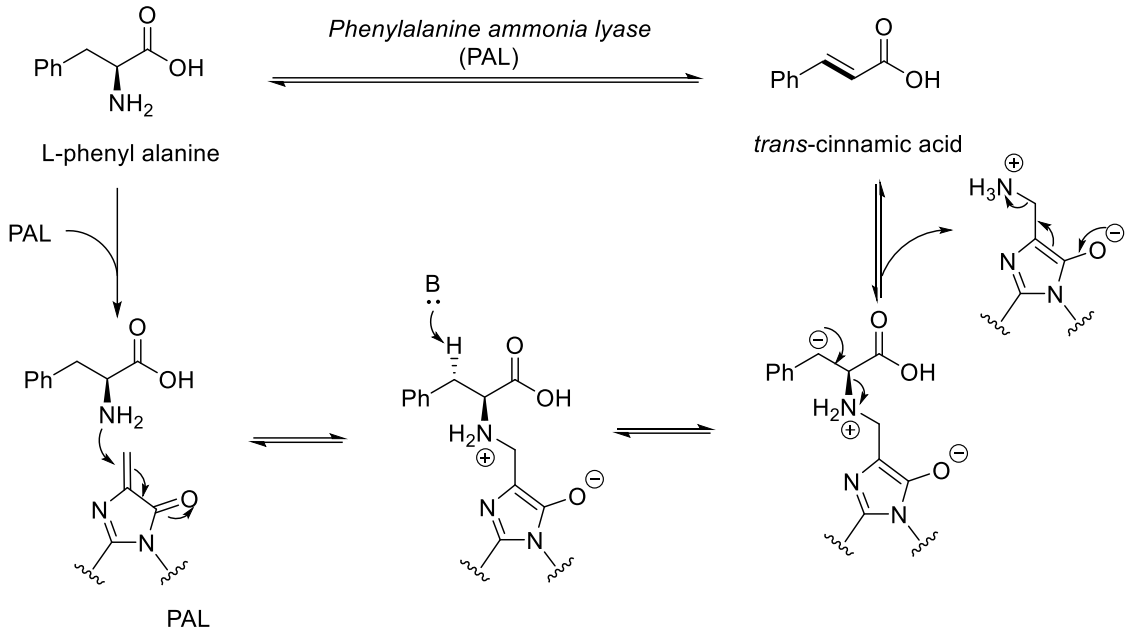

Scheme 4.1. Deamination L-phenylalanine catalyzed by PAL enzyme.

Despite recent advancements in biomimetic synthesis, it is surprising that there is a lack of readily available and mild in vitro methods for converting primary amines into alkenes.[119] The classical pathway for deaminative functionalization is *via* polar mechanism, in which the amine is first converted to a leaving group and undergoes subsequent elimination reactions. The first transformation of primary amines into olefins was developed and also named after Hofmann - a German chemist in 1881 (Scheme 4.2).[120] Hofmann elimination takes place in two-step process, which initially involves exhaustive methylation of primary amines to ammonium salts by treatment with an access amount of methyl iodides. The formed ammonium salts are followed by distillation under low pressure in presence of a stoichiometric strong base such as silver oxide. Although the method needs to be conducted in harsh conditions, it is still found practical in complex molecule synthesis of some natural products.[121]

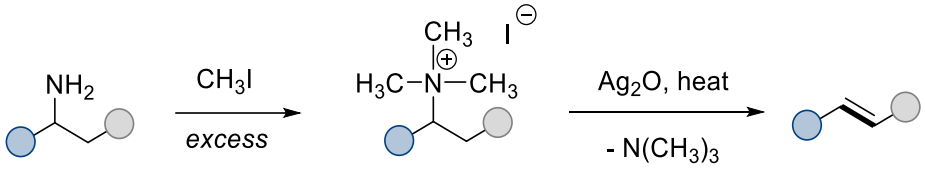

Scheme 4.2. Hofmann elimination process

The second classical strategy to convert amines into olefin is Cope elimination (Scheme 4.3). This transformation also occurs in two steps, starting with the formation of N-oxide species by reducing amines with peroxides. The further elimination to alkenes was taken place by heating up efficiently. Even this transformation is limited to tertiary amines and

requires harsh conditions (high temperature, strong oxidants), the method is still applied recently in synthesis of an alkaloid through a biomimetic strategy.[122]

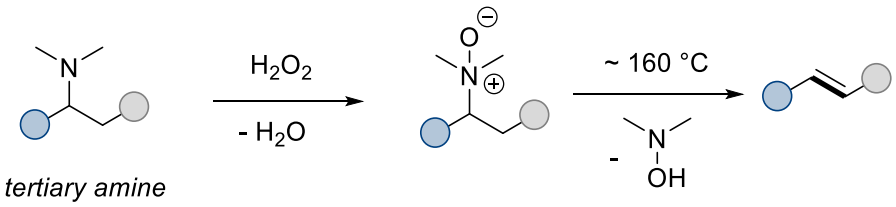

Scheme 4.3. Cope elimination process.

Surprisingly, the Burgess reagent, which is often used to convert alcohols into alkenes, has not been adopted to defunctionalize primary amines.[123] Instead of producing alkenes, the reaction between Burgess reagents and amines can only yield sulfamides.[124]

Additionally, another method of constructing C=C bonds from amines is by functional transformation of amines.[125] Specifically, a cascade of [1,2]-Stevens arrangements/ Hofmann-type elimination events is recently used to synthesize nature products (Scheme 4.4).[121a] This transformation is initiated by a cleavage of one of the C–N bond of tertiary amine and formation of C–C bond *via* alkylation process. The newly formed amine is subjected elimination process to yield the corresponding olefin.

Scheme 4.4. A cascade of [1,2]-Stevens arrangements/ Hofmann-type elimination events.

Following this strategy of masking amines, Katritzky and co-workers developed a method as a mild alternative to Hofmann elimination in 1982 (Scheme 4.5).[126] The approach begins with the condensation of amines with commercially available pyrylium ions to yield the corresponding bench-stable pyridinium salts. These ammonium salts follow the subsequent thermolysis at 150-180 °C to generate the respective olefins. In addition, the same group also demonstrated that these bulky pyridinium salts can act as efficient electrophiles to further functionalize amine through nucleophilic substitution reaction.[127]

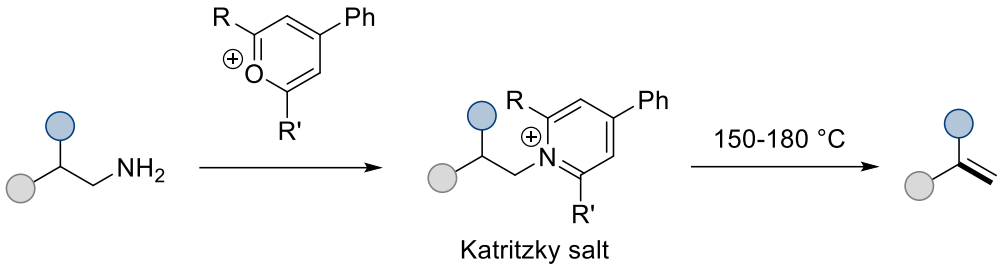

Scheme 4.5. Pyrylium-mediated conversion of primary amines into olefins via Katritzky salt

Besides the ability to engage in nucleophilic substitution, the Katritzky salts are also known as radical reservoirs to provide selective alkyl radical.[119] This behavior relies on the effective reduction of the C(sp^3)–N bonds of pyridinium substitution group that facilitate fragmentation.[128] Additionally, the low reduction potentials ($E_{1/2}$ ~ –0.90 V vs. SCE in DMF) of pyrdinium salts make them excellent electron acceptors in the redox reaction.[129] This would enable the formation of alkyl radicals in milder conditions just by applying the suitable photocatalyst reaction. Under the irradiation with the excited-state of photocatalyst, the singly reduced pyridinium salt is rapidly decomposed to the 2,4,6-triphenylpyridine and the respective alkyl radical via SET process.

Inspired from the nature transformation by phenylalanine ammonia lyase, a non-enzymatic catalytic system has been proposed to convert amines into valuable alkenes (Scheme 4.6). Based on the literature, the approach of generating C-centered radicals *via* cleaving the C–N bonds under mild condition seems like a promising alternative to classical elimination. To facilitate the cleavage of C–N bonds, primary amines are first converted into pyridinium salts using commercially available 2,4,6-triphenylpyrilium salts. Next, photocatalysts, such as organic dyes or transition metal complexes, are employed to generate alkyl radicals. A key challenge in this process is the rapid reduction of these radicals, which can lead to the formation of alkanes instead of alkenes. To address this, cobaloxime catalysis is introduced to control alkene formation based on the experiences in desaturation process from previous chapters. This approach is inspired by the natural role of methylcobalamin, which acts as a reversible free radical carrier, stabilizing reactive methyl radicals *via* weak carbon–cobalt bonds.[37, 130] Therefore, the synergistic use of two photoactive catalysts—an organic dye and cobaloxime—enables efficient dehydroamination of primary amines under mild conditions.

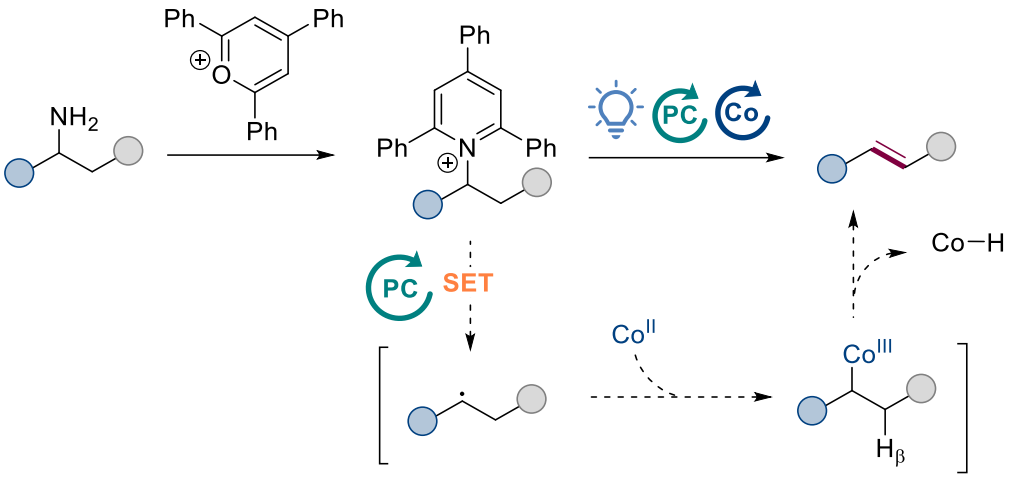

Scheme 4.6. Strategic design of dehydroamination of primary amines

4.2. Screening of reaction conditions

In this section, Dr. Chenyang Wang screened the optimal reaction conditions, with respect to the catalyst, the solvent and the base. The results are summarized in Table 4.1. In this optimization, amino acid **3.1a** derived from phenylalanine was chosen as a model system to mimic the transformation by phenylalanine ammonia lyase.

Table 4.1. Screening of the reaction conditions for the remote desaturation of amide

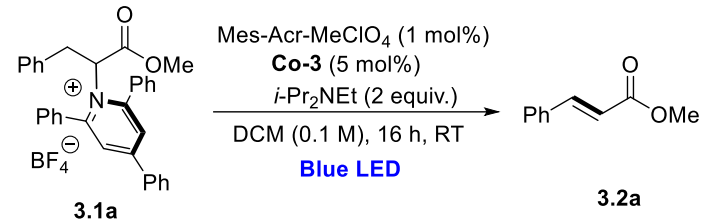

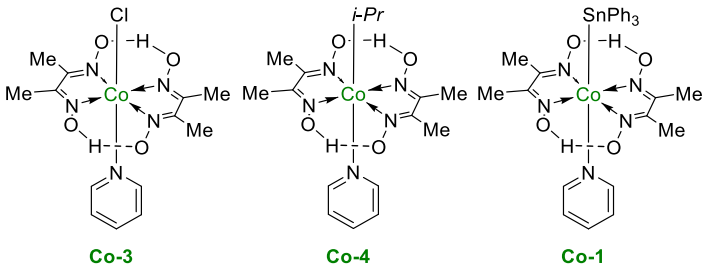

Entry	Deviations from standard conditions	Yield (%)	*E:Z* ratio
1	None	84	>20:1
2	Mes-Acr-MeBF$_4$ as PC	82	>20:1
3	Eosin Y as PC	22	>20:1

4	Riboflavin as PC	38	10:1
5	4CzIPN as PC	40	>20:1
6	CH_3CN as solvent	80	>20:1
7	DBU as base	37	>20:1
8	K_2CO_3 as base	trace	--
9	Et_3N as base	30	10:1
10	**Co-4** instead of **Co-3**	82	>20:1
11	**Co-1** (single catalyst)	23	15:1
12	No light/PC/Co/base	n.r.	--

The optimized reaction conditions utilized two commercially available catalysts: Mes-Acr-$MeClO_4$ (1 mol%) and **Co-3**, (5 mol%). The reaction was performed in a 0.1 M solution of dichloromethane (DCM) with 2 equivalents of diisopropylethylamine (*i*-Pr_2NEt) as the base, under blue LED irradiation at room temperature. Under the optimized conditions (entry 1), the reaction achieves an 84% yield with excellent *E*-selectivity (*E:Z* ratio >20:1). Substituting Mes-Acr-$MeBF_4$ for Mes-Acr-$MeClO_4$ as the photocatalyst maintains a high yield and stereoselectivity (entry 2). However, less oxidizing photocatalysts, such as Eosin Y (entry 3), Riboflavin (entry 4), and 4CzIPN (entry 5), result in significantly lower yields, although the *E*-selectivity remains high for most cases, with the exception of Riboflavin (10:1 *E:Z* ratio).

Changing the solvent from dichloromethane to acetonitrile has minimal effect on the outcome, with only a slight decrease in yield (entry 6). In contrast, altering the base has a much more pronounced effect. While DBU provides a moderate yield of 37% (entry 7), using inorganic base like K_2CO_3 leads to only trace amounts of product (entry 8), and triethylamine gives a low yield of 30% with diminished stereoselectivity (10:1, entry 9).

When the cobalt catalyst **Co-4** is used instead of **Co-3**, the yield and selectivity remain high (entry 10). However, when a single bifunctional catalyst **Co-1** is employed, both the yield and *E:Z* ratio drop significantly (entry 11). Finally, control experiments omitting any key component of the reaction (light, photocatalyst, cobalt catalyst, or base) result in no reaction (entry 12), confirming the essential roles of these elements.

4.3.Scope of deammoniation of primary amines

After establishing the optimal reaction conditions, the scope of the photoexcited cobalt-catalyzed dehydroamination of various Katritzky salts was explored (Scheme 4.7). The developed method proved to be highly versatile and exhibited tolerance toward a broad range of substrates, including primary amines, amino acids, natural products, and drug molecules (**3.1a**-**3.1ad**).

The exploration began with amino acid derivatives, where methyl and benzyl phenylalanine derivatives were successfully transformed into the corresponding cinnamates **3.2a** and **3.2b**, yielding 82% and 85% respectively. Phenylalanine derivatives bearing electron-withdrawing groups (**3.2c**-**3.2e**) furnished α, β-unsaturated esters, while electron-rich tyrosine selectively produced trans-cinnamate **3.2f**. Additionally, homophenylalanine gave ester **3.2g** with an 80% yield and moderate *E* selectivity. Aliphatic amino acids like leucine and norleucine afforded the unsaturated esters **3.2h** and **3.2i** in excellent yields. Notably, methionine, a sulfur-containing amino acid, selectively yielded the *E*-alkene **3.2k** with 71% yield, while dicarboxylic acids aspartic and glutamic acid produced **3.2l** and **3.2m**, with 60% and 71% yields respectively. Additionally, asparagine and glutamine, with their amide functionalities, furnished olefins **3.2n** and **3.2o** with high yields and stereocontrol. Even lysine and tryptophan, which contain polar and heterocyclic groups, provided the corresponding olefins **3.2p**-**3.2r** with good yields and excellent stereoselectivity.

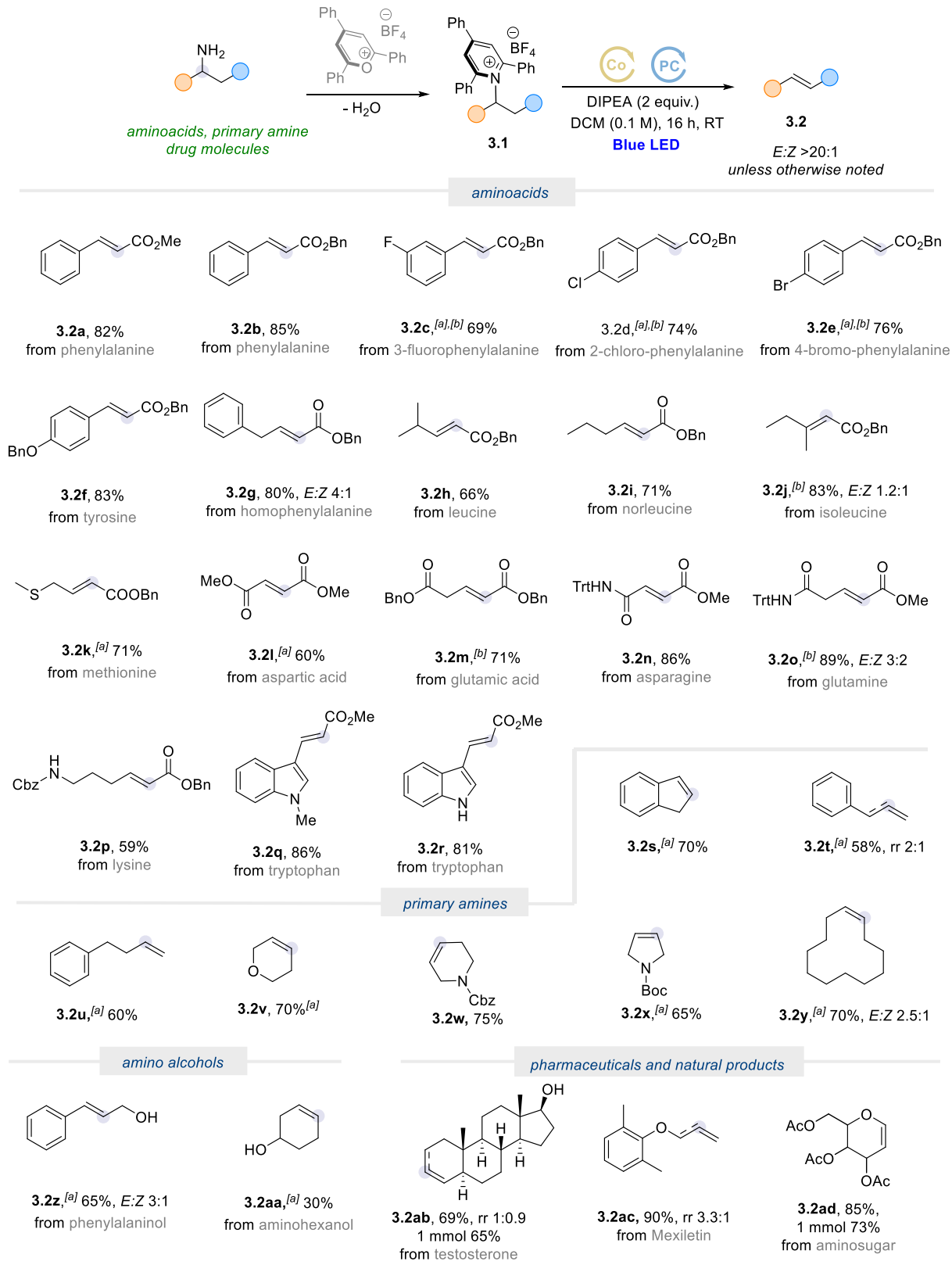

Scheme 4.7. Reaction scope of dehydroamination of primary amines. Standard conditions: pyridinium salt (0.2 mmol), ***Co-3*** *(0.01 mmol, 0.8 mg), Acr-MeClO₄ (0.002 mmol, 0.8 mg), i-Pr₂NEt (0.4 mmol, 70 µL), DCM (2 mL), RT, 16 h, the reported yields refer to the conversion of the pyridinium salts to the olefins. [a]NMR yield. [b]Contains minor amount of hydrodeamination by-product.*

Moving beyond amino acids, the reaction also demonstrated tolerance with primary amines. For example, 2-aminoindane, a designer drug, was converted into indene **3.2s** in 70% yield. Amphetamine yielded a mixture of terminal and internal olefins **3.2t** in a 58% yield, due to the competition between benzylic and terminal hydrogen atom abstraction. However, 4-phenyl-2-butanamine selectively produced the terminal alkene **3.2u**. Cyclic amines, including pyrrolidine derivatives (**3.2w**-**3.2y**), were also well-tolerated, with excellent regioselectivity seen in the formation of **3.2x**, highlighting the cobalt catalyst's tendency to abstract the less hindered β-hydrogen atom. Notably, phenylalaninol yielded cinnamyl alcohol **3.2z** in 65% yield, further demonstrating the method's functional group tolerance.

In addition to simpler substrates, the protocol was applied to more complex molecules. A testosterone derivative was dehydroaminated to form olefin **3.2ab**, albeit as a mixture of regioisomers. Mexiletine, a cardiac drug, was converted into its terminal olefin **3.2ac** with moderate regioselectivity. Notably, an application of a β-aminoglucose derivative led to the unsaturated deoxysugar **3.2ad** with the elimination of the β-OAc group instead of the β-hydrogen.

The method shows broad applicability across a wide range of substrates, including amino acids, primary amines, amino alcohols, and pharmaceuticals, providing excellent yields and stereoselectivity under mild conditions. The system effectively transforms these diverse molecules, showcasing its potential for synthetic applications in drug development and complex molecule modification.

4.4. Mechanistic insights

4.4.1. Fluorescence quenching experiment

To determine the competent quencher of the excited-state photocatalyst, a series of fluorescence measurements with Mes-Acr (0.02 mM in acetonitrile) was performed along different components in the reaction system (**Co-4**, substrate **3.1a** and DIPEA) at room temperature under inert atmosphere. Before each measurement, the cuvettes were degassed by Schlenk technique. The solutions were irradiated at 450 nm and fluorescence was recorded at 540 nm. The results are illustrated in Figure 4.1.

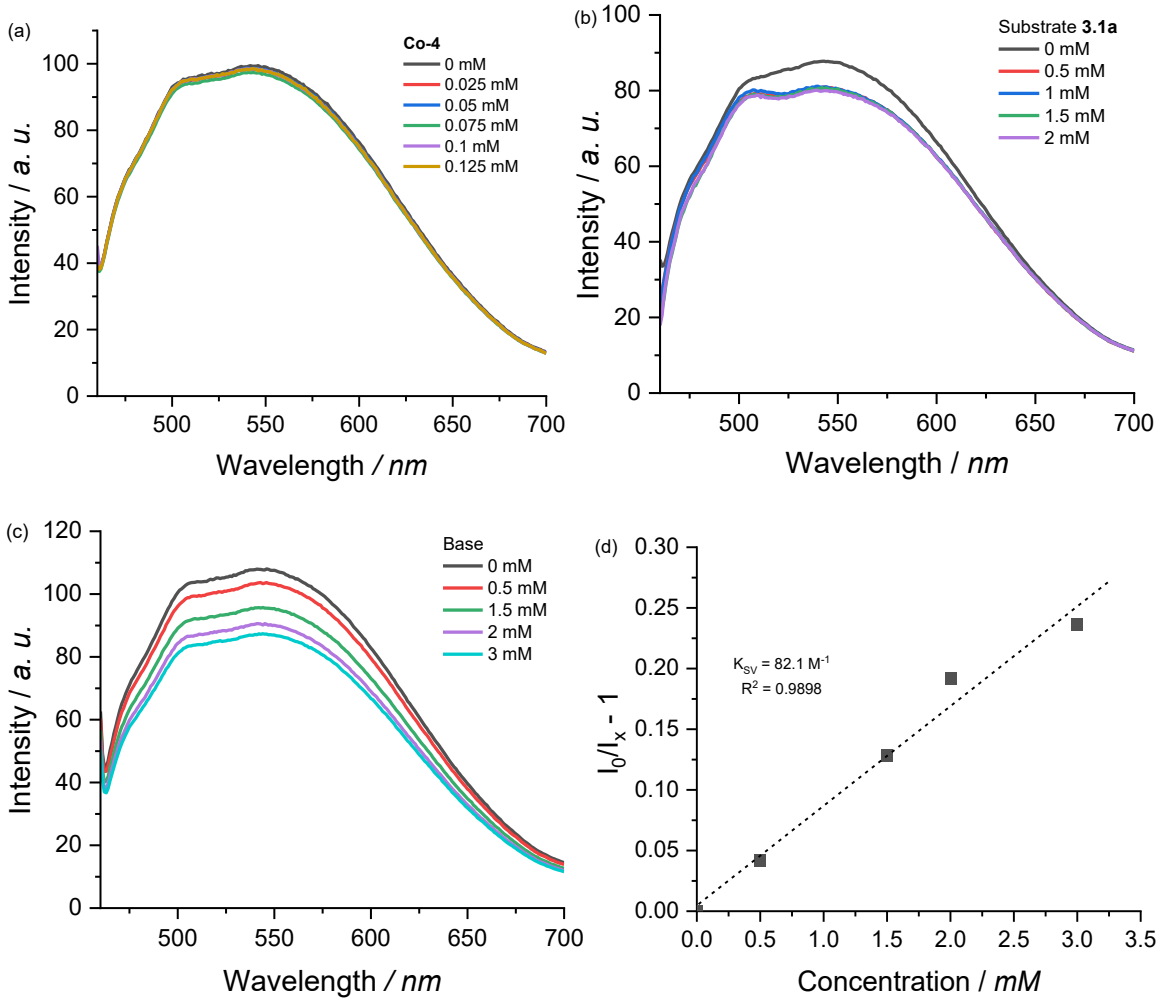

Figure 4.1. Fluorescence spectra of Mes-Acr with the presence of different concentration of (a) Co-4, (b) Substrate 3.1a and (c) DIPEA; (d) Stern-Volmer plot for fluorescence quenching of Mes-Acr with DIPEA.

According to the fluorescence spectrum of Mes-Acr, no quenching of the excited-state photocatalyst (Mes-Acr*) was observed upon the addition of varying amounts of **Co-4** and substrate **3.1a** (Figure 4.1a,b). However, increasing the concentration of DIPEA in the solution led to a gradual decrease in the emission intensity of the photocatalyst, indicating that a quenching process was taking place (Figure 4.1c). By plotting the Stern-Volmer plot, the quenching constant (K_{SV}) of 82.1 M^{-1} was obtained, confirmed that DIPEA acts as an effective quencher for Mes-Acr* (Figure 4.1d). Due to the availability of electron in DIPEA, a reductive quenching cycle, where a SET from the base to the excited state of the photocatalyst, is suggested to take place (Scheme 4.8).

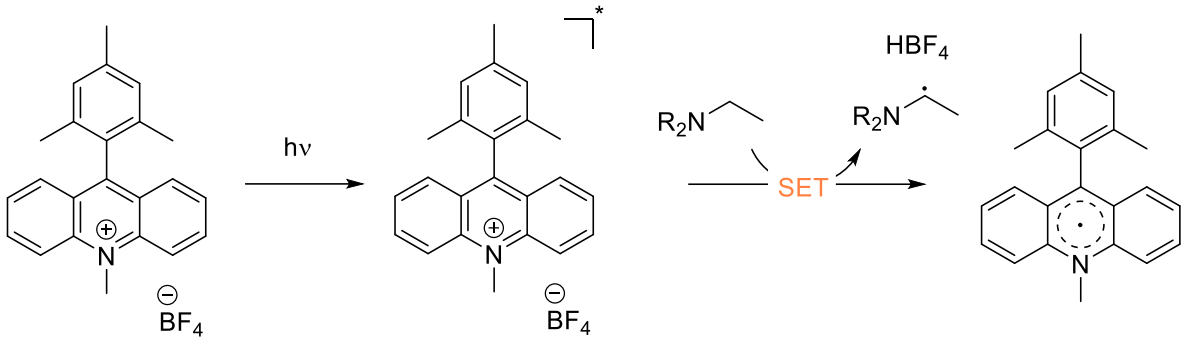

Scheme 4.8. Plausible reductive quenching pathway of Mes-Acr by DIPEA.*

4.4.2. EPR spectroscopy

To detect open-shell species in the system, EPR spectroscopy was acquired. The results are shown in Figure 4.2.

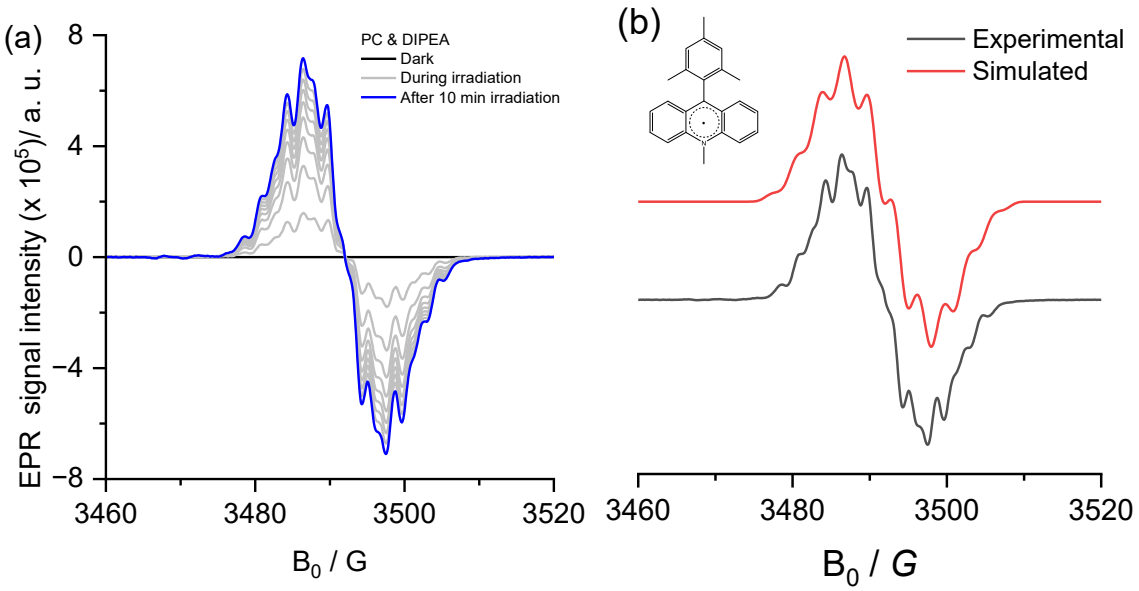

Figure 4.2. a) EPR spectra of the mixture between photocatalyst and DIPEA during the irradiation; b) Experimental and simulated EPR spectrum of the Mes-Acr• signal.

For the investigation of initial steps in the reaction, the photocatalyst was added together with the base and no EPR signal was observed in the dark (Figure 4.2a, black line). However, upon irradiation, a complicated signal of free radical at g = 2.0043, which was assigned to delocalize in the acridinium part of the photocatalyst, was detected.[131] This radical is supposed to be resulted from a quenching process of Mes-Acr* by DIPEA (Figure 4.2b). The gradual increase of the Mes-Acr• signal during prolonged irradiation suggested that the quenching process kept occurring. Theoretically, the quenching process takes place by a SET, meaning that there should be an additional existence of a radical

from DIPEA (Scheme 4.8). However, we could not observe any signals from this species, probably due to the dominance of Mes-Acr• signal.

4.4.3. Spin trapping experiments

To identify the type of radical existing in the system of Mes-Acr, DIPEA and substrate **3.1a**, an addition of DMPO to the solution was carried out. The measurement with EPR spectroscopy pointed out the existence of an organic radical through the signal of DMPO–C adduct (a_N = 14.4 G, a_H = 21.5 G) (Figure 4.3).

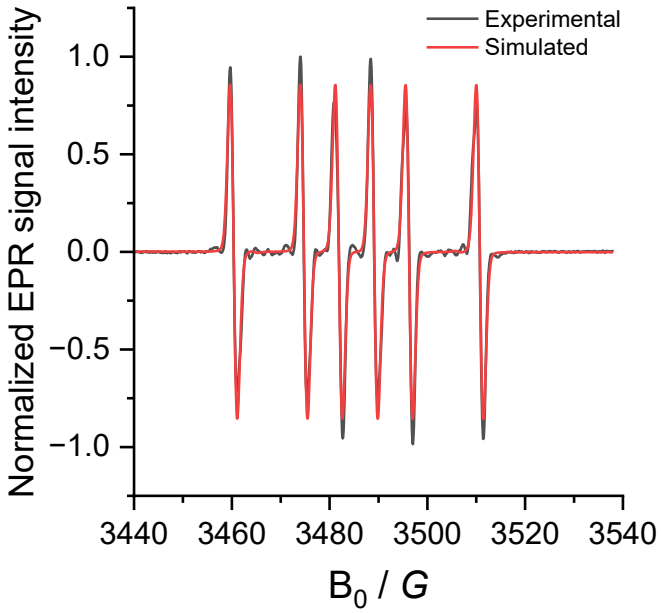

Figure 4.3. Experimental and simulated EPR spectrum of the irradiated mixture between PC and DIPEA after the addition of Substrate and DMPO.

This C-radical might be generated via a SET process from an existed radical to substrate **3.1a**. To identify the source of this radical, an additional experiment, where **3.1a** and DMPO were added to the irradiated DIPEA solution, was conducted (Figure 4.4).

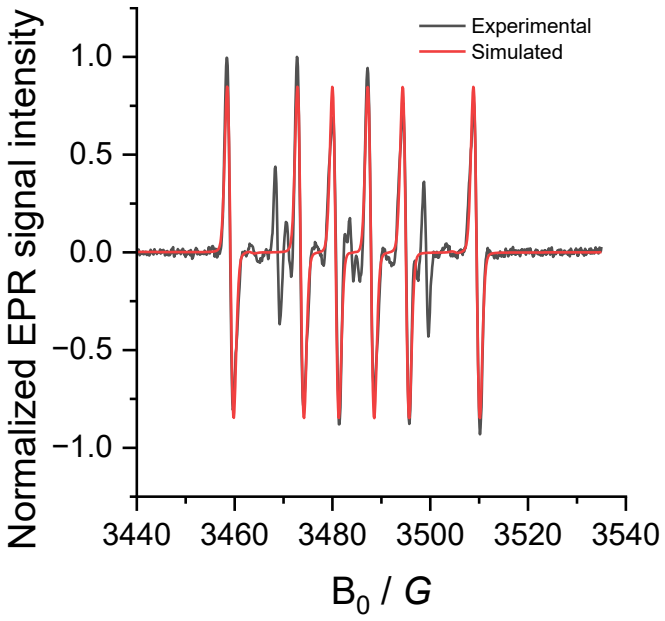

Figure 4.4. Experimental and simulated EPR spectrum of the irradiated DIPEA solution after the addition of Substrate and DMPO. The simulated result supports the formation of DMPO-C adduct (a_N = 14.4 G, a_H = 21.5 G) besides the appearance of addition signals.

Based on the literature, the irradiation of DIPEA in DCM released α-amino radical, which was also obtained by the reductive quenching of Mes-Acr*.[132] The output of the experiment also contained DMPO–C adduct as in previous one, suggesting a tentative substrate activation pathway from base radical (Scheme 4.9).

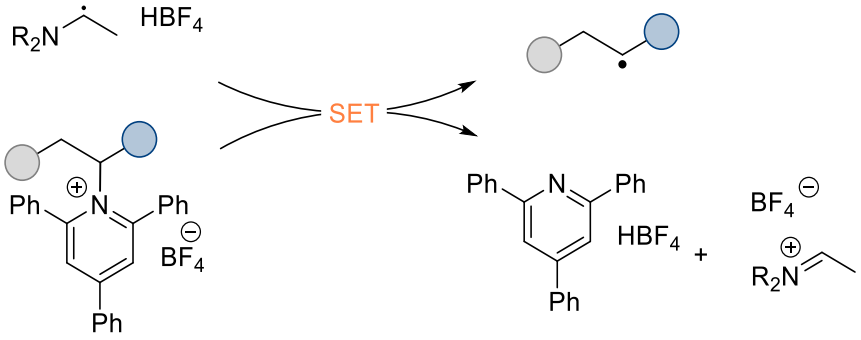

Scheme 4.9. Plausible pathway of substrate activation.

4.4.4. Low temperature EPR spectroscopy

To monitor the cobalt species during the reaction, a stepwise EPR experiment was conducted. The results are illustrated in Figure 4.5.

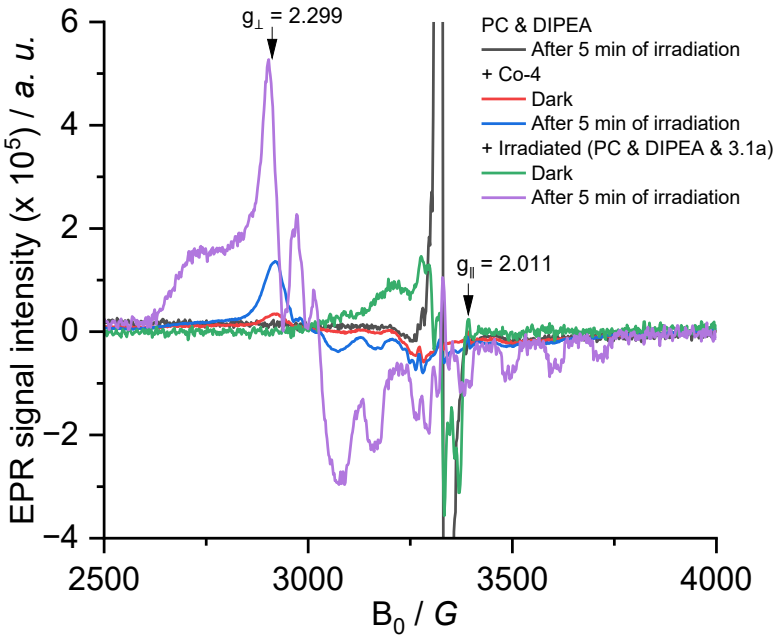

*Figure 4.5. EPR spectra recorded at -173 °C of the irradiated mixture of PC and i-Pr$_2$NEt with the addition of **Co-4**, then subsequential addition of the irradiated solution of PC, i-Pr$_2$NEt and substrate **3.1a**.*

At low temperature (-173 °C), the EPR spectrum obtained from irradiating the mixture of Mes-Acr and DIPEA exhibited an overload signal of Mes-Acr• (black line). Subsequently, the addition of **Co-4** to this mixture replaced this radical by an EPR active – [Co^{II}] species at $g_\perp$ = 2.299 and $g_\parallel$ = 2.011 (red line). This substitution can occur via a SET process, in which an electron from Mes-Acr-Me• donates to [Co^{III}] to form [Co^{II}], and simultaneously regenerating the initial Mes-Acr state to close the photoredox cycle. The intensity and resolved signal of [Co^{II}] species can be further improved by re-irradiating the mixture (blue line). Next, this mixture was added successively an irradiated solution of PC, Substrate and DIPEA, which contains a substrate radical species. This addition resulted in a disappearance of [Co^{II}] signal, indicating that the generated [Co^{II}] reacted with the substrate radical to form an inactive EPR species - [Co^{III}]–substrate complex (green line). However, irradiating the mixture led to a reappearance of [Co^{II}] species in a more intensive and highly resolved EPR signal, suggesting that more Co was involved into the catalytic cycle (purple line). The broadening in perpendicular region of [Co^{II}] signal implies the cluster formation, which might indicate for a deactivation pathway.

4.5. DFT calculation

To support the results from spectroscopic method, DFT calculations were conducted by Dr. Luis Miguel Azofra. The results of calculating potential energy surface using **3.1a** as model substrate are illustrated in Figure 4.6.

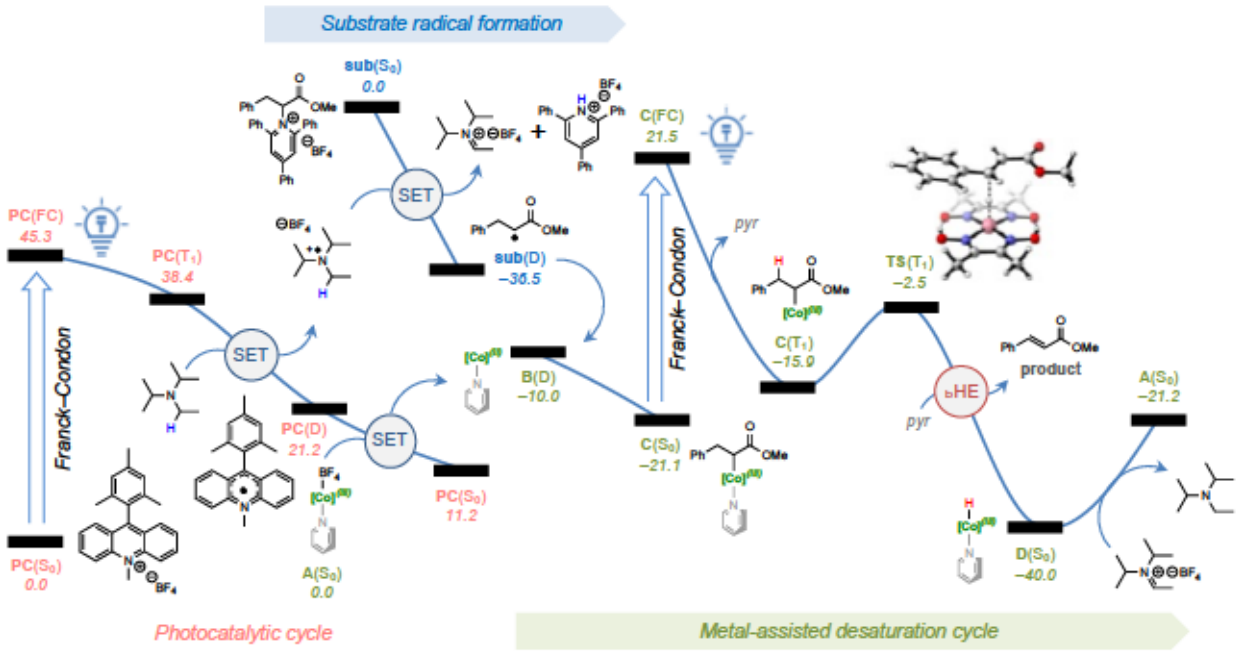

Figure 4.6. Potential energy surface (PES) for the light-assisted deamination process constituted by the photocatalytic cycle, substrate radical formation, and metal-assisted desaturation cycle. Free energies (room temperature) are shown in kcal mol^{-1} at the BP91/TZVP//BP91/SVP computational level, using acetonitrile (e = 35.688) as solvent.

DFT calculations revealed that the photocatalyst undergoes light-induced vertical Franck-Condon excitation to its triplet state [**PC**(FC)] at 45.3 kcal/mol. After relaxation, it transitions to a more stable triplet state [**PC**(T_1)] at 38.4 kcal/mol. This highly oxidizing excited species undergoes SET from *i*-Pr_2NEt, reducing the acridine photocatalyst to the radical Mes-Acr-Me• in its doublet state. The reductive quenching process is thermodynamically favorable, releasing 17.2 kcal/mol. As shown by EPR spectroscopy, the complexation of *i*-$Pr_2NEt^{\bullet+}$ and HBF_4 facilitates the exergonic formation of a carbon-centered radical, releasing 36.5 kcal/mol.

Upon the addition of the pyridinium salt **3.1a**, an organic radical intermediate in the doublet state (**sub**(D)) is formed. This intermediate is then trapped by [Co^{II}] species, which are generated *via* a spontaneous SET from the photocatalyst in its doublet state [**PC**(D)], leading to the formation of a highly stable [Co^{III}]–substrate complex, **C**(S_0), at –21.1 kcal/mol. This stabilization is due to the photolysis of relatively weak C(sp^3)–[Co^{III}] bonds (with bond dissociation energy, BDE, less than 30 kcal/mol).

Further excitation of **C**(S_0) by light results in the Franck-Condon triplet state [**C**(FC)], which relaxes to the triplet state [**C**(T_1)], releasing pyridine in the process. In this triplet state, β-hydrogen elimination occurs, leading to substrate desaturation and the formation of a [Co^{III}]–H complex, **D**(S_0), *via* homolytic cleavage of the C(sp^3)–[Co^{III}] bond. The

transition state for this process, **TS**(T_1), was calculated to be just 12.8 kcal/mol above the free energy of **C**(T_1). Finally, the [Co^{III}]–hydride complex regenerates *i*-Pr_2NEt and complex **A**(S_0), thereby completing the catalytic cycle.

4.6. Proposed mechanism

By combining the results from experimental and theoretical methods, the proposed reaction mechanism for the dehydroamination of primary amines reaction is depicted in Scheme 4.10.

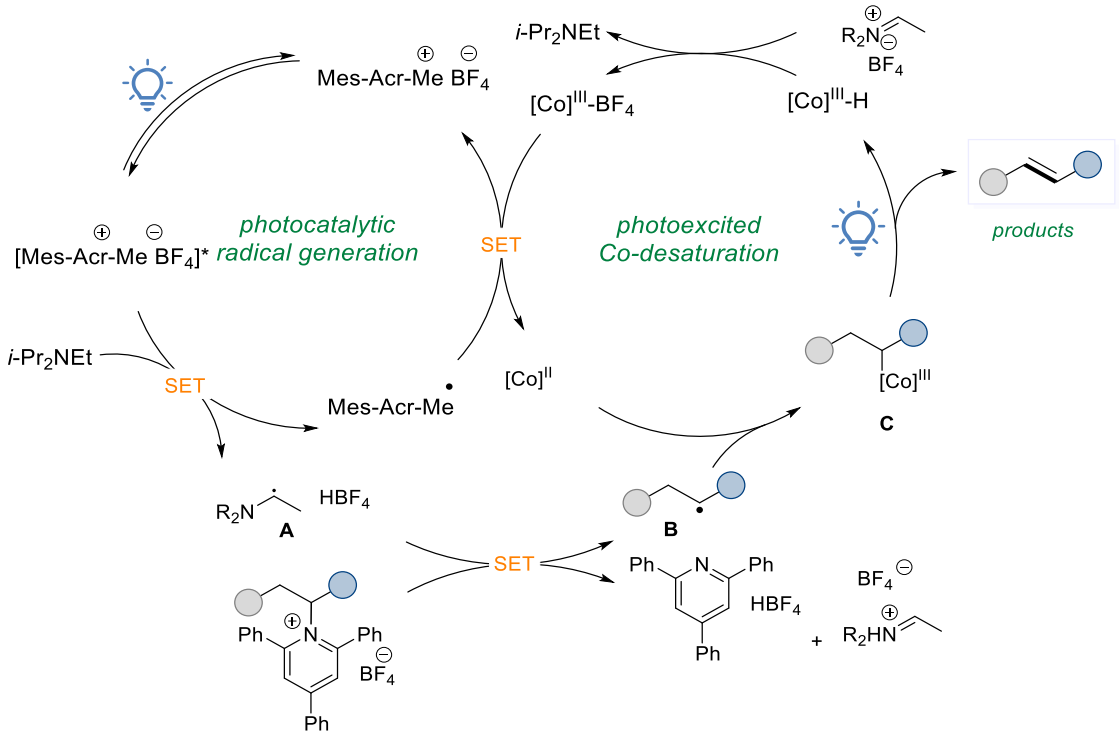

Scheme 4.10. Proposed mechanism for dehydroamination of primary amines reaction utilizing dual photoredox-cobaloxime catalysis.

Initially, the photocatalyst Mes-Acr-Me BF_4 is excited by light to form its active state [Mes-Acr-Me BF_4]*, which undergoes SET with diisopropylethylamine (*i*-Pr_2NEt), producing the radical species Mes-Acr-Me• and *α*-amino radical (**A**). The amine radical further participates in a SET with a Katritzky salt, leading to the formation of an open-shell intermediate (**B**). This organic radical is trapped by a cobalt [Co^{II}] species, which has been generated *via* a spontaneous SET from the photocatalyst. The resulting [Co^{III}]–substrate complex (**C**) undergoes β-hydrogen elimination through homolytic cleavage of the weak C(sp^3)–[Co^{III}] bond, yielding the desaturated product and a [Co^{III}]–H species. The product is released, and the cobalt catalyst is regenerated, thus completing the catalytic cycle.

4.7. Conclusion

In conclusion, we have reported a straightforward conversion of various primary amines, including amino acids, natural products, and drug molecules, into their respective alkenes with high trans-selectivity. This biomimetic transformation was achieved using a dual organic dye/photoexcited base metal catalysis system under visible light irradiation at room temperature. The protocol offers the flexibility to employ a diverse range of common amino acids and allows for the late-stage functionalization of drug molecules. Given its simplicity, effectiveness, mild reaction conditions, and broad applicability, we anticipate that this photocatalytic deaminative desaturation method will find widespread use in both academic and industrial settings.

Chapter 5: Cobalt(salen)-catalyzed remote γ, δ – desaturation and functionalization of aliphatic alcohols

5.1. Background

Aliphatic alcohols, which are easily obtainable and commonly utilized in bulk chemicals, play a crucial role as building blocks in organic chemistry.[133] However, selectively functionalizing these alcohols along the carbon chain is difficult because of the unreactive nature of C(sp^3)–H bonds and the challenges associated with achieving regioselectivity. To address these difficulties, remote functionalization of aliphatic alcohols has emerged as a powerful strategy, enabling selective modifications at positions distant from the functional group.[134] This method also promotes more sustainable chemical synthesis by reducing the need for pre-functionalized starting materials and minimizing synthetic steps.

A classical approach to achieve C(sp^3)–H functionalization is metalation *via* palladium catalysis (Scheme 5.1).[135] This strategy requires an external chelating group preinstalled onto the hydroxyl group to accelerate and direct cyclometallation, which facilitate the concerted metalation-deprotonation (CMD) pathway.[136] Driven by the ring strain of the cyclometallated intermediate, most of the products are limited in β-C–H activation. Additionally, this strategy also faces significant challenges that limit its practical applicability, such as being restricted to less hindered like primary C–H bonds. Thus, the remote functionalization of more sterically hindrance C–H bonds in aliphatic alcohols while achieving rarer regioselectivity remains intriguing.

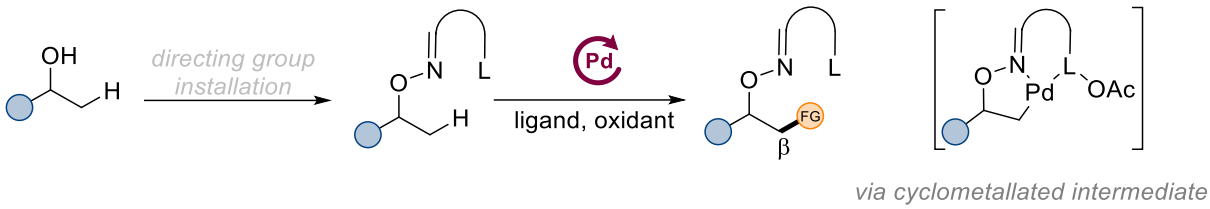

Scheme 5.1. Remote functionalization of alcohols by palladium catalysis

Another approach to achieve high regioselectivity of remote C–H functionalization involves radical mediation, which relies on the participant of intramolecular H-atom transfer (i-HAT) processes.[137] A typical example of this method involves generating

alkoxy radical intermediates directly at the hydroxyl group, frequently leading to complete δ-functionalization *via* selective internal 1,5-HAT (Scheme 5.2).[138] However, these alkoxy radical intermediates are usually challenging to handle and require harsh conditions for their generation. In addition, to generate the alkoxy radical, this method requires the pre-activation of alcohols and the corresponding precursors, such as nitrite esters, peroxy compounds, N-alkoxylpyridine-2-thiones, lead (IV) alkoxides or using strong acids, high energy UV light.

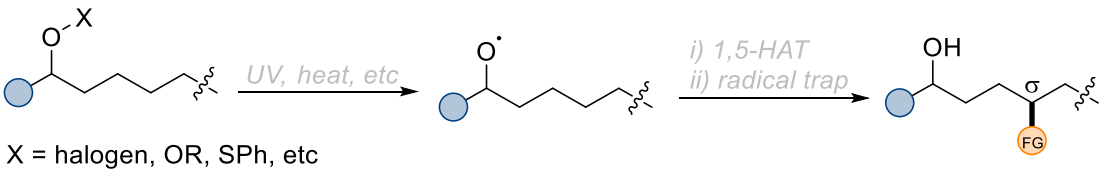

Scheme 5.2. Radical-mediated remote functionalization of alcohols via alkoxy radical

To achieve the regioselectivity at more challenging positions, using a radical chaperone as an alternative group to guide functionalization was found as an effective strategy.[139] In pioneering works by Roizen and Zare, the authors masked the aliphatic alcohols by sulfamate esters to guide functionalization at γ position. The use of this esters as radical auxiliaries demonstrated the effectiveness of this approach to promote the kinetically disfavored 1,6-HAT process.[140] This could be supported by the nature of sulfone group, as their elongated O–S and S–N bonds (ca. 1.58 Å) and compressed O–S–N bond angles (ca. 103°) geometrically favor a seven-membered-ring transition state for C–H abstraction.[140b] The radicals are proposed to be generated at nitrogen atom, which is reminiscent of the Hofmann–Löffler–Freytag amine synthesis.[141] These N-centered radicals would follow the 1,6-HAT process afterwards to deliver the radicals to γ position. Despite the versality to proceed under mild conditions, the requirement to install desired functional group onto the chaperone limits its applications.

Inspired by these works, the idea of utilizing vinyl sulfone, a much cheaper and commercially available reagent, for remote γ-functionalization of aliphatic alcohols is developed (Scheme 5.3). Indeed, using vinyl sulfone can reduce the cost for installing radical tether by two orders of magnitude than sulfamate reagent. To initiate radicals from C(sp^2) center in controlled manner, metal hydride-catalyzed HAT (MHAT) is chosen due to the well-known reputation for providing selective carbon-centered radicals to alkenes along with a H-atom.[142] This generation of organic radicals, which can easily attach to radicalophiles, allows further chemoselective functionalization under mild conditions.

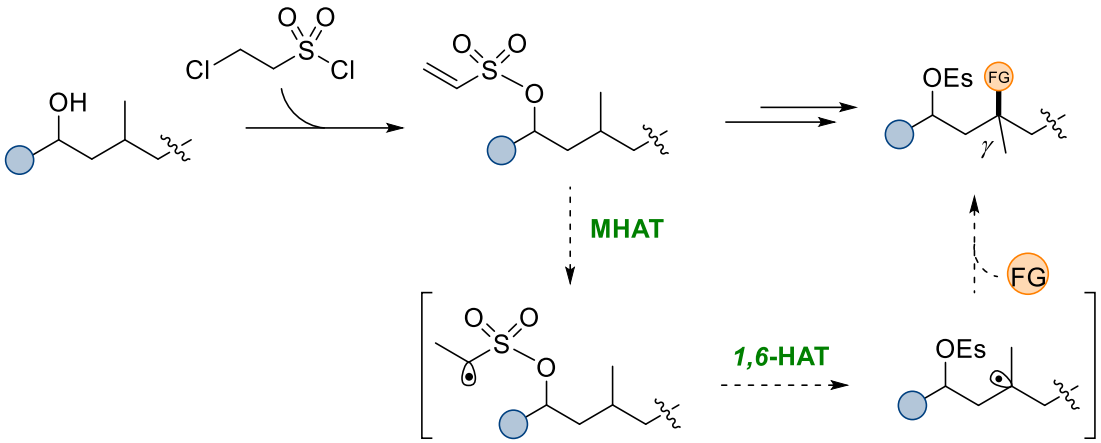

Scheme 5.3. Merging MHAT and 1,6-HAT for remote γ-C(sp^3)–H functionalization of alcohols

To promote the MHAT process, a suitable transition metal needs to be chosen. Depending on the coordination strength of ligand, transition metal-hydride species can be categorized into two groups: strong field and weak field system. The former class uses transition metal having strong field supporting ligands (e.g., carbonyls) for limited reaction such as isomerizations, cyclizations, and hydrogenations. Additionally, the rates of catalysis are generally slow. On the other hand, the second system having weak field supporting ligands based on N or O donors proceeds the reaction more rapid and at room temperature. In this class, the high reactivity of metal-hydride species lies on the formation of weak M–H bonds, which must be compensated by a strong bond in another product. Thus, the catalytic system needs hydride precursors such as silane hydride, which have Si–H bonds can be broken to form a strong bond in another product such as Si–O, Si–F bonds (Scheme 5.4).[142a]

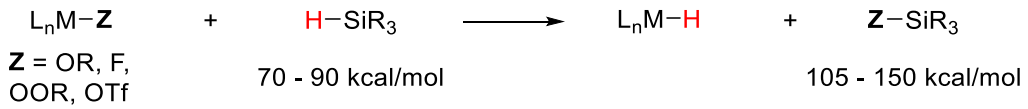

Scheme 5.4. Potential mechanism of metal-hydride formation.[142a]

Among the first-row transition metals, the most popular catalysts for MHAT alkene reactions are salen-supported cobalt complexes, which has proven to be highly active in alkene isomerization, hydroarylation, hydroalkoxylation, and epoxidation.[143] In these reactions, the catalytic system contains cobalt^{II}(salen) precatalyst and a stoichiometric amount of silane. The treatment of this mixture presumably gives cobalt hydride complex, which transfers a H atom to an alkene to form a [Co^{III}]–alkyl complex (Scheme 5.5). The cobalt–carbon bonds can reversibly dissociate to a [Co^{II}] complex and an alkyl radical.

This radical can easily be attached by a radicalophile to form a corresponding functionalized product.

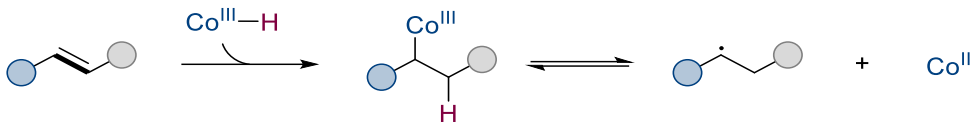

Scheme 5.5. Proposed mechanism of Co–H species catalyzing hydrofunctionalization of alkenes.

5.2. Screening of reaction conditions for remote γ- functionalization

As a proof of concept, remote chlorination was selected as a model transformation. The development of γ-chlorinated aliphatic alcohols is detailed in Table 5.1. Substrate **4.1a**, bearing tertiary γ-C(sp^3)-H bonds, was chosen for the initial optimization of the 1,6-HAT reaction.

*Table 5.1. Screening of reaction condition for γ-chlorination of alcohol **4.1a**.*

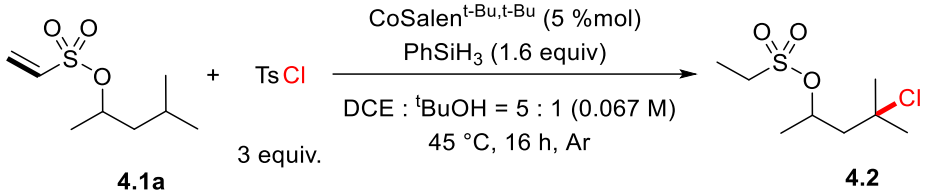

Entry	Deviation from the standard condition	Yield (%)
1	None	84
2	No Co(salen)/ $PhSiH_3$	n.d.
3	50 %mol of $PhSiH_3$	40
4	Et_3SiH instead of $PhSiH_3$	85
5	$PhSi(Oi\text{-}Pr)H_2$ instead of $PhSiH_3$	trace
6	With Selectfluor	88
7	RT instead of 45 °C	25
8	Blue LEDs instead of 45 °C	83
9	DCM/ DCE as solvent	trace
10	N-Chlorosuccinimide instead of TsCl	48
11	1,3-Dichloro-5,5-dimethylhydantoin instead of TsCl	30

The initial run with commercially available Co^{II}(*t*-Bu,*t*-Bu-cyclohexylsalen) (Co(salen)) and stoichiometric amount of $PhSiH_3$ as a typical reductant yielded excellent chlorination exclusively at the γ position by using tosyl chloride as a Cl source in a mixture of DCE and *t*-BuOH (entry 1). Control experiments demonstrated the essential roles of cobalt catalyst and silane for the successful reaction (entries 2&3). Next, the silane source screening revealed that phenyl silane was optimal, as more electron-rich substituents decreasing the yield (entries 4&5). Adding a common oxidant in the Co(salen) system, such as Selectfluor, slightly increased the yield (entry 6). Furthermore, the change from thermal conditions to room temperature reduced the reactivity of the catalyst (entry 7), suggesting the need for additional energy to overcome the reaction barrier. Meanwhile, blue LEDs were also proved to be an alternative energy source to activate the reaction (entry 8). It is worth to mentioned that no reaction took place in the absence of *t*-BuOH (entry 9), indicating the importance of a protic solvent to participate in the reaction as a reagent. Moreover, the selection of Cl source was also investigated. Specifically, other radicalophiles, such as N-succinimide derivatives, were less efficient compared to tosyl chloride (entries 10-12). Consequently, different tosyl derivatives were chosen as radical sources for further corresponding functionalizations.

5.3. Scope for remote γ- functionalization

With the optimal system in hand, the scope of remote functionalization of aliphatic alcohols was investigated (Scheme 5.6). A series of different functionalizations was explored, including halogenation, azidation, cyanation and amination. Firstly, the chlorination reaction showed good tolerance for various aliphatic secondary alcohols containing different substituent groups. Specifically, the method efficiently yields mono-chlorinated alcohol (**4.2b**) at one of the tertiary C(sp^3)–H at γ positions in excellent yield under the optimized condition. Furthermore, this approach allowed for the exclusive functionalization of a 3° γ-C(sp^3)–H bonds in a secondary alcohol (**4.2c**), even in the presence of 2° C–H bonds at another γ position, achieving good yields. Notably, a natural alcohol such as (–)-Menthol underwent the transformation smoothly, producing the desired product (**4.2d**) in 80% yield.

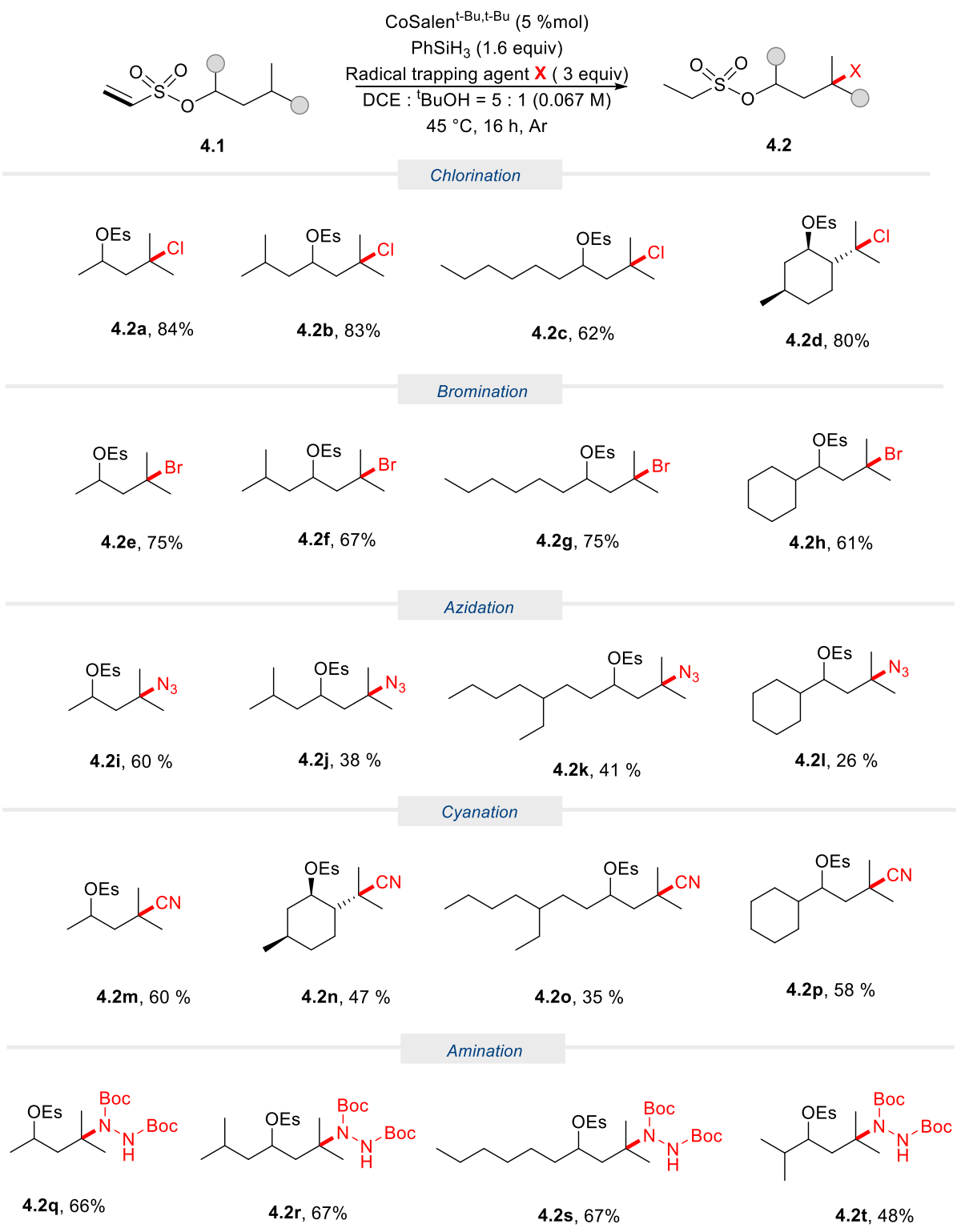

Scheme 5.6. Reaction scope of remote γ- functionalization for aliphatic alcohols. Standard conditions: , alcohols (0.2 mmol), CoSalen$^{t\text{-}Bu,t\text{-}Bu}$ (5 mol%, 6 mg), radical trap (0.6 mmol, 3 equiv.), $PhSiH_3$ (40 μL, 1.6 equiv.), DCE: t-BuOH 5:1 (V:V) (3 mL), Ar, 45 °C, 16h.

Next, the system was evaluated for another halogenated functionalization, such as bromination. Similar to chlorination, various aliphatic alcohols underwent bromination,

yielding the corresponding products (**4.2e-4.2h**) in moderate to good yields. Interestingly, in a competition between cyclic and aliphatic C(sp^3)–H bonds at γ positions, functionalization occurred merely at the latter one (**4.2h**).

However, when the protocol was applied to azidation using tosyl azide, the yields of the obtained products were influenced by the substituents. Specifically, the branched chain (**4.2j**), long straight chain (**4.2k**), and alicyclic structure (**4.2l**) lowered the yields to 38%, 41%, and 28%, respectively. Notably, an alcohol with tertiary C–H bonds at both δ and γ positions was preferentially functionalized at the γ position (**4.2k**). A similar trend was also observed in the cyanation reaction (**4.2m-4.2p**).

Finally, the scope was expanded to test an amination reaction under standard conditions. The steric hindrance of the azodicarboxylate reagent likely contributed to the reduced efficiency of the reaction, resulting in hydrazinated products (**4.2q-4.2t**) in moderate yields. Remarkably, an alcohol with two tertiary C–H bonds at both β and γ positions was exclusively functionalized at the γ position (**4.2t**), demonstrating the method's ability to achieve exclusive regioselectivity at the γ position.

5.4. Screening of reaction conditions for remote γ, δ- desaturation

Besides the investigation of cobalt salen for functionalization *via* MHAT transformation, the system was further examined for remote γ, δ- desaturation. The reaction development is detailed in Table 5.2. Substrate **4.1d**, bearing both tertiary cyclic and aliphatic γ-C(sp^3)-H bonds, was selected for initial optimization.

*Table 5.2. Screening of reaction conditions for remote γ, δ- desaturation of aliphatic alcohol **4.1d.***

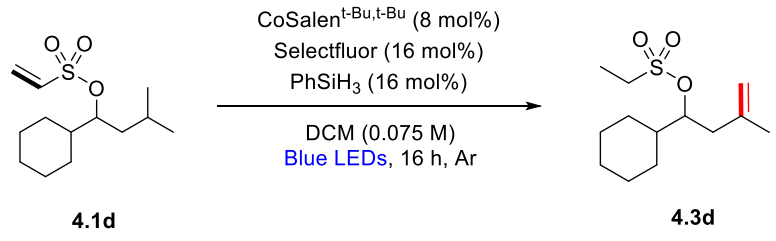

Entry	Deviation from the standard condition	Yield (%)	Ratio to reduction
1	None	62	5.5 : 1
2	CoTPP instead of Co(salen)	n.d.	-
3	No $PhSiH_3$	n.d.	-

4	No Selectfluor	57	4 : 1
5	45 °C instead of Blue LEDs	40	4 : 1

Unlike the remote functionalization, the desaturation system included the oxidant Selectfluor, excluded the protic solvent ^{t}BuOH, and used blue LEDs to activate the reaction. Especially, this new system only used a catalytic amount of $PhSiH_3$. These modifications allowed the γ, δ- desaturation to proceed at exclusively aliphatic position with moderate yield. However, there was a side reaction that alkenes were reduced to corresponding alkanes. Next, using cobalt–porphyrin complexes, such as Co^{II}–tetraphenylporphyrin (Co(TPP)) instead of Co(salen) resulted in no desired product (entry 2). The control experiments in the absence of silane highlighted its importance for the reaction (entry 3). The use of Selectfluor increased both the yield and selectivity towards the desaturation product (entry 4). Unlike the remote functionalization, the desaturation reaction system required blue LEDs to achieve a higher yield (entry 5).

In addition, the solvent selection for the reaction was also investigated, as it can influence the chemoselectivity towards desaturated product (Table 5.3). Unlike the functionalization, the desaturation reaction could proceed without a protic solvent. Specifically, the use of neat DCM and DCE produced good yields and minimized reduction product (entries 1-2). However, ^{t}BuOH, while matching DCM in yield at 62%, exhibits a significantly lower product-to-reduction ratio (2.6:1), indicating more undesired reduction byproducts (entry 3). Another protic solvent like ethanol performed poorly and is likely favoring reduction reaction (entry 4). This indicates that protic solvent would favor the reaction selectivity towards reduction product. Interestingly, the mixture of DCE and ^{t}BuOH slightly improved the yield and a decent product-to-reduction ratio (entry 5).

Table 5.3. Screening of different solvent.

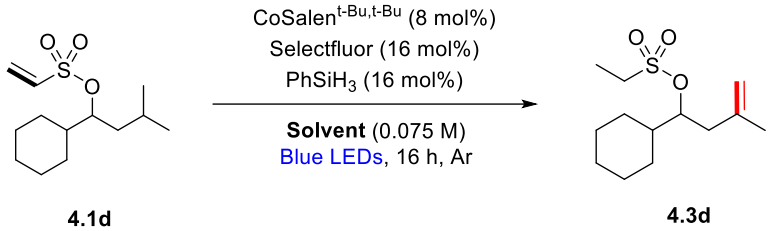

4.1d **4.3d**

Entry	**Solvent**	**Yield (%)**	**Ratio to reduction**
1	DCM	62	5.5:1
2	DCE	49	3:1

3	^{t}BuOH	62	2.6:1
4	EtOH	6	-
5	DCE: ^{t}BuOH (9:1)	63	4.2:1

Following the optimization of the solvent, the reaction conditions were evaluated with respect to the catalyst loading to ensure that the developed process is as gentle on resources as possible (Table 5.4). A catalyst loading of 8 mol% showed that the desired product was formed in the highest yield (entry 1). Reducing the amount of catalyst not only decreased the yield but also favored the formation of byproduct (entries 2-5). Lower the catalyst loading to 2 mol% - 0.5 mol% resulted in a significant decline in yield of desaturated product (entries 3-5).

Table 5.4. Screening of different catalyst loading.

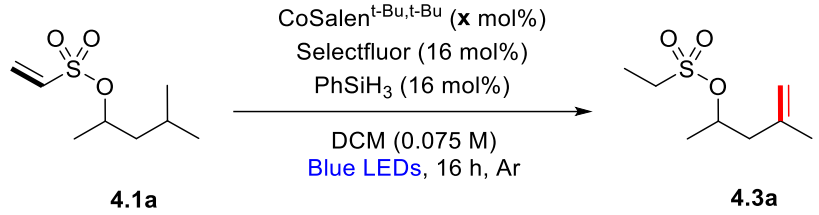

4.1a **4.3a**

Entry	**[Co] mol%**	**Yield (%)**	**Ratio to reduction**
1	8	65	2.3:1
2	5	43	1:1
3	2	8	0.12:1
4	1	4	0.05:1
5	0.5	-	-

5.5. Scope for remote γ, δ- desaturation

Having developed optimized reaction conditions, the scope of the desaturation process was examined (Scheme 5.7). A range of various aliphatic substituted alcohols afford the corresponding desaturated products (**4.3a-4.3d**) from moderate to good yields. In more details, a simple alcohol bearing a tertiary C(sp^3)–H bonds at γ position yielded 65% (**4.3a**). An alcohol with two 3° C–H bonds yielded the desaturation in only one site in excellent yield (**4.3b**). An alcohol having both secondary and tertiary C–H bonds at γ positions was preferentially desaturated of 3° (**4.3c**) in good yield.

Next, the scope was also broadened in cyclic tertiary C-H bonds at γ position. Indeed, a tertiary carbon in 1,6-position in a cyclohexyl group was also tolerated to form cyclohexenyl group in excellent yield (**4.3e**). Interestingly, the substrate bearing 3°C in both cyclic and aliphatic at γ positions yielded the product (**4.3f**) favouring the 3°C at cyclohexyl to isopropyl in a ratio of 3 to 1. This might be due to that the *in situ* formation of an radical at the cyclic site was more stable than that at the aliphatic.

Knowing that desaturation occurs only at tertiary C–H bonds, alcohols with different positions of these bonds were selected to investigate the preference of the reaction over various internal HAT processes. Specifically, under the optimized conditions, γ, δ-desaturation was exclusively favored over β, γ- or δ, ε-, yielding desaturated alcohols in moderate yields (**4.3g-4.3h**). Thus, this protocol demonstrated a preference for proceeding via intramolecular 1,6-HAT over 1,5- and 1,7-HAT processes.

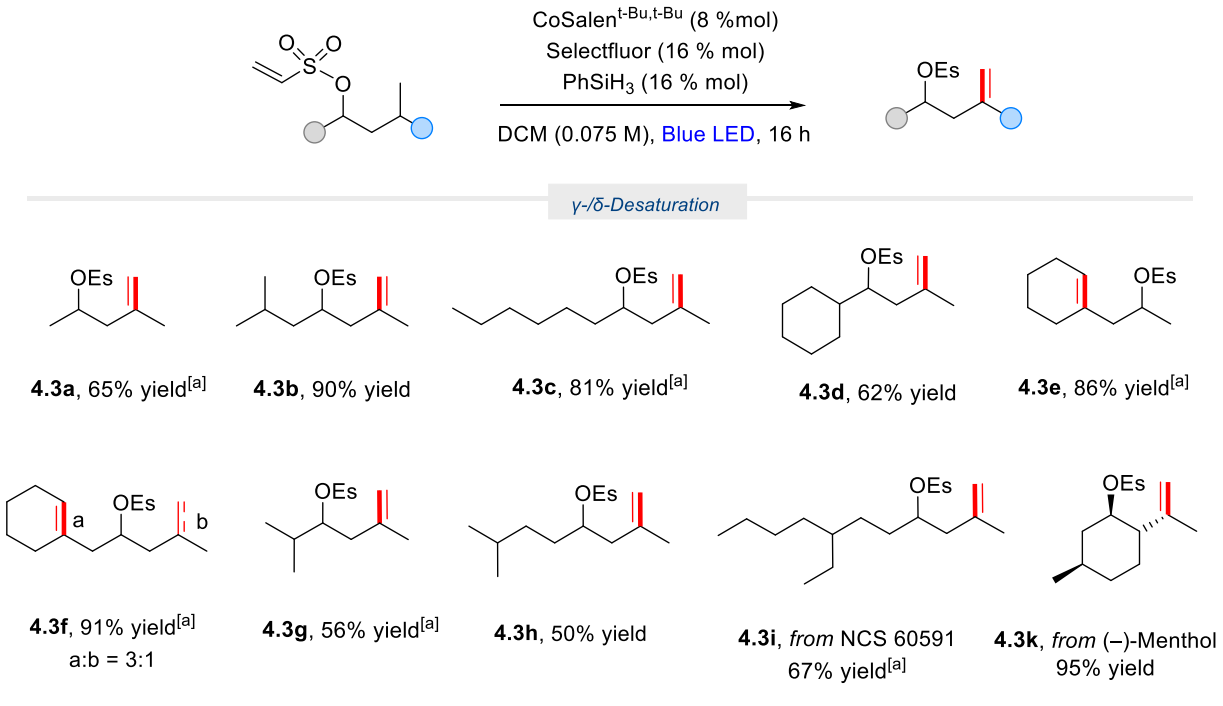

Scheme 5.7. Reaction scope of remote γ, δ- desaturation for aliphatic alcohols. Standard conditions: alcohols (0.15 mmol), CoSalen$^{t\text{-}Bu,t\text{-}Bu}$ (8 mol%, 7.2 mg), Selectfluor (16 mol%, 8.5 mg), PhSiH$_3$ (16 mol%, 3 µL) DCM (2 mL), Ar, blue-LED, 35 °C, 16 h. a) NMR yield.

To further probe the generality of this system, an alcohol found in high-value material or natural product were tested. A surface-active agent like NCS 60591 also provided desaturated alcohol (**4.3i**) with moderate yield. Pleasingly, a nature product of (–)-Menthol were exposed to our conditions and achieved an excellent yield of desaturated product (**4.3k**).

5.6. Mechanistic insights

5.6.1. In situ UV-vis spectroscopy

To explore the mechanism of the γ,δ- desaturation reaction, UV-vis spectroscopy was employed to monitor the transformation of cobalt species throughout the process. The order of adding component was proven importance, as the reaction failed to proceed if the substrate was added lastly. Therefore, experiments with stepwise addition of different components were performed to study the activation of the catalyst (Figure 5.1).

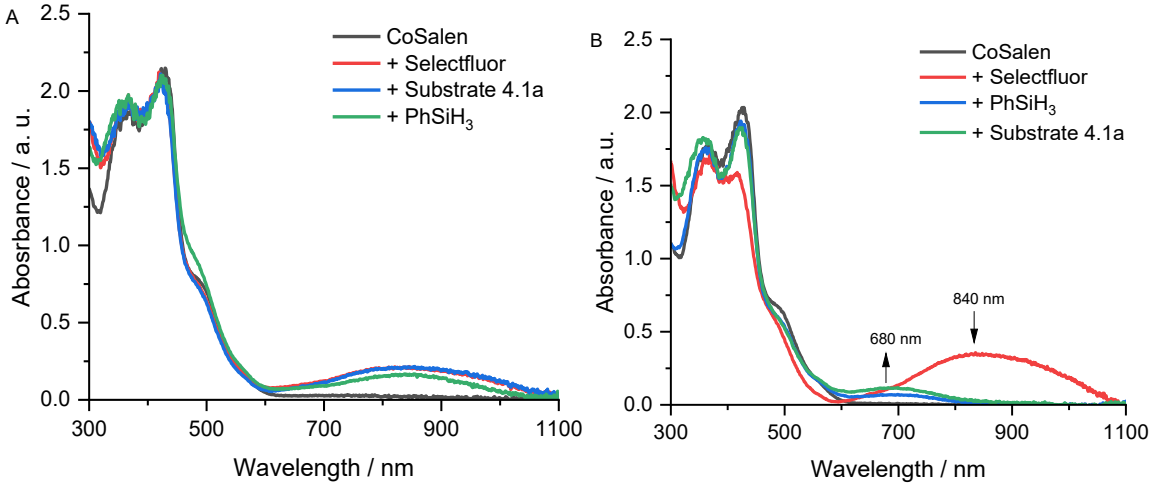

*Figure 5.1. UV-vis spectra of reaction mixture during stepwise components addition. **A**: substrate **4.1a** was added before silane; **B**: substrate **4.1a** was added after silane.*

Upon the addition of the oxidant Selectfluor, a broad absorption around 860 nm emerged, attributed to the axial ligand-to-metal charge-transfer transition in the electronic structure of the newly formed Co^{III}–F species (red curve).[144] In the order of adding alcohol before silane, the spectrum remained nearly the same and slightly decreased the intensity of the absorption band at 860 nm upon the addition of silane (Figure 5.1A). This indicates that the replacement of Co–F by Co–H species slowly took place due to the subsequent interaction between newly formed Co–H and the presented substrate (Scheme 5.8). However, in the absence of the substrate in the mixture, the absorption band of Co–F species disappeared immediately and substituted by a new absorption band at 680 nm when silane was added directly after Selectfluor (Figure 5.1B). This suggests the fast catalytic deactivation as Co–H can react actively with Co–F species. These experiments imply the high activity of Co–H species, as it can either deactivate by reacting with Co–F or catalyze the reaction by interacting with the substrate.

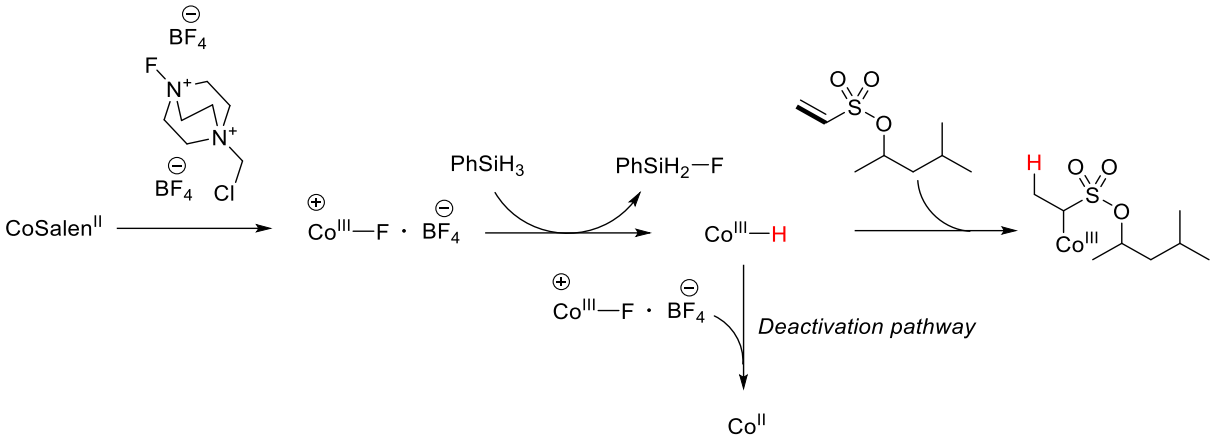

Scheme 5.8. Proposed the catalytic activation of the γ,δ-desaturation reaction

During irradiation, the MLCT band at 420 nm of cobalt(salen) gradually diminished, suggesting the participation of the precatalyst in the reaction. Additionally, a new absorption band at 750 nm, corresponding to an intermediate [Co^{III}]–alkyl species, briefly appeared before quickly disappearing.[145] Prolonged reaction overnight led to a gradual evolution of a d-d transition band at 680 nm, which are likely characteristic of decomposed cobalt species as in the previous experiment.

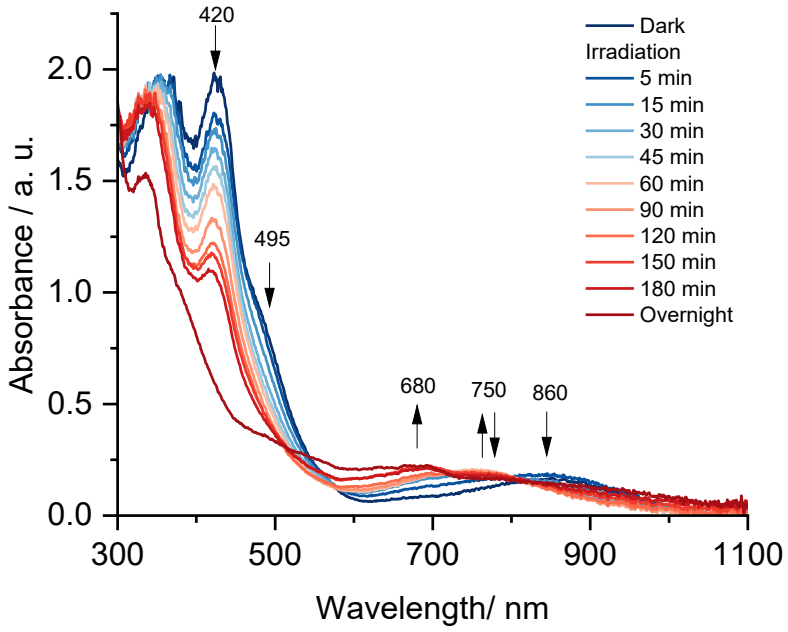

Figure 5.2. In situ UV-vis spectra of reaction mixture during the irradiation.

5.6.2. Spin trapping experiment

To confirm the formation of radical species during the reaction, an EPR experiment was conducted using 5,5-Dimethyl-1-pyrroline N-oxide (DMPO) as the spin trap (Figure 5.3).

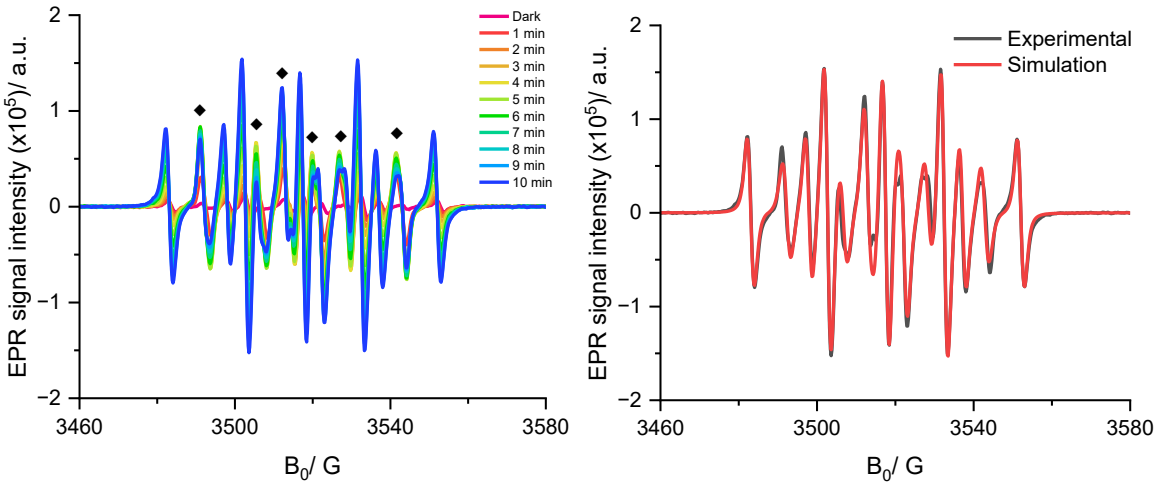

Figure 5.3. ***A****: In situ EPR spectra of a mixture for γ, δ- desaturation of* ***4.1a*** *and DMPO during irradiation;* ***B****: Experimental (black) and simulation (red) of EPR spectra of the mixture after 10 minutes of irradiation.*

In the first 4 minutes, the dominant species observed were DMPO–C adducts (rhombic, (a_N = 14.5 G, a_H = 21.5 G), which then plateaued afterwards. This is attributed to C-centered radicals likely originating from either the vinyl group or the γ-position of the alcohol. Simultaneously, another radical species was identified as DMPO–H adducts (a_N = 14.8 G, a_{H1} = 19.6 G, a_{H2} = 19.7 G). These H radicals gradually increased during irradiation, might be attributed to the H species at the δ-position of the alcohol was abstracted. Two DMPO adducts were simulated, consisting of DMPO–C and DMPO–H with the ratio of DMPO–C to DMPO–H is 2.35:1.

5.7. Conclusion

In conclusion, this study demonstrates the successful application of cobalt-catalyzed remote γ-C(sp^3)–H functionalization of aliphatic alcohols, providing a versatile method for modifying these compounds at previously inaccessible positions. The range of functionalization reactions showcases the method's broad utility and potential for use in complex molecule synthesis. While the results are promising, further exploration is needed to optimize reaction conditions and expand the substrate scope. Overall, this work contributes a valuable new strategy to the field of organic synthesis, offering potential applications in pharmaceuticals, materials science, and beyond.

Chapter 6: General conclusions and outlook

Four projects presented in the previous chapters demonstrates the widespread application of cobalt catalysis in open-shell transformations. The findings highlight the effectiveness of cobalt as an abundant and sustainable alternative to noble metal catalysts, capable of facilitating complex organic transformations under mild reaction conditions.

Throughout different organic transformations, the natural-mimic cobaloxime complex is proved to be a powerful catalyst for desaturation process. The matching between cobaloxime and radical chemistry relies on the key ability to capture radical species by persistent Co(II) metalloradicals to form cobalt–alkyl intermediates. The subsequent cleavage of these cobalt–alkyl bonds under visible light irradiation, which leads to the generation of olefinic products via β-hydrogen elimination, is a highly practical pathway in desaturation chemistry. This efficiency is evident when cobaloxime is employed as a single catalyst, as demonstrated in **chapters 2** and **3**, or in combination with a redox photocatalyst, as shown in **chapter 4**. Particularly, cobalt catalysts exhibited remarkable efficiency in remote desaturation of aliphatic amines and amides in **chapter 2**, which demonstrates potential in synthetic strategies that require precise bond manipulation. Similarly, the successful application of cobalt as a sole catalyst in the intramolecular Heck reaction in **chapter 3** revealed the metal's unique capability to promote open-shell mechanisms. Meanwhile, in **chapter 4**, combining cobaloxime with photoredox catalysis enabled desaturation alongside defunctionalization, broadening the scope of achievable transformations and underscoring cobalt’s versatility in complex organic syntheses.

With a structure distinct from cobaloxime, the cobalt salen complex described in **chapter 5** demonstrates a wider range of catalytic applications, facilitating not only desaturation but also diverse functionalization reactions. Unlike cobaloxime, cobalt salen employs a unique mechanism to generate radical species: the catalytic system includes silane, which enables the formation of cobalt-hydride species. These cobalt-hydride intermediates act as the active species, efficiently promoting radical formation from alkenes.

Through an integrated approach combining advanced experimental and theoretical methodologies, significant insights into the reactivity and selectivity of cobalt catalysts were gained. Techniques such as UV-vis and EPR spectroscopy have been essential in shedding light on catalytic activation steps and identifying key reaction intermediates. While spectroscopic analysis is valuable for observing reaction progress and intermediates,

complex mechanisms with rapid or multi-step pathways often exceed the capabilities of sole spectroscopic techniques. In such cases, computational tools like DFT analysis play a crucial role by enabling the construction of plausible reaction pathways and clarifying intricate mechanistic details. Thus, by merging experimental observations with computational modeling, this research has constructed a more comprehensive understanding of cobalt-catalyzed mechanisms, highlighting the necessity of this dual approach in elucidating the full mechanistic picture.

The application of cobalt catalysts in open-shell chemistry presents numerous exciting possibilities. There is potential for further expansion into more complex and diverse substrates, allowing cobalt catalysis to be applied in the synthesis of pharmaceuticals, agrochemicals, and materials. Additionally, the insights gained from this research could inform the design of novel cobalt-based catalytic systems that are even more selective, efficient, and environmentally friendly.

The work presented in this dissertation lays a strong foundation for the broader adoption of cobalt catalysis in green chemistry. As the need for sustainable alternatives in chemical manufacturing grows, cobalt's potential as a versatile and cost-effective catalyst is likely to become increasingly important.

Chapter 7: Experimental section

7.1. General remarks

All reactions involving moisture- or air-sensitive reagents or products were performed under an atmosphere of dry argon using standard Schlenk techniques and pre-dried glassware. Syringes for handling of dry solvents or liquid reagents were flushed with dry argon prior to use. Unless otherwise noted, all commercial reagents were purchased from commercial suppliers and used without further purification.

Chromatography

Thin layer chromatography (TLC) was performed on aluminum sheets silica gel 60 F254 from Merck. Chromatographic purification of products was accomplished by flash column chromatography using silica gel 60 (63-200 μm) from MACHEREY-NAGEL.

Analytical data

Analytical data of substances that are known in literature (marked by corresponding references) were compared with those described in the literature.

Nuclear Magnetic Resonance Spectroscopy

Nuclear magnetic resonance (NMR) spectra of ^{1}H and ^{13}C were recorded Bruker AV 300 (300 MHz), AV 400 (400 MHz) or Fourier 300 (300 MHz). Chemical shifts (δ) are given relative to solvent: references for $CDCl_3$ were 7.26 ppm (^{1}H NMR) and 77.16 ppm (^{13}C NMR), for d_4-CD_3OD were 4.78 ppm and 3.31 ppm (^{1}H NMR) and 49.15 ppm (^{13}C NMR).

And all signals were reported in parts per million (ppm) and spin-spin coupling constants (J) are given in Hz, while multiplicities are abbreviated by s (singlet), d (doublet), t (triplet), q (quartet), br (broad), m (multiplet).

UV-vis Spectroscopy

UV-vis spectra were recorded by a fiberoptical spectrometer (AvaSpec-2048, Avantes) with a probe consisting of a quartz fiber and a 1-mm-probe tip. The probe was inserted in the headspace of the schlenck tube, which was degassed three times before each measurement.

Electron Paramagnetic Resonance Spectroscopy

EPR measurements were recorded on a Bruker EMX CW-micro X-band spectrometer with a microwave power ≈ 6.9 mW, a modulation frequency of 100 kHz and modulation amplitude up to 5 G. The EPR spectrometer is equipped with a variable temperature control unit including a liquid N_2 cryostat and a temperature controller for recording the EPR spectra at low temperature down to 100 K. g values were calculated using the equation $h\nu = g\beta B_0$ with β, B_0 and ν being the Bohr magneton, resonance field and frequency, respectively. Calibration of the g values was performed using a DPPH standard (g = 2.0036 ± 0.0004).

Rapid scan EPR spectra were obtained on an ELEXYS 500 cw-EPR spectrometer (Bruker) using a Bruker ER4125RS Vers. M1 resonator.

The simulated spectrum was acquired by using software package Easyspin and Bruker SimFonia software.

Fluorescence Spectroscopy

Fluorescence spectra was recorded on Varian Cary Eclipse fluorescence spectrophotometer, using a quartz cuvette from Hellma. Before each measurement, the cuvette was degassed three time and filled with argon afterwards.

7.2. General procedures

7.2.1. General procedure 1.A: Desaturation of Amines

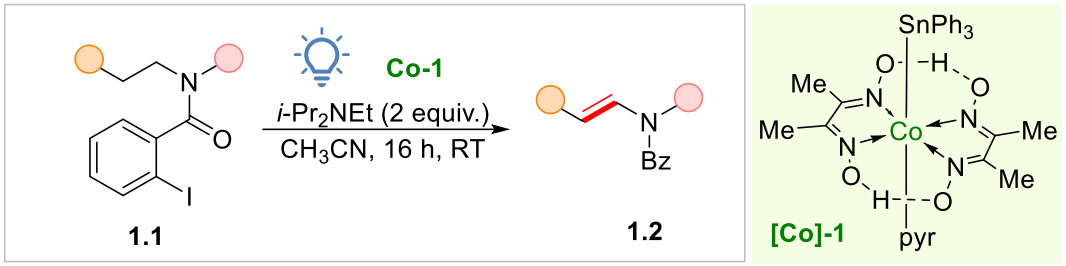

In an oven dried 15 mL Schlenk tube equipped with a magnetic stir bar, amine **1.1** (0.2 mmol), **Co-1** (5 mol%, 7.2 mg) and i-Pr_2NEt (0.4 mmol, 70 µL) were added to CH_3CN (2 mL) under the argon atmosphere. Then, the reaction mixture was stirred under blue-LED (24 W) irradiation at room temperature for 16 h. The residue was then purified by column chromatography on silica gel using hexane/EtOAc mixtures (10/1 to 4/1).as eluent to give pure enamides **1.2.**

7.2.2. General procedure 1.B: Desaturation of Amides

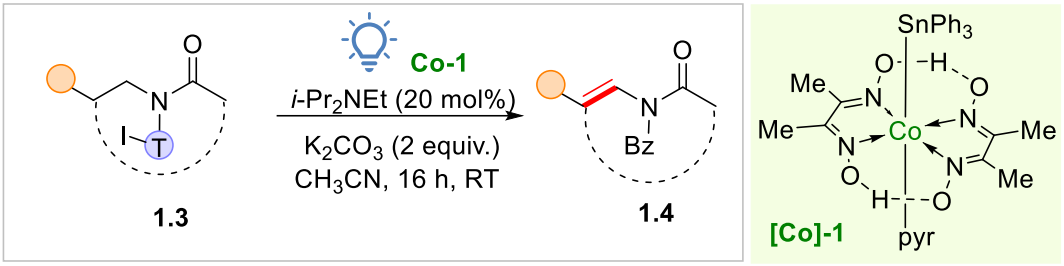

In an oven dried 15 mL Schlenk tube equipped with a magnetic stir bar, amides **1.3** (0.2 mmol), **Co-1** (10 mol%, 14.4 mg), *i*-Pr$_2$NEt (0.04 mmol, 7 µL) and K_2CO_3 (55 mg, 0.4 mmol) were added to CH_3CN (2 mL) under argon atmosphere. Then, the reaction mixture was stirred under blue-LED (24 W) irradiation at room temperature for 16 h. The residue was then purified by column chromatography on silica gel using hexane/EtOAc mixtures (10/1 to 4/1).as eluent to give pure enimides **1.4**.

7.2.3. General procedure 2.A: Intramolecular alkyl Heck Reaction

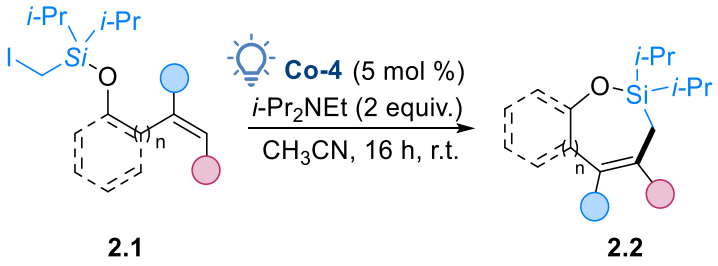

In an oven dried 25 mL Schlenk tube equipped with a magnetic stir bar, substrates **2.1** (0.2 mmol), **Co-2** (5 mol%, 3.7 mg) and *i*-Pr$_2$NEt (0.4 mmol, 70 µL) were added to degassed CH_3CN (2 mL) under the argon atmosphere. Then, the reaction mixture was stirred under blue-LED irradiation at room temperature for 16 h. The residue was then purified by column chromatography on silica gel using hexane as eluent to give pure cyclization products **2.2**.

7.2.4. General procedure 3.A: Olefination of Pyridinium Salts

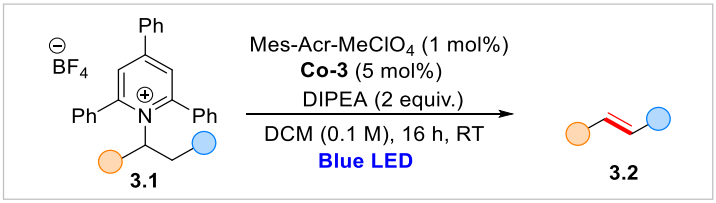

In an oven dried 15 mL Schlenk tube equipped with a magnetic stir bar, pyridinium salts **3.1** (0.2 mmol), Mes-Acr-MeClO$_4$ (1 mol%, 0.8 mg), **Co-3** (5 mol%, 4 mg), *i*-Pr$_2$NEt (0.4

mmol, 70 µL) were added to DCM (2 mL) under argon atmosphere. Then, the reaction mixture was stirred under blue-LED (24 W) irradiation at room temperature for 16 h. The residue was then purified by column chromatography on silica gel using hexane/ethyl acetate or hexane/diethyl ether mixtures (40/1 to 3/1) as eluent to give pure olefins **3.2**.

7.2.5. General procedure 4.A: Remote γ-functionalization of Alcohols

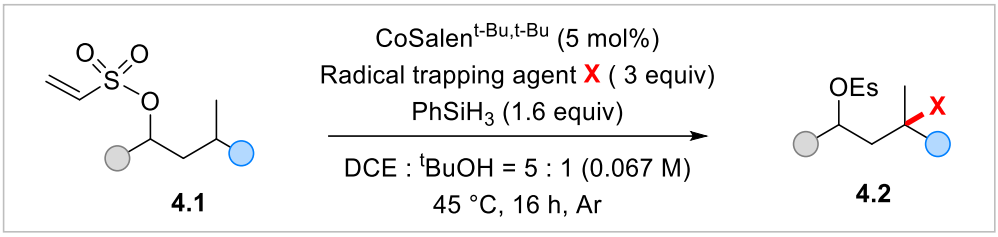

In an oven dried 25-mL-Schlenk tube equipped with a magnetic stir bar, alcohols (0.2 mmol), CoSalen$^{t\text{-}Bu,t\text{-}Bu}$ (5 mol%, 6 mg) and radical trap (0.6 mmol, 3 equiv.) were added to 3 mL of a 5:1 (V:V) DCE: *t*-BuOH mixture under argon atmosphere. Subsequently, phenyl silane (40 µL, 1.6 equiv.) was added, followed by degassed *via* 3 vacuum and argon backfill cycles. Then, the reaction mixture was stirred at 45 °C for 16h. The residue was then purified by column chromatography on either aluminum oxide neutral (for chlorination, bromination and cyanation reaction) or silica gel (for amination and azidation reaction) using hexane/ethyl acetate mixtures as eluent to give desired products.

7.2.6. General procedure 4.B: Remote γ, δ– desaturation of Alcohols

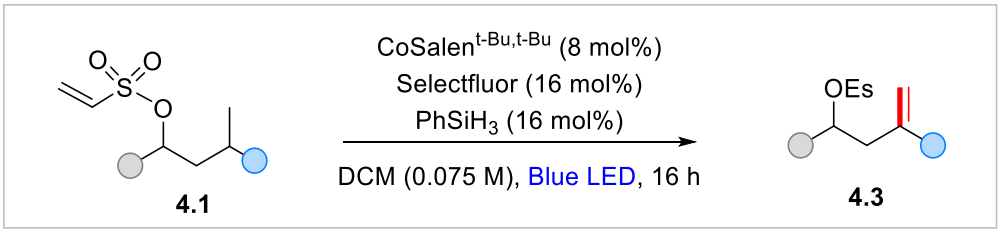

In an oven dried 25-mL-Schlenk tube equipped with a magnetic stir bar, alcohols (0.15 mmol), CoSalen$^{t\text{-}Bu,t\text{-}Bu}$ (8 mol%, 7.2 mg), Selectfluor (16 mol%, 8.5 mg) were added to DCM (2 mL) under argon atmosphere. Subsequently, phenyl silane (16 mol%, 3 µL) was added, followed by degassed *via* 3 vacuum and argon backfill cycles. Then, the reaction mixture was stirred under blue-LEDs (24 W) irradiation at 35 °C for 16 h. The residue was then purified by column chromatography on silica gel using pentane/diethyl ether mixtures as eluent to give pure olefins.

7.3. Analytical data

7.3.1. Analytical data of chapter 2

(2,3-dihydro-4*H*-1,4-oxazin-4-yl)(phenyl)methanone (1.2a)

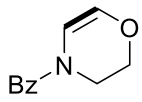

According to the general procedure method 1.A, **1.2a** was isolated in yield 99% (clear oil, 38 mg) as a mixture of rotamers, purification by chromatography (hexane/ethyl acetate = 6:1).

^{1}H NMR (300 MHz, $CDCl_3$) δ 7.63 – 7.33 (m, 5H), 6.71 – 5.88 (m, 1H), 6.21 – 5.83 (m, 1H), 4.22 – 4.01 (m, 2H), 3.95 – 3.70 (m, 2H).

^{13}C NMR (75 MHz, $CDCl_3$) δ 166.90, 133.95, 130.44, 129.11, 128.34, 128.21, 127.64, 107.52, 105.16, 64.93, 45.80, 39.98.

IR (ATR, cm^{-1}): ν = 2929, 2878, 1630, 1446, 1407, 1378, 1291, 1264, 1209, 1076, 1018, 983, 856, 787, 724, 705, 625.

(3,4-dihydropyridin-1(2*H*)-yl)(phenyl)methanone (1.2b).

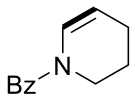

According to the general procedure method 1.A, **1.2b** was isolated in yield 91% (clear oil, 34 mg) as a mixture of rotamers, purification by chromatography (hexane/ethyl acetate = 10:1).

^{1}H NMR (300 MHz, $CDCl_3$) δ 7.54 – 7.37 (m, 5H), 7.28 – 6.43 (m, 1H), 5.23 – 4.83 (m, 1H), 3.85 – 3.56 (m, 2H), 2.15 – 2.09 (m, 2H), 1.97 – 1.80 (m, 2H).

^{13}C NMR (101 MHz, $CDCl_3$) δ 169.31, 135.07, 130.12, 128.30, 128.15, 127.46, 107.56, 41.06, 21.85, 21.63.

IR (ATR, cm^{-1}): ν = 3343, 2931, 1719, 1636, 1577, 1538, 1490, 1376, 1330, 1284, 1126, 1071, 1026, 998, 791, 698, 668.

(4-hydroxy-3,4-dihydropyridin-1(2*H*)-yl)(phenyl)methanone (1.2c)

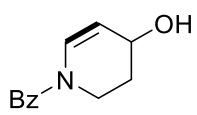

According to the general procedure method 1.A, **1.2c** was isolated in yield 90% (clear oil, 36 mg) as a mixture of rotamers, purification by chromatography (hexane/ethyl acetate = 3:1).

^{1}H NMR (300 MHz, $CDCl_3$) δ 7.49 – 7.37 (m, 5H), 7.38 – 6.57 (m, 1H), 5.33 – 4.97 (m, 1H), 4.28 – 4.13 (m, 2H), 3.63 – 3.47 (m, 1H), 2.17 – 1.96 (m, 3H).

^{13}C NMR (101 MHz, $CDCl_3$) δ 193.69, 169,70, 134.30, 131.55, 130.50, 128.44, 128.40, 126.85, 61.01, 38.12, 37.33, 35.96, 32.95, 30.57, 29.62.

IR (ATR, cm^{-1}): ν = 3339, 2928, 1621, 1576, 1538, 1445, 1415, 1344, 1290, 1244, 1144, 1063, 1026, 998, 788, 699, 628.

(4-methyl-3,4-dihydropyridin-1(2*H*)-yl)(phenyl)methanone (1.2d)

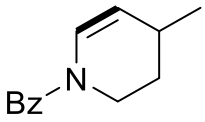

According to the general procedure method 1.A, **1.2d** was isolated in yield 96% (clear oil, 38.5 mg) as a mixture of rotamers, purification by chromatography (hexane/ethyl acetate = 10:1).

^{1}H NMR (300 MHz, $CDCl_3$) δ 7.55 – 7.33 (m, 5H), 7.37 – 6.39 (m, 1H), 5.10 – 4.70 (m, 1H), 4.05 – 4.06 (m, 1H), 3.60 (t, *J* = 11.7 Hz, 1H), 2.37 (tq, *J* = 7.6, 2.9 Hz, 1H), 2.03 – 2.04 (m, 1H), 1.60 – 1.55 (m, 1H), 1.05 (d, *J* = 7.0 Hz, 3H).

^{13}C NMR (101 MHz, $CDCl_3$) δ 169.28, 135.08, 130.13, 128.31, 128.15, 126.28, 113.76, 39.78, 29.88, 27.28, 21.18.

HRMS (ESI) m/z: $[M + H]^+$ Calcd for $C_{13}H_{15}NO$ 202.1232; Found 202.1233.

IR (ATR, cm^{-1}): ν = 2953, 2851, 1627, 1447, 1409, 1371, 1346, 1288, 1240, 1111, 1015, 970, 867, 789, 721, 702, 621.

phenyl(1,4-dioxa-8-azaspiro[4.5]dec-6-en-8-yl)methanone (1.2e)

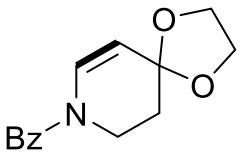

According to the general procedure method 1.A, **1.12e** was isolated in yield 86% (yellow oil, 42 mg) as a mixture of rotamers, purification by chromatography (hexane/ethyl acetate = 5:1).

^{1}H NMR (300 MHz, $CDCl_3$) δ 7.60 – 7.37 (m, 5H), 7.37 – 6.64 (m, 1H), 5.33 – 4.80 (m, 1H), 4.18 – 2.64 (m, 4H), 4.06 – 3.97 (m, 2H), 2.05 – 1.94 (m, 2H).

^{13}C NMR (101 MHz, $CDCl_3$) δ 193.56, 170.25, 144.84, 132.53, 131.84, 128.74, 128.53, 107.76, 63.60, 42.83, 35.90, 29.57.

HRMS (ESI) m/z: $[M + H]^+$ Calcd for $C_{14}H_{16}NO_3$ 246.1125; Found 246.1128.

IR (ATR, cm^{-1}): ν = 3456, 3063, 2922, 1657, 1584, 1407, 1341, 1289, 1222, 1179, 1142, 969, 885, 811, 722, 706, 629.

(propane-1,3-diylbis(3,4-dihydropyridine-4,1(2*H*)-diyl))bis(phenylmethanone) (1.2f)

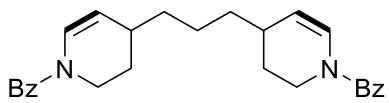

According to the general procedure method 1.A, **1.2f** was isolated in yield 93% (yellow oil, 77 mg) as a mixture of rotamers, purification by chromatography (hexane/ethyl acetate = 8:1).

^{1}H NMR (300 MHz, $CDCl_3$) δ 7.29 – 7.15 (m, 10H), 7.26 – 6.20 (m, 2H), 4.92 – 4.52 (m, 2H), 3.91 – 3.32 (m, 2H), 3.39 – 3.32 (m, 2H), 2.02 – 2.01 (m, 2H), 1.82 – 1.65 (m, 2H), 1.40 – 1.13 (m, 8H).

^{13}C NMR (75 MHz, $CDCl_3$) δ 169.14, 134.94, 130.08, 128.23, 128.05, 127.36, 126.59, 111.89, 39.85, 35.76, 32.21, 27.78, 24.01.

HRMS (ESI) m/z: $[M + H]^+$ Calcd for $C_{27}H_{30}N_2O_2$ 415.2386; Found 415.2381.

IR (ATR, cm^{-1}): ν = 2924, 1625, 1576, 1407, 1374, 1289, 1241, 1073, 959, 788, 721, 700, 623.

(3-methyl-3,4-dihydropyridin-1(2*H*)-yl)(phenyl)methanone (1.2g)

(5-methyl-3,4-dihydropyridin-1(2*H*)-yl)(phenyl)methanone (1.2g')

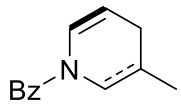

According to the general procedure method 1.A, **1.2g** and **1.2g'** were isolated in yield 95% (clear oil, 37.8 mg) as a mixture of regioisomers and rotamers, purification by chromatography (hexane/ethyl acetate = 10:1).

For major isomer **2g**, **^{1}H NMR (300 MHz, $CDCl_3$)**: δ 7.48 – 7.36 (m, 5H), 6.44 – 6.22 (m, 1H), 6.21 – 5.22 (m, 1H), 3.78 – 3.75 (m, 1H), 3.07 – 3.00 (m, 1H), 2.23 – 1.70 (m, 3H), 1.09 – 1.07 (d, 3H).

^{13}C NMR (101 MHz, $CDCl_3$) δ 169.37, 168.74, 135.73, 135.25, 135.05, 130.12, 129.96, 129.80, 128.89, 128.76, 128.40, 128.26, 128.22, 128.07, 127.29, 126.96, 126.86, 122.10, 119.72, 116.53, 107.15, 47.14, 46.02, 40.53, 30.20, 27.31, 27.07, 22.73, 22.45, 21.60, 20.80, 18.77.

HRMS (ESI) m/z: $[M + H]^+$ Calcd for $C_{13}H_{15}NO$ 202.1232; Found 202.1232.

IR (ATR, cm^{-1}): ν = 3348, 2929, 1716, 1616, 1575, 1414, 1332, 1274, 1135, 1050, 1026, 961, 925, 788, 699, 665.

ethyl 1-benzoyl-1,2,3,4-tetrahydropyridine-2-carboxylate (1.2h)

ethyl 1-benzoyl-1,4,5,6-tetrahydropyridine-2-carboxylate (1.2h')

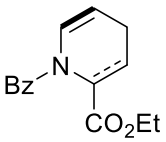

According to the general procedure method 1.A, **1.2h** (rotamers) and 1.**2h'** were isolated in yield 95% (clear oil, 48.8 mg), purification by chromatography (hexane/ethyl acetate = 10:1).

^{1}H NMR (300 MHz, $CDCl_3$) δ 7.60 – 7.33 (m, 5H), 6.84 – 6.50 (m, 1H), 5.3 – 5.21 (m, 1H), 4.86 – 4.53 (m, 1H), 4.32 – 4.14 (m, 2H), 2.49 (qt, *J* = 9.0, 3.4 Hz, 1H), 2.18 – 1.91 (m, 3H), 1.29 (t, *J* = 7.1 Hz, 3H).

^{13}C NMR (75 MHz, $CDCl_3$) δ 170.30, 169.61, 134.51, 130.35, 128.36, 128.10, 127.03, 126.69, 106.19, 61.40, 52.59, 23.43, 19.00, 14.16.

^{1}H NMR (300 MHz, $CDCl_3$) δ 7.66 – 7.53 (m, 2H), 7.53 – 7.33 (m, 3H), 6.22 (t, *J* = 3.9 Hz, 1H), 3.95 (s, 2H), 3.83 – 3.61 (m, 2H), 2.33 (td, *J* = 6.7, 3.9 Hz, 2H), 1.87 (p, *J* = 6.4 Hz, 2H), 1.12 (t, *J* = 7.1 Hz, 3H).

^{13}C NMR (75 MHz, $CDCl_3$) δ 164.07, 133.59, 130.79, 128.35, 128.24, 123.83, 61.02, 23.27, 23.03, 13.89.

HRMS (ESI) m/z: $[M + H]^+$ Calcd for $C_{15}H_{17}NO_3$ 260.1287; Found 260.1292.

IR (ATR, cm^{-1}): ν = 3339, 2935, 1730, 1637, 1601, 1530, 1446, 1369, 1192, 1156, 1095, 1022, 986, 860, 790, 700, 618.

IR (ATR, cm^{-1}): ν = 3339, 2935, 1726, 1627, 1575, 1539, 1489, 1387, 1270, 1229, 1174, 1062, 1024, 858, 793, 753, 694.

(4a,5,6,7,8,8a-hexahydroisoquinolin-2(1*H*)-yl)(phenyl)methanone (1.2i)

(4,4a,5,6,7,8-hexahydroisoquinolin-2(3*H*)-yl)(phenyl)methanone (1.2i')

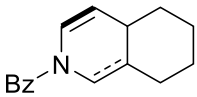

According to the general procedure method 1.A, **1.2i** and **1.2i'** were isolated in yield 94% (clear oil, 45 mg) as a mixture of rotamers, purification by chromatography (hexane/ethyl acetate = 10:1).

For major isomer **2i, ^{1}H NMR (300 MHz, $CDCl_3$)**: δ 7.51 – 7.38 (m, 5H), 6.40 – 6.19 (d, 1H), 4.62 – 4.59 (m, 1H), 3.40 – 3.30 (m, 1H), 2.12 – 1.04 (m, 10H)

^{13}C NMR (101 MHz, $CDCl_3$) δ 169.24, 168.64, 135.24, 135.16, 130.01, 129.97, 129.80, 128.35, 128.28, 128.26, 128.23, 128.16, 127.89, 127.36, 126.96, 126.16, 123.98, 120.18, 117.93, 112.35, 47.16, 45.31, 39.69, 39.09, 38.59, 34.88, 34.31, 34.18, 32.56, 32.24, 32.13, 31.87, 30.86, 30.00, 29.90, 27.45, 27.25, 26.20, 26.07, 25.93, 25.89, 25.71.

IR (ATR, cm^{-1}): ν = 3364, 2922, 2825, 1623, 1576, 1444, 1406, 1342, 1252, 1177, 1070, 1027, 973, 788, 719, 700, 662.

pyrazine-1,4-diylbis(phenylmethanone) (1.2j)

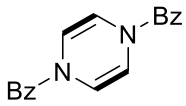

According to the general procedure method 1.A, **1.2j** was isolated in yield 75% (yellow solid, 43.5 mg) as a mixture of rotamers, purification by chromatography (DCM).

^{1}H NMR (300 MHz, $CDCl_3$) δ 7.51 – 7.34 (m, 5H), 6.93 – 5.52 (m, 2H).

^{13}C NMR (101 MHz, $CDCl_3$) δ 163.66, 132.83, 131.16, 129.85, 128.75, 128.54, 127.90, 115.87, 113.17, 112.69, 110.39.

IR (ATR, cm^{-1}): ν = 3653, 1594, 1572, 1413, 1361, 1310, 1109, 1074, 981, 937, 916, 778, 749, 715, 699, 684.

methyl (*R*)-1-benzoyl-2,3-dihydro-1*H*-pyrrole-2-carboxylate (1.2k)

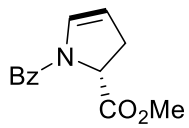

According to the general procedure method 1.A, **1.2k** was isolated in yield 88% (clear oil, 40.6 mg), purification by chromatography (hexane/ethyl acetate = 5:1).

^{1}H NMR (300 MHz, $CDCl_3$) δ 7.59 – 7.51 (m, 2H), 7.51 – 7.35 (m, 3H), 6.52 (dt, *J* = 4.8, 2.3 Hz, 1H), 5.10 (dt, *J* = 4.9, 2.6 Hz, 1H), 5.01 (dd, *J* = 11.5, 5.1 Hz, 1H), 3.79 (s, 3H), 3.10 (ddt, *J* = 16.7, 11.6, 2.4 Hz, 1H), 2.71 (dddd, *J* = 17.0, 5.0, 2.8, 2.0 Hz, 1H).

^{13}C NMR (75 MHz, $CDCl_3$) δ 171.42, 166.98, 134.87, 130.78, 130.67, 128.40, 127.80, 108.87, 58.35, 52.45, 33.70.

IR (ATR, cm^{-1}): ν = 3361, 2953, 1738, 1636, 1577, 1390, 1268, 1201, 1174, 1074, 1012, 826, 726, 699, 669.

phenyl(2,3,4,5-tetrahydro-1*H*-azepin-1-yl)methanone (1.2l)

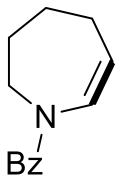

According to the general procedure method 1.A, **1.2l** was isolated in yield 95% (clear oil, 38.2 mg) as a mixture of rotamers, purification by chromatography (hexane/ethyl acetate = 10:1).

^{1}H NMR (400 MHz, $CDCl_3$) δ 7.55 – 7.30 (m, 5H), 7.30 – 6.15 (m, 1H), 5.26 – 4.99 (m, 1H), 3.95 – 3.93 (m, 1H), 2.27 – 2.23 (m, 2H), 1.91 – 1.69 (m, 4H).

^{13}C NMR (101 MHz, $CDCl_3$) δ 169.64, 135.96, 132.79, 130.02, 128.20, 127.94, 126.53, 116.59, 46.01, 27.80, 26.50, 24.67.

HRMS (ESI) m/z: $[M + H]^+$ Calcd for $C_{13}H_{16}NO$ 202.1226; Found 202.1227.

IR (ATR, cm^{-1}): ν = 3324, 2931, 1720, 1628, 1575, 1536, 1489, 1446, 1411, 1308, 1072, 999, 850, 789, 695, 667.

(*Z*)-phenyl(3,4,5,6-tetrahydroazocin-1(2H)-yl)methanone (1.2m)

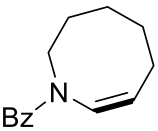

According to the general procedure method 1.A, **1.2m** was isolated in yield 93% (clear oil, 40 mg) as a mixture of rotamers, purification by chromatography (hexane/ethyl acetate = 10:1).

^{1}H NMR (300 MHz, $CDCl_3$) δ 7.46 – 7.43 (m, 2H), 7.39 – 7.30 (m, 3H), 6.22 – 6.20 (m, 1H), 4.97 – 4.95 (m, 1H), 3.92 (m, 2H), 2.27 (m, 2H), 1.92 – 1.56 (m, 8H).

^{13}C NMR (75 MHz, $CDCl_3$) δ 170.98, 170.67, 170.46, 136.48, 131.01, 129.81, 128.12, 127.91, 117.27, 73.46, 45.27, 33.48, 31.56, 31.52, 27.26, 26.54, 25.36, 25.29, 25.23, 24.50, 23.72, 23.66.

(*E*)-*N*-(but-1-en-1-yl)-*N*-butylbenzamide (1.2n)

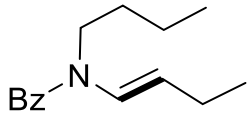

According to the general procedure method 1.A, **1.2n** was isolated in yield 84% (clear oil, 38.8 mg) as a mixture of rotamers, purification by chromatography (hexane/ethyl acetate = 10:1).

^{1}H NMR (300 MHz, $CDCl_3$) δ 7.50 – 7.33 (m, 5H), 6.35 (d, *J* = 14.2 Hz, 1H), 5.29 – 4.85 (m, 1H), 3.80 – 3.60 (m, 2H), 1.98 – 1.95 (m, 2H), 1.65 – 1.60 (m, 2H), 1.43 – 1.41 (m, 2H), 1.16 – 0.76 (m, 6H).

^{13}C NMR (75 MHz, $CDCl_3$) δ 169.94, 136.07, 129.80, 128.25, 127.94, 113.23, 43.33, 28.95, 23.50, 20.22, 14.52, 13.82.

HRMS (ESI) m/z: [M + H]+ Calcd for $C_{15}H_{21}NO$ 232.1701; Found 232.1701.

IR (ATR, cm^{-1}): ν = 2958, 2930, 2871, 1643, 1445, 1397, 1322, 1285, 1209, 1100, 944, 788, 717, 697, 655.

(*E*)-*N*-isopentyl-*N*-(3-methylbut-1-en-1-yl)benzamide (1.2o)

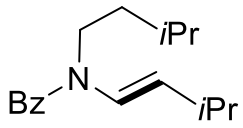

According to the general procedure method 1.A, **1.2o** was isolated in yield 89% (clear oil, 46.2 mg) as a mixture of rotamers, purification by chromatography (hexane/ethyl acetate = 10:1).

^{1}H NMR (400 MHz, $CDCl_3$) δ 7.46 – 7.35 (m, 5H), 7.35 – 6.31 (m, 1H), 5.00 – 4.95 (m, 1H), 3.85 – 3.26 (m, 2H), 2.25 – 2.08 (m, 1H), 1.77 – 1.60 (m, 1H), 1.58 – 1.46 (m, 2H), 1.09 – 0.84 (m, 12H).

^{13}C NMR (101 MHz, $CDCl_3$) δ 202.80, 169.88, 135.98, 134.84, 131.13, 129.82, 128.39, 128.19, 127.98, 127.08, 126.81, 119.02, 52.52, 42.02, 38.47, 38.30, 35.42, 29.41, 26.33, 25.90, 23.05, 22.51, 22.44.

HRMS (ESI) m/z: [M + H]+ Calcd for $C_{17}H_{25}NO$ 260.2014; Found 260.2016.

IR (ATR, cm^{-1}): ν = 3335, 2955, 2869, 1635, 1537, 1466, 1403, 1384, 1301, 1209, 1107, 944, 791, 695, 656.

(3*S*,4*R*)-3-((benzo[*d*][1,3]dioxol-5-yloxy)methyl)-1-benzyl-4-(4-fluorophenyl)-1,2,3,4-tetrahydropyridine (1.2q)

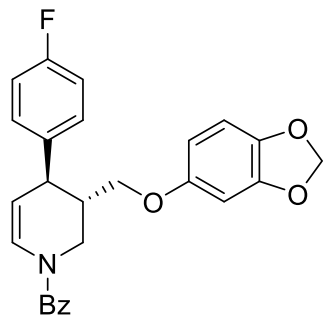

According to the general procedure method 1.A, **1.2q** was isolated in yield 44% (clear oil, 37 mg) as a mixture of rotamers, purification by chromatography (hexane/ethyl acetate = 5:1).

^{1}H NMR (300 MHz, $CDCl_3$) δ 7.66 – 6.59 (m, 2H), 7.48 – 7.37 (m, 5H), 7.15 – 7.09 (m, 2H), 6.97 – 6.91 (m, 2H), 6.39 – 6.05 (m, 2H), 5.83 (s, 2H), 5.15 – 4.76 (m, 1H), 4.26 – 4.19 (1H), 3.81 – 3.44 (m, 2H), 2.21 – 2.09 (m, 1H), 1.79 – 0.99 (m, 1H), 1.35 –1.18 (m, 2H), 0.82 – 0.76 (m, 1H).

^{13}C NMR (101 MHz, $CDCl_3$) δ 169.56, 163.06, 160.62, 148.31, 141.91, 138.90, 138.87, 130.93, 130.59, 129.66, 129.58, 128.51, 128.35, 127.82, 115.61, 115.40, 109.74, 107.95, 105.62, 101.21, 98.11, 68.55, 42.32, 40.77, 40.20.

HRMS (ESI) m/z: $[M + H]^+$ Calcd for $C_{26}H_{22}FNO_4Na$ 454.1425; Found 454.1425.

IR (ATR, cm^{-1}): ν = 2922, 1722, 1630, 1600, 1502, 1486, 1404, 1375, 1355, 1267, 1219, 1179, 1133, 1033, 992, 926, 837, 814, 785, 720, 701.

(*S*)-5-((benzo[*d*][1,3]dioxol-5-yloxy)methyl)-1-benzyl-4-(4-fluorophenyl)-1,2,3,4-tetrahydropyridine (1.2q')

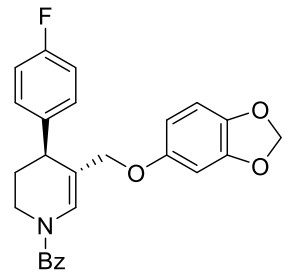

According to the general procedure method 1.A, **1.2q'** was isolated in yield 43% (clear oil, 36 mg), purification by chromatography (hexane/ethyl acetate = 5:1).

^{1}H NMR (400 MHz, $CDCl_3$) δ 7.66 – 6.81 (m, 1H), 7.48 – 7.37 (m, 5H), 7.14 – 7.08 (m, 2H), 6.96 – 6.91 (m, 2H), 6.55 (m, 1H), 6.24 – 5.81 (m, 2H), 5.86 – 5.78 (m, 2H), 4.24 – 4.00 (m, 3H), 3.68 (t, *J* = 5.1 Hz, 1H), 3.41 (t, *J* = 12.0 Hz, 1H), 2.20 – 1.93 (m, 2H)

^{13}C NMR (75 MHz, $CDCl_3$) δ 162.99, 160.55, 148.15, 141.86, 138.52, 130.94, 130.66, 129.71, 129.63, 128.53, 115.58, 115.37, 107.86, 106.44, 101.16, 98.58, 70.21, 38.33, 37.62, 30.38.

HRMS (ESI) m/z: $[M + H]^+$ Calcd for $C_{26}H_{23}FNO_3$ 432.1606; Found 432.1611.

IR (ATR, cm^{-1}): ν = 2924, 1722, 1633, 1601, 1502,1484, 1399, 1360, 1282, 1267, 1220, 1175, 1129, 1096, 991, 926, 834, 788, 717, 699, 648.

(1-(3,4-dimethoxyphenyl)-6,7-dimethoxyisoquinolin-2(1*H*)-yl)(phenyl)methanone (1.2r)

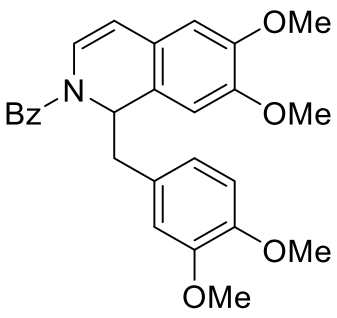

According to the general procedure method 1.A, **1.2r** was isolated in yield 45% (clear oil, 40 mg), purification by chromatography (hexane/ethyl acetate = 3:1).

^{1}H NMR (300 MHz, $CDCl_3$) δ 7.47 – 7.28 (m, 6H), 6.70 – 6.49 (m, 3H), 6.47 – 6.23 (m, 2H), 5.94 (s, 1H), 5.66 (dd, *J* = 14.6, 6.5 Hz, 2H), 4.30 – 4.16 (m, 1H), 3.80 (s, 3H), 3.76 (s, 3H), 3.70 (s, 3H), 3.50 (s, 3H), 3.06 – 2.72 (m, 2H).

^{13}C NMR (75 MHz, $CDCl_3$) δ 168.83, 167.70, 148.57, 148.33, 147.74, 147.38, 130.91, 130.68, 130.12, 128.82, 128.64, 128.40, 124.96, 124.53, 122.93, 122.41, 113.22, 111.12, 110.86, 109.24, 107.92, 66.20, 65.88, 56.44, 56.01, 55.95, 55.82, 39.70.

HRMS (ESI) m/z: $[M + H]^+$ Calcd for $C_{27}H_{28}NO_5$ 446.1962; Found 446.1967.

IR (ATR, cm^{-1}): ν = 2955, 2926, 2854, 1725, 1654, 1624, 1511, 1451, 1423, 1341, 1263, 1230, 1193, 1137, 1073, 1026, 1002, 891, 860, 725, 707, 633.

(*E*)-*N*-acetyl-*N*-(but-1-en-1-yl)benzamide (1.4a)

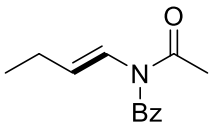

According to the general procedure method 1.B, **1.4a** was isolated in yield 89% (clear oil, 38.6 mg), purification by chromatography (hexane/ethyl acetate = 8:1).

^{1}H NMR (400 MHz, CD_3OD) δ 7.78 – 7.73 (m, 2H), 7.61 – 7.55 (m, 1H), 7.51 – 7.45 (m, 2H), 6.53 (dt, *J* = 14.2, 1.5 Hz, 1H), 5.12 (dt, *J* = 14.1, 7.0 Hz, 1H), 2.33 (s, 3H), 1.98 – 1.89 (m, 2H), 0.76 (t, *J* = 7.5 Hz, 3H).

^{13}C NMR (101 MHz, CD_3OD) δ 174.90, 174.15, 136.18, 134.65, 132.45, 131.80, 130.41, 127.77, 25.08, 25.08, 24.90, 14.29.

HRMS (ESI) m/z: $[M + Na]^+$ Calcd for $C_{13}H_{15}NO_2Na$ 240.1000; Found 240.1004.

IR (ATR, cm^{-1}): ν = 2963, 1686, 1449,1368, 1232,1073, 977, 946, 800, 714, 691, 658, 610.

(*E*)-*N*-acetyl-*N*-(hex-1-en-1-yl)benzamide (1.4b)

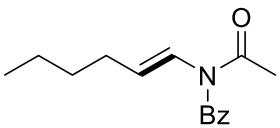

According to the general procedure method 1.B, **1.4b** was isolated in yield 87% (clear oil, 42.6 mg), purification by chromatography (hexane/ethyl acetate = 8:1).

^{1}H NMR (400 MHz, CD_3OD) δ 7.78 – 7.73 (m, 2H), 7.61 – 7.55 (m, 1H), 7.51 – 7.46 (m, 2H), 6.52 (d, *J* = 14.2 Hz, 1H), 5.08 (dt, *J* = 14.2, 7.4 Hz, 1H), 2.33 (s, 3H), 1.94 (qd, *J* = 7.1, 1.4 Hz, 2H), 1.14 – 1.05 (m, 2H), 1.05 – 0.95 (m, 2H), 0.78 – 0.73 (m, 3H).

^{13}C NMR (101 MHz, CD_3OD) δ 172.76, 171.99, 134.11, 132.48, 129.67, 129.12, 128.34, 126.28, 30.74, 29.09, 22.93, 21.38, 12.80.

HRMS (ESI) m/z: $[M + H]^+$ Calcd for $C_{15}H_{19}NO_2$ 246.1494; Found 246.1493.

IR (ATR, cm^{-1}): ν = 2965, 2927, 2857, 1686, 1368, 1239, 1177, 1074, 948, 896, 798, 713, 699, 658.

(*E*)-*N*-acetyl-*N*-(3-methylbut-1-en-1-yl)benzamide (1.4c)

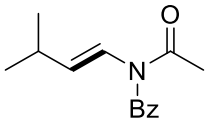

According to the general procedure method 1.B, **1.4c** was isolated in yield 90% (clear oil, 41.6 mg) as a mixture of rotamers, purification by chromatography (hexane/ethyl acetate = 8:1).

^{1}H NMR (400 MHz, CD_3OD) δ 7.89 – 7.73 (m, 2H), 7.60 – 7.54 (m, 1H), 7.51 – 7.46 (m, 2H), 6.92 – 6.47 (m, 1H), 5.56 – 4.96 (m, 1H), 2.35 (s, 3H), 2.44 – 2.17 (m, 1H), 1.09 – 0.760.73 (m, 6H).

^{13}C NMR (101 MHz, CD_3OD) δ 172.82, 172.19, 165.87, 135.91, 134.20, 133.70, 132.38, 131.53, 129.64, 128.23, 128.21, 127.12, 124.26, 122.22, 120.84, 29.16, 29.12, 22.92, 21.94, 20.72.

HRMS (ESI) m/z: $[M + Na]^+$ Calcd for $C_{14}H_{17}NO_2Na$ 254.1151; Found 254.1158.

IR (ATR, cm^{-1}): ν = 3267, 2958, 2868, 1691, 1628, 1331, 1310, 1240, 1190, 1177, 1072, 957, 800, 695, 590.

***N*-acetyl-*N*-(4-methylpent-1-en-2-yl)benzamide (1.4d)**

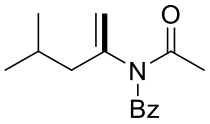

According to the general procedure method 1.B, **1.4d** was isolated in yield 60% (clear oil, 29.4 mg) as a mixture of rotamers, purification by chromatography (hexane/ethyl acetate = 8:1).

^{1}H NMR (400 MHz, $CDCl_3$) δ 7.70 – 7.66 (m, 2H), 7.56 – 7.51 (m, 1H), 7.48 – 7.41 (m, 2H), 5.25 – 5.22 (m, 1H), 5.08 (d, *J* = 0.7 Hz, 1H), 2.36 (s, 3H), 2.12 (ddd, *J* = 7.0, 1.4, 0.7 Hz, 2H), 1.86 (ddd, *J* = 13.4, 7.1, 6.5 Hz, 1H), 0.95 (d, *J* = 6.6 Hz, 6H).

^{13}C NMR (101 MHz, $CDCl_3$) δ 173.21, 173.16, 145.21, 135.54, 132.23, 128.52, 128.46, 128.44, 116.18, 44.22, 25.74, 25.25, 22.44.

HRMS (ESI) m/z: $[M + Na]^+$ Calcd for $C_{15}H_{19}NO_2Na$ 268.1313; Found 268.1316.

IR (ATR, cm^{-1}): ν = 2956, 1686, 1448, 1365, 1281, 1232, 1176, 892, 791, 697, 661, 613.

***(E)*-*N*-acetyl-*N*-styrylbenzamide (1.4e)**

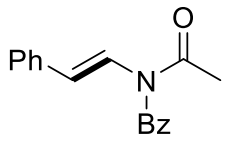

According to the general procedure method 1.B, **1.4e** was isolated in yield 90% (yellow oil, 47.7 mg) as a mixture of rotamers, purification by chromatography (hexane/ethyl acetate = 8:1).

^{1}H NMR (400 MHz, $CDCl_3$) δ 7.79 – 7.73 (m, 2H), 7.51 – 7.43 (m, 1H), 7.43 – 7.33 (m, 3H), 7.20 – 7.11 (m, 6H), 5.85 (d, *J* = 14.9 Hz, 1H), 2.28 (s, 3H).

^{13}C NMR (101 MHz, $CDCl_3$) δ 172.48, 170.58, 135.06, 133.65, 133.16, 132.05, 130.26, 128.94, 128.85, 128.75, 128.63, 128.39, 127.76, 127.66, 127.40, 126.15, 125.34, 124.32, 24.21.

HRMS (ESI) m/z: $[M + Na]^+$ Calcd for $C_{17}H_{15}NO_2Na$ 288.0995; Found 288.1001.

IR (ATR, cm^{-1}): ν = 2930, 1691, 1600, 1510, 1448, 1369, 1247, 1108, 1071, 960, 894, 798, 740, 712, 695.

(*E*)-*N*-acetyl-*N*-(3-phenylprop-1-en-1-yl)benzamide (1.4f)

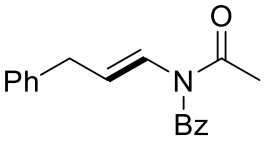

According to the general procedure method 1.B, **1.4f** was isolated in yield 93% (clear oil, 51.9 mg) as a mixture of rotamers, purification by chromatography (hexane/ethyl acetate = 8:1).

^{1}H NMR (400 MHz, $CDCl_3$) δ 7.75 – 7.71 (m, 2H), 7.61 – 7.55 (m, 1H), 7.48 – 7.43 (m, 2H), 7.16 – 7.11 (m, 3H), 6.79 – 6.73 (m, 2H), 5.24 (dt, *J* = 14.4, 7.3 Hz, 1H), 3.35 – 3.29 (m, 2H), 2.40 (s, 3H).

^{13}C NMR (101 MHz, $CDCl_3$) δ 172.60, 171.45, 138.93, 133.93, 132.82, 129.96, 128.76, 128.41, 128.38, 128.17, 128.13, 127.29, 127.06, 126.16, 36.09, 24.36.

HRMS (ESI) m/z: $[M + Na]^+$ Calcd for $C_{18}H_{17}NO_2Na$ 302.1151; Found 302.1152.

IR (ATR, cm^{-1}): ν = 3028, 1689, 1600, 1369, 1240, 1110, 1069, 1025, 949, 710, 697, 659.

(*E*)-*N*-acetyl-*N*-(2-methoxyvinyl)benzamide (1.4g)

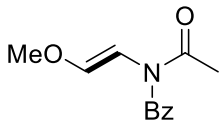

According to the general procedure method 1.B, **1.4g** was isolated in yield 85% (yellow oil, 37.2 mg) as a mixture of rotamers, purification by chromatography (hexane/ethyl acetate = 8:1).

^{1}H NMR (400 MHz, $CDCl_3$) δ 7.76 – 7.58 (m, 2H), 7.47 – 7.42 (m, 1H), 7.40 – 7.31 (m, 2H), 6.34 – 5.57 (m, 2H), 3.45 – 3.29 (m, 3H), 3.29 (s, 2H), 2.35 (s, 3H).

^{13}C NMR (101 MHz, $CDCl_3$) δ 172.86, 172.41, 150.26, 143.22, 134.79, 134.34, 134.09, 132.39, 132.21, 131.74, 129.46, 128.88, 128.66, 128.54, 127.85, 127.08, 106.91, 106.09, 104.21, 60.08, 57.18, 24.75, 24.51.

HRMS (ESI) m/z: $[M + Na]^+$ Calcd for $C_{12}H_{13}NO_3Na$ 242.0792; Found 242.0798.

IR (ATR, cm^{-1}): ν = 2930, 1691, 1510, 1484, 1448, 1369, 1247, 1108, 1071, 1000, 960, 894, 740, 712, 695.

***N*-acetyl-*N*-(cyclohexylidenemethyl)benzamide (1.4h)**

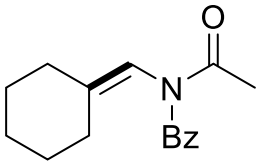

According to the general procedure method 1.B, **1.4h** was isolated in yield 65% (clear oil, 33.4 mg) as a mixture of rotamers, purification by chromatography (hexane/ethyl acetate = 10:1).

^{1}H NMR (400 MHz, $CDCl_3$) δ 7.72 – 7.66 (m, 2H), 7.54 – 7.49 (m, 1H), 7.45 – 7.39 (m, 2H), 6.05 (t, *J* = 1.2 Hz, 1H), 2.48 (s, 3H), 2.23 – 2.14 (m, 1H), 2.03 – 1.98 (m, 2H), 1.90 – 1.80 (m, 2H), 1.60 (d, *J* = 2.3 Hz, 2H), 1.37 (p, *J* = 2.3 Hz, 4H), 1.22 (p, *J* = 5.8 Hz, 2H).

^{13}C NMR (101 MHz, $CDCl_3$) δ 173.25, 172.92, 141.21, 134.74, 132.24, 129.39, 128.71, 128.03, 126.94, 118.65, 33.23, 27.80, 27.14, 25.96, 25.81, 25.11.

HRMS (ESI) m/z: $[M + Na]^+$ Calcd for $C_{16}H_{19}NO_2Na$ 280.1308; Found 280.1315.

IR (ATR, cm^{-1}): ν = 3339, 2928, 2852, 1679, 1634, 1598, 1512, 1445, 1367, 1315, 1246, 1213, 1175, 1158, 1079, 990, 974, 800, 745, 711, 692, 658, 619.

***N*-acetyl-*N*-(cyclopent-1-en-1-yl)benzamide (1.4i)**

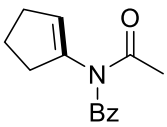

According to the general procedure method 1.B, **1.4i** was isolated in yield 39% (clear oil, 17.9 mg) as a mixture of rotamers, purification by chromatography (hexane/ethyl acetate = 10:1).

^{1}H NMR (400 MHz, CD$_3$OD) δ 7.72 – 7.67 (m, 2H), 7.60 – 7.55 (m, 1H), 7.50 – 7.44 (m, 2H), 5.44 (tt, *J* = 2.5, 1.8 Hz, 1H), 2.58 – 2.51 (m, 2H), 2.37 (s, 3H), 2.22 (ddq, *J* = 8.9, 7.6, 2.4 Hz, 2H), 1.97 – 1.88 (m, 2H).

^{13}C NMR (101 MHz, CD$_3$OD) δ 173.23, 172.99, 140.63, 135.04, 132.07, 129.23, 128.13, 128.11, 47.81, 47.60, 47.39, 31.65, 29.69, 23.44, 22.06.

HRMS (ESI) m/z: [M + Na]$^+$ Calcd for $C_{14}H_{15}NO_2Na$ 252.1000; Found 252.1002.

IR (ATR, cm^{-1}): ν = 2925, 2851, 1687, 1447, 1269, 1240, 1111, 1006, 800, 776, 713, 693, 671, 613.

1-benzoyl-3,4-dihydropyridin-2(1*H*)-one (1.4j)

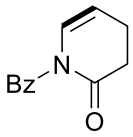

According to the general procedure method 1.B, **1.4j** was isolated in yield 81% (yellow oil, 32.6 mg) as a mixture of rotamers, purification by chromatography (hexane/ethyl acetate = 10:1).

^{1}H NMR (300 MHz, CDCl$_3$) δ 7.55 – 7.49 (m, 2H), 7.48 – 7.42 (m, 1H), 7.38 – 7.30 (m, 2H), 5.38 (dtt, *J* = 8.1, 4.4, 0.6 Hz, 1H), 2.64 (ddt, *J* = 7.8, 7.3, 0.7 Hz, 2H), 2.46 – 2.36 (m, 2H).

^{13}C NMR (75 MHz, CDCl$_3$) δ 171.18, 170.87, 135.10, 132.17, 128.39, 128.23, 126.47, 109.01, 33.11, 20.93.

HRMS (ESI) m/z: [M + Na]$^+$ Calcd for $C_{12}H_{11}NO_2Na$ 224.0686; Found 224.0686.

IR (ATR, cm^{-1}): ν = 2934, 2845, 1719, 1664, 1449, 1339, 1169, 1253, 1294, 1153, 1128, 1019, 928, 902, 732, 699, 657, 589.

7.3.2. Analytical data for chapter 3

2,2-diisopropyl-2,3-dihydrobenzo[*f*][1,2]oxasilepine (2.2a)

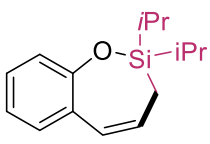

According to the general procedure 2.A, **2a** was isolated in yield 99% (49 mg, colorless oil, Endo:Exo >20:1), purification by chromatography (only hexane).

^{1}H NMR (300 MHz, CDCl$_3$) δ 7.20 – 7.06 (m, 2H), 7.02 – 6.92 (m,

2H), 6.32 – 6.25 (m, 1H), 6.14 – 6.05 (m, 1H), 1.64 (dd, *J* = 7.5, 0.9 Hz, 2H), 1.21 – 1.14 (m, 2H), 1.14 – 1.08 (m, 12H).

^{13}C NMR (101 MHz, $CDCl_3$) δ 154.11, 130.93, 128.37, 128.16, 127.81, 126.09, 121.65, 120.98, 17.73, 17.46, 13.61, 12.34.

7-fluoro-2,2-diisopropyl-2,3-dihydrobenzo[*f*][1,2]oxasilepine (2.2b)

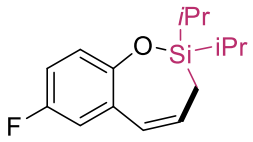

According to the general procedure for 2.A, **2.2b** was isolated in yield 90% (52 mg, colorless oil, Endo:Exo >20:1), purification by chromatography (only hexane).

^{1}H NMR (400 MHz, $CDCl_3$) δ 6.94 – 6.91 (m, 1H), 6.88 – 6.83 (m, 1H), 6.79 – 9.76 (m, 1H), 6.23 – 6.21 (m, 1H), 6.17 – 6.10 (m, 1H), 1.65 (dd, *J* = 7.3, 0.7 Hz, 2H), 1.21 – 1.14 (m, 2H), 1.12 – 1.08 (m, 12H).

^{13}C NMR (101 MHz, $CDCl_3$) δ 158.28, 155.91, 150.13, 150.11, 129.51, 129.44, 125.14, 125.12, 122.43, 122.35, 116.35, 116.13, 114.49, 114.26, 17.71, 17.45, 13.56, 12.40.

^{19}F NMR (282 MHz, CDCl3) δ -123.89 (m).
HRMS (EI) m/z: $[M]^+$ Calcd for $C_{15}H_{21}FOSi$ 264.1346; Found 264.1340.

7-chloro-2,2-diisopropyl-2,3-dihydrobenzo[*f*][1,2]oxasilepine (2.2c)

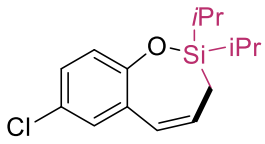

According to the general procedure for 2.A, **2.2c** was isolated in yield 94% (53 mg, colorless oil, Endo:Exo >20:1), purification by chromatography (only hexane).

^{1}H NMR (400 MHz, $CDCl_3$) δ 7.13 – 7.05 (m, 2H), 6.93 – 6.91 (m, 1H), 6.24 – 6.11 (m, 2H), 1.65 (dd, *J* = 7.3, 0.6 Hz, 2H), 1.23 – 1.14 (m, 2H), 1.13 – 1.07 (m, 12H).

^{13}C NMR (101 MHz, $CDCl_3$) δ 152.76, 130.26, 129.89, 129.55, 127.63, 125.78, 124.95, 122.89, 17.69, 17.42, 13.59, 12.42.

7-bromo-2,2-diisopropyl-2,3-dihydrobenzo[*f*][1,2]oxasilepine (2.2d)

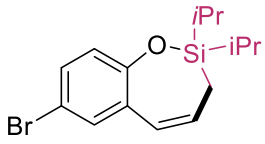

According to the general procedure for 2.A, **2.2d** was isolated in yield 95% (62 mg, colorless oil, Endo:Exo >20:1), purification by chromatography (only hexane).

^{1}H NMR (400 MHz, $CDCl_3$) δ 7.24 – 7.17 (m, 2H), 6.86 – 6.81 (m, 1H), 6.21 – 6.06 (m, 2H), 1.62 (dd, *J* = 7.3, 0.6 Hz, 2H), 1.19 – 1.11 (m, 2H), 1.09 – 1.05 (m, 12H).

^{13}C NMR (101 MHz, $CDCl_3$) δ 153.23, 133.19, 130.49, 130.41, 129.53, 124.81, 123.32, 113.15, 17.63, 17.36, 13.53, 12.37.

HRMS (EI) m/z: $[M]^+$ Calcd for $C_{15}H_{21}BrOSi$ 324.0540; Found 324.0541.

2,2-diisopropyl-7-methoxy-2,3-dihydrobenzo[*f*][1,2]oxasilepine (2.2e)

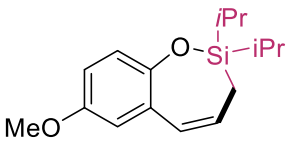

According to the general procedure for 2.A, **2.2e** was isolated in yield 97% (54 mg, colorless oil, Endo:Exo >20:1), purification by chromatography (hexane/ethyl acetate = 100 : 1).

^{1}H NMR (400 MHz, $CDCl_3$) δ 6.70 (d, *J* = 8.8 Hz, 1H), 6.52 (dd, *J* = 8.8, 3.2 Hz, 1H), 6.40 (d, *J* = 3.1 Hz, 1H), 6.06 – 6.01 (m, 1H), 5.89 (dt, *J* = 10.8, 7.5 Hz, 1H), 3.57 (s, 3H), 1.42 (dd, *J* = 7.5, 0.9 Hz, 2H), 0.99 – 0.92 (m, 2H), 0.91 – 0.86 (m, 12H).

^{13}C NMR (101 MHz, $CDCl_3$) δ 153.66, 148.13, 128.83, 128.75, 125.88, 122.18, 114.70, 113.99, 55.62, 17.78, 17.52, 13.59, 12.37.

HRMS (EI) m/z: $[M]^+$ Calcd for $C_{16}H_{24}O_2Si$ 276.1540; Found 276.1534.

2,2-diisopropyl-8-methoxy-2,3-dihydrobenzo[f][1,2]oxasilepine (2.2f)

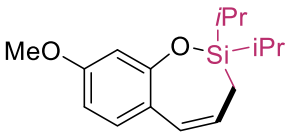

According to the general procedure for 2.A, **2.2f** was isolated in yield 95% (52 mg, colorless oil, Endo:Exo >20:1), purification by chromatography (hexane/ethyl acetate = 100 : 1).

^{1}H NMR (300 MHz, $CDCl_3$) δ 6.90 – 6.84 (m, 1H), 6.47 – 6.41 (m, 2H), 6.11 (dd, *J* = 10.8, 0.9 Hz, 1H), 5.87 (dt, *J* = 10.8, 7.4 Hz, 1H), 3.69 (s, 3H), 1.54 – 1.47 (m, 2H), 1.07 – 1.02 (m, 2H), 1.02 – 0.94 (m, 12H).

^{13}C NMR (75 MHz, $CDCl_3$) δ 159.52, 155.11, 131.64, 126.32, 125.95, 121.06, 107.57, 106.61, 55.31, 17.73, 17.69, 17.46, 17.42, 13.62, 13.60, 12.19.

6-chloro-2,2-diisopropyl-2,3-dihydrobenzo[f][1,2]oxasilepine (2.2g)

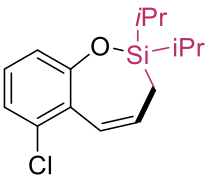

According to the general procedure for 2.A, **2.2g** was isolated in yield 95% (53 mg, colorless oil, Endo:Exo >20:1), purification by chromatography (only hexane).

^{1}H NMR (400 MHz, $CDCl_3$) δ 7.13 – 7.06 (m, 2H), 6.93 (m, 1H), 6.39 (dd, *J* = 10.9, 0.9 Hz, 1H), 6.25 (dt, *J* = 10.8, 7.7 Hz, 1H), 1.68 (dd, *J* = 7.7, 0.8 Hz, 2H), 1.24 – 1.16 (m, 2H), 1.15 – 1.09 (m, 12H).

^{13}C NMR (101 MHz, $CDCl_3$) δ 155.05, 134.25, 129.52, 128.01, 127.20, 122.88, 122.39, 120.17, 17.75, 17.47, 13.56, 12.53.

HRMS (EI) m/z: $[M]^+$ Calcd for $C_{15}H_{21}ClOSi$ 280.1045; Found 280.1049.

6-bromo-2,2-diisopropyl-2,3-dihydrobenzo[*f*][1,2]oxasilepine (2.2h)

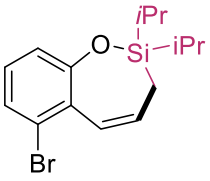

According to the general procedure for 2.A, **2h** was isolated in yield 98% (63 mg, colorless oil, Endo:Exo >20:1), purification by chromatography (only hexane).

^{1}H NMR (400 MHz, $CDCl_3$) δ 7.15 – 7.09 (m, 2H), 6.76 – 6.74 (m, 1H), 6.09 (d, *J* = 10.9, 1H), 6.02 (dt, *J* = 7,2, 10.9, 1H),1.55 – 1.50 (d, *J* = 6.8, 2H), 1.10 – 1.02 (m, 2H), 1.00 – 0.96 (m, 12H).

^{13}C NMR (101 MHz, $CDCl_3$) δ 153.28, 133.25, 130.54, 130.47, 129.59, 124.86, 123.37, 113.21, 17.69, 17.42, 13.59, 12.43.

HRMS (EI) m/z: $[M]^+$ Calcd for $C_{15}H_{21}BrOSi$ 324.0540; Found 324.0542.

6-bromo-8-chloro-2,2-diisopropyl-2,3-dihydrobenzo[*f*][1,2]oxasilepine (2.2i)

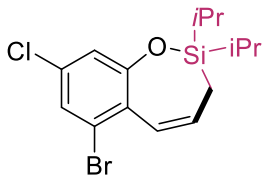

According to the general procedure for 2.A, **2i** was isolated in yield 99% (71 mg, colorless oil, Endo:Exo >20:1), purification by chromatography (only hexane).

^{1}H NMR (400 MHz, $CDCl_3$) δ 7.44 (d, *J* = 2.6, 1H), 7.02 (d, *J* = 2.6, 1H), 6.19 – 6.15 (m, 2H), 1.67 (dd, *J* = 4.8, 1.8 Hz, 2H), 1.27 – 1.18 (m, 2H), 1.12 (m, 12H).

^{13}C NMR (101 MHz, $CDCl_3$) δ149.33, 130.71, 130.41, 129.83, 125.70, 124.66, 116.68, 17.55, 17.17, 13.67, 12.60.

HRMS (EI) m/z: $[M]^+$ Calcd for $C_{15}H_{20}BrClOSi$ 358.0150; Found 358.0150.

7,9-dichloro-2,2-diisopropyl-2,3-dihydrobenzo[*f*][1,2]oxasilepine (2.2j)

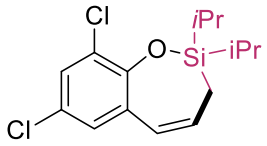

According to the general procedure for 2.A, **2.2j** was isolated in yield 99% (62 mg, colorless oil, Endo:Exo >20:1), purification by chromatography (only hexane).

^{1}H NMR (400 MHz, $CDCl_3$) δ 7.05 (d, *J* = 2.7, 1H), 6.76 (d, *J* = 2.7, 1H), 5.97 – 5.94 (m, 2H), 1.44 (dd, *J* = 4.8, 1.9 Hz, 2H), 1.02 – 0.94 (m, 2H), 0.90 (m, 12H).

^{13}C NMR (101 MHz, $CDCl_3$) δ 148.48, 130.76, 130.46, 128.99, 127.78, 126.92, 125.38, 124.53, 17.49, 17.15, 13.64, 12.69.

HRMS (EI) m/z: $[M]^+$ Calcd for $C_{15}H_{20}Cl_2OSi$ 314.0655; Found 314.0656.

2,2-diisopropyl-2,3-dihydronaphtho[2,3-*f*][1,2]oxasilepine (2.2k)

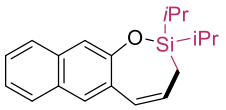

According to the general procedure for 2.A, **2.2k** was isolated in yield 99% (59 mg, colorless oil, Endo:Exo >20:1), purification by chromatography (only hexane).

^{1}H NMR (400 MHz, $CDCl_3$) δ 7.83 – 7.81 (m, 1H), 7.69 – 7.67 (m, 1H), 7.59 – 7.57 (m, 1H), 7.39-7.34 (m, 1H), 7.30-7.24 (m, 1H), 7.12 – 7.09 (m, 1H), 6.61 (d, *J* = 10.7 Hz, 1H), 6.24 (dt, *J* = 10.8, 7.7 Hz, 1H), 1.59 (dd, *J* = 7.8, 0.9 Hz, 2H), 1.16 – 1.06 (m, 2H), 1.05 – 1.00 (m, 12H).

^{13}C NMR (101 MHz, $CDCl_3$) δ 151.78, 133.48, 129.49, 129.45, 128.48, 128.11, 126.03, 123.95, 123.74, 123.02, 122.31, 121.07, 17.87, 17.56, 13.71, 12.82.

HRMS (EI) m/z: $[M]^+$ Calcd for $C_{19}H_{24}OSi$ 296.1591; Found 296.1592.

2,2-diisopropyl-5-phenyl-2,3-dihydrobenzo[*f*][1,2]oxasilepine (2.2l)

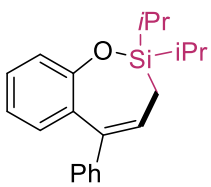

According to the general procedure for 2.A, **2.2l** was isolated in yield 98% (63 mg, colorless oil, Endo: Exo >20:1), purification by chromatography (only hexane).

^{1}H NMR (400 MHz, $CDCl_3$) δ 7.21 – 7.07 (m, 6H), 6.98 – 6.94 (m, 1H), 6.87 – 6.79 (m, 2H), 6.24 (t, *J* = 8.1 Hz, 1H), 1.63 (d, *J* = 8.1 Hz, 2H), 1.14 – 1.05 (m, 2H), 1.01 – 0.97 (m, 12H).

^{13}C NMR (101 MHz, $CDCl_3$) δ 154.88, 143.89, 137.08, 132.01, 130.72, 128.34, 128.03, 126.54, 126.04, 121.63, 121.29, 17.81, 17.55, 13.56, 13.44.

2,2-diisopropyl-4-methyl-2,3-dihydrobenzo[*f*][1,2]oxasilepine (2.2m, and other isomers, **2.2m'**, **2.2m"**, **2.2m"')**

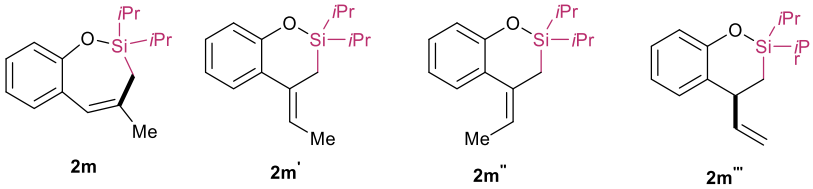

6.4:1:1.6:1.6

According to the general procedure for 2.A, **2.2m,** and other isomers, **2.2m'**, **2.2m"**, **2.2m"'** were obtained in 91% NMR yield (Ratio = 6.4:1:1.6:1.6), purification by chromatography (only hexane).

^{1}H NMR (400 MHz, $CDCl_3$) δ ppm only olefinic proton were analyzed: 2m = 6.10 (s, 6.4H), 2m'= 5.66-5.71 (q, 1H), 2m''=5.50 – 5.55 (q, 1.6H), 2m'''= 5.08-5.17 (dd, 3.2H).

^{13}C NMR (101 MHz, $CDCl_3$) δ 155.03, 155.00, 154.15, 154.00, 151.73, 142.40, 137.19, 134.01, 132.86, 131.62, 131.46, 130.71, 129.59, 129.54, 129.37, 129.05, 128.52, 128.42, 128.29, 127.92, 127.84, 127.76, 127.63, 127.28, 127.24, 126.33, 126.15, 126.06, 125.58, 121.89, 121.85, 121.64, 121.27, 121.25, 121.12, 121.01, 120.67, 120.60, 120.58, 120.13, 119.72, 119.62, 119.40, 119.27, 119.02, 114.44, 40.59, 34.27, 30.37, 27.71, 19.07, 18.89, 17.76, 17.72, 17.69, 17.65, 17.51, 17.46, 17.42, 17.38, 17.33, 17.17, 17.15, 17.10, 17.04, 17.00, 16.93, 16.89, 15.31, 14.07, 13.84, 13.66, 13.53, 13.27, 13.23, 12.95, 12.89, 12.76, 12.69, 12.57, 10.40.

2,2-diisopropyl-4-phenyl-2,3-dihydrobenzo[*f*][1,2]oxasilepine (2.2n)

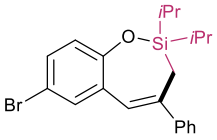

According to the general procedure for 2.A, **2.2n** was isolated in yield 90% (72 mg, colorless oil, Endo:Exo >20:1), purification by chromatography (hexane).

^{1}H NMR (300 MHz, $CDCl_3$) δ 7.24 – 7.12 (m, 4H), 7.12 – 7.03 (m, 3H), 6.84 (d, *J* = 8.6 Hz, 1H), 6.46 (d, *J* = 1.6 Hz, 1H), 2.00 (d, *J* = 1.5 Hz, 2H), 1.25 – 1.12 (m, 3H), 1.11 – 1.04 (m, 13H).

^{13}C NMR (75 MHz, $CDCl_3$) δ 154.46, 137.22, 133.65, 132.36, 131.89, 129.96, 129.02, 128.13, 126.50, 126.44, 121.32, 112.11, 29.74, 20.17, 17.10, 16.84, 12.89.

2,2-diisopropyl-7-phenyl-2,3,4,7-tetrahydro-1,2-oxasilepine (2.2o)

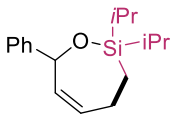

According to the general procedure for 2.A, **2.2o** was isolated in yield 78% (43 mg, colorless oil, Endo:Exo >20:1), purification by chromatography (hexane/ethyl acetate = 100 : 1).

^{1}H NMR (400 MHz, $CDCl_3$) δ 7.49 – 7.45 (m, 2H), 7.42 – 7.40 (m, 2H), 7.32 – 7.28 (m, 1H), 6.02 – 6.00 (m, 1H), 5.67 – 5.57 (m, 1H), 5.19 – 5.16 (dd, J = 9.0, 2.4 Hz, 1H), 2.70 – 2.48 (m, 2H), 1.89 – 1.70 (m, 2H), 1.28 – 1.09 (m, 14H).

^{13}C NMR (101 MHz, $CDCl_3$) δ 145.85, 128.19, 128.06, 126.74, 125.79, 125.29, 74.33, 40.10, 17.83, 17.74, 17.72, 17.64, 13.12, 12.94, 11.63.

2,2-diisopropyl-2,3,5a,6,7,8,9,9a-octahydrobenzo[*f*][1,2]oxasilepine (2.2p)

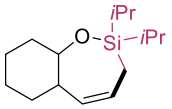

According to the general procedure for 2.A, **2.2p** was isolated in yield 89% (45 mg, colorless oil, Endo:Exo > 20:1), purification by chromatography (hexane/ethyl acetate = 100 : 1).

^{1}H NMR (400 MHz, $CDCl_3$) δ 5.77 – 5.71 (m, 1H), 5.15 – 5.10 (m, 1H), 3.60 (m, 1H), 2.22 (m, 1H), 1.99 (m, 1H), 1.76 – 1.47 (m, 5H), 1.37 – 1.07 (m, 4H), 1.03 – 0.92 (m, 14H).

^{13}C NMR (101 MHz, $CDCl_3$) δ 132.54, 125.20, 46.43, 36.42, 32.60, 25.53, 25.08, 17.83, 17.67, 17.50, 13.50, 13.25, 11.27.

2,2-diisopropyl-7-methyl-7-phenyl-2,3,6,7-tetrahydro-1,2-oxasilepine (2.2q)

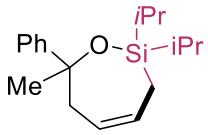

According to the general procedure for 2.A, **2.2q** was isolated in yield 75% (43 mg, colorless oil, Endo:Exo >20:1), purification by chromatography (hexane/ethyl acetate = 100:0 to 100:1).

^{1}H NMR (300 MHz, $CDCl_3$) δ 7.52 – 7.47 (m, 2H), 7.36 – 7.28 (m, 2H), 7.24 – 7.17 (m, 1H), 5.96 – 5.90 (m, 1H), 5.45 – 5.42 (m, 1H), 2.80 – 2.60 (m, 2H), 1.76 – 1.57 (m, 2H), 1.53 (s, 3H), 1.13 – 0.97 (m, 14H).

^{13}C NMR (75 MHz, $CDCl_3$) δ 149.59, 129.51, 127.75, 126.10, 124.86, 124.42, 40.94, 31.73, 29.72, 18.02, 17.83, 17.68, 17.62, 14.34, 13.78, 11.84.

HRMS (EI) m/z: $[M]^+$ Calcd for $C_{18}H_{28}OSi$ 288.1909; Found 288.1910.

2,2-diisopropyl-5-phenyl-2,3,6,7-tetrahydro-1,2-oxasilepine (2.2r)

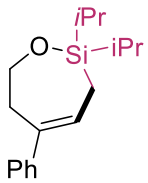

According to the general procedure for 2.A, **2.2r** was isolated in yield 89% (49 mg, colorless oil, Endo:Exo>20:1), purification by chromatography (hexane/ethyl acetate = 100 : 1).

^{1}H NMR (300 MHz, $CDCl_3$) δ 7.27 – 7.22 (m, 5H), 6.14 (t, *J* = 7.5, 1H), 4.01 – 3.95 (m, 2H), 2.81 – 2.75 (m, 2H), 1.74 (d, *J* = 7.5 Hz, 2H), 0.97 (m, *J* = 3.3, 1.8 Hz, 14H).

^{13}C NMR (75 MHz, $CDCl_3$) δ 143.53, 137.43, 128.34, 128.30, 126.30, 126.08, 125.52, 63.58, 34.88, 17.68, 17.59, 13.36, 13.04.

(*E*)-2,2-diisopropyl-5-phenyl-3,6,7,8-tetrahydro-2H-1,2-oxasilocine (2.2s)

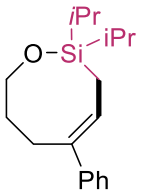

According to the general procedure for 2.A, **2.2s** was produced in 78% (NMR yield)

^{1}H NMR (400 MHz, $CDCl_3$) δ 7.42 – 7.20 (m, 5H), 6.22 (t, *J* = 8.24, 1H), 3.76 – 3.73 (m, 2H), 2.74 (m, 2H), 1.83 (d, *J* = 8.2 Hz, 2H), 1.77 (m, 2H), 1.13 (m, 14H).

2,2-diisopropyl-8-methyl-5-methylenedecahydrobenzo[*f*][1,2]oxasilepine (2.2t)

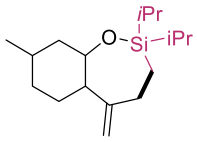

According to the general procedure for 2.A, **2.2t** was isolated in yield 80% (45 mg, colorless oil, Endo:Exo >20:1), purification by chromatography (hexane/ethyl acetate = 100:1).

^{1}H NMR (400 MHz, $CDCl_3$) δ 4.91 – 4.72 (m, 2H), 3.52 – 3.55 (m, 1H), 2.32 – 2.36 (m, 1H), 2.27 – 2.20 (m, 1H), 2.06 – 1.92 (m, 2H), 1.62 – 1.57 (m, 2H), 1.44 – 1.46 (m, 1H), 1.38 – 1.25 (m, 1H), 1.13 – 0.86 (m, 19H), 0.84 – 0.77 (m, 2H).

^{13}C NMR (101 MHz, $CDCl_3$) δ 155.35, 111.76, 74.98, 53.37, 44.68, 34.51, 31.89, 31.78, 29.54, 22.15, 17.93, 17.49, 17.36, 13.68, 12.77, 11.87.

7.3.3. Analytical data for chapter 4

methyl cinnamate (3.2a)

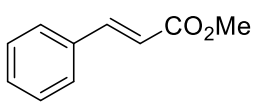

According to the general procedure for 3.A, **3.2a** was isolated in 82% yield (white solid, 27 mg), (E:Z) > 20:1, purification by chromatography (hexane/ethyl acetate = 20:1).

^{1}H NMR (300 MHz, $CDCl_3$) δ 7.75 – 7.70 (d, *J* = 16.0 Hz, 1H), 7.59 – 7.51 (m, 2H), 7.44 – 7.38 (m, 3H), 6.47 (d, J = 16.0 Hz, 1H), 3.83 (s, 3H).

^{13}C NMR (75 MHz, $CDCl_3$) δ167.4, 144.9, 134.4, 130.3, 128.9, 128.1, 117.8, 51.7.

benzyl cinnamate (3.2b)

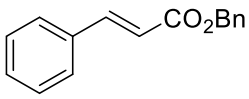

According to the general procedure for 3.A, **3.2b** was isolated in yield 85% (white solid, 40 mg), (E:Z) > 20:1, purification by chromatography (hexane/ethyl acetate = 20:1 to 10:1).

^{1}H NMR (300 MHz, $CDCl_3$) δ 7.65 (d, *J* = 16.0 Hz, 1H), 7.45 – 7.41 (m, 2H), 7.37 – 7.21 (m, 8H), 6.40 (d, *J* = 16.0 Hz, 1H), 5.17 (s, 2H).

^{13}C NMR (101 MHz, $CDCl_3$) δ 166.8, 145.2, 136.1, 134.4, 130.4, 128.9, 128.6, 128.3, 128.3, 128.2, 117.9, 66.4.

benzyl (*E*)-3-(3-fluorophenyl)acrylate (3.2c)

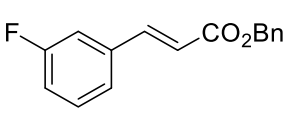

According to the general procedure for 3.A, **3.2c** was determined by NMR yield: 69%, (E:Z) > 20:1, purification by chromatography (hexane/ethyl acetate = 10:1).

^{1}H NMR (300 MHz, $CDCl_3$) δ 7.60 (dd, *J* = 16.0, 0.7 Hz, 1H), 7.39 – 7.00 (m, 9H), 6.40 (d, *J* = 16.0 Hz, 1H), 5.18 (s, 2H).

^{13}C NMR (101 MHz, $CDCl_3$) δ 166.4, 161.4, 143.8, 135.9, 130.5, 130.4, 128.7, 128.4, 124.1, 119.3, 117.4, 117.1, 114.5, 114.2, 66.6.

^{19}F NMR (282 MHz, $CDCl_3$) δ -112.46 (td, *J* = 8.9, 5.5 Hz)

benzyl (*E*)-3-(4-chlorophenyl)acrylate (3.2d)

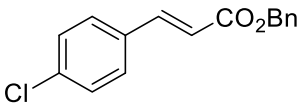

According to the general procedure for 3.A, **3.2d** was determined by NMR yield: 74%, (E:Z) > 20:1, purification by chromatography (hexane/ethyl acetate = 10:1).

^{1}H NMR (300 MHz, $CDCl_3$) δ 7.68 (d, *J* = 16.0 Hz, 1H), 7.49 – 7.32 (m, 9H), 6.46 (d, *J* = 16.0 Hz, 1H), 5.26 (s, 2H).

^{13}C NMR (101 MHz, $CDCl_3$) δ 166.6, 143.7, 136.3, 136.0, 132.9, 129.3, 129.2, 128.7, 118.5, 66.5.

benzyl (*E*)-3-(4-bromophenyl)acrylate (3.2e)

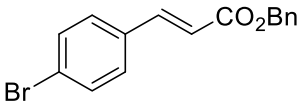

According to the general procedure for 3.A, **3.2e** was determined by NMR yield: 76%, (E:Z) > 20:1, purification by chromatography (hexane/ethyl acetate = 5:1).

^{1}H NMR (300 MHz, $CDCl_3$) δ 7.57 (d, *J* = 16.0 Hz, 1H), 7.47 – 7.38 (m, 2H), 7.37 – 7.24 (m, 7H), 6.39 (d, *J* = 16.0 Hz, 1H), 5.17 (s, 2H).

^{13}C NMR (101 MHz, $CDCl_3$) δ 166.5, 143.8, 135.9, 133.3, 132.2, 129.5, 128.7, 128.4, 124.6, 118.6, 66.5.

benzyl (*E*)-3-(4-(benzyloxy)phenyl)acrylate (3.2f)

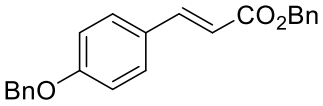

According to the general procedure for 3.A, **3.2f** was isolated in yield 83% (white solid, 57 mg), (E:Z) > 20:1, purification by chromatography (hexane/ethyl acetate = 10:1).

^{1}H NMR (300 MHz, $CDCl_3$): δ 7.59 (d, J = 16.0 Hz, 1H), 7.41 – 7.17 (m, 12H), 6.90 – 6.82 (m, 2H), 6.26 (d, *J* = 16.0 Hz, 1H), 5.14 (s, 2H), 4.97 (s, 2H).

^{13}C NMR (101 MHz, $CDCl_3$) δ 167.1, 160.7, 144.8, 136.5, 136.3, 129.8, 128.7, 128.6, 128.3, 128.2, 128.2, 127.5, 127.4, 115.5, 115.3, 70.1, 66.2.

HRMS (EI) m/z: $[M]^+$ Calcd for $C_{23}H_{20}O_3$ 344.1412; Found 344.1407.

benzyl (*E*)-4-phenylbut-2-enoate (3.2g)

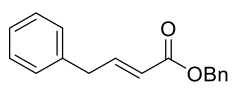

According to the general procedure for 3.A, **3.2g** was isolated in yield 80% (colorless oil, 40 mg), (E:Z) = 4 :1, purification by chromatography (hexane/diethyl ether = 20:1).

^{1}H NMR for the major product: **^{1}H NMR (300 MHz, $CDCl_3$)** δ 7.45 – 7.15 (m, 11H), 6.59 – 5.88 (m, 1H), 5.22 (s, 2H), 3.58 – 3.34 (m, 2H).

^{13}C NMR for the major product: **^{13}C NMR (75 MHz, $CDCl_3$)** δ 166.3, 148.1, 137.6, 136.1, 135.9, 133.6, 128.9, 128.8, 128.6, 128.3, 126.8, 122.1, 121.6, 66.2, 38.4.

benzyl (*E*)-4-methylpent-2-enoate (3.2h)

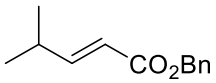

According to the general procedure for 3.A, **3.2h** was isolated in yield 66% (clear oil, 27 mg), (E:Z) > 20:1, purification by chromatography (hexane/diethyl ether = 30:1).

^{1}H NMR (300 MHz, $CDCl_3$) δ 7.39 – 7.19 (m, 5H), 6.99 (dd, *J* = 15.7, 6.6 Hz, 1H), 5.80 (d, *J* = 15.7, 1H), 5.10 (s, 2H), 2.48 – 2.44 (m, 1H), 1.08 (s, 3H), 1.06 (s, 3H).

^{13}C NMR (75 MHz, $CDCl_3$) δ 166.9, 156.2, 136.2, 128.6, 128.3, 118.3, 66.1, 31.0, 21.2.

benzyl (*E*)-hex-2-enoate (3.2i)

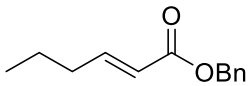

According to the general procedure for 3.A, **3.2i** was isolated in yield 71% (clear oil, 30 mg), (E:Z) > 20:1, purification by chromatography (hexane/diethyl ether = 30:1).

^{1}H NMR (300 MHz, $CDCl_3$): δ 7.34 – 7.21 (m, 5H), 6.9 – 6.94 (m, 1H), 5.80 (dt, *J* = 15.7, 1.6 Hz, 1H), 5.10 (s, 2H), 2.15 – 2.06 (m, 2H), 1.45 – 1.38 (m, 2H), 0.86 (t, J = 7.4 Hz, 3H).

^{13}C NMR (101 MHz, $CDCl_3$) δ ^{13}C NMR (75 MHz, $CDCl_3$) δ 166.5, 150.0, 136.2, 128.6, 128.2, 128.2, 121.1, 66.0, 34.3, 21.2, 13.7.

benzyl (*E*)-3-methylpent-2-enoate (3.2j)

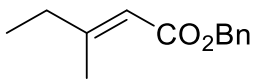

According to the general procedure for 3.A, **3.2j** was determined by NMR yield: 83%, (E:Z) = 1.2:1, purification by chromatography (hexane/diethyl ether = 30:1). The NMR data of the major product (*E*) is shown.

^{1}H NMR (300 MHz, $CDCl_3$) δ 7.46 – 7.34 (m, 5H), 5.8 (m, 1H), 5.2 (s, 2H), 2.26 (d, *J* = 1.3 Hz, 3H), 2.22 (dd, *J* = 7.4, 1.3 Hz, 2H), 2.25 (d, 3H), 1.15 (t, *J* = 7.6 Hz, 1H).

benzyl (*E*)-4-(methylthio)but-2-enoate (3.2k)

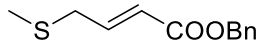

According to the general procedure for 3.A, **3.2k** was determined by NMR yield: 71%, (E:Z) > 20:1, purification by chromatography (hexane/diethyl ether = 10:1).

^{1}H NMR (300 MHz, $CDCl_3$) δ 7.43 – 7.36 (m, 5H), 6.94 (dt, *J* = 15.5, 7.5 Hz, 1H), 5.96 – 5.91 (m, 1H), 5.22 (s, 2H), 3.21 (dd, *J* = 7.4, 1.3 Hz, 2H), 2.05 (s, 3H).

^{13}C NMR (101 MHz, $CDCl_3$) δ 165.8, 143.8, 135.9, 128.6, 128.3, 122.6, 66.3, 34.9, 14.7.

HRMS (EI) m/z: $[M]^+$ Calcd for $C_{12}H_{14}O_2S$ 222.0715; Found 222.0706.

methyl (*R*)-1-benzoyl-2,3-dihydro-1*H*-pyrrole-2-carboxylate (3.2l)

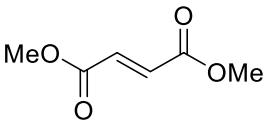

According to the general procedure for 3.A, **3.2l** was determined by NMR yield in 60% without further purification.

^{1}H NMR (400 MHz, $CDCl_3$) δ 6.82 (s, 2H), 3.76 (s, 6H).

dibenzyl (*E*)-pent-2-enedioate (3.2m)

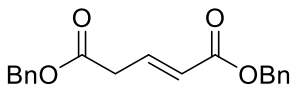

According to the general procedure for 3.A, **3.2m** was isolated in yield 71% (clear oil, 42 mg), (E:Z) > 20:1, purification by chromatography (hexane/ ethyl acetate = 10:1).

^{1}H NMR (300 MHz, $CDCl_3$) δ7.39 – 7.33 (m, 10H), 7.09 (dt, *J* = 15.7, 7.2 Hz, 1H), 6.00 (dt, *J* = 15.7, 1.6 Hz, 1H), 5.22 – 5.16 (m, 4H), 3.29 (dd, *J* = 7.2, 1.6 Hz, 2H).

^{13}C NMR (75 MHz, $CDCl_3$) δ 169.6, 165.5, 140.1, 135.9, 135.4, 128.7, 128.6, 128.5, 128.4, 128.3, 128.2, 124.6, 67.0, 66.4, 37.42.

methyl (*E*)-4-oxo-4-(tritylamino)but-2-enoate (3.2n)

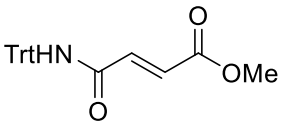

According to the general procedure for 3.A, **3.2n** was isolated in yield 86% (white solid, 39 mg), (E:Z) > 20:1, purification by chromatography (hexane/ ethyl acetate = 5:1),

^{1}H NMR (300 MHz, $CDCl_3$) δ 7.36 – 7.26 (m, 9H), 7.23 – 7.17 (m, 6H), 7.03 (d, *J*= 15.3, 1H), 6.88 (s, 1H), 6.79 (d, *J*=15.3, 1H), 3.78 (s, 3H).

^{13}C NMR (75 MHz, $CDCl_3$) δ 166.0, 162.5, 144.1, 137.1, 130.6, 128.6, 128.1, 127.3, 71.1, 52.2.

HRMS (EI) m/z: $[M]^+$ Calcd for $C_{24}H_{21}NO_3$ 371.1521; Found 371.1514.

(benzyl-5-oxo-5-(tritylamino)pent-2-enoate (3.2o)

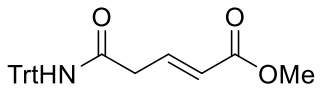

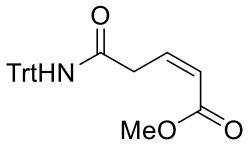

According to the general procedure for 3.A, **3.2o** was determined by NMR yield: 81%, (E:Z) > 1.5:1, purification by chromatography (hexane/ ethyl acetate = 10:1). NMR signals of the major (*E*)-product are shown.

^{1}H NMR (300 MHz, $CDCl_3$) δ 7.21-7.32 (m, 15 H), 7.05 (dt, *J* = 15.7, 7.2 Hz, 1H). 6.7 (m, 1H), 5.95 (dt, *J* = 15.7, 1.5 Hz, 1H), 3.76 (3H, m), 3.17-3.19 (m, 2H).

HRMS (EI) m/z: $[M]^+$ Calcd for $C_{25}H_{23}NO_3$ 385.1678; Found 385.1672.

benzyl (*E*)-6-(((benzyloxy)carbonyl)amino)hex-2-enoate (3.2p)

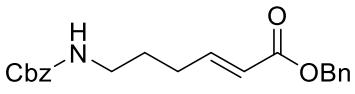

According to the general procedure for 3.A, **3.2p** was isolated in yield 59% (yellow oil, 42 mg), (E:Z) > 20:1, purification by chromatography (hexane/ ethyl acetate = 5:1).

^{1}H NMR (400 MHz, $CDCl_3$) δ 7.40 – 7.28 (m, 10H), 6.99 (dt, *J* = 15.6, 6.9 Hz, 1H), 5.89 (d, *J* = 15.7, 1H), 5.17 (s, 2H), 5.10 (s, 2H), 4.86 (s, 1H), 3.21 (q, *J* = 6.7 Hz, 2H), 2.29 – 2.18 (m, 2H), 1.69 – 1.64 (m, 2H).

^{13}C NMR (101 MHz, $CDCl_3$) δ 166.3, 156.4, 148.5, 136.5, 136.1, 128.6, 128.6, 128.2, 128.2, 128.2, 128.1, 121.7, 66.7, 66.1, 40.5, 29.4, 28.4.

HRMS (EI) m/z: $[M]^+$ Calcd for $C_{21}H_{23}NO_4$ 353.1627; Found 353.1623.

methyl (*E*)-3-(1-methyl-1H-indol-3-yl)acrylate (3.2q)

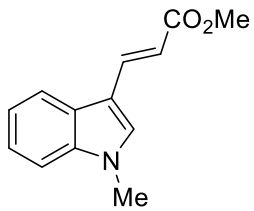

According to the general procedure for 3.A, **3.2q** was isolated in yield 86% (yellow solid, 37 mg), (E:Z) > 20:1, purification by chromatography (hexane/ ethyl acetate = 5:1).

^{1}H NMR (300 MHz, $CDCl_3$) δ 7.98 – 7.88 (m, 2H), 7.40 – 7.24 (m, 4H), 6.44 (d, J = 16.0 Hz, 1H), 3.84 (s, 3H), 3.81 (s, 3H).

^{13}C NMR (101 MHz, $CDCl_3$) δ 168.8, 138.3, 138.1, 133.2, 126.0, 123.0, 121.3, 120.6, 112.1, 112.0, 110.0, 51.4, 33.2.

methyl (*E*)-3-(1H-indol-3-yl)acrylate (3.2r)

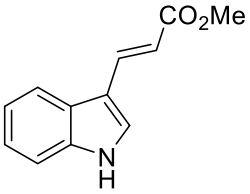

According to the general procedure for 3.A, **3.2r** was isolated in yield 81% (yellow solid, 33 mg), (E:Z) > 20:1, purification by chromatography (hexane/ ethyl acetate = 5:1).

^{1}H NMR (400 MHz, $CDCl_3$) δ 8.57 (s, 1H), 7.92 – 7.79 (m, 2H), 7.40 – 7.39 (m, 1H), 7.37 – 7.31 (m, 1H), 7.25 – 7.13 (m, 2H), 6.40 (dd, J = 16.0, 0.4 Hz, 1H), 3.74 (s, 3H).

^{13}C NMR (75 MHz, $CDCl_3$) δ 168.8, 138.5, 137.1, 128.9, 125.3, 123.4, 121.6, 120.5, 113.6, 113.0, 111.8, 51.5.

1H-indene (3.2s)

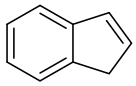

According to the general procedure for 3.A, **3.2s** was determined by NMR yield: 70%, purification by chromatography (hexane).

^{1}H NMR (400 MHz, $CDCl_3$) δ 7.52 – 7.51 (m, 1H), 7.49 – 7.48 (m, 1H), 7.29 – 7.18 (m, 2H), 6.92 – 6.90 (m, 1H), 6.59 – 6560 (m, 1H), 3.43 – 3.42 (m, 2H).

^{13}C NMR (101 MHz, $CDCl_3$) δ 144.8, 143.6, 134.08, 132.07, 126.21, 124.53, 123.69, 120.94, 39.03.

Allylbenzene (3.2t)

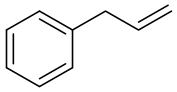

According to the general procedure for 3.A, **3.2t** was determined by NMR yield in 58% without further purification. The ^{1}H NMR data of the olefin part is shown.

^{1}H NMR (300 MHz, $CDCl_3$) δ5.98 – 5.84 (m, 1H), 5.11 – 5.04 (m, 2H).

but-3-en-1-ylbenzene (3.2u)

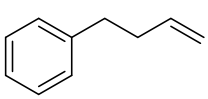

According to the general procedure for 3.A, **3.2u** was determined by NMR yield in 60% NMR yield without further purification. The ^{1}H NMR data of the olefin part is shown.

^{1}H NMR (300 MHz, $CDCl_3$) δ 4.93 – 4.74 (m, 2H).

3,6-dihydro-2H-pyran (3.2v)

According to the general procedure for 3.A, **3.2v** was determined by NMR yield in 70% NMR yield without further purification. The ^{1}H NMR data of the olefin part is shown.

^{1}H NMR (300 MHz, CD_3CN) δ 5.90 – 5.80 (m, 1H), 5.78 – 5.68 (m, 1H).

benzyl 3,6-dihydropyridine-1(2H)-carboxylate (3.2w)

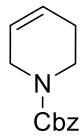

According to the general procedure for 3.A, **3.2w** was isolated in yield 75% (yellow oil, 33 mg), (E:Z) > 20:1, purification by chromatography (hexane/ ethyl acetate = 10:1).

^{1}H NMR (400 MHz, $CDCl_3$) δ 7.30 – 7.24 (m, 5H), 5.77 – 5.74 (m, 1H), 5.58 – 5.58 (m, 1H), 5.08 (s, 2H), 3.93 – 3.84 (m, 2H), 3.49 (t, J = 5.7 Hz, 2H), 2.07 – 2.06 (m, 2H).

^{13}C NMR (101 MHz, $CDCl_3$) δ 155.5, 136.9, 128.6, 128.5, 128.3, 128.0, 127.9, 125.5, 124.5, 123.9, 77.5, 77.1, 76.6, 67.0, 43.5, 43.5, 40.3, 24.9, 24.9.

tert-butyl 2,5-dihydro-1H-pyrrole-1-carboxylate (3.2x)

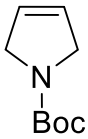

According to the general procedure for 3.A, **3.2x** was determined in 65% NMR yield without further purification. The ^{1}H NMR data of the olefin part is shown.

^{1}H NMR (300 MHz, CD_3CN) δ 5.87–5.67 (m, 2H).

Cyclododecene (3.2y)

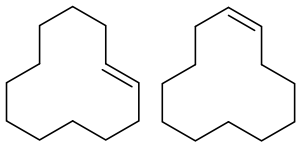

According to the general procedure for 3.A, **3.2y** was determined in 70% NMR yield, (E:Z) = 2.5 :1, purification by chromatography (hexane). NMR signals of the major (*E*)-product are shown.

^{1}H NMR (400 MHz, $CDCl_3$) δ 5.41 – 5.39 (m, 2H), 2.11 – 2.03 (m, 4H), 1.50 – 1.41 (m, 4H), 1.33 – 1.28 (m, 8H).

^{13}C NMR (101 MHz, $CDCl_3$) δ 131.4, 130.4, 32.1, 31.6, 26.9, 26.2, 25.6, 24.9, 24.6, 24.6, 24.3, 23.9, 22.7, 22.0.

3-phenylprop-2-en-1-ol (3.2z)

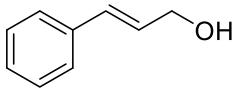

According to the general procedure for 3.A, **3.2z** was determined in 65% NMR yield, (E:Z) = 3 :1, purification by chromatography (hexane/ ethyl acetate = 10:1). NMR signals of the major (*E*)-product are shown.

^{1}H NMR (300 MHz, $CDCl_3$) δ 7.35 – 7.11 (m, 5H), 6.55 (m, 1H), 6.30 (m, 1H), 4.26 (dd, *J* = 5.7, 1.5 Hz, 2H).

^{13}C NMR (75 MHz, CD_3OD) δ 136.6, 131.2, 128.6, 128.5, 127.7, 126.5, 63.8.

cyclohex-3-en-1-ol (3.2aa)

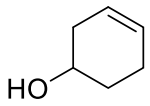

According to the general procedure for 3.A, **3.2aa** was determined in 65% NMR yield without further purification. The ^{1}H NMR data of the C–H part is shown.

^{1}H NMR (300 MHz, CD$_3$CN) δ 3.88 – 3.80 (m, 1H).

(5*S*,8*R*,9*S*,10*S*,13*S*,14*S*,17*S*)-10,13-dimethyl-4,5,6,7,8,9,10,11,12,13,14,15,16,17-tetradecahydro-1H-cyclopenta[a]phenanthren-17-ol (3.2ab)

(5*S*,8*R*,9*S*,10*S*,13*S*,14*S*,17*S*)-10,13-dimethyl-2,5,6,7,8,9,10,11,12,13,14,15,16,17-tetradecahydro-1H-cyclopenta[a]phenanthren-17-ol (3.2ab')

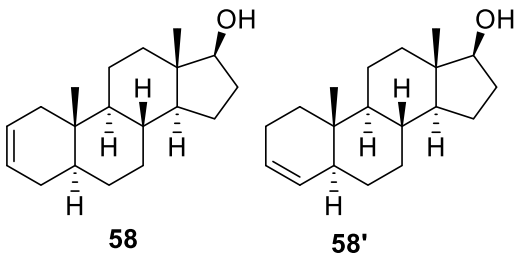

58 **58'**

According to the general procedure for 3.A, **3.2ab** and **3.2ab'** were determined in 65% NMR yield, the ratio of **3.2ab**/**3.2ab'** is 1:1. Purification was done by chromatography (hexane/ ethyl acetate = 10:1).

The ^{1}H NMR data of the olefin part is shown: **^{1}H NMR (300 MHz, CDCl$_3$)** δ 5.65 – 5.50 (m, 3H), 5.30 – 5.26 (m, 1H).

The ^{13}C NMR data of **58** and **58'** is shown: **^{13}C NMR (75 MHz, CDCl$_3$)** δ 131.3, 125.9, 125.8, 125.5, 82.0, 54.2, 53.5, 51.1, 51.0, 46.0, 43.2, 42.9, 41.5, 39.8, 36.8, 36.8, 35.7, 35.0, 34.7, 34.1, 31.6, 31.4, 30.6, 30.5, 30.3, 28.6, 27.3, 23.5, 23.4, 20.6, 20.5, 11.9, 11.7, 11.2, 11.1.

2-(allyloxy)-1,3-dimethylbenzene (3.2ac)

1,3-dimethyl-2-(prop-1-en-1-yloxy)benzene(3.2ac')

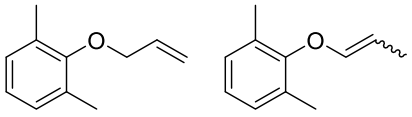

According to the general procedure for 3.A, **3.2ac** and **3.2ac'** were determined in 65% NMR yield, the ratio of **3.2ab**/**3.2ab'** is 3.3:1. Purification was done by chromatography (hexane/ ethyl acetate = 8:1). The ^{1}H NMR signals of the major (*E*)-product is shown.

^{1}H NMR (300 MHz, CDCl$_3$) δ 6.97 – 6.90 (m, 3H), 6.08 –5.99 (m, 1H), 5.39 – 5.32 (m, 1H), 5.20 – 5.16 (m, 1H), 4.25 – 4.23 (m, 2H), 2.21 (s, 6H).

^{13}C NMR (75 MHz, CDCl$_3$) δ 155.9, 134.2, 131.0, 130.7, 123.8, 117.1, 73.1.

(*E*)-*N*-acetyl-*N*-(2-methoxyvinyl)benzamide (3.2ad)

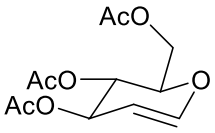

According to the general procedure for 3.A, **3.2ad** was isolated in yield 85% (yellow oil, 46 mg), purification by chromatography (hexane/ethyl acetate = 5:1).

^{1}H NMR (400 MHz, $CDCl_3$) δ 6.47 (dd, J = 6.2, 1.4 Hz, 1H), 5.34 – 5.33 (m, 1H), 5.23 (dd, J = 7.5, 5.7 Hz, 1H), 4.87 – 4.83 (m, 1H), 4.43 – 4.38 (m, 1H), 4.29 – 4.14 (m, 2H), 2.10 (s, 3H), 2.08 (s, 3H), 2.05 (s, 3H).

^{13}C NMR (101 MHz, $CDCl_3$) δ 170.6, 170.4, 169.6, 145.6, 99.0, 73.9, 67.4, 67.17, 61.4, 21.0, 20.8, 20.7.

HRMS (EI) m/z: $[M]^+$ Calcd for $C_{12}H_{17}O_6$ 272.0896; Found 272.0899.

7.3.4. Analytical data for chapter 5

4-chloro-4-methylpentan-2-yl ethanesulfonate (4.2a)

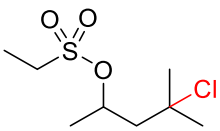

According to the general procedure 4.A with the use of p-Toluenesulfonyl chloride as radical trap, **4.1a** was isolated in 84% yield (38 mg, 0.162 mmol), purification by chromatography (gradient elution from pure n-hexane to n-hexane/ethyl acetate (v/v 10:1)).

^{1}H NMR (300 MHz, $CDCl_3$) δ = 5.18 – 5.08 (m, 1H), 3.12 (q, *J*=7.5, 2H), 2.26 (dd, *J*=15.4, 6.8, 1H), 2.03 (dd, *J*=15.4, 3.9, 1H), 1.65 (d, *J*=8.6, 6H), 1.52 (d, *J*=6.3, 3H), 1.43 (t, *J*=7.4, 3H).

^{13}C NMR (75 MHz, $CDCl_3$) δ 68.17, 52.19, 46.58, 33.89, 32.07, 29.84, 23.29, 8.28.

2-chloro-2,6-dimethylheptan-4-yl ethanesulfonate (4.2b)

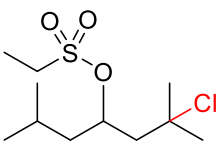

According to the general procedure 4.A with the use of p-Toluenesulfonyl chloride as radical trap, 4.1b was isolated in 83% yield (44 mg, 0.166 mmol), purification by chromatography (gradient elution from pure n-hexane to n-hexane/ethyl acetate (v/v 10:1)).

^{1}H NMR (300 MHz, $CDCl_3$) δ = 5.07 (m, 1H), 3.12 (q, *J*=7.5, 2H), 2.22 (dd, *J*=15.5, 5.8, 1H), 2.14 (dd, *J*=15.4, 4.5, 1H), 1.81 – 1.71 (m, 2H), 1.66 (d, *J*=10.9, 6H), 1.43 (t, *J*=7.4, 3H), 0.98 (dd, *J*=6.4, 3.2, 6H).

^{13}C NMR (75 MHz, $CDCl_3$) δ 79.04, 68.36, 50.36, 46.77, 45.61, 34.06, 32.15, 24.81, 22.68, 22.63, 8.30.

2-chloro-2-methyldecan-4-yl ethanesulfonate (4.2c)

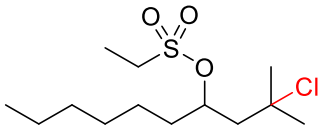

According to the general procedure 4.A with the use of p-Toluenesulfonyl chloride as radical trap, **4.2c** was isolated in 62% yield (36 mg, 0.124 mmol), purification by chromatography (gradient elution from pure n-hexane to n-hexane/ethyl acetate (v/v 10:1)).

^{1}H NMR (300 MHz, $CDCl_3$) δ = 5.07 – 4.97 (m, 1H), 3.12 (q, *J*=7.5, 2H), 2.20 (dd, *J*=15.5, 6.2, 1H), 2.11 (dd, *J*=15.5, 4.1, 1H), 1.93 – 1.75 (m, 2H), 1.65 (d, *J*=7.8, 6H), 1.44 (d, *J*=7.4, 3H), 1.40 – 1.20 (m, 8H), 0.92 – 0.84 (m, 3H).

^{13}C NMR (75 MHz, $CDCl_3$) δ 80.29, 68.43, 49.77, 46.71, 36.38, 33.95, 32.06, 31.78, 29.15, 24.49, 22.68, 14.18, 8.30.

(1R,2S,5R)-2-(2-chloropropan-2-yl)-5-methylcyclohexyl ethanesulfonate (4.2d)

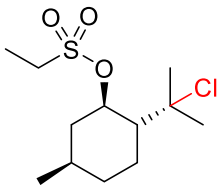

According to the general procedure 4.A with the use of p-Toluenesulfonyl chloride as radical trap, **4.2d** was isolated in 80% yield (45 mg, 0.160 mmol), purification by chromatography (gradient elution from pure n-hexane to n-hexane/ethyl acetate (v/v 10:1)).

^{1}H NMR (300 MHz, $CDCl_3$) δ = 4.79 (ddd, *J*=11.0, 10.0, 4.4, 1H), 3.14 (q, *J*=7.5, 2H), 2.37 (dddd, *J*=12.3, 4.5, 3.4, 2.2, 1H), 2.22 (dq, *J*=13.7, 3.5, 1H), 1.86 (ddd, *J*=12.0, 10.0, 3.7, 1H), 1.68 (d, *J*=3.2, 6H), 1.44 (t, *J*=7.4, 3H), 1.39 – 1.22 (m, 4H), 0.94 (d, *J*=6.5, 3H).

^{13}C NMR (75 MHz, $CDCl_3$) δ 82.42, 73.10, 52.84, 47.35, 42.86, 33.81, 33.40, 31.46, 31.27, 27.65, 21.69, 8.18.

4-bromo-4-methylpentan-2-yl ethanesulfonate (4.2e)

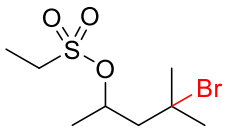

According to the general procedure 4.A with the use of p-Toluenesulfonyl bromide as radical trap, **4.2e** was isolated in 75% yield (40 mg, 0.150 mmol), purification by chromatography (gradient elution from pure n-hexane to n-hexane/ethyl acetate (v/v 10:1)).

^{1}H NMR (300 MHz, $CDCl_3$) δ = 5.21 – 5.07 (m, 1H), 3.13 (q, *J*=7.5, 2H), 2.30 (dd, *J*=15.6, 7.0, 1H), 2.15 (dd, *J*=15.6, 3.6, 1H), 1.84 (d, *J*=5.5, 6H), 1.53 (d, *J*=6.3, 3H), 1.43 (t, *J*=7.4, 3H).

^{13}C NMR (75 MHz, $CDCl_3$) δ 63.99, 53.59, 46.65, 35.64, 33.77, 23.22, 8.29.

2-bromo-2,6-dimethylheptan-4-yl ethanesulfonate (4.2f)

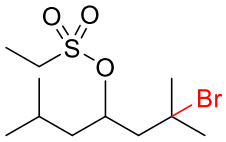

According to the general procedure 4.A with the use of p-Toluenesulfonyl bromide as radical trap, **4.2f** was isolated in 67% yield (42 mg, 0.134 mmol), purification by chromatography (gradient elution from pure n-hexane to n-hexane/ethyl acetate (v/v 10:1)).

^{1}H NMR (300 MHz, $CDCl_3$) δ = 5.12 – 5.02 (m, 1H), 3.12 (q, *J*=7.5, 2H), 2.26 (dd, *J*=5.1, 1.5, 2H), 1.84 (d, *J*=6.8, 6H), 1.79 – 1.58 (m, 4H), 1.42 (t, *J*=7.4, 3H), 0.98 (d, *J*=6.1, 6H).

^{13}C NMR (75 MHz, $CDCl_3$) δ 79.79, 64.24, 51.69, 46.84, 45.52, 35.84, 33.81, 24.79, 22.79, 22.57, 8.29.

2-bromo-2-methyldecan-4-yl ethanesulfonate (4.2g)

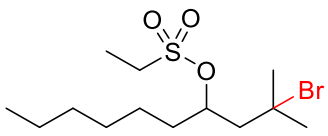

According to the general procedure 4.A with the use of p-Toluenesulfonyl bromide as radical trap, **4.2g** was isolated in 75% yield (51 mg, 0.150 mmol), purification by chromatography (gradient elution from pure n-hexane to n-hexane/ethyl acetate (v/v 10:1)).

^{1}H NMR (300 MHz, $CDCl_3$) δ = 5.08 – 4.99 (m, 1H), 3.17 – 3.08 (m, 2H), 2.26 – 2.22 (m, 2H), 1.84 (d, *J*=3.2, 6H), 1.43 (t, J=7.5, 1H), 1.41 – 1.19 (m, 10H), 0.91 – 0.85 (m, 3H).

^{13}C NMR (75 MHz, $CDCl_3$) δ 81.02, 64.36, 51.12, 46.78, 36.31, 35.73, 33.71, 31.77, 29.16, 24.41, 22.68, 14.18, 8.30.

3-bromo-1-cyclohexyl-3-methylbutyl ethanesulfonate (4.2h)

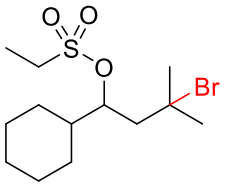

According to the general procedure 4.A with the use of p-Toluenesulfonyl bromide as radical trap, **4.2h** was isolated in 61% yield (41 mg, 0.122 mmol), purification by chromatography (gradient elution from pure n-hexane to n-hexane/ethyl acetate (v/v 10:1)).

^{1}H NMR (300 MHz, $CDCl_3$) δ = 4.98 – 4.90 (m, 1H), 3.12 (qd, *J*=7.5, 1.0, 2H), 2.30 (dd, *J*=15.8, 2.8, 1H), 2.08 (dd, *J*=15.8, 7.1, 1H), 1.97 (tq, *J*=11.8, 2.8, 1H), 1.83 (d, *J*=2.0, 6H), 1.80 – 1.67 (m, 5H), 1.43 (t, *J*=7.5, 3H), 1.28 – 1.07 (m, 5H).

^{13}C NMR (75 MHz, $CDCl_3$) δ 84.71, 64.82, 47.31, 47.06, 43.10, 35.74, 33.52, 28.22, 26.83, 26.50, 26.20, 26.12, 8.31.

4-azido-4-methylpentan-2-yl ethanesulfonate (4.2i)

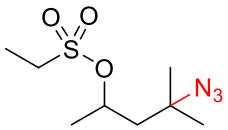

According to the general procedure 4.A with the use of p-Toluenesulfonyl azide as radical trap, **4.2i** was isolated in 60% yield (28 mg, 0.120 mmol), purification by chromatography (gradient elution from pure n-hexane to n-hexane/ethyl acetate (v/v 5:1)).

^{1}H NMR (300 MHz, $CDCl_3$) δ = 5.01 (m, 1H), 3.12 (q, *J*=7.4, 2H), 2.00 (dd, *J*=15.1, 7.0, 1H), 1.70 (dd, *J*=15.0, 4.4, 1H), 1.49 (d, *J*=6.3, 3H), 1.43 (t, *J*=7.4, 3H), 1.36 (d, *J*=5.4, 6H).

^{13}C NMR (75 MHz, $CDCl_3$) δ 75.92, 60.05, 47.69, 46.49, 27.09, 26.02, 23.04, 8.26.

2-azido-2,6-dimethylheptan-4-yl ethanesulfonate (4.2j)

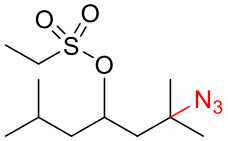

According to the general procedure 4.A with the use of p-Toluenesulfonyl azide as radical trap, **4.2j** was isolated in 38% yield (21 mg, 0.076 mmol), purification by chromatography (gradient elution from pure n-hexane to n-hexane/ethyl acetate (v/v 5:1)).

^{1}H NMR (300 MHz, $CDCl_3$) δ = 4.98 – 4.91 (m, 1H), 3.17 – 3.07 (m, 2H), 1.96 (dd, *J*=15.1, 5.9, 1H), 1.79 (dd, J=15.1, 5.1, 1H), 1.73 – 1.57 (m, 3H), 1.43 (t, *J*=7.5, 3H), 1.36 (d, *J*=6.3, 6H), 0.96 (dd, *J*=6.4, 4.8, 6H).

^{13}C NMR (75 MHz, $CDCl_3$) δ 78.26, 60.10, 46.60, 45.95, 45.28, 27.17, 26.04, 24.75, 22.74, 22.46, 8.27.

2-azido-7-ethyl-2-methylundecan-4-yl ethanesulfonate (4.2k)

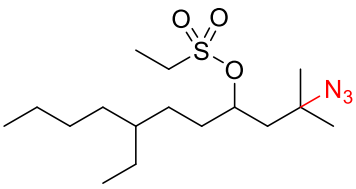

According to the general procedure 4.A with the use of p-Toluenesulfonyl azide as radical trap, **4.2k** was isolated in 41% yield (28 mg, 0.082 mmol), purification by chromatography (gradient elution from pure n-hexane to n-hexane/ethyl acetate (v/v 5:1)).

^{1}H NMR (300 MHz, $CDCl_3$) δ = 4.93 – 4.84 (m, 1H), 3.12 (qd, *J*=7.5, 0.9, 2H), 1.95 (dd, *J*=15.1, 6.5, 1H), 1.76 (dd, J=15.1, 4.6, 1H), 1.81 – 1.64 (m, 2H), 1.43 (t, *J*=7.5, 3H), 1.36 (d, *J*=6.4, 6H), 1.33 – 1.22 (m, 11H), 0.86 (dt, J=13.9, 7.0, 6H).

^{13}C NMR (75 MHz, $CDCl_3$) δ 79.95, 79.92, 60.15, 46.53, 45.34, 38.75, 38.71, 33.33, 32.74, 29.00, 28.96, 27.80, 27.09, 26.02, 25.79, 23.19, 14.25, 10.92, 10.88, 8.28.

3-azido-1-cyclohexyl-3-methylbutyl ethanesulfonate (4.2l)

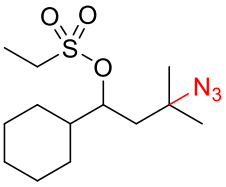

According to the general procedure 4.A with the use of p-Toluenesulfonyl azide as radical trap, **4.2l** was isolated in 28% yield (15 mg, 0.052 mmol), purification by chromatography (gradient elution from pure n-hexane to n-hexane/ethyl acetate (v/v 5:1)).

^{1}H NMR (300 MHz, $CDCl_3$) δ = 4.83 – 4.77 (m, 1H), 3.14 (qd, *J*=7.5, 1.3, 2H), 1.82 – 1.65 (m, 8H), 1.43 (t, *J*=7.4, 3H), 1.35 (d, *J*=6.1, 6H), 1.20 – 0.91 (m, 5H).

^{13}C NMR (75 MHz, $CDCl_3$) δ 83.32, 60.28, 46.79, 42.97, 41.53, 27.94, 27.37, 26.89, 26.48, 26.21, 26.14, 26.11, 8.31.

4-cyano-4-methylpentan-2-yl ethanesulfonate (4.2m)

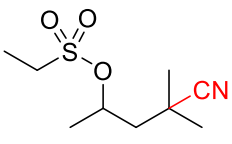

According to the general procedure 4.A with the use of p-Toluenesulfonyl cyanide as radical trap, **4.2m** was isolated in 60% yield (26 mg, 0.120 mmol), purification by chromatography (gradient elution from pure n-hexane to n-hexane/ethyl acetate (v/v 1:1)).

^{1}H NMR (300 MHz, $CDCl_3$) δ = 5.11 – 4.99 (m, 1H), 3.22 – 3.11 (m, 2H), 2.10 (dd, *J*=14.9, 8.9, 1H), 1.67 (dd, *J*=14.9, 3.8, 1H), 1.53 (d, *J*=6.2, 3H), 1.44 (t, *J*=7.5, 3H), 1.43 (s, 6H).

^{13}C NMR (75 MHz, $CDCl_3$) δ 129.56, 74.30, 46.92, 46.32, 30.04, 27.96, 26.28, 22.54, 8.07.

(1R,2R,5R)-2-(2-cyanopropan-2-yl)-5-methylcyclohexyl ethanesulfonate (4.2n)

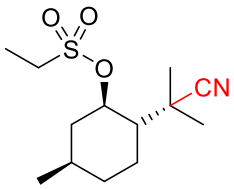

According to the general procedure 4.A with the use of p-Toluenesulfonyl cyanide as radical trap, **4.2n** was isolated in 47% yield (25 mg, 0.094 mmol), purification by chromatography (gradient elution from pure n-hexane to n-hexane/ethyl acetate (v/v 1:1)).

^{1}H NMR (300 MHz, $CDCl_3$) δ = 4.74 – 4.64 (m, 1H), 3.35 – 3.12 (m, 2H), 2.46 – 2.38 (m, 1H), 1.98 – 1.78 (m, 2H), 1.78 – 1.69 (m, 1H), 1.43 (t, *J*=7.4, 3H), 1.40 (d, *J*=4.9, 6H), 1.35 – 1.23 (m, 2H), 1.20 – 1.05 (m, 1H), 0.94 (d, *J*=6.4, 3H).

^{13}C NMR (75 MHz, $CDCl_3$) δ 129.68, 79.69, 48.10, 46.70, 42.41, 33.58, 31.25, 26.08, 25.36, 22.19, 21.58, 21.55, 7.98.

2-cyano-7-ethyl-2-methylundecan-4-yl ethanesulfonate (4.2o)

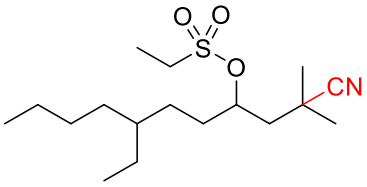

According to the general procedure 4.A with the use of p-Toluenesulfonyl cyanide as radical trap, **4.2o** was isolated in 35% yield (24 mg, 0.070 mmol), purification by chromatography (gradient elution from pure n-hexane to n-hexane/ethyl acetate (v/v 1:1)).

^{1}H NMR (300 MHz, $CDCl_3$) δ = 4.98 – 4.88 (m, 1H), 3.31 – 3.11 (m, 2H), 2.07 (dd, *J*=14.9, 8.4, 1H), 1.87 – 1.81 (m, 1H), 1.73 (dd, *J*=14.9, 3.9, 1H), 1.47 – 1.40 (m, 9H), 1.36 – 1.19 (m, 12H), 0.91 – 0.81 (m, 6H).

^{13}C NMR (75 MHz, $CDCl_3$) δ 129.71, 78.37, 46.36, 44.54, 38.78, 32.96, 32.76, 30.08, 30.04, 29.02, 28.00, 27.76, 26.44, 25.80, 23.17, 14.24, 10.94, 8.12.

3-cyano-1-cyclohexyl-3-methylbutyl ethanesulfonate (4.2p)

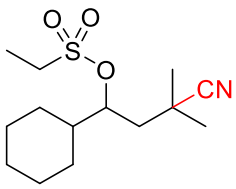

According to the general procedure 4.A with the use of p-Toluenesulfonyl cyanide as radical trap, **4.2p** was isolated in 60% yield (26 mg, 0.120 mmol), purification by chromatography (gradient elution from pure n-hexane to n-hexane/ethyl acetate (v/v 1:1)).

^{1}H NMR (400 MHz, $CDCl_3$) δ = 4.84 – 4.80 (m, 1H), 3.30 – 3.12 (m, 2H), 1.97 (dd, *J*=15.2, 8.7, 2H), 1.84 – 1.67 (m, 7H), 1.43 (t, *J*=7.4, 3H), 1.41 (d, *J*=5.4, 6H), 1.21 – 0.95 (m, 5H).

^{13}C NMR (101 MHz, $CDCl_3$) δ 129.66, 81.76, 46.41, 42.35, 40.56, 30.02, 29.97, 28.16, 27.92, 27.06, 26.38, 26.31, 26.06, 25.99, 8.09.

di-tert-butyl 1-(4-((ethylsulfonyl)oxy)-2-methylpentan-2-yl)hydrazine-1,2-dicarboxylate (4.2q)

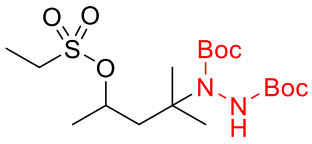

According to the general procedure 4.A with the use of di-tert-butyl azodicarboxylate as radical trap, **4.2q** was isolated in 66% yield (56 mg, 0.132 mmol), purification by chromatography (gradient elution from pure n-hexane to n-hexane/ethyl acetate (v/v 1:1)).

^{1}H NMR (300 MHz, $CDCl_3$) δ = 6.48 (s, 1H), 6.36 (s, 1H), 4.49 (s, 2H), 1.96 – 1.82 (m, 3H), 1.44 (s, 18H), 1.32 (d, *J*=6.2, 6H), 1.28 (s, 3H), 1.22 (s, 2H).

^{13}C NMR (75 MHz, $CDCl_3$) δ 156.26, 81.59, 69.86, 58.52, 44.14, 29.74, 28.16, 26.26, 20.94, 20.59.

di-tert-butyl 1-(4-((ethylsulfonyl)oxy)-2,6-dimethylheptan-2-yl)hydrazine-1,2-dicarboxylate (4.2r)

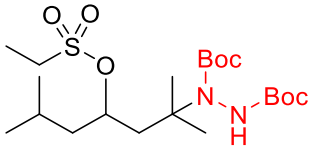

According to the general procedure 4.A with the use of di-tert-butyl azodicarboxylate as radical trap, **4.2r** was isolated in 67% yield (62 mg, 0.134 mmol), purification by chromatography (gradient elution from pure n-hexane to n-hexane/ethyl acetate (v/v 1:1)).

^{1}H NMR (300 MHz, $CDCl_3$) δ = 6.52 (s, 1H), 6.41 (s, 1H), 4.39 (s, 2H), 1.89 – 1.80 (m, 4H), 1.62 (ddd, *J*=14.2, 8.3, 6.0, 2H), 1.44 (s, 18H), 1.22 (s, 2H), 0.91 (s, 3H), 0.89 (d, *J*=1.5, 6H), 0.88 (s, 3H).

^{13}C NMR (75 MHz, $CDCl_3$) δ 156.26, 81.54, 71.76, 58.49, 43.68, 42.90, 29.73, 28.16, 26.25, 24.05, 22.98, 22.27.

di-tert-butyl 1-(4-((ethylsulfonyl)oxy)-2-methyldecan-2-yl)hydrazine-1,2-dicarboxylate (4.2s)

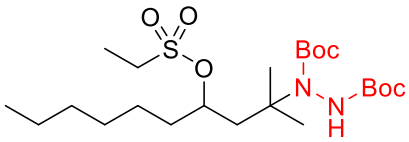

According to the general procedure 4.A with the use of di-tert-butyl azodicarboxylate as radical trap, **4.2s** was isolated in 67% yield (66 mg, 0.134 mmol), purification by chromatography (gradient elution from pure n-hexane to n-hexane/ethyl acetate (v/v 1:1)).

^{1}H NMR (300 MHz, $CDCl_3$) δ = 6.50 (s, 1H), 6.37 (s, 1H), 4.31 (s, 2H), 1.93 – 1.79 (m, 3H), 1.72 – 1.58 (m, 2H), 1.44 (s, 18H), 1.29 – 1.25 (m, 11H), 1.22 (s, 2H), 0.89 – 0.80 (m, 6H).

^{13}C NMR (75 MHz, $CDCl_3$) δ 156.28, 81.57, 73.47, 58.47, 42.46, 34.68, 31.71, 29.74, 29.09, 28.16, 26.24, 24.81, 22.58, 14.09.

di-tert-butyl 1-(4-((ethylsulfonyl)oxy)-2,5-dimethylhexan-2-yl)hydrazine-1,2-dicarboxylate (4.2t)

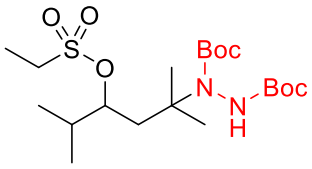

According to the general procedure 4.A with the use of di-tert-butyl azodicarboxylate as radical trap, **4.2t** was isolated in 48% yield (43 mg, 0.096 mmol), purification by chromatography (gradient elution from pure n-hexane to n-hexane/ethyl acetate (v/v 2:1)).

^{1}H NMR (300 MHz, $CDCl_3$) δ = 6.44 (s, 1H), 6.30 (s, 1H), 4.09 (s, 2H), 1.84 (m, *J*=6.7, 4H), 1.44 (s, 18H), 1.23 (s, 2H), 0.99 (s, 3H), 0.97 (s, 3H), 0.95 (s, 3H), 0.93 (s, 3H).

^{13}C NMR (75 MHz, $CDCl_3$) δ 156.30, 81.65, 77.97, 58.36, 39.37, 31.70, 29.78, 28.20, 26.19, 17.95, 17.74.

4-methylpent-4-en-2-yl ethanesulfonate (4.3a)

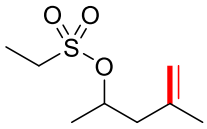

According to the general procedure 4.B, **4.3a** was determined by 65% NMR yield. Purification was done by chromatography gradient elution from pure pentane to pentane/diethyl ether (v/v 10:1).

^{1}H NMR (300 MHz, $CDCl_3$) δ = 5.02 – 4.90 (m, 1H), 4.87 (p, *J*=1.5, 1H), 4.80 (dq, *J*=1.9, 1.0, 1H), 3.08 (q, *J*=7.4, 2H), 2.49 (ddd, *J*=14.1, 7.1, 1.1, 1H), 2.27 (ddd, *J*=14.0, 6.2, 1.1, 1H), 1.77 (dd, *J*=1.5, 1.0, 3H), 1.43 – 1.40 (m, 6H).

^{13}C NMR (75 MHz, $CDCl_3$) δ 140.65, 114.54, 78.28, 46.14, 45.33, 22.58, 21.34, 8.35.

2,6-dimethylhept-1-en-4-yl ethanesulfonate (4.3b)

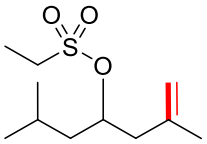

According to the general procedure 4.B, **4.3b** was isolated in 90% yield (31.9 mg, 0.135 mmol), purification by chromatography (gradient elution from pure pentane to pentane/diethyl ether (v/v 20:1)).

^{1}H NMR (300 MHz, $CDCl_3$) δ = 4.97 – 4.88 (m, 1H), 4.86 (p, *J*=1.5, 1H), 4.79 (dq, *J*=2.0, 1.0, 1H), 3.09 (q, *J*=7.4, 2H), 2.51 (ddd, *J*=14.0, 6.6, 1.2, 1H), 2.34 (ddd, *J*=14.1, 6.5, 1.2, 1H), 1.78 (dd, *J*=1.5, 0.9, 3H), 1.65 (ddd, *J*=13.7, 8.4, 5.2, 1H), 1.49 – 1.36 (m, 2H), 1.41 (t, *J*=7.4, 3H), 0.94 (dd, *J*=6.6, 4.3, 6H).

^{13}C NMR (75 MHz, $CDCl_3$) δ 140.89, 114.56, 79.74, 46.31, 44.03, 43.73, 24.49, 23.16, 22.59, 22.03, 8.38.

2-methyldec-1-en-4-yl ethanesulfonate (4.3c)

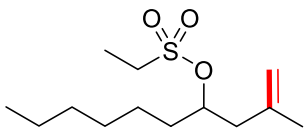

According to the general procedure 4.B, **4.3c** was determined by 81% NMR yield. Purification was done by chromatography gradient elution from pure pentane to pentane/diethyl ether (v/v 10:1).

^{1}H NMR (300 MHz, $CDCl_3$) δ = 4.89 – 4.86 (m, 1H), 4.86 – 4.81 (m, 1H), 4.80 (dq, *J*=2.0, 1.0, 1H), 3.09 (q, *J*=7.4, 2H), 2.48 (ddd, *J*=14.1, 7.0, 1.1, 1H), 2.34 (ddd, *J*=14.1, 6.2, 1.2, 1H), 1.78 (dd, *J*=1.5, 0.9, 3H), 1.71 – 1.64 (m, 2H), 1.44 – 1.38 (m, 1H), 1.41 (t, *J*=7.5, 3H), 1.36 – 1.24 (m, 7H), 0.92 – 0.88 (m, 3H).

^{13}C NMR (75 MHz, $CDCl_3$) δ 140.91, 114.51, 81.39, 46.21, 43.39, 34.72, 31.77, 29.14, 25.00, 22.69, 22.59, 14.18, 8.38.

1-cyclohexyl-3-methylbut-3-en-1-yl ethanesulfonate (4.3d)

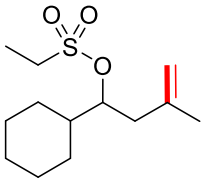

According to the general procedure 4.B, **4.3d** was isolated in 62% yield (24 mg, 0.093 mmol), purification by chromatography (gradient elution from pure pentane to pentane/diethyl ether (v/v 20:1)) .

^{1}H NMR (300 MHz, $CDCl_3$) δ = 4.86 (p, *J*=1.6, 1H), 4.81 (dq, *J*=2.1, 1.1, 1H), 4.75 – 4.69 (m, 1H), 3.08 (q, *J*=7.4, 2H), 2.44 (ddd, *J*=14.3, 7.8, 1.0, 1H), 2.36 (ddd, *J*=14.3, 5.4, 1.3, 1H), 1.79 – 1.63 (m, 9H), 1.40 (t, *J*=7.4, 3H), 1.29 – 1.12 (m, 5H).

^{13}C NMR (75 MHz, $CDCl_3$) δ 141.26, 114.45, 85.19, 46.28, 41.66, 40.24, 28.97, 27.60, 26.40, 26.19, 26.16, 22.43, 8.42.

1-(cyclohex-1-en-1-yl)propan-2-yl ethanesulfonate (4.3e)

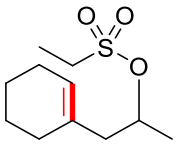

According to the general procedure 4.B, **4.3e** was determined by 86% NMR yield. Purification was done by chromatography gradient elution from pure pentane to pentane/diethyl ether (v/v 5:1).

^{1}H NMR (300 MHz, $CDCl_3$) δ = 5.53 – 5.50 (m, 1H), 4.97 – 4.79 (m, 1H), 3.10 – 3.03 (m, 2H), 2.39 (ddd, *J*=13.9, 7.2, 1.1, 1H), 2.17 (ddd, *J*=13.9, 6.2, 0.9, 1H), 1.99 (dd, *J*=4.3, 2.0, 2H), 1.67 – 1.50 (m, 6H), 1.40 (d, *J*=1.2, 3H), 1.40 – 1.37 (m, 3H).

^{13}C NMR (75 MHz, $CDCl_3$) δ 132.90, 125.77, 78.22, 46.08, 45.70, 28.60, 25.42, 22.94, 22.31, 21.46, 8.38.

1-cyclohexyl-4-methylpent-4-en-2-yl ethanesulfonate (4.3f)

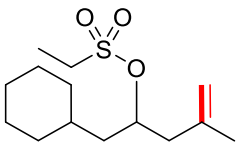

The desaturation reaction was conducted according to GP3 with compound **S6** (41.1 mg, 0.150 mmol).

Isolated yield of **6b**: 10% (4 mg, 0.015 mmol); NMR yield: 23%.

Eluent composition: gradient elution from pure pentane to pentane/diethyl ether (v/v 10:1).

^{1}H NMR (300 MHz, $CDCl_3$) δ = 5.00 – 4.91 (m, 1H), 4.87 – 4.84 (m, 1H), 4.78 (dq, *J*=1.9, 1.1, 1H), 3.09 (q, *J*=7.4, 2H), 2.50 (ddd, *J*=14.0, 6.6, 1.2, 1H), 2.34 (ddd, *J*=14.0, 6.5, 1.2, 1H), 1.77 (dd, *J*=1.5, 0.9, 3H), 1.75 – 1.54 (m, 9H), 1.41 (t, *J*=7.4, 3H), 1.33 – 1.14 (m, 4H).

^{13}C NMR (75 MHz, $CDCl_3$) δ 140.94, 114.51, 79.26, 46.29, 44.07, 42.32, 33.85, 33.80, 32.80, 26.56, 26.33, 26.14, 22.60, 8.39.

2,5-dimethylhex-5-en-3-yl ethanesulfonate (4.3g)

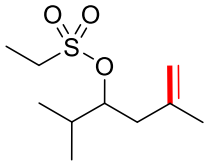

According to the general procedure 4.B, **4.3g** was determined by 56% NMR yield. Purification was done by chromatography gradient elution from pure pentane to pentane/diethyl ether (v/v 10:1).

^{1}H NMR (300 MHz, $CDCl_3$) δ = 4.86 (p, *J*=1.6, 1H), 4.82 (dq, *J*=2.1, 1.1, 1H), 4.78 – 4.72 (m, 1H), 3.09 (q, *J*=7.5, 2H), 2.44 (ddd, *J*=14.3, 8.0, 1.0, 1H), 2.32 (ddd, *J*=14.3, 5.3, 1.3, 1H), 2.04 (heptd, *J*=6.8, 3.9, 1H), 1.79 (t, *J*=1.3, 3H), 1.40 (t, *J*=7.4, 3H), 1.02 (d, *J*=6.9, 3H), 0.97 (d, *J*=6.9, 3H).

^{13}C NMR (75 MHz, $CDCl_3$) δ 141.15, 114.43, 85.38, 46.28, 39.94, 31.77, 22.37, 18.34, 17.06, 8.42.

2,7-dimethyloct-1-en-4-yl ethanesulfonate (4.3h)

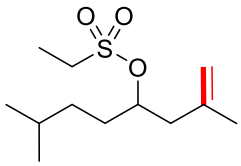

According to the general procedure 4.B, **4.3h** was isolated in 50% yield (18 mg, 0.075 mmol), purification by chromatography (gradient elution from pure pentane to pentane/diethyl ether (v/v 5:1)).

^{1}H NMR (300 MHz, $CDCl_3$) δ = 4.88 – 4.86 (m, 1H), 4.85 – 4.82 (m, 1H), 4.80 (dq, *J*=2.0, 1.0, 1H), 3.09 (q, *J*=7.4, 2H), 2.48 (ddd, *J*=14.2, 7.1, 1.1, 1H), 2.34 (ddd, *J*=14.1, 6.1, 1.2, 1H), 1.78 (dd, *J*=1.5, 0.9, 3H), 1.71 – 1.67 (m, 1H), 1.41 (t, *J*=7.4, 3H), 1.36 – 1.27 (m, 4H), 0.91 – 0.88 (m, 6H).

^{13}C NMR (75 MHz, $CDCl_3$) δ 140.91, 114.52, 81.58, 46.21, 43.33, 33.95, 32.57, 28.01, 22.69, 22.61, 22.52, 8.39.

7-ethyl-2-methylundec-1-en-4-yl ethanesulfonate (4.3i)

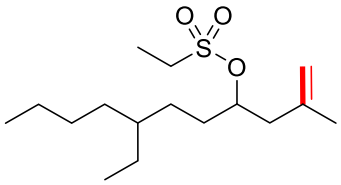

According to the general procedure 4.B, **4.3i** was determined by 67% NMR yield. Purification was done by chromatography gradient elution from pure pentane to pentane/diethyl ether (v/v 5:1).

^{1}H NMR (300 MHz, $CDCl_3$) δ = 4.88 – 4.86 (m, 1H), 4.85 – 4.81 (m, 1H), 4.80 (dq, *J*=1.9, 0.9, 1H), 3.09 (q, *J*=7.4, 2H), 2.49 (ddd, *J*=14.2, 7.1, 1.2, 1H), 2.35 (ddd, *J*=14.2, 6.2, 1.2, 1H), 1.78 (dd, *J*=1.5, 0.9, 3H), 1.41 (t, 3H), 1.32 – 1.18 (m, 13H), 0.99 – 0.85 (m, 6H).

^{13}C NMR (75 MHz, $CDCl_3$) δ 140.92, 114.50, 81.76, 46.21, 43.31, 38.77, 32.84, 31.84, 29.02, 28.17, 25.88, 23.21, 22.61, 14.27, 10.94, 8.40.

(1R,2S,5R)-5-methyl-2-(prop-1-en-2-yl)cyclohexyl ethanesulfonate (4.3j)

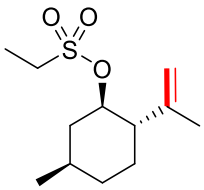

According to the general procedure 4.B, **4.3j** was isolated in 95% yield (35.1 mg, 0.142 mmol), purification by chromatography (gradient elution from pure pentane to pentane/diethyl ether (v/v 10:1)).

^{1}H NMR (300 MHz, $CDCl_3$) δ = 4.88 – 4.79 (m, 2H), 4.61 (td, *J*=10.9, 4.6, 1H), 3.11 – 2.95 (m, 2H), 2.31 (dddd, *J*=12.2, 4.9, 3.3, 1.8, 1H), 2.26 – 2.10 (m, 1H), 1.78 – 1.59 (m, 5H), 1.58 – 1.39 (m, 2H), 1.36 (t, *J*=7.4, 3H), 1.33 – 1.23 (m, 1H), 0.95 (d, *J*=6.5, 3H).

^{13}C NMR (101 MHz, $CDCl_3$) δ 145.64, 112.83, 82.18, 50.97, 46.28, 42.29, 33.78, 31.69, 30.72, 21.94, 19.70, 8.31.

Appendix

Procedure to determine photon flux of the Blue LEDs setup

Preparation of acetate buffer solution:

2.48 g of NaOAc and 0.5 ml of H_2SO_4 were dissolved in H_2O to a final volume of 50 mL.

Preparation of potassium ferrioxalate solution:

118 mg of $K_3[Fe(C_2O_4)_3].3H_2O$, and 56 µL of H_2SO4 were dissolved in H_2O to a final volume of 20 mL.

2 mL of the potassium ferrioxalate solution were irradiated for 10 sec using the same setup for the catalytic reactions. Then the solution was diluted by the addition of 4 mL of the buffer solution containing 2 mg 1,10-phenanthroline and 6 mL of water. Subsequently the absorbance of this solution was determined at 510 nm by Avantes with a 1-mm-tip.

The same procedure was followed for an unirradiated sample.

Calculation of Photon number:

Absorption of Fe^{2+} (at 510 nm) = 0.6670 (after irradiation of 10 sec)

Absorption of Fe^{2+} (at 510 nm) = 0.1225 (no irradiation)

Absorption of Fe^{2+} (at 510 nm) = 0.6670 - 0.1225 = 0.5445

Mol of Fe^{2+}:

$$n_{Fe^{2+}} = \frac{\text{Abs of } Fe^{2+}(\text{at 510 nm}) \times V}{\varepsilon_{510\text{ nm}} \times l} = \frac{0.5445 \times 0.01\text{ L}}{11100\text{ M}^{-1}\text{cm}^{-1} \times 0.1\text{ cm}} = 4.905 \times 10^{-6}\text{ mol}$$

With quantum yield of 0.805 for the absorption of ferrioxalate actinometer, number of photons generated by the Blue LED:

$$n_{(photons)} = \frac{n_{Fe^{2+}}}{\phi} = \frac{4.905 \times 10^{-6}\text{ mol}}{0.805} = 6.093 \times 10^{-6}\text{ mol}$$

The photon flux of the Blue LED:

$$n_{(photons/s)} = \frac{n_{(photons)}}{t} = \frac{6.093 \times 10^{-6}\text{ mol}}{10} = 6.093 \times 10^{-7}\text{ mol/s}$$

List of abbreviations

ATR	Attenuated Total Reflection
BDE	Bond dissociation energy
CCC	Carbon-carbon coupling
CDC	Cross dehydrogenative coupling
DABCO	1,4-diazabicyclo[2.2. 2]octane
DBU	1,8-Diazabicyclo[5.4.0]undec-7-ene
DCE	Dichloroethane
DCM	Dichloromethane
DFT	Density function theory
DIPEA	Diisopropylethylamine
DMAP	4-Dimethylaminopyridine
DMF	Dimethylformamide
DMPO	5,5-Dimethyl-1-pyrroline N-oxide
EDA	Electron donor-acceptor
EI	Electron ionization
EPR	Electron paramagnetic resonance
ESI	Electrospray ionization
FC	Franck-Condon
GC	Gas chromatography
HAT	Hydrogen-atom transfer
HRMS	High resolution mass spectroscopy
IR	Infrared
ISET	Internal single electron transfer
LED	Light-emitting diode
LMCT	Ligand-to-metal charge transfer

MHAT	Metal-hydride atom transfer
MLCT	Metal-to-ligand charge transfer
NHC	N-heterocyclic carbene
NMR	Nuclear magnetic resonance
PAL	Phenylalanine ammonia-lyase
PC	Photocatalyst
PCET	Proton-coupled electron transfer
PES	Potential energy surface
PT	Proton transfer
RM	Reaction mixture
RT	Room temperature
SCE	Saturated calomel electrode
SET	Single electron transfer
TEMPO	2,2,6,6-tetramethyl-1-piperidinyloxy
THF	Tetrahydrofuran
TLC	Thin layer chromatography
TPP	Tetraphenylporphyrin
TS	Transition state
UV	Ultraviolet
Vis	Visible
XAT	Halogen atom transfer

List of figures

List of tables

List of schemes

References

[1] V. I. Minkin, *Pure and Applied Chemistry* **1999**, *71*, 1919-1981.
[2] A. I. Krylov, in *Reviews in Computational Chemistry*, **2017**, pp. 151-224.
[3] S. A. Bonke, T. Risse, A. Schnegg, A. Brückner, *Nature Reviews Methods Primers* **2021**, *1*.
[4] I. Ratera, J. Veciana, *Chemical Society Reviews* **2012**, *41*, 303-349.
[5] J.-M. Savéant, in *Advances in Physical Organic Chemistry, Vol. 35*, Academic Press, **2000**, pp. 117-192.
[6] P. Muller, *Pure and Applied Chemistry* **1994**, *66*, 1077-1184.
[7] M. Gomberg, *Journal of the American Chemical Society* **1900**, *22*, 757-771.
[8] G. Herzberg, *The Spectra and Structures of Simple Free Radicals: An Introduction to Molecular Spectroscopy*, Dover Publications, **1988**.
[9] F. Paneth, W. Lautsch, *Nature* **1930**, *125*, 564-564.
[10] D. H. Hey, W. A. Waters, *Chemical Reviews* **1937**, *21*, 169-208.
[11] B. Giese, *Tetrahedron* **1985**, *41*, 3887-4364.
[12] A. G. Davies, in *Chemistry of Tin* (Ed.: P. J. Smith), Springer Netherlands, Dordrecht, **1998**, pp. 265-289.
[13] J. K. Matsui, S. B. Lang, D. R. Heitz, G. A. Molander, *ACS Catalysis* **2017**, *7*, 2563-2575.
[14] A. L. J. Beckwith, *Chemical Society Reviews* **1993**, *22*, 143-151.
[15] aM. W. Wong, A. Pross, L. Radom, *Journal of the American Chemical Society* **1993**, *115*, 11050-11051; bJ. M. Tedder, J. C. Walton, *Tetrahedron* **1980**, *36*, 701-707.
[16] V. W. Bowry, J. Lusztyk, K. U. Ingold, *Journal of the American Chemical Society* **1991**, *113*, 5687-5698.
[17] J. M. Tedder, *Angewandte Chemie International Edition in English* **1982**, *21*, 401-410.
[18] aM. Graetzel, *Accounts of Chemical Research* **1981**, *14*, 376-384; bH. Takeda, O. Ishitani, *Coordination Chemistry Reviews* **2010**, *254*, 346-354; cK. Kalyanasundaram, M. Grätzel, *Coordination Chemistry Reviews* **1998**, *177*, 347-414.
[19] aD. A. Nicewicz, D. W. C. MacMillan, *Science* **2008**, *322*, 77-80; bM. A. Ischay, M. E. Anzovino, J. Du, T. P. Yoon, *Journal of the American Chemical Society* **2008**, *130*, 12886-12887; cJ. M. R. Narayanam, J. W. Tucker, C. R. J. Stephenson, *Journal of the American Chemical Society* **2009**, *131*, 8756-8757.
[20] L. Buglioni, F. Raymenants, A. Slattery, S. D. A. Zondag, T. Noël, *Chemical Reviews* **2022**, *122*, 2752-2906.
[21] D. M. Schultz, T. P. Yoon, *Science* **2014**, *343*, 1239176.
[22] aR. F. Heck, *Journal of the American Chemical Society* **1968**, *90*, 5518-5526; bT. Mizoroki, K. Mori, A. Ozaki, *Bulletin of the Chemical Society of Japan* **2006**, *44*, 581-581.
[23] aN. Miyaura, A. Suzuki, *Journal of the Chemical Society, Chemical Communications* **1979**, 866-867; bN. Miyaura, K. Yamada, A. Suzuki, *Tetrahedron Letters* **1979**, *20*, 3437-3440.
[24] A. O. King, N. Okukado, E.-i. Negishi, *Journal of the Chemical Society, Chemical Communications* **1977**, 683-684.
[25] aJ. K. Kochi, *Accounts of Chemical Research* **1974**, *7*, 351-360; bM. F. Lappert, P. W. Lednor, in *Advances in Organometallic Chemistry, Vol. 14* (Eds.: F. G. A. Stone, R. West), Academic Press, **1976**, pp. 345-399.

[26] U. Jahn, in *Radicals in Synthesis III* (Eds.: M. Heinrich, A. Gansäuer), Springer Berlin Heidelberg, Berlin, Heidelberg, **2012**, pp. 121-189.
[27] X. Wang, J. He, Y.-N. Wang, Z. Zhao, K. Jiang, W. Yang, T. Zhang, S. Jia, K. Zhong, L. Niu, Y. Lan, *Chemical Reviews* **2024**, *124*, 10192-10280.
[28] J. Iqbal, B. Bhatia, N. K. Nayyar, *Chemical Reviews* **1994**, *94*, 519-564.
[29] P. I. Dalko, *Tetrahedron* **1995**, *51*, 7579-7653.
[30] Y. Sumida, H. Ohmiya, *Chemical Society Reviews* **2021**, *50*, 6320-6332.
[31] F. Juliá, *ChemCatChem* **2022**, *14*.
[32] J. W. Verhoeven, **1996**, *68*, 2223-2286.
[33] R. L. Carter, *Molecular symmetry and group theory*, J. Wiley, New York, **1998**.
[34] M. Ramprasad, S. P. Bhattacharyya, in *Intramolecular Charge Transfer*, **2018**, pp. 1-27.
[35] J. Demarteau, A. Debuigne, C. Detrembleur, *Chemical Reviews* **2019**, *119*, 6906-6955.
[36] B. D. Martin, R. G. Finke, *Journal of the American Chemical Society* **1992**, *114*, 585-592.
[37] Y. Wang, T. P. Begley, *Journal of the American Chemical Society* **2020**, *142*, 9944-9954.
[38] G. N. Schrauzer, J. Sibert, R. J. Windgassen, *Journal of the American Chemical Society* **1968**, *90*, 6681-6688.
[39] G. N. Schrauzer, *Accounts of Chemical Research* **1968**, *1*, 97-103.
[40] V. Artero, M. Chavarot‐Kerlidou, M. Fontecave, *Angewandte Chemie International Edition* **2011**, *50*, 7238-7266.
[41] aH. Bhandal, G. Pattenden, J. J. Russell, *Tetrahedron letters* **1986**, *27*, 2299-2302; bB. P. Branchaud, M. S. Meier, Y. Choi, *Tetrahedron letters* **1988**, *29*, 167-170; cA. Ghosez, T. Göbel, B. Giese, *Chemische Berichte* **1988**, *121*, 1807-1811; dB. Giese, J. Hartung, J. He, O. Hüter, A. Koch, *Angewandte Chemie International Edition in English* **1989**, *28*, 325-327; eM. Tada, K. Kaneko, *The Journal of Organic Chemistry* **1995**, *60*, 6635-6636.
[42] aM. Okabe, M. Abe, M. Tada, *The Journal of Organic Chemistry* **1982**, *47*, 1775-1777; bS. Torii, T. Inokuchi, T. Yukawa, *The Journal of Organic Chemistry* **1985**, *50*, 5875-5877; cB. P. Branchaud, W. D. Detlefsen, *Tetrahedron letters* **1991**, *32*, 6273-6276; dB. Giese, P. Erdmann, T. Göbel, R. Springer, *Tetrahedron letters* **1992**, *33*, 4545-4548; eW. Affo, H. Ohmiya, T. Fujioka, Y. Ikeda, T. Nakamura, H. Yorimitsu, K. Oshima, Y. Imamura, T. Mizuta, K. Miyoshi, *Journal of the American Chemical Society* **2006**, *128*, 8068-8077.
[43] M. E. Weiss, L. M. Kreis, A. Lauber, E. M. Carreira, *Angewandte Chemie International Edition* **2011**, *47*, 11125-11128.
[44] aX.-W. Gao, Q.-Y. Meng, J.-X. Li, J.-J. Zhong, T. Lei, X.-B. Li, C.-H. Tung, L.-Z. Wu, *ACS Catalysis* **2015**, *5*, 2391-2396; bJ. G. West, D. Huang, E. J. Sorensen, *Nature communications* **2015**, *6*, 10093; cG. Zhang, C. Liu, H. Yi, Q. Meng, C. Bian, H. Chen, J.-X. Jian, L.-Z. Wu, A. Lei, *Journal of the American Chemical Society* **2015**, *137*, 9273-9280.
[45] K. C. Cartwright, J. A. Tunge, *ACS Catalysis* **2018**, *8*, 11801-11806.
[46] D. D. Wayner, D. McPhee, D. Griller, *Journal of the American Chemical Society* **1988**, *110*, 132-137.
[47] A. C. Frisch, M. Beller, *Angewandte Chemie International Edition* **2005**, *44*, 674-688.
[48] G. P. Cerai, B. Morandi, *Chemical Communications* **2016**, *52*, 9769-9772.
[49] H. Cao, H. Jiang, H. Feng, J. M. C. Kwan, X. Liu, J. Wu, *Journal of the American Chemical Society* **2018**, *140*, 16360-16367.

[50] T. Constantin, M. Zanini, A. Regni, N. S. Sheikh, F. Juliá, D. Leonori, *Science* **2020**, *367*, 1021-1026.
[51] W. Zhou, S. Wu, P. Melchiorre, *Journal of the American Chemical Society* **2022**, *144*, 8914-8919.
[52] G. E. Dobereiner, R. H. Crabtree, *Chemical Reviews* **2010**, *110*, 681-703.
[53] K. C. Cartwright, A. M. Davies, J. A. Tunge, *European Journal of Organic Chemistry* **2020**, *2020*, 1245-1258.
[54] M.-J. Zhou, L. Zhang, G. Liu, C. Xu, Z. Huang, *Journal of the American Chemical Society* **2021**, *143*, 16470-16485.
[55] R. Wohlgemuth, *ChemSusChem* **2022**, *15*, e202200402.
[56] D. J. Abrams, J. G. West, E. J. Sorensen, *Chemical Science* **2017**, *8*, 1954-1959.
[57] X. Sun, J. Chen, T. Ritter, *Nature chemistry* **2018**, *10*, 1229-1233.
[58] H. Zhao, A. J. McMillan, T. Constantin, R. C. Mykura, F. Juliá, D. Leonori, *Journal of the American Chemical Society* **2021**, *143*, 14806-14813.
[59] aX. Wang, Y. Li, X. Wu, *ACS Catalysis* **2022**, *12*, 3710-3718; bL. Huang, T. Ji, C. Zhu, H. Yue, N. Zhumabay, M. Rueping, *Nature Communications* **2022**, *13*, 809.
[60] aU. D. S, F. Julia, A. Luridiana, J. J. Douglas, D. Leonori, *Nature* **2020**, *584*, 75-81; bH. Zhao, H. P. Caldora, O. Turner, J. J. Douglas, D. Leonori, *Angewandte Chemie International Edition* **2022**, *61*, e202201870; cH. P. Caldora, Z. Zhang, M. J. Tilby, O. Turner, D. Leonori, *Angewandte Chemie International Edition* **2023**, *62*, e202301656.
[61] Q. Yang, L. Zhang, C. Ye, S. Luo, L. Z. Wu, C. H. Tung, *Angewandte Chemie International Edition* **2017**, *56*, 3694-3698.
[62] Z. Jia, L. Zhang, S. Luo, *Journal of the American Chemical Society* **2022**, *144*, 10705-10710.
[63] T. Risse, D. Hollmann, A. Brückner, in *Catalysis: Volume 27, Vol. 27* (Eds.: J. Spivey, K. Dooley, Y.-F. Han), The Royal Society of Chemistry, **2015**, p. 0.
[64] M. J. Davies, *Methods* **2016**, *109*, 21-30.
[65] D. Rehorek, *Chemical Society Reviews* **1991**, *20*, 341-353.
[66] O. Augusto, D. R. Truzzi, E. Linares, *Redox Biochemistry and Chemistry* **2023**, *5-6*, 100009.
[67] G. R. Eaton, S. S. Eaton, D. P. Barr, R. T. Weber, *Quantitative EPR*, Springer Vienna, **2010**.
[68] D. C. F.E. Mabbs, *Electron Paramagnetic Resonance of d Transition Metal Compounds, Vol. 16*, Elsevier Science, **2013**.
[69] M. Picollo, M. Aceto, T. Vitorino, **2019**, *4*.
[70] H.-H. Perkampus, *UV-VIS Spectroscopy and its Applications*, Springer Science & Business Media, **2013**.
[71] L. Antonov, D. Nedeltcheva, *Chemical Society Reviews* **2000**, *29*, 217-227.
[72] H. Förster, in *Characterization I Molecular Sieves – Science and Technology* (Eds.: H. G. Karge, J. Weitkamp), Springer Berlin Heidelberg, Berlin, Heidelberg, **2004**, pp. 337-426.
[73] aZ. Rappoport, *The Chemistry of Enamines, Part 1*, Wiley & Sons, New York, **1994**; bZ. Rappoport, *The chemistry of enamines. Part 2*, Wiley & Sons, New York, **1994**.
[74] R. J. Ouellette, J. D. Rawn, in *Organic Chemistry (Second Edition)* (Eds.: R. J. Ouellette, J. D. Rawn), Academic Press, **2018**, pp. 763-800.
[75] T. Courant, G. Dagousset, G. Masson, *Synthesis* **2015**, *47*, 1799-1856.
[76] aT. B. Poulsen, *Accounts of Chemical Research* **2021**, *54*, 1830-1842; bL. N. Berntsen, T. N. Solvi, K. Sørnes, D. S. Wragg, A. H. Sandtorv, *Chemical Communications* **2021**, *57*, 11851-11854.

[77] J. R. Dehli, J. Legros, C. Bolm, *Chemical Communications* **2005**, 973-986.
[78] aB. M. Trost, J. J. Cregg, N. Quach, *Journal of the American Chemical Society* **2017**, *139*, 5133-5139; bL. Wang, C. Liu, R. Bai, Y. Pan, A. Lei, *Chemical Communications* **2013**, *49*, 7923-7925.
[79] aG. R. Cook, N. S. Barta, J. R. Stille, *The Journal of Organic Chemistry* **1992**, *57*, 461-467; bN. Sotomayor, T. Vicente, E. Domínguez, E. Lete, M.-J. Villa, *Tetrahedron* **1994**, *50*, 2207-2218; cJ. Genovino, B. Lagu, Y. Wang, B. B. Touré, *Chemical Communications* **2012**, *48*, 6735-6737.
[80] aM. V. J. Villa, S. M. Targett, J. C. Barnes, W. G. Whittingham, R. Marquez, *Organic Letters* **2007**, *9*, 1631-1633; bR. K. Dieter, R. R. Sharma, *The Journal of Organic Chemistry* **1996**, *61*, 4180-4184.
[81] aL. Jiang, G. E. Job, A. Klapars, S. L. Buchwald, *Organic Letters* **2003**, *5*, 3667-3669; bY. Bolshan, R. A. Batey, *Angewandte Chemie International Edition* **2008**, *47*, 2109-2112.
[82] aB. Gourdet, H. W. Lam, *Journal of the American Chemical Society* **2009**, *131*, 3802-3803; bL. L. Baldassari, A. de la Torre, J. Li, D. S. Lüdtke, N. Maulide, *Angewandte Chemie International Edition* **2017**, *56*, 15723-15727.
[83] aS. Yudha S, Y. Kuninobu, K. Takai, *Organic Letters* **2007**, *9*, 5609-5611; bN. Panda, R. Mothkuri, *The Journal of Organic Chemistry* **2012**, *77*, 9407-9412.
[84] H. Liu, Y. Zhou, X. Yan, C. Chen, Q. Liu, C. Xi, *Organic Letters* **2013**, *15*, 5174-5177.
[85] S. Lin, Z.-Q. Yang, B. H. B. Kwok, M. Koldobskiy, C. M. Crews, S. J. Danishefsky, *Journal of the American Chemical Society* **2004**, *126*, 6347-6355.
[86] A. D. Bolig, M. Brookhart, *Journal of the American Chemical Society* **2007**, *129*, 14544-14545.
[87] aC. B. Bheeter, R. Jin, J. K. Bera, P. H. Dixneuf, H. Doucet, *Advanced Synthesis & Catalysis* **2014**, *356*, 119-124; bP. Chuentragool, M. Parasram, Y. Shi, V. Gevorgyan, *Journal of the American Chemical Society* **2018**, *140*, 2465-2468.
[88] G. Li, P. A. Kates, A. K. Dilger, P. T. Cheng, W. R. Ewing, J. T. Groves, *ACS Catalysis* **2019**, *9*, 9513-9517.
[89] P. Spieß, M. Berger, D. Kaiser, N. Maulide, *Journal of the American Chemical Society* **2021**, *143*, 10524-10529.
[90] P. H. Buist, *Natural Product Reports* **2004**, *21*, 249-262.
[91] C. Kim, Y. Dong, L. Que, *Journal of the American Chemical Society* **1997**, *119*, 3635-3636.
[92] A. Fürstner, *ACS Central Science* **2016**, *2*, 778-789.
[93] R. Bam, A. S. Pollatos, A. J. Moser, J. G. West, *Chemical Science* **2021**, *12*, 1736-1744.
[94] D. Mandal, B. D. Gupta, *Organometallics* **2005**, *24*, 1501-1510.
[95] B. L. Wadsworth, A. M. Beiler, D. Khusnutdinova, S. I. Jacob, G. F. Moore, *ACS Catalysis* **2016**, *6*, 8048-8057.
[96] J. Niklas, K. L. Mardis, R. R. Rakhimov, K. L. Mulfort, D. M. Tiede, O. G. Poluektov, *The Journal of Physical Chemistry B* **2012**, *116*, 2943-2957.
[97] P. Maillard, J. C. Massot, C. Giannotti, *Journal of Organometallic Chemistry* **1978**, *159*, 219-227.
[98] M. Oestreich, *The Mizoroki-Heck Reaction*, John Wiley & Sons, Ltd, **2009**.
[99] aH. Dieck, R.-F. Heck, *Journal of the American Chemical Society* **1974**, *96*, 1133-1136; bR. F. Heck, *Journal of the American Chemical Society* **1969**, *91*, 6707-6714.
[100] R. F. Heck, J. P. Nolley, Jr., *The Journal of Organic Chemistry* **1972**, *37*, 2320-2322.

[101] M. Mori, K. Chiba, Y. Ban, *Tetrahedron Letters* **1977**, *18*, 1037-1040.
[102] D. Kurandina, M. Parasram, V. Gevorgyan, *Angewandte Chemie International Edition* **2017**, *56*, 14212-14216.
[103] L. Firmansjah, G. C. Fu, *Journal of the American Chemical Society* **2007**, *129*, 11340-11341.
[104] K. S. Bloome, R. L. McMahen, E. J. Alexanian, *Journal of the American Chemical Society* **2011**, *133*, 20146-20148.
[105] D. Kurandina, P. Chuentragool, V. Gevorgyan, *Synthesis* **2019**, *51*, 985-1005.
[106] S. Busato, O. Tinembart, Z.-d. Zhang, R. Scheffold, *Tetrahedron* **1990**, *46*, 3155-3166.
[107] M. Koreeda, L. G. Hamann, *Journal of the American Chemical Society* **1990**, *112*, 8175-8177.
[108] M. Parasram, V. O. Iaroshenko, V. Gevorgyan, *Journal of the American Chemical Society* **2014**, *136*, 17926-17929.
[109] X. Dong, Y. Han, F. Yan, Q. Liu, P. Wang, K. Chen, Y. Li, Z. Zhao, Y. Dong, H. Liu, *Organic letters* **2016**, *18*, 3774-3777.
[110] M. Ladlow, G. Pattenden, *Tetrahedron letters* **1984**, *25*, 4317-4320.
[111] aY. Ikeda, T. Nakamura, H. Yorimitsu, K. Oshima, *Journal of the American Chemical Society* **2002**, *124*, 6514-6515; bY. Ikeda, H. Yorimitsu, H. Shinokubo, K. Oshima, *Advanced Synthesis & Catalysis* **2004**, *346*, 1631-1634.
[112] G. N. Schrauzer, J. W. Sibert, R. J. Windgassen, *J. Am. Chem. Soc.* **1968**, *90*, 6681-6688.
[113] aP. Ertl, E. Altmann, J. M. McKenna, *Journal of Medicinal Chemistry* **2020**, *63*, 8408-8418; bM. D. Kärkäs, *Chemical Society Reviews* **2018**, *47*, 5786-5865.
[114] J. Bariwal, E. Van der Eycken, *Chemical Society Reviews* **2013**, *42*, 9283-9303.
[115] aT. Sandmeyer, *Berichte der deutschen chemischen Gesellschaft* **1884**, *17*, 2650-2653; bG. Balz, G. Schiemann, *Berichte der deutschen chemischen Gesellschaft (A and B Series)* **1927**, *60*, 1186-1190; cK. Kikukawa, T. Matsuda, *Chemistry Letters* **2006**, *6*, 159-162.
[116] R. A. Sheldon, D. Brady, *ChemSusChem* **2022**, *15*, e202102628.
[117] E. L. Camm, G. H. N. Towers, *Phytochemistry* **1973**, *12*, 961-973.
[118] S. L. Lovelock, R. C. Lloyd, N. J. Turner, *Angewandte Chemie International Edition* **2014**, *53*, 4652-4656.
[119] K. J. Berger, M. D. Levin, *Organic & Biomolecular Chemistry* **2021**, *19*, 11-36.
[120] A. W. Hofmann, *Berichte der deutschen chemischen Gesellschaft* **1881**, *14*, 659-669.
[121] aT. P. McFadden, C. I. Nwachukwu, A. G. Roberts, *Organic & Biomolecular Chemistry* **2022**, *20*, 1379-1385; bD. Trauner, *Angewandte Chemie International Edition* **2015**, *54*, 11910-11916.
[122] A. V. Serna, L. Kürti, J. H. Siitonen, *Angewandte Chemie International Edition* **2021**, *60*, 27236-27240.
[123] G. M. Atkins, Jr., E. M. Burgess, *Journal of the American Chemical Society* **1968**, *90*, 4744-4745.
[124] K. C. Nicolaou, S. A. Snyder, D. A. Longbottom, A. Z. Nalbandian, X. Huang, *Chemistry – A European Journal* **2004**, *10*, 5581-5606.
[125] Z. Schwartz, C. Valiton, M. Lovasz, A. G. Roberts, *Synthesis* **2023**, *56*, 87-106.
[126] A. R. Katritzky, A. M. El-Mowafy, *The Journal of Organic Chemistry* **1982**, *47*, 3506-3511.
[127] A. R. Katritzky, C. M. Marson, *Angewandte Chemie International Edition in English* **1984**, *23*, 420-429.

[128] A. M. Yousif, S. Colarusso, E. Bianchi, *European Journal of Organic Chemistry* **2023**, *26*, e202201274.
[129] J. T. M. Correia, V. A. Fernandes, B. T. Matsuo, J. A. C. Delgado, W. C. de Souza, M. W. Paixão, *Chemical Communications* **2020**, *56*, 503-514.
[130] B. E. Daikh, R. G. Finke, *Journal of the American Chemical Society* **1992**, *114*, 2938-2943.
[131] S. Fukuzumi, K. Ohkubo, T. Suenobu, K. Kato, M. Fujitsuka, O. Ito, *Journal of the American Chemical Society* **2001**, *123*, 8459-8467.
[132] A. Böhm, T. Bach, *Chemistry – A European Journal* **2016**, *22*, 15921-15928.
[133] H. T. Luk, C. Mondelli, D. C. Ferré, J. A. Stewart, J. Pérez-Ramírez, *Chemical Society Reviews* **2017**, *46*, 1358-1426.
[134] P. Gandeepan, T. Müller, D. Zell, G. Cera, S. Warratz, L. Ackermann, *Chemical Reviews* **2019**, *119*, 2192-2452.
[135] Q. Zhang, B.-F. Shi, *Chemical Science* **2021**, *12*, 841-852.
[136] G. Xia, Z. Zhuang, L.-Y. Liu, S. L. Schreiber, B. Melillo, J.-Q. Yu, *Angewandte Chemie International Edition* **2020**, *59*, 7783-7787.
[137] aL. M. Stateman, K. M. Nakafuku, D. A. Nagib, *Synthesis* **2018**, *50*, 1569-1586; bS. Sarkar, K. P. S. Cheung, V. Gevorgyan, *Chemical Science* **2020**, *11*, 12974-12993.
[138] aY. Zhu, K. Huang, J. Pan, X. Qiu, X. Luo, Q. Qin, J. Wei, X. Wen, L. Zhang, N. Jiao, *Nature Communications* **2018**, *9*, 2625; bX. Wu, M. Wang, L. Huan, D. Wang, J. Wang, C. Zhu, *Angewandte Chemie International Edition* **2018**, *57*, 1640-1644; cA. Hu, J.-J. Guo, H. Pan, H. Tang, Z. Gao, Z. Zuo, *Journal of the American Chemical Society* **2018**, *140*, 1612-1616.
[139] M. Nechab, S. Mondal, M. P. Bertrand, *Chemistry* **2014**, *20*, 16034-16059.
[140] aS. Sathyamoorthi, S. Banerjee, J. Du Bois, N. Z. Burns, R. N. Zare, *Chemical science* **2018**, *9*, 100-104; bM. A. Short, J. M. Blackburn, J. L. Roizen, *Angewandte Chemie* **2018**, *130*, 302-305.
[141] aA. W. Hofmann, *Berichte der deutschen chemischen Gesellschaft* **1883**, *16*, 558-560; bK. Löffler, C. Freytag, *Berichte der deutschen chemischen Gesellschaft* **1909**, *42*, 3427-3431.
[142] aS. L. Shevick, C. V. Wilson, S. Kotesova, D. Kim, P. L. Holland, R. A. Shenvi, *Chemical Science* **2020**, *11*, 12401-12422; bS. W. Crossley, C. Obradors, R. M. Martinez, R. A. Shenvi, *Chemical reviews* **2016**, *116*, 8912-9000.
[143] aS. Jana, V. J. Mayerhofer, C. J. Teskey, *Angewandte Chemie International Edition* **2023**, *62*, e202304882; bC. V. Wilson, D. Kim, A. Sharma, R. X. Hooper, R. Poli, B. M. Hoffman, P. L. Holland, *Journal of the American Chemical Society* **2022**, *144*, 10361-10367.
[144] T. Kurahashi, H. Fujii, *Inorganic Chemistry* **2013**, *52*, 3908-3919.
[145] C. V. Wilson, P. L. Holland, *Journal of the American Chemical Society* **2024**, *146*, 2685-2700.